2024

U.S. Department of Transportation
Federal Highway Administration

NEBRASKA
DEPARTMENT OF TRANSPORTATION

NEBRASKA
TRANSPORTATION CENTER

Report PR-FY21(002)

Final Report

Development of Guideline for the Use of Geosynthetics in Different Roadway Layered System in Nebraska

Jongwan Eun, PhD, PE
Associate Professor
Department of Civil and Environmental Engineering
University of Nebraska-Lincoln

Seunghee Kim, PhD, PE
Assistant Professor

Daniel Robertson
Graduate Research Assistant

Yusuf Alhowaidi
Graduate Research Assistant

Hung Van
Graduate Research Assistant

Laith Ibdah
Graduate Research Assistant

Kenaz Owusu
Graduate Research Assistant

Nebraska Department of Transportation Research
Headquarters Address
1400 Nebraska Parkway
Lincoln, NE 68509
ndot.research@nebraska.gov
(402) 479-4697
https://dot.nebraska.gov/business-center/research/

Nebraska Transportation Center
262 Prem S. Paul Research Center at Whittier School
2200 Vine Street
Lincoln, NE 68583-0851
(402) 472-1932
http://ntc.unl.edu

This report was funded in part through grant[s] from the Federal Highway Administration [and Federal Transit Administration], U.S. Department of Transportation. The views and opinions of the authors [or agency] expressed herein do not necessarily state or reflect those of the U.S. Department of Transportation.

Development of Guideline for the Use of Geosynthetics in Different Roadway Layered System in Nebraska

Jongwan Eun, Ph.D., P.E.
Associate Professor
Department of Civil and Environmental Engineering
University of Nebraska-Lincoln

Seunghee Kim, Ph.D., P.E.
Assistant Professor
Department of Civil and Environmental Engineering
University of Nebraska-Lincoln

Daniel Robertson
Graduate Research Assistant
Department of Civil and Environmental Engineering
University of Nebraska-Lincoln

Yusuf Alhowaidi
Graduate Research Assistant
Department of Civil and Environmental Engineering
University of Nebraska-Lincoln

Hung Van
Graduate Research Assistant
Department of Civil and Environmental Engineering
University of Nebraska-Lincoln

Laith Ibdah
Graduate Research Assistant
Department of Civil and Environmental Engineering
University of Nebraska-Lincoln

Kenaz Owusu
Graduate Research Assistant
Department of Civil and Environmental Engineering
University of Nebraska-Lincoln

Sponsored By

Nebraska Department of Transportation and U.S. Department of Transportation Federal Highway Administration

January 2024

TECHNICAL REPORT DOCUMENTATION PAGE

1. Report No. PR-FY21(002)	**2. Government Accession No.**	**3. Recipient's Catalog No.**
4. Title and Subtitle Development of Guideline for the Use of Geosynthetics in Different Roadway Layered System in Nebraska		**5. Report Date** January 2024 **6. Performing Organization Code**
7. Author(s) Jongwan Eun, Seunghee Kim, Daniel Robertson, Yusuf Alhowaidi, Hung Van, Laith Ibdah, Kenaz Owusu		**8. Performing Organization Report No.**
9. Performing Organization Name and Address Board of Regents, University of Nebraska-Lincoln		**10. Work Unit No.** **11. Contract** PR-FY21(002)
12. Sponsoring Agency Name and Address Nebraska Department of Transportation Research Section 1400 Nebraska Parkway Lincoln, NE 68502		**13. Type of Report and Period Covered** Final Report July 2020 – Jan 2024 **14. Sponsoring Agency Code**

15. Supplementary Notes
If applicable, enter information not included elsewhere, such as translation of (or by), report supersedes, old edition number, alternate title (e.g. project name), or hypertext links to documents or related information.

16. Abstract
This study evaluated the design properties of the geosynthetic reinforced soils for the roadway pavement and compared the reinforcing performance depending on different geosynthetics and soil types, particularly for a subgrade layer in Nebraska. The results obtained from a large direct shear test, pullout test, and soil chamber test with a dynamic cone penetrometer (DCP) showed that geosynthetic improves soil properties associated with the pullout and interface shear resistance, strength related parameters. The Large Scale Tracking Wheel Test also showed how the performance of biaxial geogrid reinforced pavement improved the strength/stiffness and reduced the total permanent deformation and pressure acting on the base/subgrade interface. Among the geosynthetic, three geogrids consistently showed better enhancement than geotextile, significantly improving all soils, including sand, red shale, and clay. Numerical modeling employing the input parameters obtained from the lab tests to simulate practical pavement layers for reinforced and unreinforced cases with geosynthetic application proved a significant enhancement when applying geosynthetics to reduce settlement and vertical stress. During the soil chamber test, the dynamic cone penetrometer index (DPI) successfully identified the depth of the geosynthetic installation, and the confined zone reinforced by the geosynthetic compared to the unreinforced case. Thus, in designing and analyzing geosynthetic reinforced subgrades in roadway pavements, it was found that the DCP test provides a valid and reliable method to evaluate the performance of geosynthetic reinforced soils. Furthermore, the Large-Scale Tracking Wheel test, performed for both reinforced and unreinforced cases, successfully showed improvement in strength/stiffness and total deformation reduction of a biaxial geogrid reinforced pavement. Based on these results, different percentage increases in the resilient modulus of reinforced subgrades were proposed for different soil and geosynthetic types. Finally, the relationships with DPI and other design properties, such as interface friction angle, subgrade reaction, and resilient modulus, were suggested for the geosynthetic reinforced soils.

17. Key Words Geosynthetics, subgrade, numerical modeling, pullout test, direct shear test, dynamic cone penetrometer test, large-scale tracking wheel test	**18. Distribution Statement** No restrictions. This document is available through the National Technical Information Service. 5285 Port Royal Road Springfield, VA 22161		
19. Security Classification (of this report) Unclassified	**20. Security Classification (of this page)** Unclassified	**21. No. of Pages** 277	**22. Price**

Form DOT F 1700.7 (8-72) Reproduction of completed page authorized

Table of Contents

List of Figures

List of Tables

Disclaimer

The contents of this report reflect the views of the authors, who are responsible for the facts and the accuracy of the information presented herein. The contents do not necessarily reflect the official views or policies neither of the Nebraska Department of Transportations nor the University of Nebraska-Lincoln. This report does not constitute a standard, specification, or regulation. Trade or manufacturers' names, which may appear in this report, are cited only because they are considered essential to the objectives of the report.

The United States (U.S.) government and the State of Nebraska do not endorse products or manufacturers. This material is based upon work supported by the Federal Highway Administration under SPR-P1(see your contract for this #. Any opinions, findings and conclusions or recommendations expressed in this publication are those of the author(s) and do not necessarily reflect the views of the Federal Highway Administration."

This report has been reviewed by the Nebraska Transportation Center for grammar and context, formatting, and Section 508 compliance.

Abstract

This study evaluated the design properties of the geosynthetic reinforced soils for the roadway pavement and compared the reinforcing performance depending on different geosynthetics and soil types, particularly for a subgrade layer in Nebraska. The results obtained from a large direct shear test, pullout test, and soil chamber test with a dynamic cone penetrometer (DCP) showed that geosynthetic improves soil properties associated with the pullout and interface shear resistance, strength related parameters. The Large Scale Tracking Wheel Test also showed how the performance of biaxial geogrid reinforced pavement improved the strength/stiffness and reduced the total permanent deformation and pressure acting on the base/subgrade interface. Among the geosynthetic, three geogrids consistently showed better enhancement than geotextile, significantly improving all soils, including sand, red shale, and clay. Numerical modeling employing the input parameters obtained from the lab tests to simulate practical pavement layers for reinforced and unreinforced cases with geosynthetic application proved a significant enhancement when applying geosynthetics to reduce settlement and vertical stress.

During the soil chamber test, the dynamic cone penetrometer index (DPI) successfully identified the depth of the geosynthetic installation, and the confined zone reinforced by the geosynthetic compared to the unreinforced case. Thus, in designing and analyzing geosynthetic reinforced subgrades in roadway pavements, it was found that the DCP test provides a valid and reliable method to evaluate the performance of geosynthetic reinforced soils. Furthermore, the Large-Scale Tracking Wheel test, performed for both reinforced and unreinforced cases, successfully showed improvement in strength/stiffness and total deformation reduction of a biaxial geogrid reinforced pavement. Based on these results, different percentage increases in the resilient modulus of reinforced subgrades were proposed for different soil and geosynthetic types. Finally, the relationships with DPI and other design

properties, such as interface friction angle, subgrade reaction, and resilient modulus, were suggested for the geosynthetic reinforced soils.

Chapter 1 Introduction

1.1 Problem Statement

Geosynthetics have been widely utilized as an effective solution for stabilizing the subgrade of roadway pavement construction in regions with problematic soil conditions. Geogrids and geotextiles are among the most common geosynthetics used in roadway applications (Kaswell 1963, Haliburton et al. 1980, Myles and Carswell 1986, and Koerner 2005). According to a study conducted by Wang et al. (2021), geosynthetics have been found to significantly improve the performance of pavements constructed on soft subgrade soils. The use of geosynthetics can reduce not only the thickness of the aggregate base required but also extend the service life of the pavement.

Geosynthetics are marketed as a viable alternative to traditional pavement systems, with the ability to reduce construction costs while maintaining equivalent structural performance. Figure 1.1 illustrates the benefits of using geosynthetics, which include improved pavement durability and reduced maintenance requirements. Although the initial construction cost of using geosynthetics may be higher than traditional methods, the overall life cycle cost is lower due to reduced maintenance requirements and increased pavement durability. Using geosynthetics, pavement conditions remain stable over time and traffic loads, resulting in improved driving conditions and increased safety for roadway users.

Typically, the geosynthetics are promoted as either having the ability to lengthen asphalt pavement design life by controlling the damage to the pavement, or they are used as a more cost-efficient substitute to reduce aggregate base thickness without jeopardizing the level of designed strength, as is the case with traditional pavement systems. Geosynthetic reinforcement is more effective in enhancing the performance of flexible asphalt pavements compared to rigid concrete pavements. The benefits speak for themselves, as roads that incorporate geosynthetics show longer serviceability and slower deterioration. Indeed,

pavement conditions are much better over time under gradual traffic loads when geosynthetic is used. The initial cost of construction would rise due to the added reinforcement, but the long-term cost would decrease as maintenance would be mitigated and become more infrequent (Barksdale et al. 1989, Zornberg 2010, Koerner 2012, Christopher 2014, and Zornberg 2017).

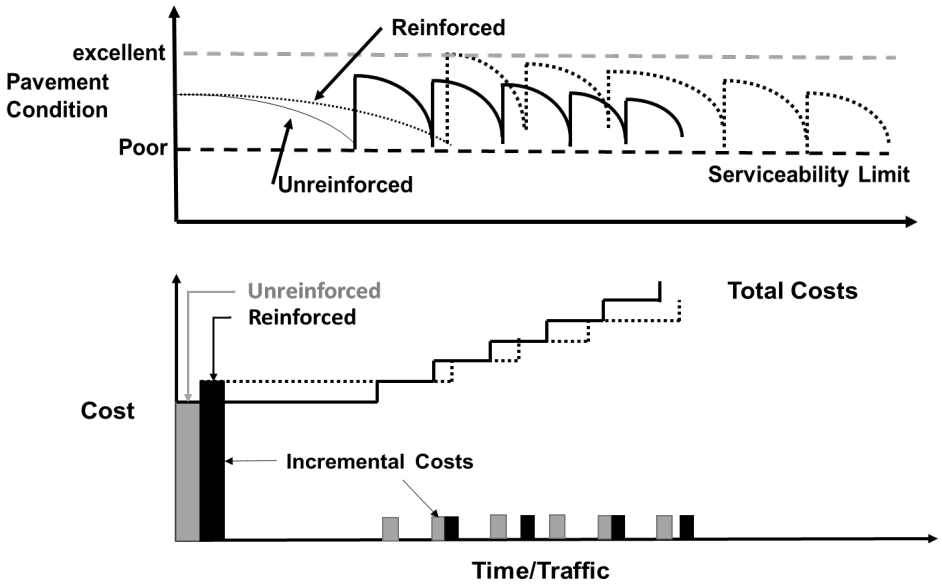

Figure 1.1 Conceptual illustration of life-cycle cost for reinforced and unreinforced pavements (adapted from Perkins et. al, 2004)

The key idea behind a geosynthetic is its ability to redistribute vehicle load, which in turn, is a redistribution of stress in the pavement structure. Geosynthetic reinforcement is commonly placed between the base and subgrade layers, though it can be placed deeper in the subgrade section. Separation is important because it does not allow for the intermingling of layers and improves the stabilization of flexible pavements. The stress distribution is reallocated to the horizontal direction along the geosynthetic. The horizontal tensile strains are reduced as the confinement and interlocking between layers are intensified (Zornberg 2017).

On a sub-surface level, it can be understood that vertical stresses under these concentrated loads from repetitive traffic are displayed as a deep upside-down bell-shaped curve where the most substantial stress develops directly under the load. Pressures are highest near the surface, gradually approaching zero at a certain depth. For pavement, the load at the surface is not a point load because it is distributed over an ellipse area by the tire; however, it follows the pattern of a point load for the variation of stress with depth as shown in Figure 1.2 (Giroud and Noirav 1981, Holtz et al. 1998, Giroud and Han 2004, and Berg et al. 2000).

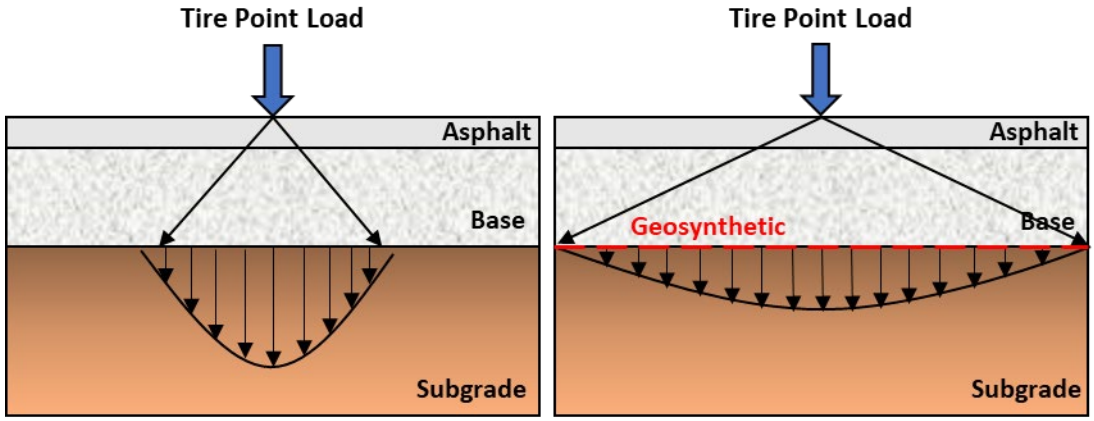

Figure 1.2 Cross-sectional roadway showing load distribution with and without geosynthetics (modified from Zornberg and Gupta 2010)

There have been several studies that have investigated the effects of geosynthetics under flexible pavements. Nonetheless, only a handful of states have implemented this technique, most presumably due to the lack of familiarity with this product among contractors and state departments and the initial increase in the cost. The Federal Highway Administration (FHWA) published a reference manual for its design and construction in 2008, which showed a general procedure for properly applying geosynthetics in roadway design with different California Bearing Ratio (CBR) values for soils. There are still some

uncertainties regarding region-specific material properties and the types of geosynthetic products to calibrate the design process accurately.

Thus, the implementation of geosynthetic reinforcement should be a case-by-case study, claiming dependencies for variable site conditions, soil types, and in particular, sensitive subgrade soil stability. These sensitive subgrade soils are usually predicted as soft or problematic foundation soils. Softer soils have lower shear strength causing excessive settlement (Pancar and Akpinar 2016). Subgrade soils with higher moisture and silt contents show greater excess rutting – even subgrade soils with 3% moisture above optimum are considered unstable (IDOT 2005). The problem is evident that there is very limited research conducted to identify the performance evaluation of geosynthetics for different soil types in Nebraska. Consequently, there are no current well-defined provisions in the Nebraska Department of Transportation (NDOT) Standard Specifications for Highway Construction regarding geosynthetic reinforcement design for roadway systems.

1.2 Objective Statement

The proposed research aims to achieve two primary goals: (1) evaluate the design parameters of geosynthetic reinforced roadway pavement for subgrade soils in Nebraska, and (2) suggest a design recommendation for geosynthetic reinforced roadway pavement. The proposed scope of work is as follows:

1. Extensive review: this task focused on conducting extensive surveys and reviews of practical cases and applications of geosynthetics to the roadway pavement in other states and other countries, as well as Nebraska. In addition, the current design and construction processes of geosynthetic-reinforced roadway pavement in other states were investigated.

2. Evaluation of design parameters: this task investigated selected subgrade soil - geosynthetic interaction using two representative laboratory tests, the large pullout box testing, and the direct shear testing method.
3. Evaluate the strength and bearing of geosynthetic-reinforced soil using a soil chamber test accompanying the Dynamic Cone Penetrometer (DCP) test. Also, the team prepared Large-Scale Tracking Wheel (LSTW) testing system close to a field condition. The performance of geosynthetic reinforcement was evaluated with the different grades of subgrade soils in Nebraska.
4. Numerical investigation: this task was conducted mainly via numerical simulation to examine the full-scale performance of geosynthetic-reinforced roadway pavement that can be implemented in Nebraska to improve cost-effectiveness.
5. Design recommendation: an improved design and construction recommendation for the geosynthetic-reinforced roadway pavement were developed. The aim is: 1) to potentially reduce the cost and to enhance the constructability and maintenance; 2) to provide a best practice of geosynthetic reinforcement for the roadway pavement system, in particular, subgrade in Nebraska; to promote the implementation of geosynthetic reinforcement to control pavement layers, in particular, subgrade in Nebraska; to suggest NE design protocol or specification of the geosynthetic-reinforced roadway layered system and subgrades, with reference to FHWA guidelines and AASHTO.

The four main aspects of the research were conducted through three new experimental tests and one simulation. The testing apparatuses were fabricated for the University of Nebraska-Lincoln Geotechnical Engineering Laboratory in coordination with the regional machine shop, Puritan Manufacturing, Inc (Omaha, NE). The research team newly designed and prepared the Large Direct Shear Box, the Large-Scale Pullout Box, and the soil chamber

test using DCP and LSTW tests. These machines define the bulk of this research to determine the best-fit geosynthetic-soil relationship for roadway application. The larger nature of the machines more aptly replicates real conditions. This magnitude of work surrounding pavement design consideration helps verify the test results and the outcomes between the design instruments.

The large direct shear test was conducted to evaluate the shear resistance at the soil-geosynthetic interface. Similar to a traditional direct shear test, this apparatus evaluated the interface response between soils and geosynthetics. Considering the geogrid aperture dimension, the box was designed to be 15 times larger than the aperture size. Different types of geosynthetics, soils, and normal pressures were considered to evaluate the interface resistance. The pullout box was designed to evaluate the pullout resistance of soil and geosynthetics. The box itself was fabricated to be large enough to eliminate the boundary effect and ensure the process was compliable with real-world application. Both tests were compared for soil-geosynthetic interface properties.

To evaluate the performance of geosynthetic reinforcement with the different grades of subgrade soils in Nebraska close to the field scale, the team prepared the LSTW testing system. The design of the tracking wheel test was based largely on preexisting setups in literature, such as the Georgia Department of Transportation (Kim et al. 2018) and New Zealand (Bagshaw et al. 2015). The mechanical performance of the geosynthetic-reinforced pavement system was evaluated to determine rutting and how well the geosynthetic could stabilize the layers. Further information and details about the LSTW apparatus can be seen in Appendix C and Appendix D.

As an alternative, a soil chamber test using DCP was conducted to evaluate the strength of the pavement and compare its performance of the pavement between geosynthetic reinforced and non-reinforced ones. The DCP tests were conducted with three different

subgrade materials: Sand, Red Shale, and clay. Gravel was used as the base course material in both cases. DPI was then used in estimating the CBR for the Sand subgrade and Gravel base course layer based on the US Army Corps of Engineers equations.

A numerical study was also conducted using the Fast Lagrangian Analysis of Continua (FLAC) software. The focus was to evaluate the performance of geosynthetic-reinforced roadway systems, specifically looking at the settlement. The input parameters were obtained from the direct shear and pullout tests, as well as the soil properties found from standard soil tests and literature. This parametric study investigated the best reinforcement type along established depths. It evaluated the system's performance and serviceability over a long-term period to examine the improved design with a reduced base thickness. Based on the results, construction recommendations were prepared for a geosynthetic-reinforced roadway pavement system.

Chapter 2 Literature Review

2.1 History of Geosynthetics

The structure of road design is straightforward, consisting of a surface layer, a base layer, and a subgrade layer. These simple components have been the driving force in roadway construction for years in the United States. The game changed in 1926. The South Carolina Highway Department is credited as being the forerunner for geosynthetic use in low-volume roadway construction. They had the idea to separate the subgrade and base layers of an unpaved road by means of a cotton fabric, which in fact led to better stabilization after an eight-year period before the material eventually degraded. It showed impressive results for the time, revealing a reduction in cracking, raveling, and surface failures (Koerner et al. 1997).

This led to a new field of study. It proved to be a slow start, especially in the United States, seeing that no one paid much attention to their research. However, in 1956, the Netherlands reported using geotextiles as part of a maritime protection effort which lasted into the 1960's, becoming an integral part of their design process (John 1987). They were used in place of soil filters. Next, the Dutch capitalized on their successes by stitch-bonding two layers of geotextiles together to create a more durable formwork for concrete revetments. They even introduced high-strength products that could be used on soft saturated soils. France caught wind of the experiment and created needle-punched non-woven fabrics from continuous filaments in the 1960's (Giroud 1986). The 1960's proved to be the rise to prominence for geosynthetic applications. Geotextiles in particular had made a mark in society.

It was not until 1968 that geosynthetics were first used on unpaved roads. During the 1970s, their usage for pavement systems grew steadily. At that time there were less than 10 types of geosynthetics available worldwide, and most products were chosen based on trial

and error (Holtz 2001). In 1971, the first field geosynthetic was used to improve the stability of an embankment in Nol, Sweden, which was successful and led to further laboratory research (Holtz 2001).

The United Kingdom developed a heat-bonded non-woven fabric for use on unpaved roads, while the US Department of Agriculture Forest Service developed some geosynthetic design methodologies for low-volume rural forest roads using a trial-and-error approach. This resulted in one of the first guidelines for fabric construction and maintenance for unpaved roads in the US, as detailed in the finalized report by Steward et al. (1977). This report helped to increase awareness of geotextiles in America.

By the mid-1970s, there was an increase in technical papers about geosynthetics and their applications. The U.S. Department of Agriculture Forest Service (USFS), using the trial-and-error basis, developed some geosynthetic design methodologies for its low-volume rural forest roads (Powell et al. 1999). It proved to be one of the first guidelines for fabric construction and maintenance for unpaved roads in the United States. In 1977, the first international conference on construction fabrics was held in Paris, France, which highlighted both woven and non-woven geotextiles. This conference marked the mainstreaming of geosynthetics, and afterward, ideas and products were traded globally, creating a sort of renaissance in the field (Koerner 2016).

Geosynthetics have become increasingly popular in roadway construction over the past few decades, resulting in a billion-dollar industry. They have been highly successful in roadway design and account for the majority of the market. Paving fabric interlayers are the most commonly, but there is ongoing research and development for geosynthetic reinforcement in subgrade and base layers. In the late 1990s, North America spent over $800 million on engineering projects related to geosynthetics. By 2001, the United States had a $1.1 billion geosynthetic market. According to Emergent Research (2021), the global

geosynthetic market was worth $9.4 billion in 2020, and despite the disruption caused by the Covid-19 pandemic, it increased to $9.9 billion in 2021 (Markets and Markets 2021).

The geosynthetics industry has expanded significantly, with a range of products available, such as geogrids, geotextiles, geomembranes, geocells, and geocomposites. Geosynthetics are now included in many standards, including those set by federal agencies like the FHWA and EPA, as well as state governments. It is crucial not to overlook their importance, given their significant progress in a relatively short period. The future of geosynthetics remains uncertain and can only be determined with time.

2.2 Geosynthetic Materials

Geosynthetics are planar materials made from polymers, strategically combined with soil or rock in civil engineering projects. These materials come in various types, with a specific emphasis on geogrids and geotextiles for our focus.

2.2.1 Geogrids

Geogrids are planar polymeric products consisting of a mesh-like network of open apertures with integrally connected tensile-resistant elements intersecting at the junctions. Generally, the apertures are stretched, making the respective product known as extruded geogrid. Further, a biaxial (triaxial) geogrid is produced by stretching heavy strands of plastic in the longitudinal and transverse (and diagonal) directions of a regularly punched polymer sheet (Shukla et al. 2006). The benefit to geogrid is its apertures, which help with its reinforcement. The apertures capture and hold aggregates together, creating a better interlock between them. In this way, redistribution of load over a wider area is better achieved, creating a longer-lasting road by a reduction in lateral aggregate movement. Geogrid acts as a restraining mechanism capable of controlling unwanted deformations. As the base acts as a more uniform unit, stresses are dissipated into the subgrade. This, too, will lead to an increase in bearing capacity.

2.2.2 Geotextiles

Geotextiles are a planar and permeable flexible textile sheet. They can be manufactured in two separate ways, resulting in woven or non-woven. A woven product is produced by interlacing synthetic fibers at right angles, while a non-woven product is produced from directionally oriented synthetic fibers bonded with bonding agents (Shukla et al. 2006). Geotextiles which may also be known as filter fabrics or construction clothes, are nonbiodegradable polymer fabrics (Koerner, 2016). They are often woven or non-woven permeable textiles used to increase soil stability, drainage, or erosion control. Similar to geogrids, they are made of polypropylene, polyester, polyethylene, or polyamide synthetic. Non-woven geotextiles are more pliable and provide better flow rates, making them more desirable in high filtration circumstances. Woven geotextiles consist of interlacing strands at right angles, making them more durable in high-strength situations. This type of fabric is preferred to reduce shear failure in soft subgrade conditions (US Fabrics). They also show greater separation qualities due to their structure, which keeps soil particles in place. Separation provides aggregate from sinking into the weaker subgrade or vise-versa where the subgrade pumps into the aggregate.

Geosynthetic can be placed underneath flexible pavements to improve strength – the structural stability of soil is compounded with the additional tensile robustness. Interlocking between particles provides for reinforcement, creating a resistant force. Steadfast mechanical properties provided by these materials should include high tensile modulus (to resist stretching under load), elastic response under dynamic loading, opposition to creep, and great durability. For subgrade stabilization, fabric helps to prevent granular material from seeping into the soft foundation soils, known as base punching or localized shear failure (Haas et al. 1980). Soil piping occurs when finer soil particles escape through the fabric's voids, leaving behind an undesirable gradation of larger particles. The simple prevention is to make the

voids in the geotextile small enough to retain all particles (Koerner 2005). Sand is expected to perform poorly with geotextile because it will slide across the surface interface, while clay should not do as well with geogrids because the particle size is too small to be effective with the aperture size. On the other hand, sand is expected to work well with geogrids due to the interlocking nature and higher friction angle of the particles. There has been rapid growth of these products globally over the past few decades, primarily because of their non-corrosiveness, high resistance to chemical degradation, and long-term durability (Shukla et al. 2006).

2.3 Proven Geosynthetic Improvement

2.3.1 General

Several methods have been used for the ground improvement of soil, including additives, higher compaction levels, and geosynthetics. These are supposed to be cost-effective alternatives, which result in reduced construction times and simplified foundation design. Generally, pavement structures come in two categories: flexible and rigid. Yoder and Witczak (1975) define a pavement functional failure as one that cannot carry out its intended function without causing discomfort to drivers. With constant demands from traffic on the road structure systems, stresses in the horizontal and vertical directions often show local settlements and cracking. Geosynthetics act as an extremely low-cost insurance that can prevent premature failure (Holtz et al. 1998). Their application has been in practice under asphalt roadways since the 1970's, and beginning in the 1980's, geosynthetics took on the reinforcement role to minimize reflective cracking in asphalt overlays, primarily by reducing stress concentration from overhead pressures (Zornberg 2017). The principal function is allotted to additional tensile resistance which absorbs strain and reduces fatigue; geosynthetics change insufficient bearing capacities. When the geogrid is tensioned, it creates an upward force that resists rutting at the surface level (Mounes et al. 2011). Geosynthetics

have a role to reduce soil settlement, improve bearing capacity, and reduce base layer aggregate. In short, they improve the performance of unpaved roads by increasing their lifetime while minimizing the maintenance cost and road thickness.

The design of geosynthetics in soft soils can lead to increased tensile strength, increased resistance to reflective cracking and bottom-up fatigue cracking, and increased shearing resistance which reduces rutting (Zofka et al. 2017). Geotextiles have been the most popular product, and their most common use is for separation and stabilization (Perkins et al. 2005). Meanwhile, polypropylene geotextiles have a low manufacturing cost. This is because polypropylene itself is a reliable, cost-effective raw material (Shukla et al. 2006). However, this product works best in non-critical structures since it tends to lose efficiency as proposed loads increase, thus making it more desirable in low-volume environments. Roughly two-thirds of roads are considered low-volume and do not receive this suitable technological attention (Keller 2016).

2.3.2 Geosynthetic Construction Procedures

A general summation of state specifications was created after evaluating several states across America that use geosynthetics for roadway design practices. These states included California, Colorado, Iowa, Kansas, Louisiana, Maryland, Minnesota, Montana, Nevada, New Jersey, North Carolina, North Dakota, South Dakota, Texas, and Virginia. The information pertains to geogrid and geotextiles specifically, and a more complete list of particulars can be found with each states' specifications and AASHTO M288, which gives accounts for classes with better survivability rates and recommendations for certain situations. The proper selection of a geosynthetic is governed by the load that will be placed upon it as well as the type of function it will serve.

Barksdale et al. (1989) states that the importance of proper construction procedure for geosynthetic reinforcement cannot be overemphasized. Most failures associated with

geosynthetic usage can be linked back to improper construction practices (Holtz 2001). In fact, estimations say that over 99.9% of the time, paving fabrics meet their design criteria without failure. It would seem the greatest cause of geosynthetic failure is due to human error – improper installment (Baker and Marienfeld, 1999). The most common examples include excessive UV exposure (resulting in loss of strength), improper overlap (especially over soft soils), or too high installation stresses (Koerner 2005). In accordance with AASHTO M288, geosynthetic rolls shall be elevated off the ground and stored in a waterproof cover to protect against ultraviolet radiation; southern climates are particularly susceptible. The ground should be relatively undisturbed. Rolls shall be covered with a suitable wrapping and stored to protect against moisture and natural elements, such as dirt, mud, or debris. Geosynthetics shall not be installed when weather conditions are not suitable. Do not operate any construction equipment atop the bare geogrid. Once the geosynthetic has been laid, it must be immediately backfilled (Caltrans 2018, Minnesota DOT 2018, South Dakota DOT 2015, Texas DOT 2014, and Virginia DOT 2020).

When placing the geogrid, it shall be laid longitudinally in the direction of traffic along the ground without any wrinkles or folds (Texas DOT 2014, Iowa DOT 2015, and Virginia DOT 2020). The stiffness of the geogrid is important. The geogrid may be cut to conform to curves along the roadway. Damaged geogrid should not be used, or, if salvageable, the damaged area must be covered an additional 24-36 inches in all directions (Texas DOT 2014, North Dakota DOT 2014, and Virginia DOT 2020). Geotextiles shall either overlap or be sewn to an adjacent roll. Overlap shall cover at least 24-36 inches. The previous roll should lie atop the new one. Tencate (2018) suggests that when the shear strength of subgrade soils is less than a 1.0 CBR value, the geotextiles should be seamed. Preferably the seams should be sown in a factory rather than the field, as it generally provides higher seam efficiencies. Seams are to be either J-seams or butterfly seams. Threads should

use polyester, polypropylene, or Kevlar with a durability greater or equal to the material. Compose all geosynthetics of at least 85% by weight polyesters, polyolefins, or polyamides. Geotextiles shall have fibers consisting of polymers, composed of 95% by weight polyesters or polyolefins (Caltrans 2018, Colorado DOT 2019, Iowa DOT 2012, Louisiana DOT 2016, Maryland DOT 2020, Minnesota DOT 2018, Montana DOT 2020, Nevada DOT 2020, New Jersey DOT 2019, North Carolina DOT 2018, North Dakota DOT 2014, South Dakota DOT 2015, and Texas DOT 2014). More detailed information is introduced in Section 2.4.

2.3.3 Stiffness Improvement

Geotextiles are good for separation as they prevent the base and subgrade layers from mixing, thus keeping stability as well. Geogrids are used for reinforcement. These methods can allow for long-term stress reduction in the surface layer in their own ways. When the aggregate is forced to interlock, it is made to act as one unit and uniformly repulses surface-level loading. In this way, it is able to maintain a high compressive strength. Soil stabilization helps improve the reactive properties to support structures because reinforced soils often show better performance than traditional soils under dynamic loads. Additionally, the soil below hardly changes volume since the rock is not penetrating from above, thus keeping rigidity and structural stability.

This was proven in a study conducted by Al-Qadi et al. (2011) where geogrid was used to improve pavement performance. The test was constructed over weak subgrade where a unilateral dual tire assembly passed overhead at a low speed. It was shown that, indeed, the reinforced sections saw reduced rutting and delayed surface cracking as well as a reduction in horizontal movement of granular material. The study stated that for weak subgrades, the geogrid should be placed at the base-subgrade interface, as this would help to reduce vertical deflection. According to Motanelli et al. (1997), geogrid placed between a gravel base and sand subgrade showed an increase in CBR for the subgrade. Adams et al. (2015) conducted a

CBR test and determined that triaxial geogrid (the same used in the present study) created a 12-31% increase in penetration resistance for soaked and unsoaked conditions when placed in the aggregate layer. Abu-Farsakh et al. (2012) ran a repeated load triaxial test under optimum moisture content. It was concluded that the addition of geogrid reinforcement in granular base specimens showed fewer permanent deformations compared to unreinforced specimens. It also proved that the higher the tensile modulus of the geogrid, the lower the permanent deformation. A triaxial geogrid did the best in this regard. The test showed, though, that geogrid did not greatly improve the resilient modulus of a granular specimen.

Rahman et al. (2014) conducted repeated load triaxial tests with different types of base materials and biaxial and triaxial geogrids. The resilient modulus proved to be higher for reinforced specimens rather than unreinforced. In fact, recycled concrete aggregate (RCA) with biaxial increased by 24% while the RCA with triaxial increased 34%. For the same specimens, permanent deformation decreased by 29% and 36%. Oliver et al. (2016) reviewed geogrid stabilization over weak subgrades, specifically the modulus of unbound layers to control particle movement. The research concluded that under triaxial conditions, the resilient modulus was raised by 10% and the stiffness by 5-20% with the addition of geogrid. The bound aggregate had a much lower axial strain after 20,000 cycles. This concept was then applied in the field where geogrid-reinforced subgrade outperformed the control section.

Geosynthetics do not actually increase the structural reinforcement of the pavement itself, but they have been known to decrease earlier on-set damages to roads. Mechanical stabilization with dense granular soil or aggregate base layers can strengthen the subgrade. It has been shown that adding a geotextile layer to reinforce the granular soil raises the CBR strength (Zumrawi and Abdalgadir 2019). Geotextiles increase the load carrying capacity of soil while the settlement decreases. Moreover, they allow for filtration and drainage and aid in rapid dissipation of excess subgrade pore pressure. In a report by Ogundare et al. (2018), a

non-woven geotextile was used as reinforcement and compared against poor subgrade A-7-5 and A-7-6 soils. After conducting a CBR test, it was determined there was an overall 15-20% value increase when reinforcement was added. Additionally, their application, regardless of depth in the subgrade during testing, increased the strength of the soil. Muhmood et al. (2021) showed that the performance of non-woven geotextiles, placed between soft subgrade and the base layer, improved the CBR value roughly 20%.

2.3.4 Rutting Improvement

Geosynthetic reinforcement can lead to rut depth reduction due to the fact that it leads to an increase in bulk stress, aggregate layer confinement and stiffness, and decreases the vertical stress on the top of the subgrade. Explained by Nunn (1998), rutting could be the result of continuous traffic over too soft of a surface pavement or because of a greater problem beneath the surface. Addition of geosynthetic reinforcement is imperative for roadways to prevent rutting, specifically a small live load (rutting 2-4 inches) or a large live load (rutting greater than 4 inches) on a thin roadway (Holtz et al. 1998). If the actual problem resides in the subgrade, it is determined to be a structural deformation.

For example, many rural roads in India are of poor quality, but are obligated to withstand heavy loads. Without an asphalt cover, the granular base is forced to take the entire load. Latha and Nair (2014) ran both a field and lab test to compare different geosynthetics against load capacity and rut depth. The geosynthetics were placed at the base-subgrade interface. Looking at the final model result, the unreinforced section handled the least amount of pressure while still showing the greatest amount of settlement. The geogrids showed greater pressure resistance. Giroud and Han (2004) suggested an improvement factor for geogrid reinforced unpaved roads. From the field results, it was seen that only planar geosynthetics at higher pressures make a considerable difference, while those at lower pressures are ineffective due to the lack of tensile strain. Barksdale et al. (1989) confirmed

this theory and stated that when the aggregate was put under pre-rutting stress, there was greater rut resistance. However, this process is considered expensive, and so a stiff geogrid was offered as a viable substitute.

Imjai et al. (2019) conducted a series of full-scale field tests to determine the performance of geosynthetics as reinforcement for flexible pavements. The geosynthetic was embedded at different depths, but geosynthetics placed underneath the base layer had the greatest improvement and least amount of rutting. The results showed that vertical static and dynamic stresses were reduced more than 50% in some instances. It also effectively reduced lateral spreading of the aggregate, having the highest lateral strain at only 0.13%. In a static plate loading test conducted by El-Maaty (2016), a woven geotextile and a polyethylene geogrid were compared against a changing base layer thickness to determine a favorable outcome. The test also ran a 0.2 square inch area geogrid, but it should be thrown out of consideration because it was only used in one case. It was conducted with ¾-inch nominal aggregate, 0.75 foot thick silty soil subgrade and the geosynthetic was placed at the soil-aggregate interface. In the end, the higher area geogrid was the best because it could hold the aggregate in a tighter manner. It showed the greatest contribution when the base layer was the same depth as the subgrade layer. All three geosynthetics showed better resistance to deformation over the unreinforced section.

Appea (1997) used a geotextile, a geogrid, and a control section beneath a granular base to prevent the base and subgrade from mixing. Three different base course thicknesses were constructed (4, 6, and 8 inch), giving nine total test sections, each over a weak clay subgrade. The test lasted over 30 months, and in the end, both geosynthetics performed better than the control section, reducing rutting by nearly 40%. Rutting was the greatest in the 4-inch base course layer, while the other base layers relatively showed the same rutting. Hoppe et al. (2019), in conjunction with the Virginia Department of Transportation, conducted a

similar test with the same aggregate base thickness and geosynthetic layout. Using a Falling Weight Deflectometer (FWD), results showed the geotextile sections had lower average deflections, while the geogrid sections proved inconclusive. A belief is because of subtle subgrade differences.

Tingle and Jersey (2005) also performed a test in weak soil and indicated that the control section had the greatest amount of deformation while the use of a geotextile provided the lowest permanent deformation. Geogrids were in the middle of the pack in both tests. The study also concluded the increase in base layer strength was due to cementation during curing. Kermani et al. (2018) wanted to use geotextile as a separator to eliminate unwanted subgrade pumping into the base layer. The study reported an approximate 30% reduction in pavement rutting when geosynthetic was used at the base-subgrade interface, and pumping also decreased. Kazmee et al. (2015) conducted a test where they had untreated Reclaimed Asphalt Pavement (RAP) to act as a subbase layer. A mechanical tire drove in a unilateral direction across the strip. It was determined that the three different aggregate types showed virtually little difference from one another, all with poor rutting improvement. One conclusion drawn from this paper is that it is not effective to use untreated RAP as against virgin crush stone aggregate; a geosynthetic could withstand many more cycles before failure was declared.

Fannin and Sigurdsson (1996) conducted a field test with geotextile and geogrid on five reinforced and unreinforced sections of unpaved road. The reinforced sections showed significant improvement. The improvement was the greatest for the thinner layers of base course (1 inch). Leng and Gabr (2002) saw that higher modulus geogrid provided the best reduction in plastic surface deformation. Tensar (2017) ran an in-house test and proved that their triaxial geogrid could reduce surface rutting and permanent deformation by 60% and 35% after 800,000 passes. It showed that aperture size affects the performance for certain

aggregate nominal sizes. Sharbaf (2016) determined that rutting was best reduced when either the biaxial or triaxial geogrid was placed in the middle of base layer and not at the bottom of the base.

In the research, Wasage et al. (2004) fabricated a small lab wheel tracking test to measure the rutting resistance of geosynthetic-reinforced low-volume pavement by analyzing the surface rut depth and base deformation. They utilized asphalt, 12-inch thick base and subgrade layers, and six test specimens consisting of two non-woven geotextiles, two biaxial geogrids, and two control sections. The geotextile was placed between the base-subgrade interface layer while the geogrid was placed at the surface-base interface layer. The test concluded at either 10,000 wheel passes or the rut depth became greater than 2 inches. The surface profiles had rut depths which were recorded in accordance with ASTM E1703E 1703M – 95. It was seen that the control sections did not reach 10,000 passes, instead reaching 2 inches at about 8,000 passes. The geotextile had only ¾-inch rutting depth. However, the geogrid specimen showed the greatest rut resistance with less than ½-inch rutting depth. The most evident problem with this research, though, is the inconsistent placement of the geosynthetics. This kills the comparison. It is believed that if the geogrid were placed under the base layer, it would supply better support, separation, and dissipation from the load.

2.3.5 Chemical Stabilization vs. Geosynthetic Stabilization

Jones and Jones (1987) stated that damage to roadways from expansive soils cost the United States more than $4.5 billion annually. This is in part due to the swelling causing greater unwanted upward pressure on these structures (Tiwari et al., 2021). The mitigation of these soils is imperative in any construction project so the stability is not compromised. One of the best-known solutions to the problem is through chemical stabilization, and Qubain et al. (2000) states that lime is the oldest agent of this practice. The addition of lime to clay soil

allows for improvement to the soil plasticity, workability, and strength. The lime decreases the liquid limit of clay soils, lowering the plasticity index, and hardening the soil so it becomes “rock-like” and cannot expand any further (Pancar and Akpinar 2016). Overall, these properties to the soil can be maintained for over 20 years (Biczysko 1996 and Kelley 1977). Lab studies have found that the CBR of fine-grained soils increases with the introduction of lime treatment. Thompson (1969) saw CBR values in treated specimens rise more than three times in relation to their untreated counterparts. Wang et al. (2017) found that geo-polymer concrete and cement were the best stabilizers to eliminate the heave cycles of the expansive clays in Louisiana. Long-term effects of chemical stabilization often result in a greater stiffness of the soil, or a higher resilient modulus. However, lime-stabilized soils are prone to lose strength in an environment where cyclic freezing and thawing are common. When such is the case, some soils can lose an average strength of 14.5 psi per freeze-thaw cycle for typical mixture designs (Dempsey and Thompson 1970).

Geosynthetics make a good alternative to treated subgrade. For soft subgrade soils, Subgrade Enhancement Geosynthetic (SEG) can be used to replace lime stabilizing elements or other chemical materials (Caltrans 2013). A four-year study conducted by Zheng et al. (2019) monitored the vertical displacement of expansive clay subgrade soil cycling through heave and settlement with a geosynthetic-stabilized base. The study had a subbase that was chemically treated and ranged from 6 to 8 inches. In the end, the longitudinal cracks showed lower percentages with the addition of geogrid. The triangular geogrid with the larger aperture size continuously showed less cracking than the other geogrid due to better soil-geosynthetic interaction. It was also shown that the addition of geogrid had little impact on the vertical deformation of the road, meaning geogrid should only be used for lateral confinement. Again, it was proven by Roodi and Zornberg (2020) that geosynthetics perform better than the lime cement-treated subbase. Geosynthetics showed lower longitudinal

cracking and pushed the cracking to the shoulder of the road. The simple use of lime showed no greater improvement in longitudinal cracking. Interestingly, the use of lime and geosynthetics together actually saw a relative decrease in performance.

On the contrary, Pancar and Akpinar (2016) conducted a plate loading test for clayey soil where different lime percentages were added and compared against geosynthetics. The peak load simulated a single tire under an ESAL load, resulting in a 9,000 force-lbs (40 kN) applied load with 80 psi (550 kPa) tire pressure. Bases in the study were 9 inches thick. Results showed that lime and geosynthetics produced the greatest resistance to settlement, while geosynthetics alone outperformed lime alone. The test also showed that the modulus of subgrade reaction increased as lime content increased, with or without geosynthetic.

Tiwari et al. (2021) used a geotextile as a substitute for any conventional treatment methods. Unconfined compression-like tests and large direct shear box tests were used. The soil was prepped to an optimum, and the reinforcement was placed at various levels of the specimen. The test showed improvement in soil swelling prevention and an increase in friction angle. The geotextile not only controlled the upward swelling pressure and expansion rate, but it also reduced these properties. The shear strength of the geotextile increased with greater expansion from the clay and the unconfined compressive strength also improved. However, once the geotextile was placed too low, about 2/3 depth of the chamber, in the specimen, the improvement was not as significant.

2.3.6 Case Studies

Barksdale et al. (1989) conducted a large-scale moving wheel laboratory test. A 1,500 force-pound load was applied over an asphalt surface layer that was 1-1.5 inches thick with an aggregate base of 6-8 inches thick. A silty clay was used as subgrade having a CBR of 2.5%. It was decided that reinforcement on soft subgrades should be at the bottom of the base layer. Further, weak subgrades (CBR $\leq$ 3) benefit the most and could lead to a 20-40%

reduction in rutting as well as a 10-20% reduction in base thickness. Miuara et al. (1990) reaffirmed the fact that geogrid should be placed at the bottom of the base layer when using poor subgrades ($3 < CBR \leq 6$) to experience greater rutting resistance. Webster (1993) found that stiffer geogrids work best under the aggregate layer and atop weak subgrades, and they could reduce the total pavement thickness (surface and base layers) by up to 40%. Holtz et al. (1998) as well as Carmichael and Marienfeld (1999) both concluded that the addition of geosynthetics can increase the life of surface roadways by a few years and decrease its thickness need by nearly two inches.

Cuelho and Perkins (2009) performed a field investigation of 10 differing geosynthetics on top of a weak sandy clay soil used for subgrade stabilization in conjunction with the Montana Department of Transportation. Longitudinal rutting was also monitored. A dual-tandem truck was driven over the test strip until rutting failure occurred, pre-decided at 4 inches. For all cases, the subgrade underperformed before the expected cycles were reached, as only 88 out of 1,000 passes were conducted. It proved that stiffer geogrids provided the best performance and stabilization as opposed to geotextiles and the control section, presumably due to a higher tensile resistance. Additionally, Chen et al. (2019) determined through numerical pullout analysis that the higher stiffness of a geogrid led to greater active zones with sand particles, which increased resistance. Since geogrid reinforcement is mobilized by the interaction between geosynthetics and soil, it proves that geogrid stiffness plays a foremost role in reinforcement application. Abdi and Arjomand (2011) showed that geogrid resistance is greater in sand than in clay, even if the sand is only a thin layer.

Sun (2015) utilized a large geotechnical test box to find the effect of geogrid-stabilized base over weak subgrade. Cyclic loads were applied at different intervals to evaluate the correlation between the geogrid-subgrade interface. The study used a Dynamic

Cone Penetrometer (DCP) to find the CBR value of the subgrade. The equation used was introduced by Webster et al. in 1992. DCP measurements were taken at four different locations along the surface and then averaged for the base course and subgrade after every test. The test concluded that the vertical stresses were reduced with geogrid inclusion or with the increase of a thicker base course. Higher reductions in permanent deformations were also seen. However, the resilient deformations of the geogrid-reinforced sections were larger than the unreinforced sections. It is believed to be due to a bearing failure.

2.3.7 Design Apparatuses

Bagshaw et al. (2015) performed a laboratory wheel tracking test in a 5.5 ft × 5.5 ft × 1.0 f dimension box. Aggregate was set to the desired moisture and compacted to roughly 95%. A 4,500 force-pound (20 kN) tire load was applied and run in a unilateral direction at a constant speed of around 1 mph. A measurement was taken after every 500 passes. The study measured rutting and deformation of the surface layer. Tests showed that improvement was made with the addition of a geogrid at the base–sub-base interface, cutting the rut depth in half. The test compared large aperture triaxial geogrid and smaller aperture biaxial geogrid. The results showed that biaxial outperformed triaxial. It is presumed that the aggregate size was better suited for the biaxial geogrid with its appropriate aperture size.

Kim et al. (2018) performed a similar test. The study created a 6 ft × 6 ft × 2 ft box that ran in a unilateral direction under a 2,250 force-pound (10 kN) load. The speed was recorded at 1 mph. A foot of aggregate was placed atop a foot of subgrade. Then a geosynthetic was placed at the interface to determine rutting and subgrade strength. Pressure cells and strain gauges were used to measure the forces in the soil. Data was collected and analyzed after 5,400 passes. Results showed that the geosynthetic reinforcement reduced the vertical pressure transmitted to the subgrade layer by 30-40%, as compared to traditional

unreinforced pavement. As such, pressure reduction varied depending upon the depth at which the geosynthetic was placed and its soil type.

2.3.8 Function of Geosynthetics in Flexible Pavement

The objective of using geosynthetic reinforcement is to increase the structural and load-carrying capacity of the pavement system. Typical functions of geosynthetic reinforcement adapted in the flexible pavement can be divided primarily into three parts, as follows (Holtz et al. 1998): (1) lateral restraint; (2) increased bearing capacity; and (3) the tensioned membrane effect produced by the geosynthetic reinforcement. Figure 2.1 shows the typical functions of geosynthetic reinforcement.

1. Lateral restraint: Geosynthetics can provide lateral restraint to the pavement layers, preventing the lateral movement of the base and subgrade soils due to traffic loads or other external factors. This helps to maintain the pavement's structural integrity and prevent deformation or rutting.
2. Increased bearing capacity: By distributing the load over a larger area, geosynthetics can help increase the pavement system's bearing capacity. This can be especially useful in weak subgrade conditions where the pavement's load-carrying capacity would be limited.
3. Tensioned membrane effect: When geosynthetics are placed in tension, they can act as a "tensioned membrane" that helps to distribute stresses and strains across the pavement system. This can help to prevent cracking and other types of pavement distress by reducing the tensile stresses that would otherwise be concentrated on the pavement surface.

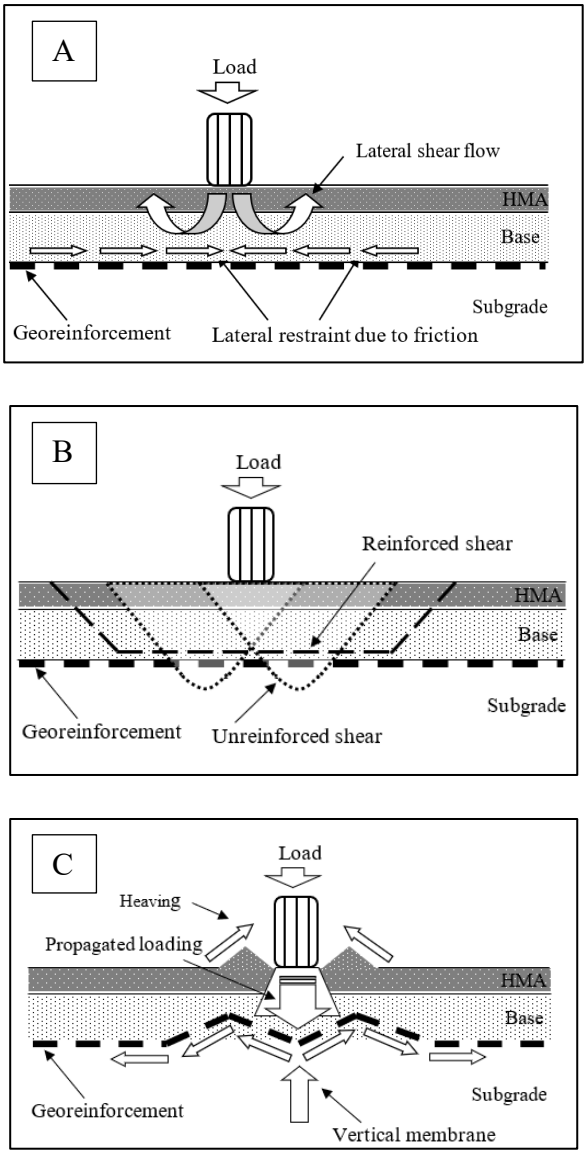

Figure 2.1 Reinforcement mechanisms induced by geosynthetics (Holtz et. al 1998): (a) Lateral restraint; (b) Increased bearing capacity; and (c) Membrane-type support (continued)

2.4 Established Parameters

2.4.1 Large Direct Shear

Like a simple direct shear test, the aim of this apparatus is to establish a friction angle (φ) between the shear force over the displacement of the soil as well as finding the cohesion. The benefit of a large-scale box is to see if the results are similar to those of the traditional small direct shear box. Another benefit is to see the interface shear properties when a

geosynthetic is used. As defined by Sakleshpur et al. (2019), the interfacial shear resistance coefficient is given as

$$\alpha = \frac{\tau_{reinforced}}{\tau_{unreinforced}} = \frac{\tau_{soil-geosynthetic}}{\tau_{soil-soil}} \quad (2.1)$$

where α is the interfacial shear resistance coefficient, and τ is the peak shear stress for both the geosynthetic-reinforced and unreinforced case. And also, shear stress equals resistance shear force over the plane area of the large direct shear box.

2.4.2 Large Pullout Box

The study wanted to find the interaction ratio (Ci), formally taken from the friction coefficient (*f**). Researchers such as Ingold (1983), Ochai et al. (1996), Wang and Richwien (2002), and Prashanth et al. (2016) have expressed the pullout results with the friction coefficient. Similar to the direct shear, it is a ratio of the force it takes to pull a geosynthetic against its displacement. As defined by Hegde et al. (2017), the interaction ratio is expressed with maximum pullout resistance per unit width (P_{max}), as

$$C_i = \frac{P_{max}}{2\ l\ \sigma_n\ tan\varphi} \quad (2.2)$$

where l is the length of the embedded geosynthetic, σ_n is the normal force exerted on the specimen, and φ is the friction angle taken from the direct shear apparatus. Additionally, stiffness modules can be found from the data. The research wants to investigate both the interfacial shear modulus and secant stiffness of the materials entrenched in the soil.

Based on the pullout testing results, the Interaction Modulus of the material was determined. The secant modulus was determined at the 2-centimeter mark and taken at a 2%

displacement of the geosynthetic. The Interaction Ratio (WI DOT 2005) is expressed with maximum pullout resistance per unit width (F_p or P_{max}), as

$$M_i = \frac{F_p / W\, L_g}{\Delta_f / L_g} \tag{2.3}$$

where Mi is the interaction modulus (an index of in-situ extensibility), F_p is the maximum pullout force, and W is the width of the geosynthetic. Δ_f is the front displacement of the geosynthetic. According to Figure 2.2, we also determined the initial pullout modulus and secant modulus. The secant modulus can be defined as the slope of plots at a 2% strain level between pullout stress and pullout strain obtained from the pullout test. The initial modulus can be defined as the initial slope of plots between pullout force and displacement, which are obtained from the pullout test.

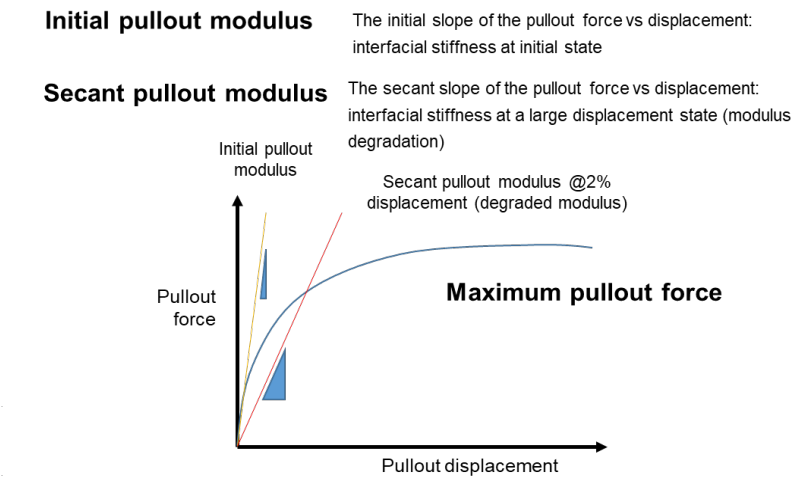

Figure 2.2 Determination of initial pullout modulus and secant pullout modulus

2.5 Specifications and Guidelines of Other States' Department of Transportation

In this section, we conducted extensive research and carefully summarized the specifications and guidelines pertaining to the use of geosynthetics in roadways from 15 different state Departments of Transportation (DOTs). The comprehensive analysis summarized to present representative documents from five states, which provide a detailed overview of the most relevant and critical information on the use of geosynthetics in roadways.

Additionally, we created Table 2.6 at the end of this section, which describes and summarizes the remaining information that we gathered from the other thirteen state DOTs. Table 2.6 provides a valuable resource for those interested in further exploring the nuances of geosynthetic applications in roadways across various states.

Furthermore, based on our thorough analysis of the gathered information, we have discussed the specific requirements for the state of Nebraska regarding using geosynthetics in roadways. Our findings are based on a careful examination of the other states' specifications and guidelines, as well as our in-depth understanding of the best practices and industry standards in this field.

Overall, the literature review provided a comprehensive and detailed analysis of geosynthetic applications in roadways, focusing on the state of Nebraska. The findings are based on a robust analysis of various state DOT guidelines and regulations. The summary and findings can serve as valuable resources for researchers, practitioners, and policymakers for the application of geosynthetics in Nebraska.

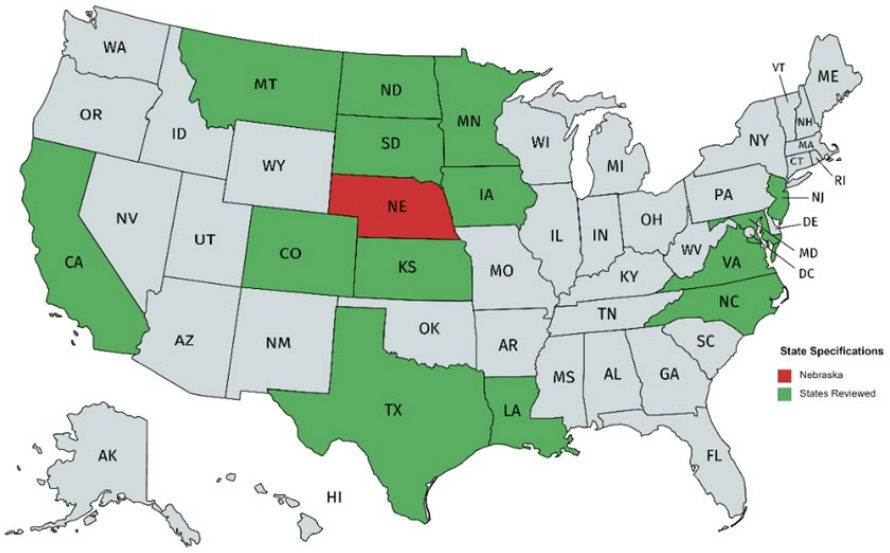

Figure 2.3 Total of fifteen states are surveyed for geosynthetic applications

2.5.1 California

Caltrans, or the California Department of Transportation, uses geosynthetics in a variety of applications throughout the state. Geosynthetics are synthetic materials used in civil engineering applications to provide reinforcement, separation, filtration, or drainage functions. Here are some additional specifics and construction methods for geosynthetics:

2.5.1.1 Geotextile Specifics:

- Geotextiles are permeable fabrics made from polyester or polypropylene fibers.
- They have a range of permeability values depending on the application, with a minimum permittivity of 0.05 sec^{-1}.
- They are available in woven, non-woven, and knitted forms.
- They can be used for filtration, separation, drainage, and erosion control.

2.5.1.2 Geogrid Specifics:

- Geogrids are high-strength, low-elongation polymer grids used for reinforcement.
- They are typically made from polypropylene or polyester.
- They are available in uniaxial and biaxial forms.

- Biaxial geogrids are made from punched and drawn polypropylene and are similar to the Tensar material used for testing.
- They can be used to reinforce soil slopes, retaining walls, and roadways.

2.5.1.3 Construction Methods:

- Geosynthetics should be placed longitudinally along the roadway with no wrinkles.
- They may be cut or folded to conform to curves.
- Overlap of adjacent materials must be at least 24 inches to ensure proper functioning.
- Material may be held in place with ties, staples, pins, or aggregate subbase.
- Installation should be carried out in accordance with manufacturer's recommendations and industry best practices to ensure effective performance.

2.5.1.4 Construction Practices

- Do not operate machinery directly upon the geogrid.
- Damaged areas of geogrid should be patched, covering over 36 inches.

Table 2.1 Characteristics of filter fabric, California DOT

Filter Fabric

Quality characteristic	Test method	Requirement		
		Class A	Class B	Class C
Permittivity, (min, sec^{-1})	ASTM D4491	0.5	0.2	0.1
Apparent opening size, average roll value, (max, US standard sieve size)	ASTM D4751	40	60	70
Grab breaking load, 1-inch grip, in each direction, (min, lb)	ASTM D4632	157		
Apparent elongation, in each direction, (min, percent)	ASTM D4632	50		
Puncture strength, (min, lb)	ASTM D6241	310		
Trapezoid tearing strength, (min, lb)	ASTM D4533	56		
UV resistance, retained grab breaking load, 500 hours, (min, percent)	ASTM D4355	70		

Table 2.2 Subgrade enhancement geotextile, California DOT

Subgrade Enhancement Geotextile

Quality characteristic	Test method	Requirement[a]				
		Class A1	Class A2	Class B1	Class B2	Class B3
Elongation at break, (percent)	ASTM D4632	<50	≥50	<50	<50	≥50
Grab breaking load, 1-inch grip in each direction, (min, lb)	ASTM D4632	250	160	--	320	200
Wide width tensile strength at 5 percent strain, (min, lb/ft)	ASTM D4595	--	--	2,000	--	--
Wide width tensile strength at ultimate strength, (min, lb/ft)	ASTM D4595	--	--	4,800	--	--
Tear strength, (min, lb)	ASTM D4533	90	60	--	120	80
Puncture strength, (min, lb)	ASTM D6241	500	310	620	620	430
Permittivity, (min, sec^{-1})	ASTM D4491	0.05	0.05	0.20	0.20	0.20
Apparent opening size, (max, inches)	ASTM D4751	0.012	0.012	0.024	0.012	0.012
UV resistance, retained grab breaking load, 500 hours, (min, percent)	ASTM D4355	70	70	70	70	70

[a]Values are based on minimum average roll value in the weaker principal direction except apparent opening size is based on maximum average roll value.

Table 2.3 Biaxial geogrid, California DOT

Biaxial Geogrid

Quality characteristic	Test method	Requirement
Aperture size, (min and max, inch)[a]	Calipered	0.8-1.3 x 1.0-1.6
Rib thickness, (min, inch)	Calipered	0.04
Junction thickness, (min, inch)	Calipered	0.150
Tensile strength, 2% strain, (min, lb/ft)[a]	ASTM D6637	410 x 620
Tensile strength at ultimate, (min, lb/ft)[a]	ASTM D6637	1,310 x 1,970
UV resistance, retained tensile strength, 500 hours, (min, percent)	ASTM D4355	100
Junction strength, (min, lb/ft)[a]	ASTM D7737	1,220 x 1,830
Overall flexural rigidity, (min, mg-cm)	ASTM D7748	750,000
Torsional rigidity at 20 cm-kg, (min, mm-kg/deg)[b]	GRI GG9	0.65

[a]Machine direction x cross direction
[b]Geosynthetic Research Institute, Test Method GG9, Torsional Behavior of Bidirectional Geogrids When Subjected to In-Plane Rotation

2.5.2 Kansas

The Kansas Department of Transportation (KDOT) uses geosynthetics in a variety of applications to enhance the performance of transportation infrastructure. Geosynthetics are man-made materials used in construction and civil engineering projects for their ability to

provide reinforcement, separation, filtration, drainage, and containment. Here are some specifics regarding geosynthetics made of at least 85% by weight polyesters or polyolefins:

- Polyester: This type of geosynthetic is strong and resistant to chemicals, UV radiation, and biological degradation. It is commonly used in applications such as geotextiles, geogrids, and geomembranes.
- Polypropylene: This type of geosynthetic is lightweight, flexible, and resistant to chemicals and UV radiation. It is commonly used in applications such as geotextiles, geogrids, and erosion control mats.
- Kevlar: This type of geosynthetic is extremely strong and resistant to impact and abrasion. It is commonly used in applications such as reinforcement for embankments and retaining walls.

2.5.2.1 Construction Methods:

When it comes to construction methods, there are a few things to keep in mind:

- Overlap: Adjacent strips of geosynthetic should overlap by 12 to 36 inches, depending on the specific application and the strength of the material. This overlap helps ensure that the geosynthetic functions correctly and can withstand its stresses.
- Seams: Seams should be constructed using polyester, polypropylene, or Kevlar thread with durability more excellent than the geosynthetic material being used. Butterfly seams or securing pins at least 18 inches long should ensure a strong and secure connection between the geosynthetics (
- Installation: Geosynthetics should be installed by trained professionals who understand the specific requirements of the project and the materials being used. Proper installation is crucial to the long-term performance and effectiveness of geosynthetics.

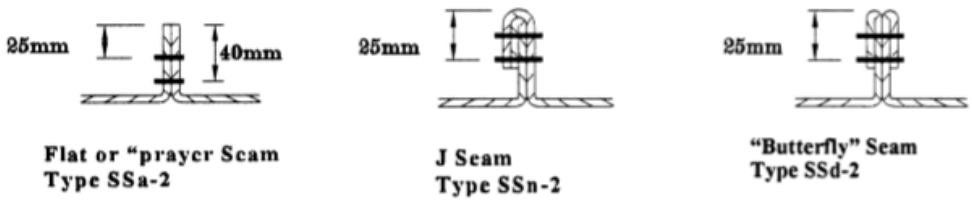

Figure 2.4 Method to seam two geosynthetics

2.5.2.2 Construction Practices

When working with geosynthetics:

- Avoid placing construction equipment or machinery directly on top of them.
- Store them in a way that protects them from sunlight and UV rays, and keeps them away from mud, dirt, and debris.
- Follow ASTM D4873 guidelines for proper wrapping during storage.

Table 2.4 Subgrade stabilization geosynthetic minimum average roll values, California DOT

TABLE 1710-2: SUBGRADE STABILIZATION GEOSYNTHETIC MIMIMUM AVERGE ROLL VALUES			
Property	**Test Method**	**Requirements**	
Tensile Strength (at 5% strain)	ASTM D4595	810 lb/ft MD	1340 lb/ft CD
Tensile Strength (at 2% strain)	ASTM D4595	410 lb/ft MD	620 lb/ft CD
Coefficient of Soil Interaction	GRI-GT6/GG5	0.8	
Junction Strength (geogrid)	GRI:GG2	25 lbs	
Permittivity (geotextile)	ASTM D4491	0.40 sec^{-1}	
Apparent Opening Size[a] (geotextile)	ASTM D4751	30 U.S. Sieve (0.0232 inches)	

[a]ASTM D 4751: AOS is a Maximum Opening Diameter Value

2.5.3 Montana

The Montana Department of Transportation (MDT) uses geosynthetics in various applications to enhance the performance and longevity of transportation infrastructure. Some of the geosynthetic applications used by MDT include geosynthetic requirements, installation, and guidelines.

2.5.3.1 Geosynthetic Requirements

The fibers used in geotextiles must be polymers, with a composition of at least 95% by weight of either polyesters or polyolefins. Polypropylene or polyester thread should be used for sewing.

2.5.3.2 Geosynthetic Installation

Adjacent rolls should be overlapped by a minimum of 36 inches, and sewing seams is also a viable option for construction.

2.5.3.3 Geosynthetic Guidelines

Avoid operating construction equipment directly on geosynthetic materials.

Table 2.5 Geotextile strength property requirements, Montana DOT

GEOTEXTILE STRENGTH PROPERTY REQUIREMENTS

			Geotextile Survivability[1]			
			Moderate Survivability		High Survivability	
Property	Test Methods	Units	Woven	Nonwoven	Woven	Nonwoven
Grab elongation	ASTM D4632	%	< 50	≥ 50	< 50	≥ 50
Grab strength	ASTM D4632	lbs.	250	160	315	200
Sewn seam strength[2]	ASTM D4632	lbs.	225	145	285	180
Tear strength	ASTM D4533	lbs.	90	55	110	80
Puncture strength	ASTM D6241	lbs.	495	310	619	433
Apparent opening size	ASTM D4751	sieve size	Required property values for AOS, permittivity, and UV stability are based on the geotextile applications. Refer to Table 716-2 for separation geotextile, Table 716-3 for stabilization geotextile, Table 716-4 for subsurface drainage geotextile filter, and Table 716-5 for erosion control geotextile.			
Permittivity	ASTM D4491	$sec.^{-1}$				
Ultraviolet stability (retained strength)	ASTM D4355	%				

Notes:
1. All numeric values represent MARV in the weaker principal direction.
2. When sewn seams are required. Refer to Subsection 622.03 for overlap requirements.

2.5.4 Louisiana

The Louisiana Department of Transportation and Development (LaDOTD) has implemented geosynthetics in various applications throughout the state. Geosynthetics are

man-made materials that are used to improve soil stability, reinforce foundations, and prevent soil erosion. Here are some examples of geosynthetic applications by Louisiana DOT:

2.5.4.1 Geosynthetic Specifications:

The geotextile fabric must consist of a minimum of 85% polyester, polyolefin, or polyamide by weight. The durability of the fibers should be comparable to that of the geotextile fabric.

2.5.4.2 Geosynthetic Construction Guidelines:

To ensure proper construction, the following guidelines should be followed:

- The overlap of adjacent rolls should be at least 18 inches.
- Sew rolls together using polyester or Kevlar thread with a J-seam or butterfly seam.
- Place the fabric on the ground without any wrinkles or folds.
- Folds are permitted on curved road sections.
- The fold should be in the direction of construction and secured with pins or staples.
- To fix a damaged geotextile, use a fabric extruder that extends 24 inches in all directions of the affected region.

2.5.4.3 Geosynthetic Storage

The material used must possess resistance to chemicals, rot, and mildew, and must be free of tears. Additionally, rolls should come with waterproof wrapping to protect against ultraviolet rays. It is essential for the geosynthetic material to possess the necessary characteristics that enable it to withstand exposure to various environmental conditions, such as temperature fluctuations, moisture, and chemical exposure. In particular, it is crucial to ensure the material is resistant to chemicals, rot, and mildew, as these factors can significantly impact the effectiveness and durability of the material. In addition to chemical and biological resistance, the geosynthetic material must also be free of tears, punctures, or other damage that could compromise its integrity. Even small tears or defects can lead to

significant problems, such as water infiltration or soil erosion, which can ultimately undermine the stability of the structure. To protect against environmental factors such as ultraviolet (UV) rays, it is recommended that rolls of geosynthetic material come with waterproof wrapping. This provides an additional layer of protection during transportation and storage, helping to prevent damage from exposure to UV rays or moisture.

Overall, selecting the right geosynthetic material is critical for ensuring the success and longevity of a project. Careful consideration of factors such as chemical resistance, tear resistance, and UV protection can help to ensure that the material is up to the task and will provide reliable performance over the long term.

2.5.5 Maryland

The Maryland Department of Transportation (MDOT) has published several specifications and guidelines related to geosynthetics. Here are some key ones:

2.5.5.1 Specifics for Geosynthetics

- The composition of the fibers in the geotextiles should be made up of polymers consisting of 95% by weight of either polyesters or polyolefins.
- Nonwoven needle-punched geotextile: This specification, MD 604.01, provides requirements for nonwoven geotextiles made from synthetic fibers and used in various geotechnical applications, such as filtration, separation, and soil stabilization.
- Woven geotextile: MD 604.02 is the specification for woven geotextiles made from synthetic yarns or fibers. These geotextiles are used for separation, filtration, and reinforcement applications.
- Geogrid: MD 604.03 provides requirements for geogrids made from synthetic materials, such as high-density polyethylene (HDPE) or polyester. These products are used for soil reinforcement applications, such as retaining walls, embankments, and slopes.

- Geocomposite: MD 604.04 is the specification for geocomposites, composed of two or more geosynthetic materials, such as geotextiles and geogrids, combined to form a single product. These products are used in various applications, such as drainage, filtration, and erosion control.

2.5.5.2 Methods for Geosynthetic Construction

- As the geotextile is being unrolled, ensure that there are no wrinkles or folds by stretching it and pinning it down. When folding the material, do so along the curves in the direction of traffic. Ensure that there is an overlap of at least 30 inches between materials. For subsequent rolls, place the old roll-on top of the new one*, overlapping them in the direction of traffic. Secure the edges by pinning them down and finish by sewing them up using a J-seam or butterfly seam. This is the only specification that makes this point.
- To fix impaired regions, overlay another 36-inch layer of geosynthetic material.

These specifications and guidelines are intended to ensure that geosynthetics are properly selected, installed, and maintained in transportation infrastructure projects in Maryland.

2.5.6 Summary of findings from the review of other DOT specifications

Table 2.6 Geosynthetic specifications of other states

State	Specifications
California	Place the geogrid material longitudinally along the roadway without wrinkles
	Material may be cut or folded along curves to conform to curve
	Overlap should be at least 24 inches
	Material may be held in place with ties, staples, pins, or aggregate subbase
	Do not operate machinery directly upon the
	Damaged areas of geogrid should be patched, covering over 36 inches
	Geogrid must have a regular and defined open area, where the open area consists of 50% - 90% of the total area
	ASTM D4491 - geotextile permittivity must be at least 0.05 sec^{-1}
	Biaxial geogrid must be a punched and drawn polypropylene
Colorado	Geosynthetic rolls shall be covered with a suitable wrapping and stored to protect against moisture and natural elements
	Rolls shall be elevated off the ground and stored in a waterproof cover
	Overlap shall be at least 12 inches for 3:1 slope and 24 inches for any greater slope
	Unroll geotextile smoothly, with no folds, and in the direction of traffic
	Geotextile may be folded to conform to curves
Iowa	The fabric must be maintained in a suitable environment
	It must be stored to prevent against sunlight, dirt, debris, mildew, or other elements

Table 2.7 Geosynthetic specifications of other states. (continued)

State	Specifications
Kansas	Do not expose geosynthetic to sunlight or ultraviolet rays
	Store the geosynthetic so it avoids mud, dirt, and debris
	Store in accordance with ASTM D4873 by use of proper wrapping
	Overlap the adjacent strips by 12 to 36 inches
	Do not allow construction or machinery directly upon the geosynthetic
	Compose all geosynthetics of at least 85% by weight polyesters or polyolefins
	Use butterfly seams
	Use polyester, polypropylene, or Kevlar thread with a durability greater or equal to the material
	Securing pins must be 18 inches long
	Subgrade stabilization utilizes Table 1710-2 for subgrade CBR values greater than 1
Louisiana	Geotextile fabric shall be composed of at least 85% by weight of polyesters, polyolefins, or polyamides
	The material shall be resistant to chemical, rot, mildew, and have no tears
	Durability of the fibers shall be similar to that of the geotextile fabric
	Rolls shall be furnished with waterproofing wrapping for protection against ultraviolet rays
	Overlap of adjacent rolls shall be at least 18 inches
	Sew rolls with polyester or Kevlar thread using a J-seam or butterfly seam
	Place the fabric onto the ground with no wrinkles or folds
	Folds are allowed along curved road sections
	The fold shall be in the direction of construction and it shall be pinned or stapled
	Repair damaged geotextile with a fabric extruding 24 inches in all directions of damaged area

Table 2.8 Geosynthetic specifications of other states. (continued)

State	Specifications
Maryland	Remove wrinkles and folds of geotextile as one is unrolling it by stretching it and pinning it
	Overlap the material at least 30 inches
	Overlap the roll in the direction of traffic with the old roll on top of the next roll
	Pin edges
	Fold material along the curves in the direction of traffic
	Repair damaged areas by covering over another 36 inches
	Geotextiles shall have fibers consisting of polymers, composed of 95% by weight of polyesters or polyolefins
	Seam it up with a J-seam or a butterfly seam
Minnesota	Provide adequate geotextiles
	Need yarns made of polyester, polypropylene, or polyamide
	Needs to be free of debris or flaws
	Rolls should be covered so as to avoid ultraviolet rays from sun, dirt, or debris
Montana	Geotextile fibers should be polymers, composed of at least 95% by weight of polyesters or polyolefins
	Use thread of polypropylene or polyester for sewing
	Overlap adjacent rolls a minimum of 36 inches
	Sewing seams is also an option
	Do not directly operate construction equipment upon geosynthetics
New Jersey	Geotextile wrapping should be protection against moisture and against ultraviolet radiation
	Fibers should be polyester
North Carolina	Place geotextile on relatively undisturbed ground
	Do not operate machinery upon the geosynthetic
	Overlap the geotextiles at least 18 inches unless sewn together
	It should be laid with no wrinkles or folds
	The use of staples or pins is an alternative option
	Utilize AASHTO M288 for geotextile shipping

Table 2.9 Geosynthetic specifications of other states. (continued)

State	Specifications
North Dakota	Rolls should avoid damage and be elevated off the ground
	Fabric should have polymeric yarn (such as polyester, polypropylene, or polyamide)
	Overlap or sew joints using Kevlar, polyester, or polypropylene thread
	Use J-seam
	Overlap geogrid a minimum of 30 inches at all joints
	Along curves, geogrid may be cut to conform to the curve
	Damaged areas should be patched with an additional 36 inches
South Dakota	See Table 2.7
Virginia	Meet AASHTO M288 requirements
	Rolls shall be stored off the ground and protected against ultraviolet radiation
	Geosynthetics rolls shall be elevated off the ground and stored in a waterproof cover to protect against ultraviolet radiation. The ground should be relatively undisturbed. Rolls shall be covered with a suitable wrapping and stored to protect against moisture and natural elements, such as dirt, mud, or debris.
	Place the geogrid longitudinally in the direction of traffic along the ground without any wrinkles or folds. The geogrid may be cut to conform to curves along the roadway, if need be. Damaged geogrid should not be used, or, if salvageable, the damaged area must be covered an additional 24-36 inches in all directions. Do not operate any construction equipment atop the bare geogrid.
	Geogrid shall either overlap or be sewn to an adjacent roll. Overlap shall cover at least 24-36 inches. Make sure the previous roll lies atop the new one. Seams are to be either J-seams or butterfly seams. Threads should use polyester, polypropylene, or Kevlar with a durability greater or equal to the material.
	Compose all geosynthetics of at least 85% by weight polyesters, polyolefins, or polyamides. Geotextiles shall have fibers consisting of polymers, composed of 95% by weight polyesters or polyolefins.

Table 2.10 Geosynthetic specification of South Dakota

Filter Fabric

Quality characteristic	Test method	Requirement		
		Class A	Class B	Class C
Permittivity, (min, sec^{-1})	ASTM D4491	0.5	0.2	0.1
Apparent opening size, average roll value, (max, US standard sieve size)	ASTM D4751	40	60	70
Grab breaking load, 1-inch grip, in each direction, (min, lb)	ASTM D4632	157		
Apparent elongation, in each direction, (min, percent)	ASTM D4632	50		
Puncture strength, (min, lb)	ASTM D6241	310		
Trapezoid tearing strength, (min, lb)	ASTM D4533	56		
UV resistance, retained grab breaking load, 500 hours, (min, percent)	ASTM D4355	70		

Paving Fabric

Quality characteristic	Test method	Requirement
Mass per unit area, (min, oz/sq yd)	ASTM D5261	4.1
Grab breaking load, 1-inch grip in each direction, (min, lb)	ASTM D4632	100
Apparent elongation in each direction, (min, percent)	ASTM D4632	50
Hydraulic bursting strength, (min, psi)	ASTM D3786	200
Melting point, (min, °F)	ASTM D276	325
Asphalt retention, (min, gal/sq yd)	ASTM D6140	0.2

2.5.6.1 Consensus Details from the Specifications of Other DOTs

All geosynthetics must comprise a minimum of 85% weight of polyesters, polyolefins, or polyamides. Geotextiles must have fibers that comprise 95% weight of polyesters or polyolefins polymers. This requirement is due to the excellent strength, durability, and chemical resistance properties of these materials, making them suitable for various geotechnical applications. Polyesters, polyolefins, and polyamides are known for their high tensile strength, low elongation, and resistance to UV degradation, making them ideal for use in soil stabilization, erosion control, and drainage systems.

Furthermore, geotextiles, a type of geosynthetic, must have fibers that comprise at least 95% of the weight of polyesters or polyolefins polymers. These materials make it possible for geotextiles to be used for filtration, separation, and drainage purposes since they need high porosity.

It is essential to note that using other materials in geosynthetics, such as PVC or nylon, is not recommended, as they may not provide the required level of performance and durability. Therefore, to ensure the highest quality and performance of geosynthetics, it is necessary to adhere to the minimum weight requirements of polyesters, polyolefins, or polyamides.

2.5.6.2 Geosynthetic Practices and Construction Methods

- Place the geogrid longitudinally in the direction of traffic along the ground without any wrinkles or folds. The geogrid may be cut to conform to curves along the roadway, if need be. Damaged geogrid should not be used, or, if salvageable, the damaged area must be covered an additional 24-36 inches in all directions. Do not operate any construction equipment atop the bare geogrid.
- Geogrid shall either overlap or be sewn to an adjacent roll. Overlap shall cover at least 24-36 inches. Make sure the previous roll lies atop the new one. Seams are to be either J-seams or butterfly seams. The product should use polyester, polypropylene, or Kevlar with a durability greater or equal to the material.
- After the geogrid has been appropriately placed and overlapped, secure it with stakes or pins to prevent any movement during the construction process. The stakes or pins should be at least 12 inches long and driven into the ground at a depth of at least 6 inches. They should be placed approximately 3 feet apart along the edges of the geogrid and at a maximum spacing of 6 feet along the centerline.
- When placing the geogrid on slopes, the overlap should be increased to 36-48 inches to ensure stability. In addition, the geogrid should be anchored with additional stakes or pins to prevent any slippage.
- It is essential to note that the geogrid should not be exposed to UV radiation for an extended period of time. If construction activities will not occur immediately after

installation, the geogrid should be covered with a UV-resistant material to prevent degradation.

- Once the geogrid has been properly installed, construction activities may begin. However, it is important to note that heavy construction equipment should not be operated directly on top of the geogrid. Instead, a layer of aggregate should be placed on top of the geogrid before equipment operation.
- Proper installation and maintenance of the geogrid will ensure that it performs as intended and provides the necessary support for the roadway or other construction project.

2.5.6.3 Geosynthetic Storage

- Geosynthetics rolls shall be elevated off the ground and stored in a waterproof cover to protect against ultraviolet radiation. The ground should be relatively undisturbed. Rolls shall be covered with a suitable wrapping and stored to protect against moisture and natural elements, such as dirt, mud, or debris.
- Meet AASHTO M288 requirements (geotextiles).
- In addition to the above-mentioned precautions, geosynthetic rolls should be stored in a dry and well-ventilated area, away from direct sunlight or any heat source. It is recommended to store geosynthetics at temperatures between 10°C and 30°C to prevent damage to the material.
- When storing geosynthetics, it is important to avoid stacking the rolls too high, as this may lead to deformation and damage to the rolls. The recommended maximum stacking height is two rolls high. The rolls should also be stored in a way that allows for easy access and handling during installation.
- It is essential to follow the American Association of State Highway and Transportation Officials (AASHTO) M288 standard for geotextiles. This standard

specifies the requirements for geotextiles used in transportation applications such as drainage, separation, and erosion control. The standard covers the physical, mechanical, and hydraulic properties of geotextiles, as well as the durability and performance characteristics required for their use in transportation applications.

- To ensure compliance with AASHTO M288, geotextiles should be tested according to the standard's requirements before installation. The tests should include properties such as thickness, mass per unit area, tensile strength, elongation, puncture resistance, and water permeability.
- In summary, proper storage and handling of geosynthetics are critical to ensuring their performance and longevity in transportation applications. Following the guidelines mentioned above, including compliance with the AASHTO M288 standard, can help ensure that geosynthetics are installed and maintained correctly, providing reliable and long-lasting solutions for transportation infrastructure.

Table 2.11 Geotextile characteristics of state specifications

Geosynthetic Parameters		
Index Properties	Range	Mode
Permittivity (Min, sec-1)	0.05 - 1.0	0.05, 0.5
Opening Size (Max, in.)	0.0083 - 0.0331	0.012
Elongation (Min, %)	40 - >50	50
Tensile Strength @ Ultimate Strain (Min, lbs./ft.)	685 - 4800	
Tensile Strength @ 5% Strain (Min, lbs./ft.)	2000	
Structural Integrity		
Grab Tensile Strength (Min, lbs.)	75 - 315	180, 200
Grab Tensile Strength Retained after Weathering (Min, %)	70	70
Puncture Strength (Min, lbs.)	25 - 75, 180 - 620	
Tearing Strength (Min, lbs.)	25 - 120	50

Table 2.12 Geogrid characteristics of state specifications

Geosynthetic Parameters	State Specifications			Tensar BiAxial	
Index Properties	Range	MD	XMD	MD	XMD
Aperature Size (Min, Max, in.)	0.8-1.6, 0.5-2.0	0.8-1.3, 0.5-2.0	1.0-1.6, 0.5-2.0	1.0	1.3
Rib Thickness (Min, in.)	0.04			0.05	0.05
Junction Thickness (Min, in.)	0.15				
Tensile Strength @ 2% Strain (Min, lbs./ft.)	400 - 620	410, 410	620, 620	34.2	620
Tensile Strength @ 5% Strain (Min, lbs./ft.)	800 - 1340	810	1340	67.5	1340
Tensile Strength @ Ultimate (Min, lbs./ft.)	1300 - 1310	1310	1300	109.2	1970
Structural Integrity					
Junction Strength (Min, lbs./ft.)	25 - 1220	800, 1220	800, 1830		
Flexural Rigidity (Min, mg-cm)	750,000			750,000	
Durability					
UV Resistance (Min, %)	70			100	

2.5.7 Notes regarding Nebraska

Currently, the Nebraska Standard Specifications for Highway Construction (2017) do not call for geosynthetics in their road design and there are no clear guidelines for overall application. Hence, once decided upon with NDOT at the start of the project, the main area of focus became geogrids and geotextiles due to their heavy use in roadway application from other states.

- Nebraska has selected geosynthetic material specifications. However, there are no precise specifications or direct guideline parameters for using geosynthetics beneath pavements.
- Different soil types require appropriate geosynthetic.
- From our tests, we can provide these performance design parameters.

Regarding geosynthetic applications, it is important to note that there are no clear specifications or direct guideline parameters for their overall use in Nebraska. The type of geosynthetic required will vary depending on the soil type and intended application.

Different soil types require different geosynthetics to achieve optimal performance. For example, clay soils require geosynthetics that are designed to withstand high loads and resist puncture and tear, while sandy soils require geosynthetics with a high-water flow rate

to prevent soil erosion. It is also important to consider the overall design parameters when selecting geosynthetics for use in Nebraska. These design parameters can include factors such as the anticipated loads, soil conditions, and environmental factors such as temperature and moisture. To determine the appropriate geosynthetic for a specific application, it is recommended to conduct tests to identify the necessary design parameters. These tests can help ensure that the geosynthetic is able to provide the required level of performance and durability over time.

Overall, using geosynthetics in Nebraska can provide many benefits, including improved soil stability, erosion control, and reduced maintenance costs over time. However, it is crucial to consider the specific soil type carefully and its intended application to select the appropriate geosynthetic and achieve optimal performance.

Chapter 3 Materials

3.1 Soil Types

The soil samples were outlined and chosen with NDOT before the start of the project. They provided representative soil types for Nebraska. More specifically, the soils were known as glacial till, clay, red shale, and sand. Though windblown Peoria loess is found along the eastern and central region of the state, it was not considered as it would not be used for a subgrade soil (Muhs 2013). Figure 3.1 shows the soil types used for this study.

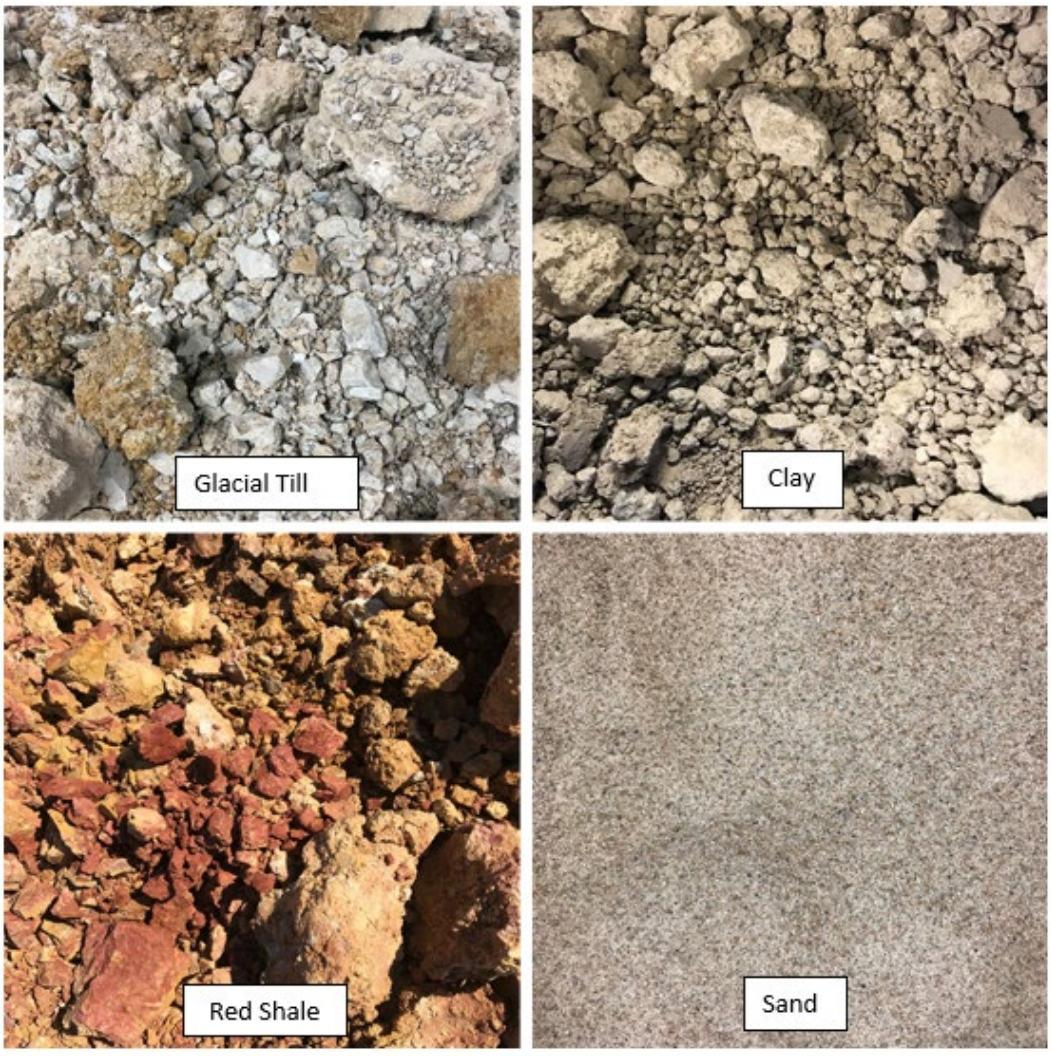

Figure 3.1 Four types of soil chosen with NDOT

The glacial till, clay, and red shale were all collected from a construction site in Lincoln, Nebraska. Lincoln approved construction for its South Beltway project which began in 2020 to the tune of $352 million. The infrastructure is a new highway that will bypass the city along its southern edge, where it breaks off Highway 77 and extends east until it links back up with Highway 2. Hence, for nearly 8 miles, the earthwork has been performed, including excavation, backfill, grading, and compaction. Figure 3.2 shows where soils were amassed at various parts of the new roadway. The rough outline of the Beltway roads can also be seen in the Figure 3.2, even though it is still early in the project.

The sand was taken from a location south of Omaha in Louisville, Nebraska. It is a small town, home to over 1,000 people and one cement processing plant just south of the Platte River and Highway 50. The plant was gracious enough to donate the sand for the present research where it was collected from a stockpile as shown in Figure 3.3. In total, approximately 150 gallons of soil were collected for the clay, red shale, and sand each. Figure 3.4 shows the research team's soil collection work.

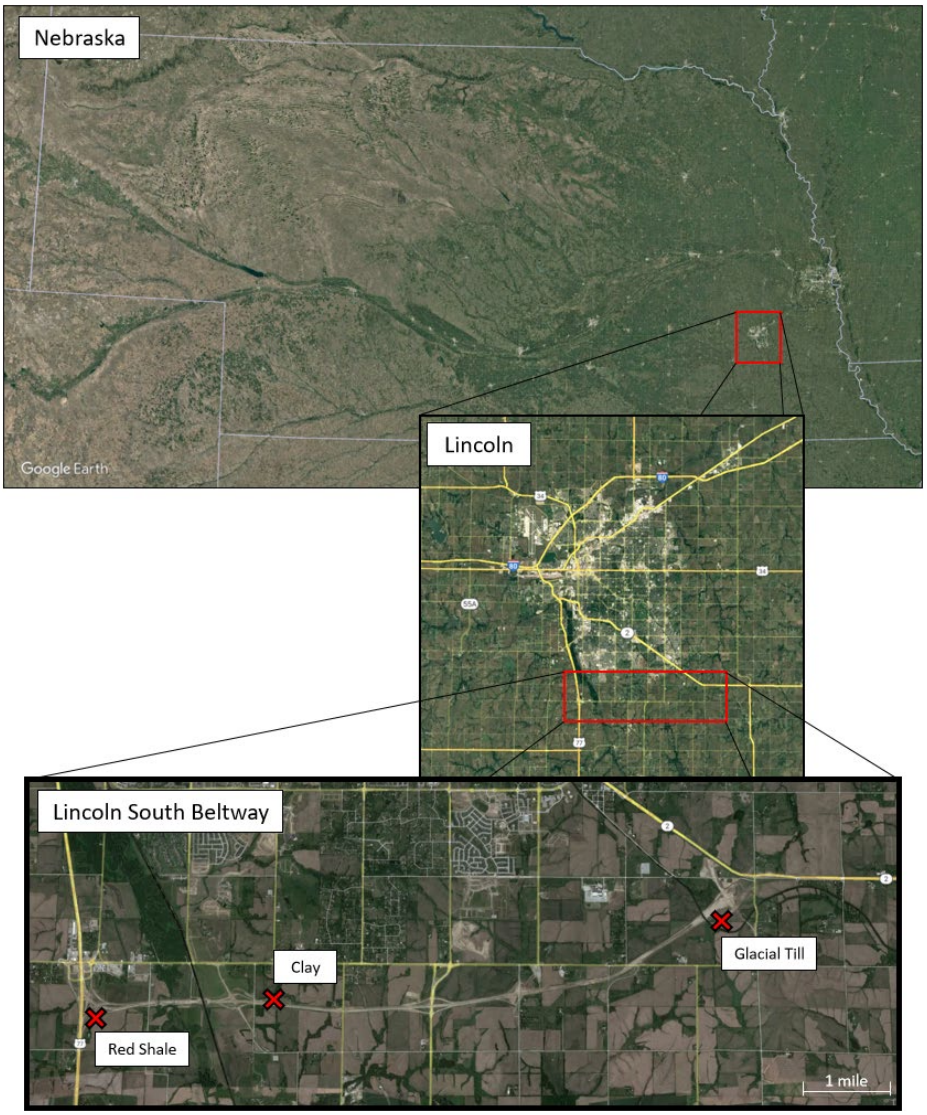

Figure 3.2 Location of soil collection areas

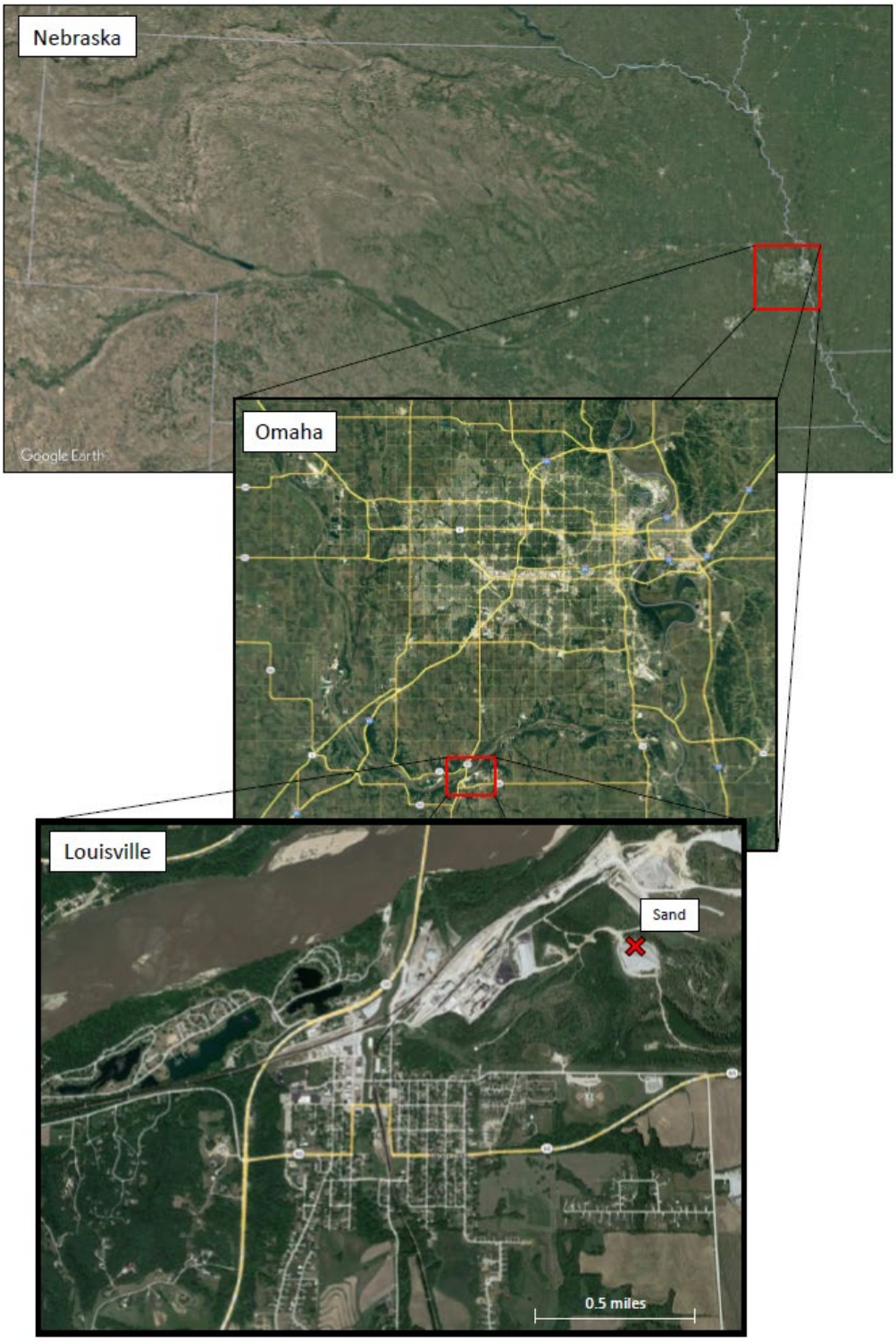

Figure 3.3 Location of sand collection area

Figure 3.4 Collection of soil for testing

3.2 Soil Characteristics

Small samples were pulled for testing purposes to determine their properties. Many preliminary tests were conducted to find the soil characteristics and were performed following ASTM guidelines – the results of which can be seen in Table 3.1. This is an important process because it allows for an ability to assess how the soil will relate as it is used for subgrade. Better gradation of the material leads to better particle packing and, moreover, a stronger reaction from the foundation.

Figure 3.5 shows the grain size distribution of the collected sand. The soil is referred to as poorly graded sand. The other three soils showed few particles that were retained on the #200 sieve, effectively concluding they were clays and silts. Figure 3.6 shows the results from the hydrometer tests. All soils were classified using the Unified Soil Classification System (USCS) and ASTM D2487.

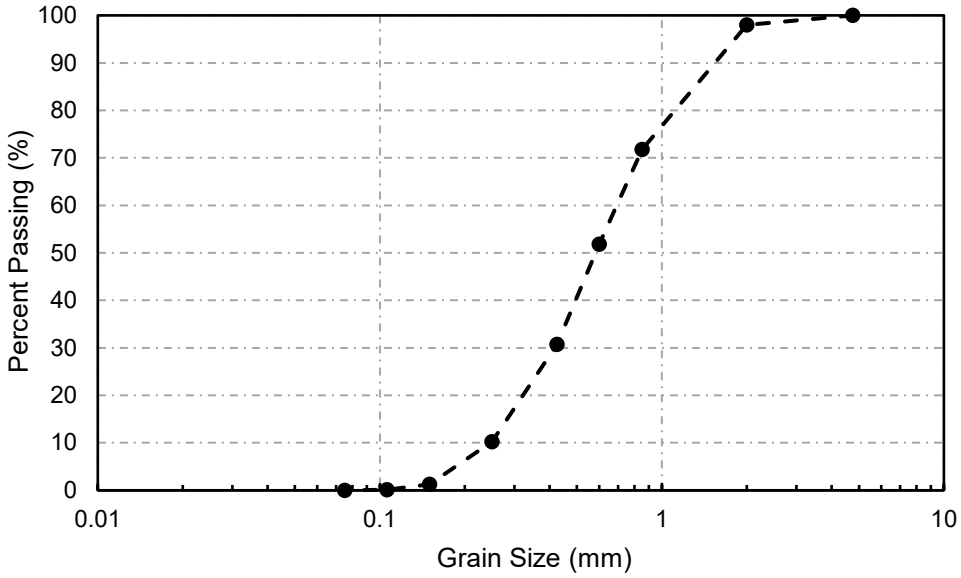

Figure 3.5 Grain size distribution graph for sand

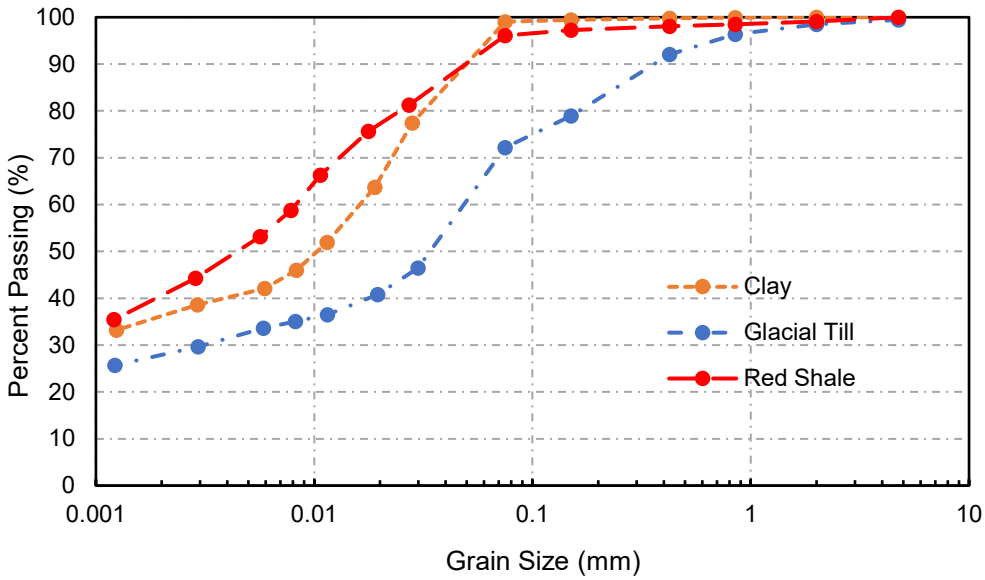

Figure 3.6 Gradations for glacial till, clay, and red shale

The graphs show the soils were sufficient for the study. All soils were mixed to their optimum moisture contents and appropriate compaction levels. Figure 3.7 shows the compaction curves for the soils.

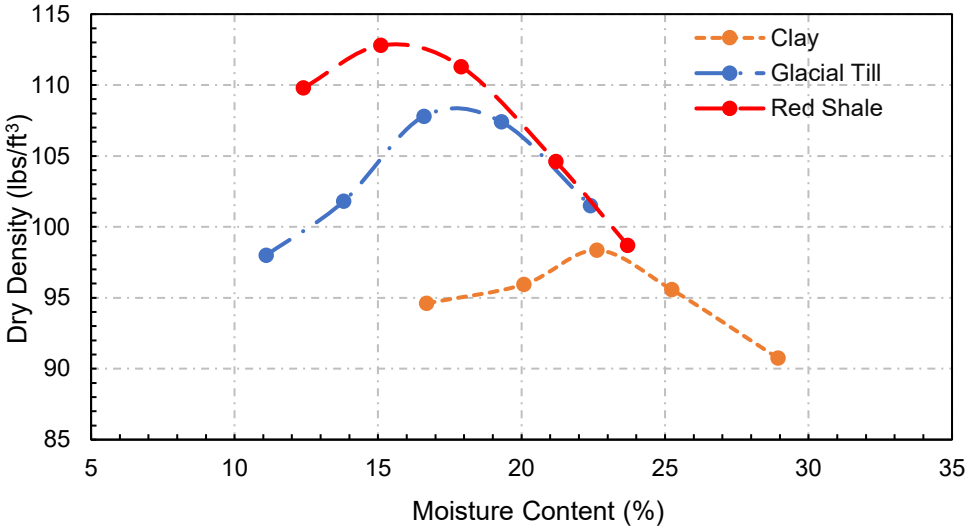

Figure 3.7 Compaction curves for glacial till, clay, and red shale

3.3 Aggregate Characteristics

The aggregate was a well-graded crushed limestone. It was a 1-inch nominal size gradation. It was stored in an aggregate bin located outside the Peter Kiewit Institute where it remained relatively untouched. Figure 3.8 shows the distribution for the aggregate.

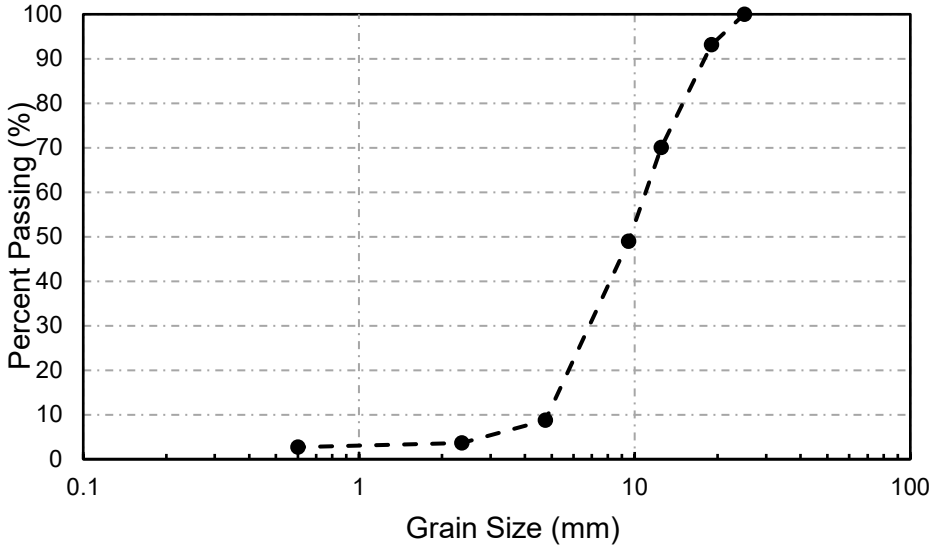

Figure 3.8 Grain size distribution graph for aggregate

Table 3.1 Properties of the soil

Glacial Till		Clay		Red Shale	
Property	Value	Property	Value	Property	Value
Liquid Limit (%)	46.0	Liquid Limit (%)	47.0	Liquid Limit (%)	36.7
Plastic Limit (%)	14.6	Plastic Limit (%)	16.8	Plastic Limit (%)	15.6
Plasticity Index (%)	31.4	Plasticity Index (%)	30.3	Plasticity Index (%)	21.1
OMC (%)	17.0	OMC (%)	22.5	OMC (%)	15.5
MDD (lbs/ft^3)	108.0	MDD (lbs/ft^3)	98.0	MDD (lbs/ft^3)	113.0
USCS Classification	CL	USCS Classification	CL	USCS Classification	CL
AASHTO Classification	A-7-6	AASHTO Classification	A-7-6	AASHTO Classification	A-6
Specific Gravity (G_s)	2.70	Specific Gravity (G_s)	2.70	Specific Gravity (G_s)	2.70

Sand	
Property	Value
D_{60}	0.69
D_{30}	0.41
D_{10}	0.22
Uniformity Coefficient (C_u)	3.14
Coefficient of Curvature (C_c)	1.11
Friction Angle (°)	30
AASHTO Classification	A-1-b
Specific Gravity (G_s)	2.65

3.4 Geosynthetic Types

Four geosynthetics were selected due to their best overall representation, common use in field application, popularity among DOTs, and abundant use. The geosynthetics used in this study were donated by Tensar International Corporation and Tencate Geosynthetics Americas. Namely, Tensar donated a roll of BX1200 geogrid and a roll of TX160 geogrid, while Tencate donated a roll of 2XT geogrid and a roll of 500X geotextile. The geosynthetics are known henceforth as GG1, GG2, GG3, and GT as indicated in Figure 3.9. The selected geosynthetics promised more reliable results with improved outcomes in Nebraska. These are commonly-used geosynthetics from both government and industrial perspectives and are in reference to the specifications of the FHWA and AASHTO guidelines. The Tensar BX1200 has especially been mentioned due to its role as a prominent initially-patented geogrid where other companies later replicated the design. Likewise, Tensar TX160 has become popular due to its triangular shape and redistribution of aggregate confinement.

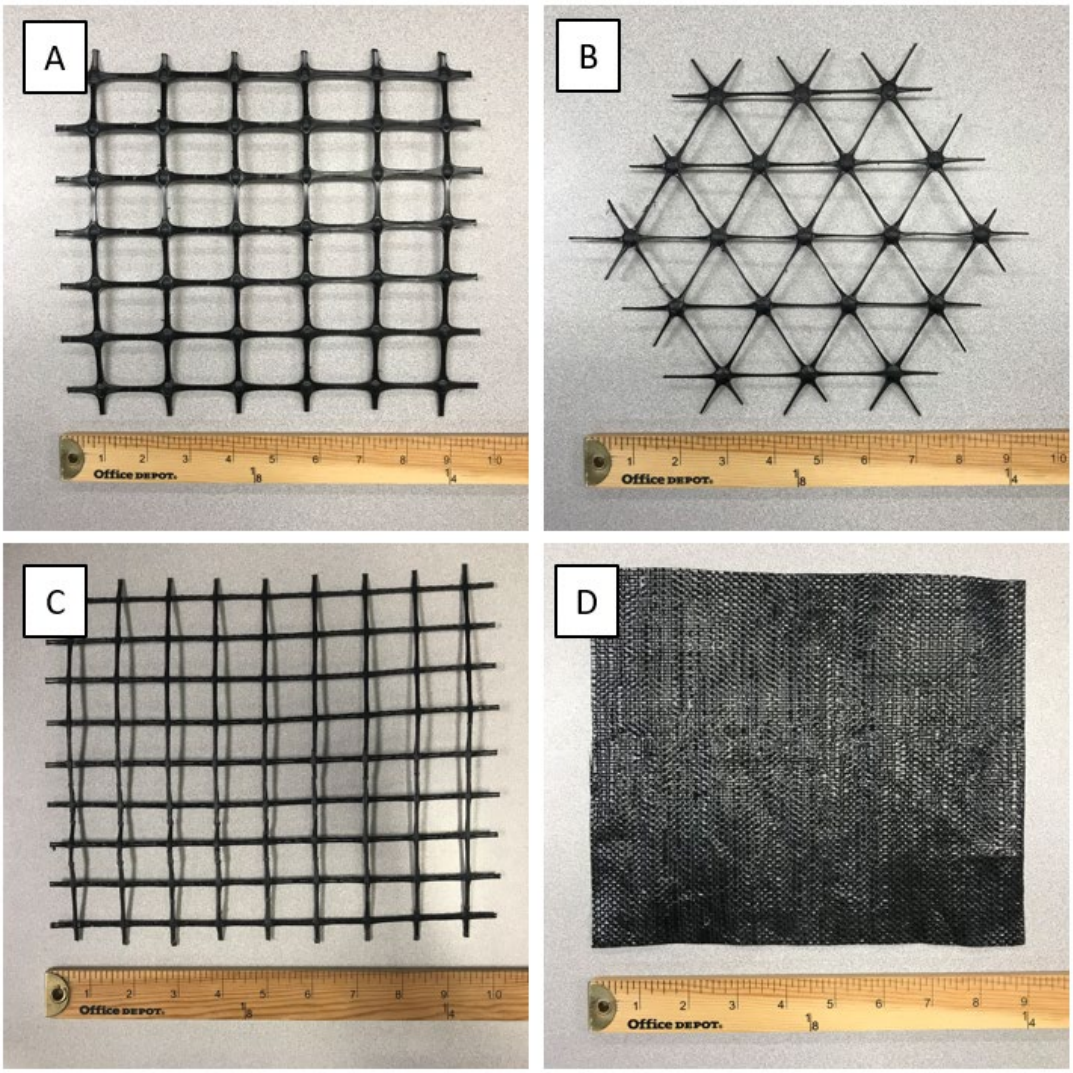

Figure 3.9 Geosynthetics used for testing, including A) BX1200 (GG1) geogrid, B) TX160 (GG2) geogrid, C) 2XT (GG3) geogrid, and D) 500X (GT) geotextile

3.4.1 Geogrid Characteristics

The GG1 and GG2 biaxial and triaxial geogrids are integrally formed polypropylene materials. The biaxial geogrids own square-shaped apertures, while the triaxial geogrids have a triangular aperture shape. The intersection points are known as junctions. The ribs are the stretched strands that complete the shape at said intersections. As can be inferred, the ribs are the weakest part of the geogrid. Table 3.2 and Table 3.3 show the characteristics of these geogrids.

The GG3 geogrid is a woven biaxial composed of polyester multifilament yarns finished with a PVC coating. This geogrid is not meant directly for preventative subgrade rutting deformation, rather its primary purpose is for soil reinforcement and slope stability (Tencate). It is the weakest of its class because its ribs are only two strands wide in the transverse direction. The geogrid also has only two strands in its longitudinal direction. Since this is the case, the values are the same for both the machine and cross-machine directions as depicted in Table 3.4.

3.4.2 Geotextile Characteristics

The GT geotextile is primarily a woven silt tape material composed of polypropylene fibers. It holds equal value in both the machine and cross-machine direction. Further, its primary use is for separation, and it meets the minimum requirements for the Class 3 Separation for AASHTO M288-17 (Tencate). During ongoing research, Tencate discontinued the Mirafi 500X (GG3) geotextile in favor of the Mirafi 140N geotextile. It seems non-woven products are better to resist continued moisture intrusion, and many states have moved away from silt tape-based geotextiles. Table 3.5 shows the characteristics of the geotextile.

Table 3.2 GG1 Geogrid Characteristics

Structural Integrity		
	MD[1]	XMD[2]
Aperture Dimension, in	1.0	1.3
Minimum Rib Thickness, in	0.05	0.05
Tensile Strength at 2% Strain, lbs/ft	34.2	620.0
Tensile Strength at 5% Strain, lbs/ft	67.5	1340.0
Ultimate Tensile Strength, lbs/ft	109.2	1970.0
Index Properties		
Junction Efficiency, %	93.0	
Flexural Stiffness, ft-lbs	0.054	
Aperture Stability, N-m/deg	0.650	

[1] Machine Direction
[2] Cross-Machine Direction

Table 3.3 GG2 Geogrid Characteristics

Structural Integrity			
Junction Efficiency, %	93.0		
Isotropic Stiffness Ratio	0.60		
Radial Stiffness at 0.5% Strain, lbs/ft	20,580[a]		
Index Properties			
	Longitudinal	Transverse	Diagonal
Rib Pitch, in	1.60	1.60	1.60
Mid-Rib Depth, in	0.06	0.06	0.06
Mid-Rib Width, in	0.05	0.05	0.04

[a] Radial stiffness was determined from tensile stiffness measured in any in-plane axis from testing in accordance with ASTM D6637-10

Table 3.4 GG3 Geogrid Characteristics

Structural Integrity		
	MD[1]	XMD[2]
Ultimate Tensile Strength, lbs/ft	2000.0	2000.0
Creep Rupture Strength, lbs/ft	1385.0	1385.0
Long-Term Design Strength, lbs/ft	1200.0	1200.0

[1] Machine Direction
[2] Cross-Machine Direction

Table 3.5 GT Geotextile Characteristics

Structural Integrity		
	MD[1]	XMD[2]
Grab Tensile Strength[3], lbs	200.0	200.0
Grab Tensile Elongation, %	15.0	15.0
Trapezoid Tear Strength, lbs	75.0	75.0
Index Properties		
Apparent Opening Size, U.S. Sieve	40	
Permittivity, sec^{-1}	0.05	
Flow Rate, $gal/min/ft^2$	4.0	
UV Resistance, %	70.0	

[1] Machine Direction
[2] Cross-Machine Direction
[3] Minimum Average Roll Value

Chapter 4 Methodology

4.1 Large Direct Shear Box

4.1.1 Apparatus Set-Up

The design of the box was taken in part from ASTM D5321 and fabricated at a local manufacturing plant in Omaha, Nebraska. It is a test that is conducted for soil-soil interaction, however specifically tailored to add a geosynthetic if desired. The box was equipped with perimeter wall segments so if the sample needed to be submerged, water would not escape. These could be taken off if the test did not require submersion, and usually were for ease of setup. The whole apparatus was made of stainless steel so that rusting wouldn't become a problem. Everything was either bolted or welded to the base for stability across the entire system. The large direct shear box was constructed with 1.7-foot-wide, 1.7-foot-long, and 0.33-foot-tall (0.5 meter × 0.5 meter × 0.25 meter) internal dimensions per shearing box – that is, for both the top and bottom. This was large enough to minimize the aperture size effect. See Figure 4.1.

Figure 4.1 Initially fabricated direct shear apparatus

A singular hydraulic piston was attached to its own base plate that applied the shear force to the top box. It was mounted at the mid-height of the top box so it would be completely horizontal. It had a direct capacity of 2,500-psi of pressure. There was also an “s-shaped” load cell attached to the hydraulic piston which displayed the force that was needed when shearing the box at the same rate. It connected to a piece of “c-shaped” steel that went over the walls and still provided rigidity when the force needed to be applied. The boxes rested on one another with the aid of smooth plastic plates to negate any undesired friction. The boxes themselves were rather heavy and did not get much soil in between them during tests. It was cleaned in between tests.

A 10,000-psi hydraulic pump was used to push the oil through 3,000-psi capacity hoses which had male quick-release couplings at their ends. These led to female couplings inserted in the hydraulic piston along with pressure gauges and needle valves. The needle valves were used to control the rate at which the oil entered the hydraulic piston, and thus, how slowly it moved.

There were three linear variable displacement transducers used to measure the displacements of the apparatus. One was fixed in the horizontal direction and two were fixed in the vertical direction shown in Figure 4.2. The horizontal was screwed down into a wooden block on the hydraulic piston that attached to a glued wooden block on the c-shaped steel. It remained parallel to the hydraulic piston and the floor, so it confidently captured the displacement. The verticals were screwed into wooden beams attached to the metal reaction rods. The verticals captured the displacement of the wooden board while the horizontals captured the movement of the top box. Since the geosynthetic did not move, it was unnecessary to tie anything to it or measure its displacement.

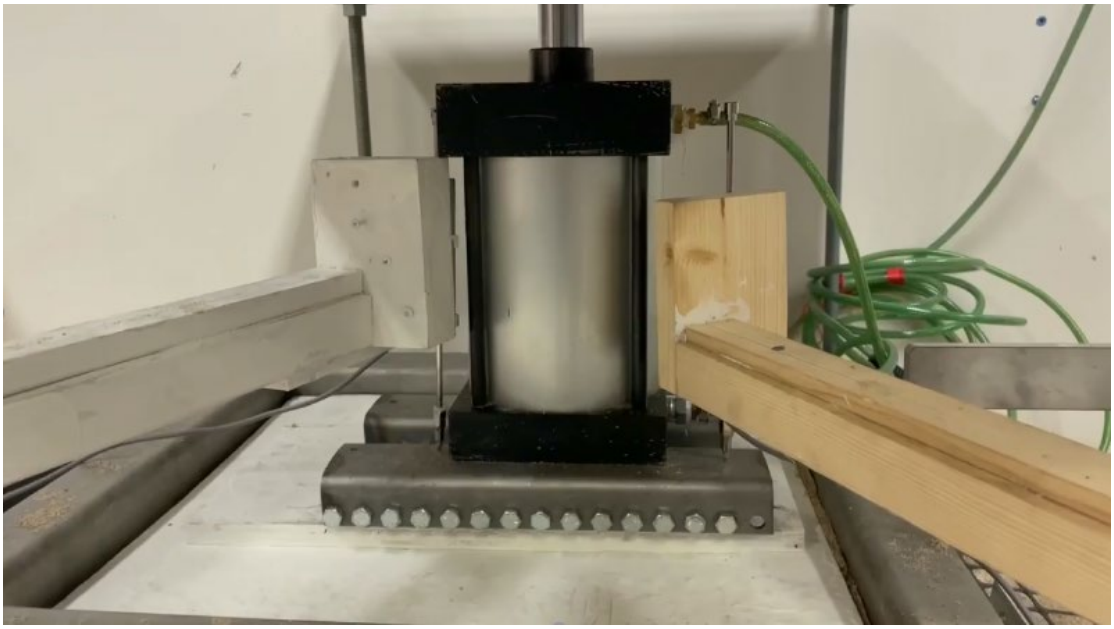

Figure 4.2 Positioning of LVDTs in the A) vertical and B) horizontal direction

Figure 4.2 cont. Positioning of LVDTs in the A) vertical and B) horizontal direction

4.1.2 Testing Procedure

The soil was initially air-dried until the test, and then the appropriate moisture was added to bring it to optimum. The clay was passed through the No. 4 sieve before it was tested. The amount of soil was known from previous calculation to determine the correct volume needed. The soil was laid into the box, one sub-layer at a time. There were two layers – one layer was below the geosynthetic while the other was above it. In total, that made for four sub-layers, each 2 inches tall. Each sub-layer was compacted to the desired 75% standard proctor and the soil height observation was confirmed. Compaction was from an 8-inch × 8-inch square steel tamper dropped from the same height with the same force. The geosynthetic was clamped in the machine direction, and it was held in place to the outside of the bottom box where it did not move during the test.

After the second layer of soil was compacted, it was covered with a wooden board which acted as a uniform load. The board was large enough to cover the whole surface of the internal dimension. An air cylinder was used to provide the normal pressure. It had a flat base which was modified to roll in a unilateral direction with the aid of conveyor-type galvanized rolling wheels. The idea was to keep the normal force constant and allow the air cylinder to remain in place as the box moved beneath it. Therefore, when the top box was sheared, the cylinder stayed in place while the wooden board moved beneath it with the top shear box. However, during testing with the original clay, the wooden board was brought into question because the soil tended to stiffen on one end of the shear box. Therefore, when the clay tests were repeated, a heavier metal plate of similar size was cut to conform to the box dimensions and used. The soil showed a more uniform texture once the test was concluded.

The cylinder provided a consistent normal force similar to that of a small direct shear box. The cylinder itself pushed off a reactionary plate. It was a stiff metal plate leveled and stationed into place with washers and nuts. The plate had a hole in the middle for the air cylinder. The stroke of the cylinder shaft elongated through this hole when air was supplied and made contact with the load cell that was bolted to the top of the plate. This load cell, rated for 30,000-psi capacity, measured vertical pressure. It can be seen it Figure 4.3.

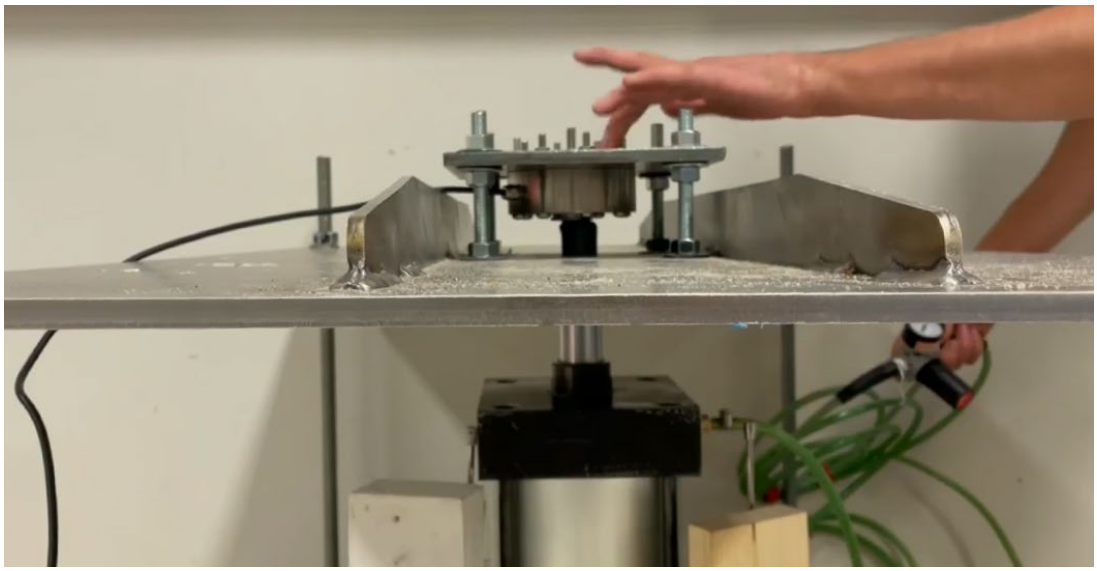

Figure 4.3 Supplication of the cylinder shaft into the load cell

The air cylinder was subjected to three different pressures of 1.89 psi, 4.06 psi, and 5.95 psi (13 kPa, 28 kPa, and 41 kPa). The difference in pressure was 0.44 psi (3.0 kPa) between the direct shear test and the pullout test. An air pressure regulator was purchased and supplied the pressures safely within its capacity. After the vertical pressure was stabilized, a data logger from Keysight DAQ970A with a 20-channel multiplexer was used to record the information. A power supply was also used to read the voltage that was exerted from the LVDTs and load cell. Benchvue software was provided to obtain the data. The top box had a shearing rate determined to be 0.04 in/min (1 mm/minute). Testing was concluded when the top box reached 10% of the box dimension, or a displacement of 2 inches (50 mm). The complete testing setup can be seen in Figure 4.4.

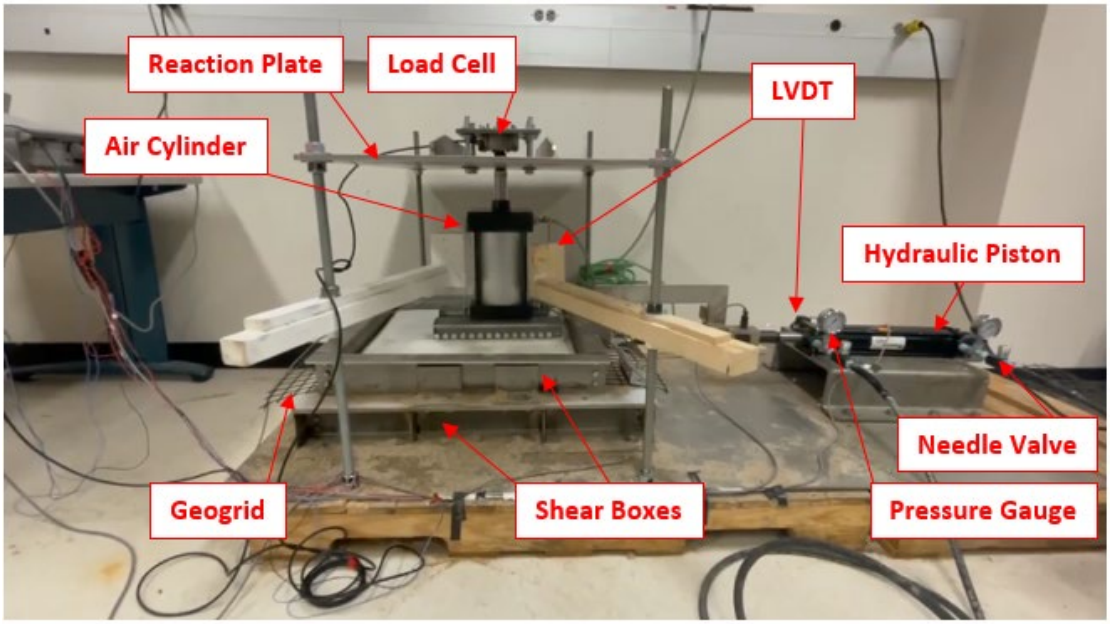

Figure 4.4 Completed setup of the large direct shear box

4.2 Large-Scale Pullout Box

4.2.1 Apparatus Set-Up

The design of the box was taken in part from ASTM D6706-01 and fabricated at Puritan Inc. which is a local manufacturing plant in Omaha, Nebraska. HUESKER does a similar test to prove its materials' capabilities. It is a test that is conducted for soil-geosynthetic interaction, specifically tailored for small displacement failure of a geosynthetic. The geosynthetic, as it works as a tensile member, is unique for its reinforcing qualities as part of an anchorage mechanism. This anchorage is known as the pullout and helps to support a planar load (Jewell 1996 and Koerner 2005). The Omaha box design was equipped with several individual wall segments to raise or lower the height of the box to account for multilayered soil tests. These wall segments were easily removable due to their bolted connections (Appendix A). The interior of the box was cleaned and spray-painted with a black gloss to minimize friction and to prevent

rust. The walls connected to a base which was immovable and was welded to one section of steel. Furthermore, this base sat atop four large caster wheels which were locked.

The large-scale pullout box was constructed with 5-foot-wide, 6.5-foot-long, and 5-foot-tall (1.5 m × 2 m × 1.5 m) internal dimensions (Figure 4.5). It was modified in the PKI Structural lab to its new dimensions. Seen in Figure 4.6, the modified volume became a 2.7-foot-wide, 4.3-foot-long, and a 1.0-foot-deep (0.85 m × 1.35 m × 0.30 m) box to allow for a more desirable set-up for the test. The set-up does not infringe upon any data misrepresentation. The two inner wall pieces were bolted down to the bottom of the apparatus and used as the outer boundary of the test, keeping in mind the geosynthetic would only be 1.7 feet (0.5 m) in width and 3.3 feet (1.0 m) in length to negate the boundary condition. The boundary condition phenomenon is where the geosynthetic material rubs against the wall of the apparatus, creating undesirable fiction, while under normal stress conditions.

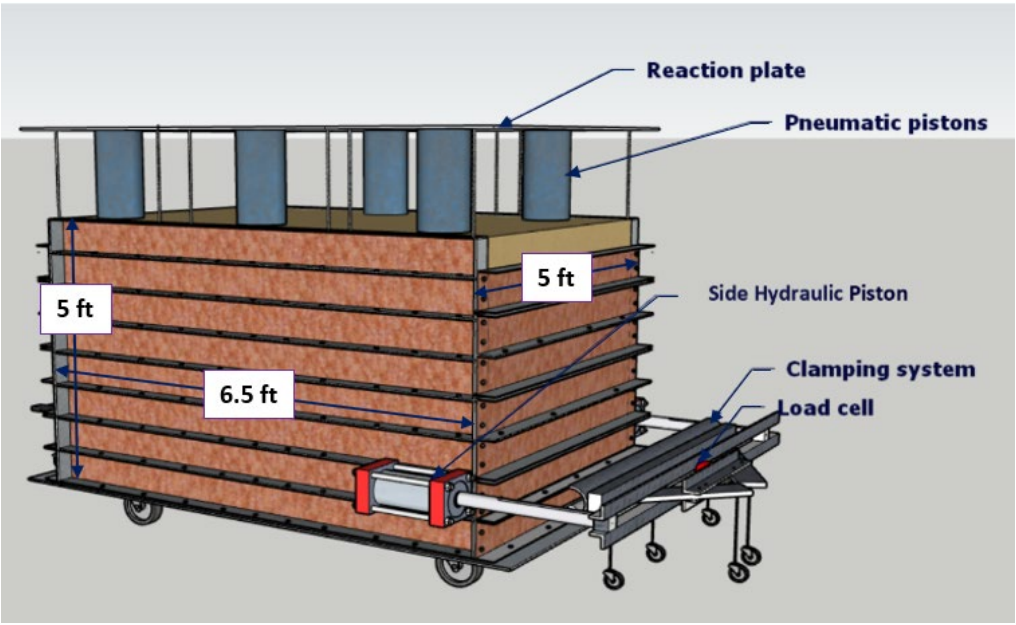

Figure 4.5 Fully-assembled design

Figure 4.6 Modified large-scale pullout box

Two hydraulic pistons were attached to the outer walls in the horizontal direction to apply the pullout force. The pistons could withstand 2,500-psi of pressure and were connected to the lower two sections of the steel wall. The pistons were important and special care had to be taken so as not to apply too much pressure, lest they burst, as one did during a preliminary test. Pressure gauges were installed. The hydraulic pistons connected to a front cross-bar which allowed them to move together and conjointly pull the geosynthetic out from the machine. The cross-bar was supported by the pistons and three individual caster wheels. Since these wheels were connected by nuts and washers along a rod that went through the roller clamp, the height of the roller clamp could be minorly raised or lowered to align the geosynthetic. In this way, it ensured the geosynthetic would be pulled out at an exact parallel surface to the box. The geosynthetic hooked around the roller clamp during the test. The top of the clamp had a flat steel bar that could be bolted down to hold the geosynthetic in place. The geosynthetic was additionally bolted to the underside with another steel bar. This geosynthetic connection was

important to hold the specimen properly, so as not to allow for any slippage due to the high tensile force exerted upon the specimen. A 30,000-pound capacity load cell was attached on the front of the cross-bar which displayed the required tensile force needed to pull the geosynthetic.

A 10,000-psi hydraulic pump was used to push the oil through 3,000-psi capacity hoses which had male quick-release couplings at their ends. These could be inserted into female release couplings attached to the hydraulic pistons on the box. The oil fed through the needle valve, past the pressure gauge, and into the piston. The needle valve, pressure gauge, and female coupling were attached together using appropriate hardware and were lubricated with PTFE Thread Sealing Compound to prevent any oil leaks. The lubrication became known as the “toothpaste” due to its consistency and blue color. The pump had two main hose lines which bisected and led into an inlet on the front and another inlet on the rear on each of the hydraulic pistons, shown in Figure 4.7. The rear inlet expanded the hydraulic piston forward.

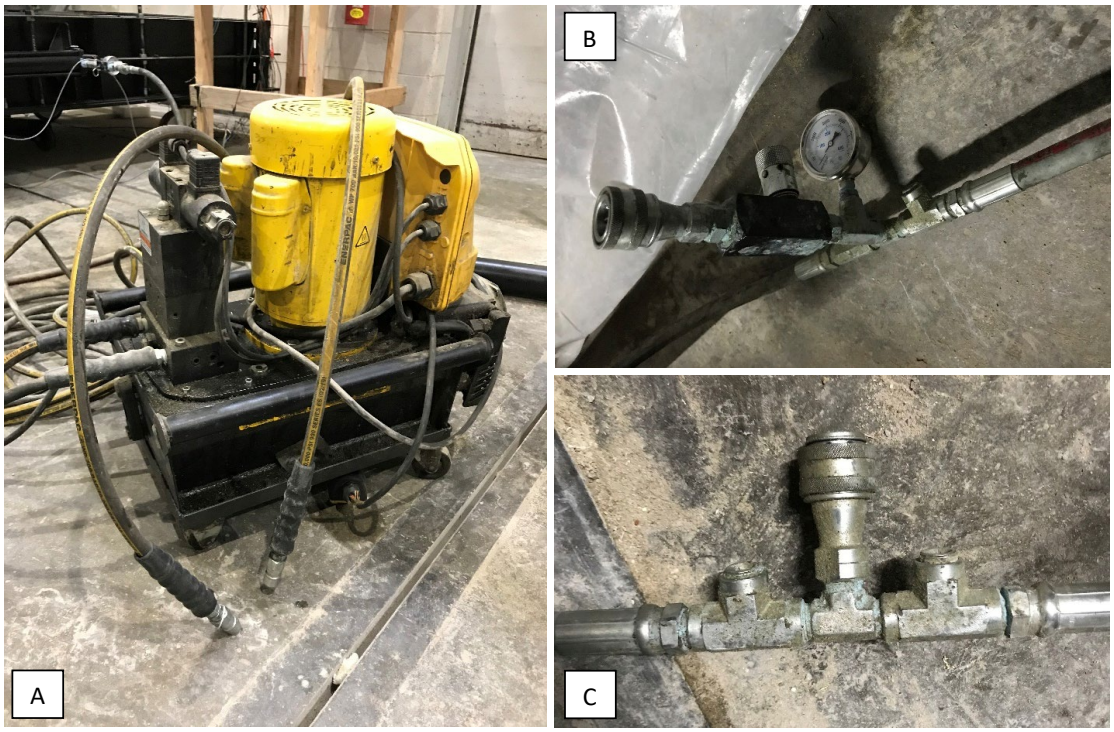

Figure 4.7 A) The hydraulic pump used in this test with the two main hose lines, bisecting into B), and C) quick disconnects which led to the hydraulic pistons

Linear variable displacement transducers (LVDTs) were used to measure the horizontal displacements. Also known as telltales, they are position transducers installed across the geogrid specimen to measure the internal displacement along the confined portion of the geogrid while it is being pulled. This indicates the gradual mobilization with the pullout force (Bakeer et al. 1998, Eun et al. 2017, Roodi et al. 2018, and Ghaaowd and McCartney 2020). Two of them were attached from the side-wall pistons to the cross-bar to record the actual horizontal displacement, one for each piston. These LVDTs were labeled as “0”. The LVDTs were screwed into blocks of wood, which in turn, were secured to the pistons and cross-bar. The hydraulic pistons started at the same length, about 20 inches, so that the constantly-controlled pullout rate would be even between them. The start of the test represented a zero displacement for the LVDTs. The back of the box laid claim to five additional LVDTs, all of which were screwed into a wooden platform

that extended from the back of the apparatus, labeled “1” through “5”. They were used to determine the soil-geosynthetic interaction and horizontal displacement of the geosynthetic while in between the soil layers during the test. Tensioned fishing line was used to tie the LVDTs to their desired destinations shown in Figure 4.8. A strong fishing line was considered a good material to use due to its low stain and thin circumference, keeping the recorded deformation values accurate. It minimized friction with the soil. Additionally, two wooden boards were screwed together and placed in the rear portion of the pullout box with a gap in between them to allow the LVDT lines to run through as shown in Figure 4.9. The gap was placed at a 0.5-foot height to coincide with the height of the first layer of soil. The wooden board was marked at 4.3 feet from the front of the box. Strategic points along the geosynthetic were chosen to tie the lines to keep testing repeatability consistent, accounting for different depths on the material and locations to provide a better understanding of how the geosynthetic interacts with the soil under loading and pullout conditions as shown in Figure 4.10.

Figure 4.8 LVDTs (telltales) attached to the rear portion of the box


Figure 4.9 Slit in the backwall for LVDTs extension cable to pass through

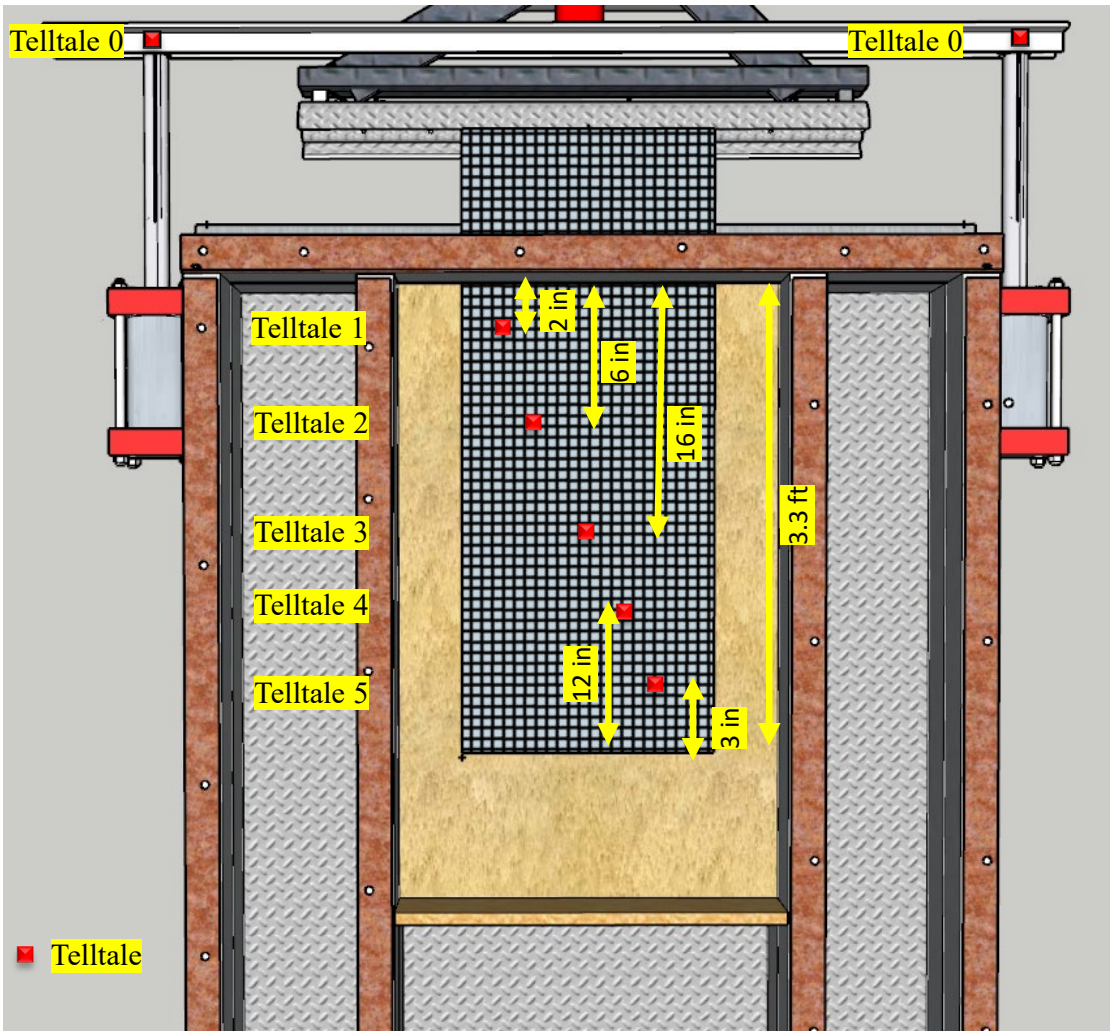

Figure 4.10 Location of LVDTs (telltales) across the tested sample

4.2.2 Testing Procedure

The soil was stored in 50-gallon drums until it was needed for testing. It was air-dried extensively to represent field conditions before it was used, then a moisture content was taken to evaluate the how much additional water had to be added to the soil to reach its optimum moisture content.

Once the box was cleaned, soil was poured into the modified dimensions, one sub-layer at a time. There were two layers – one layer was below the geosynthetic while the other was above it. A layer needed to be 0.5-foot-tall, to match the height of the wall segment. This

thickness complied with the minimum thickness specified by the ASTM D6706 standard. Likewise, each layer was compacted into three sub-layers, where each sub-layer was a third of the 0.5-foot height. From previous calculation it was known, for each sub-layer, the proper weight of soil needed before it was placed into the box to achieve a relative density of 75%. Then, each sub-layer was compacted by dropping an 8-inch × 8-inch square steel tamper from the same height with the same force.

When the geosynthetic was laid in the machine direction, it covered an area of 5.45 square feet (1.65 ft × 3.3 ft) in the box and extended through a slot in the front wall section. The geosynthetic was then properly attached to the clamp and held there for the remainder of the test while the LVDTs from the back of the box were tied to it. Figure 4.11 shows the sample preparation for testing. Many papers have determined that there is lateral earth pressure developed at the front wall which causes an increase in pullout resistance (Palmeira 1987, Palmeira and Milligan 1989, Raju 1995, and Sugimoto et al. 2001). Alternatives have been suggested to minimize this effect, such as using sleeves to keep the pullout load away from the front wall (Christopher et al. 1985). The testing slot in the front wall where the geosynthetic passed through was deemed big enough that it did not encroach upon any additional earth lateral pressure.

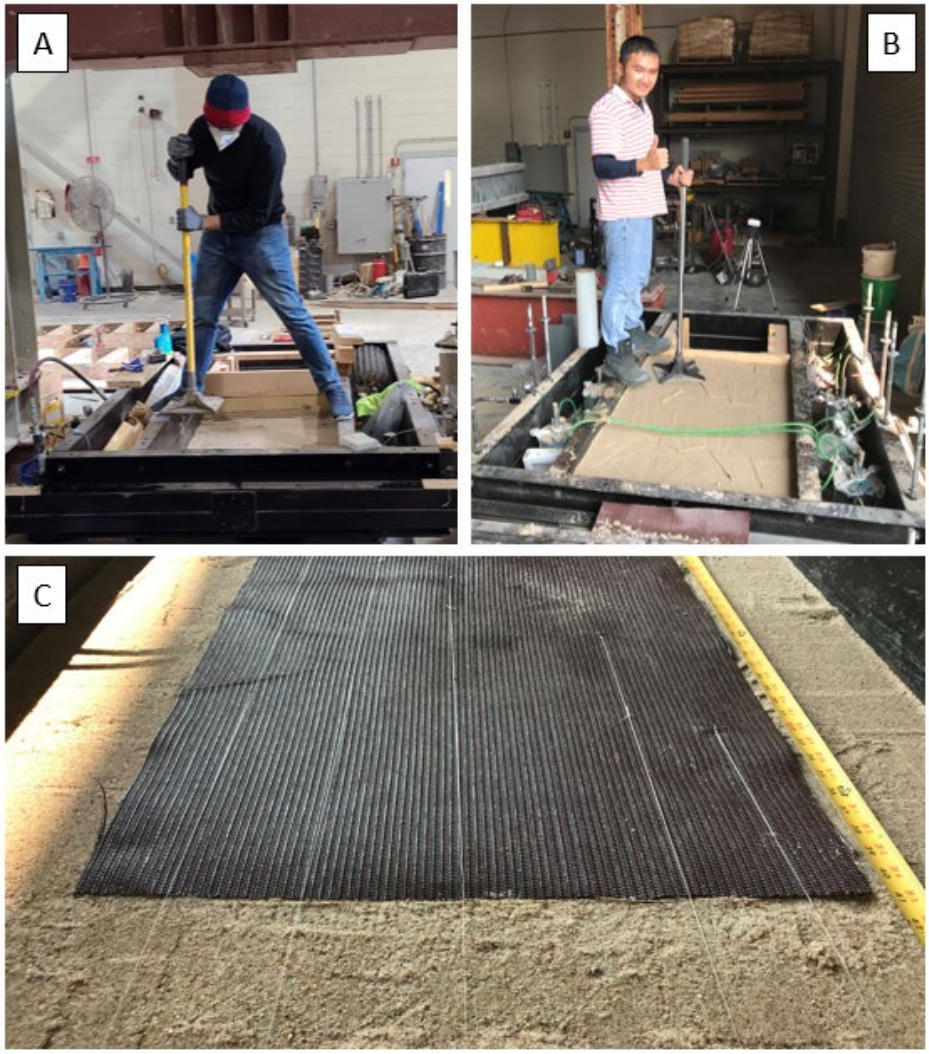

Figure 4.11 A) compaction of the bottom soil layer, B) compaction of the topsoil, and C) deploying geosynthetic specimen on the compacted soil in the chamber

After the second layer of soil was compacted, it was covered with a wooden plate which acted as a uniform load. Roodi (2016) performed this test with pyramidal wooden structures beneath the air cylinders. It proved to show no difference in uniform loading, so the idea was not pursued in this study. Six air cylinders (pneumatic pistons) were placed atop the wood; however, because of their inability to stand erect due to an awkward hump, a stiff piece of Styrofoam was laid beneath them. The Styrofoam was chipped away so there would be a space for the hump to rest comfortably and keep the cylinder upright. All the cylinders were connected with tubes and

were supplied with an air hose adjacent to the box on the wall. Each cylinder was subjected to different air pressures of 1.45 psi, 3.60 psi, and 5.50 psi (10 kPa, 25 kPa, and 38 kPa) respectively. An air pressure regulator was used to control the applied pressure. The cylinders shown in Figure 4.12 created the confining pressure to represent the same pressure soil undergoes in the field at various depths. They used a manufactured ceiling (the reaction plate) on the box as a counterforce to help displace the load into the soil. The reaction plate was quite stiff, and its deformation was minimal. A steel rod was placed through both holes of the reactionary plates to help stiffen the ceiling.

Figure 4.12 Pneumatic pistons used to apply the confinement pressure over the tested sample

After the confining pressure was stabilized, the systems were turned on and quickly checked. A data logger from Keysight DAQ970A with a 20-channel multiplexer was used to read the data from the load cell and the LVDTs. This was coupled with two power supplies which read the voltage from the LVDTs and the load cell. It was then possible to convert the voltage into applicable data. Benchvue software was provided to obtain the data as shown in Figure 4.13. Once everything was stabilized and ready, the geosynthetic was pulled out at a constant hydraulic flow rate of 0.04 in/min (1 mm/minute). Testing stopped when there was no increase in force but there remained increasing displacement. Failure occurred when the geosynthetic was ruptured or had been pulled 2 inches (50 mm). Appendix B has additional imagery.

Figure 4.13 Data acquisition system used to obtain the results from the pullout box

After the testing was completed, the soil was put back into the drum and stored with a lid, so no moisture escaped. The top layer of soil under the apparatus, after testing, was evaluated and moisture was added if necessary. Most of the time it was not. Soil fell from the apparatus but was cleaned and placed back into the barrel with the rest of the soil, keeping the volume change

throughout testing negligible. More importantly, soil weight was satisfactory. The complete testing setup with labeled parts is shown in Figure 4.14.

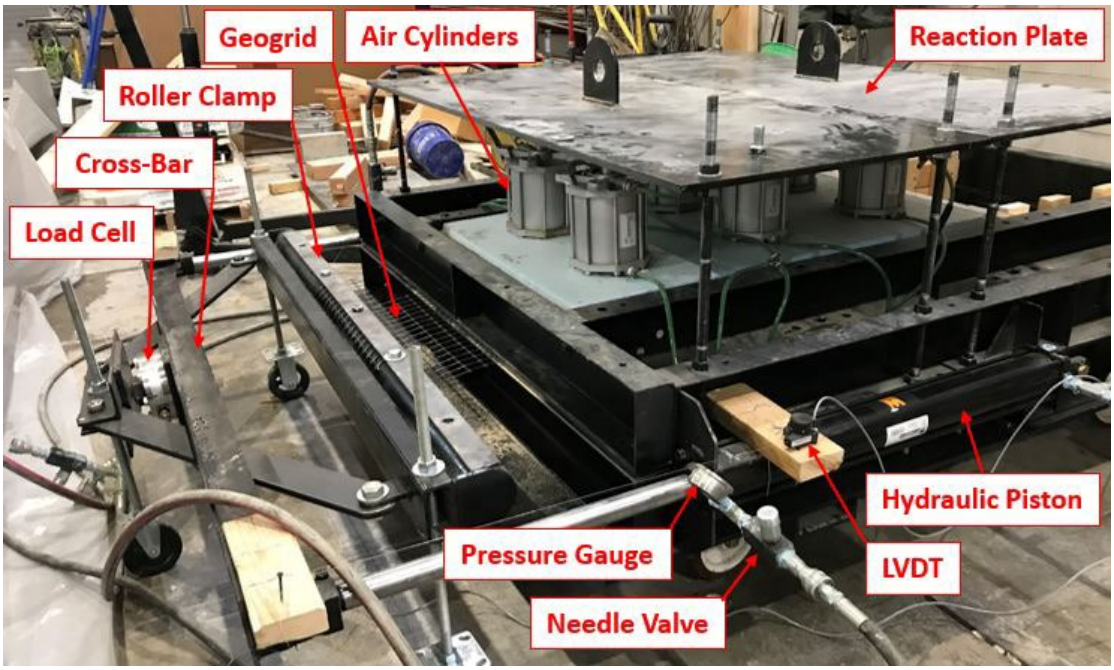

Figure 4.14 Completed setup of the large-scale pullout box

4.3 Dynamic Cone Penetrometer (DCP) Test in Soil Chamber Simulating Base and Subgrade

4.3.1 Soil Chamber Set-up for DCP test

To assess the durability of the pavement layers at various depths between geosynthetic reinforced and unreinforced scenarios, a soil chamber test using DCP was performed. The DCP offers a comprehensive estimation of the measured outcomes at different depths. Subsequently, we analyzed the most effective performance observed in a large-scale test. The testing barrel was made of steel with a diameter of 23 inches and a height of 34 inches as shown in Figure 4.15. Hooks were welded at different points around the circumference of the steel barrel, 19 inches from the bottom as shown in Figure 4.16 to provide tension in the geosynthetic material used. DCP test measures the penetration rate of a 17.6 lb (8.0 kg) hammer from a height of 22.6 inches

(575 mm) through undisturbed or compacted material. The penetration rate can be correlated to the in situ the in-situ California Bearing Ratio (CBR) based on equations developed by the U.S. Army Corps of Engineering.

Figure 4.15 Steel barrel for DCP test

Figure 4.16 Hooks welded in steel barrel

4.3.2 Testing Procedure

The different soil types which were used for testing were first air dried. Two different soil types were chosen as a subgrade material – Sand and Red Shale. Gravel was used as the base course material for this test. The amount of subgrade and base course material that was required was pre-determined from the dry density and volume of each layer in the steel barrel. To reduce the effect of boundary condition, 7 inches of sand was placed at the bottom of the steel barrel.

For the first case, which involved conducting the DCP test on the compacted base and subgrade layers with no geosynthetics, 12 inches of sand was placed on the 7-inch layer of sand already in the barrel. The 12-inch sand layer was compacted in three lifts each being 4 inches tall to a relative dry density of 75% as shown in Figure 4.18. Figure 4.19 shows the base course

material which was prepared at Optimum moisture content and placed on the compacted sand layer in three lifts each being 4 inches tall as well and compacted to 95% standard proctor dry density. A schematic of the various soil layers for the first case can be found in Figure 4.17. Compaction was done using a 10-inch x 10-inch square steel tamper. DCP tests were conducted for four different geosynthetic materials namely, BX1200 (GG1) geogrid, TX160 (GG2) geogrid, 2XT (GG3) geogrid and 500X (GT) geotextile with the gravel as a base course material and sand being the selected subgrade material for the first case (Figure 4.29). Figure 4.20, Figure 4.21, Figure 4.22 and Figure 4.23 show the various geosynthetic material on the compacted sand layer. Penetrations in the prepared soil layer for the DCP tests were recorded after every three blows through the entire 12-inch gravel base course layer and the 12-inch sand layer.

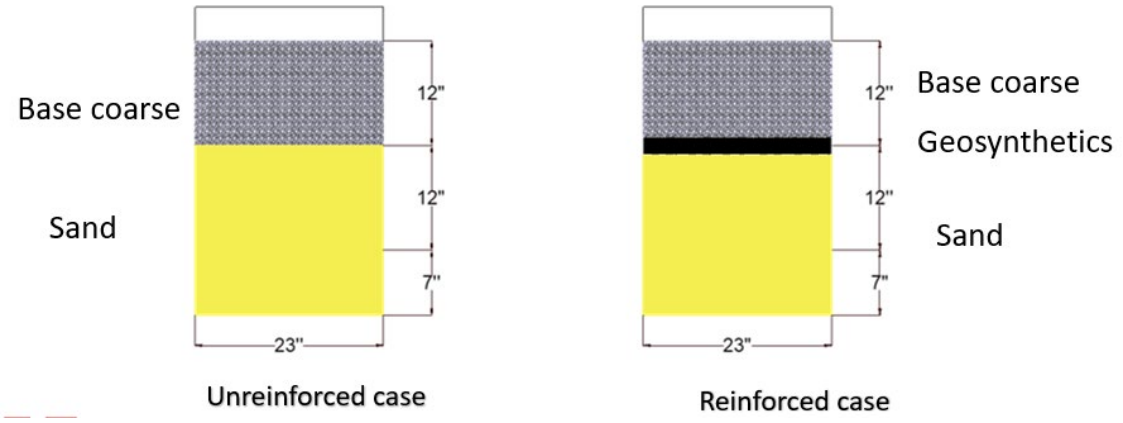

Figure 4.17 Schematic of soil layer in steel barrel for unreinforced and reinforced cases

Figure 4.18 Compacted sand subgrade layer

Figure 4.19 Compacted gravel base course layer

Figure 4.20 BX1200 (GG1) geogrid on compacted sand subgrade

Figure 4.21 TX160 (GG2) geogrid on compacted sand subgrade

Figure 4.22 2XT (GG3) geogrid on compacted sand subgrade

Figure 4.23 500X (GT) geotextile on compacted sand subgrade

For the second and third case, red shale and clay were used as the subgrade material, respectively. A schematic of the various soil layers in the steel barrel is shown in Figure 4.24. Figure 4.24 shows the 12 inches of red Shale and clay material placed on 7 inches of sand in the steel barrel. The 7-inch sand layer at the bottom was to reduce the effect of boundary condition. The soil material used was prepared at Optimum Moisture Content and compacted in 3 lifts to 75% standard proctor dry density (Figure 4.25). Figure 4.25 shows the compacted red shale layer. GG1 was placed on the subgrade layer as shown in Figure 4.27. The base course layer was then placed on the red shale and clay layers (Figure 4.26). DCP tests were conducted for both reinforced and unreinforced cases. For the reinforced case, the geosynthetics used were BX1200 (GG1) and TX160 (GG2) for red shales and GG1, GG2, and GT for clay.

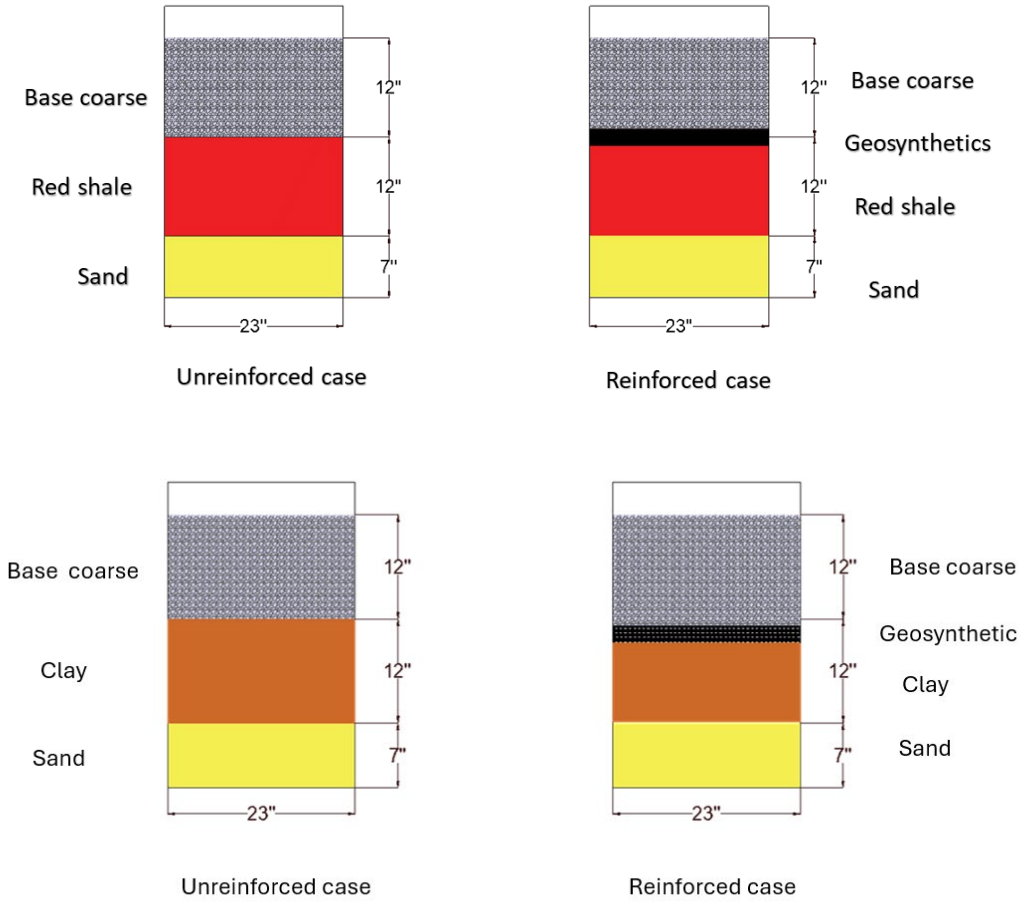

Figure 4.24 Schematic of various soil layer within steel barrel - case II and III

Figure 4.25 Compacted red shale subgrade layer

Figure 4.26 Compacted red shale base course layer

Figure 4.27 BX1200 (GG1) on compacted red shale subgrade

For the current research, a Dynamic Cone Penetrometer (DCP) was planned for use. Defined by ASTM D6951, the DCP measures the in-situ stiffness of base course and subgrade layers. To operate a dynamic cone penetrometer, one gently places the tip at the desired location. Keeping the DCP plumb, the initial height is marked and the weight is raised to the appropriate height where it falls freely. Continually drop the weight at the desired location until the maximum depth of penetration is reached. DCP testing is completed when either the penetration depth of 39 inches is reached or the penetration depth is greater than 24 inches and at least 10 consecutive blows return a PR of less than 0.04 in/blow. DCP measurements would have been taken at the four corners of the box and then averaged – four measurements taken per layer, resulting in eight total measurements per test. Figure 4.28 shows ASTM standard DCP equipment.

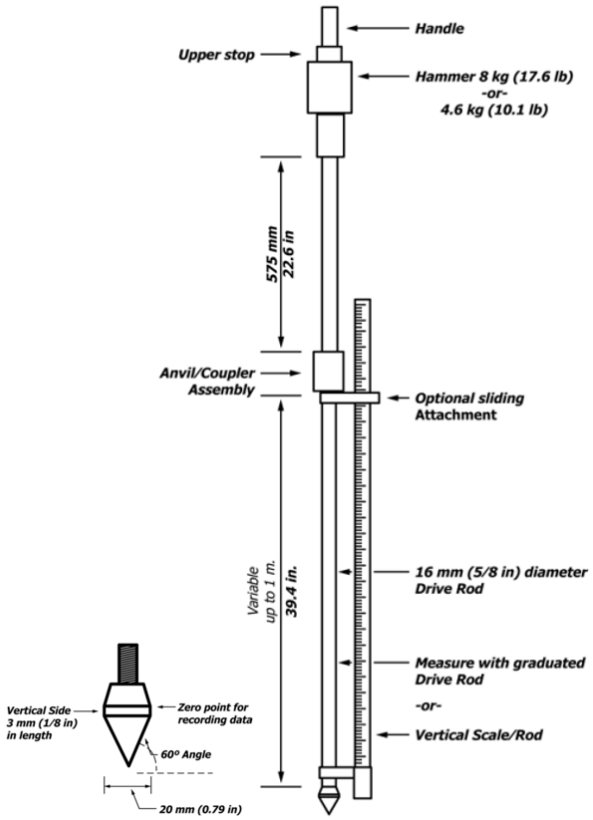

Figure 4.28 ASTM dynamic cone penetrometer

Figure 4.29 DCP test on compacted base course and sand layer

Iowa Specifications (2013) explain that a subgrade should hold a CBR of at least 10, otherwise, it will deflect under traffic loads. A proper knowledge of soil properties, water influences, and grading practices would go a long way to achieve a greater subgrade. AASHTO M288 identifies a CBR of 3 as the threshold between separation and stabilization. Predicted soil values are expressed in Table 4.1.

Table 4.1 Type of soil and expected values

Type	USCS Classification	k-value (psi/inch)	Strength Rating	M_R (psi)	Typical CBR (%)
Crushed Stone	-	220 to 250	High	M_R > 5,700	30 to 80
Gravel	GW or GP	200 to 220	Medium-High	4,500 to 5,700	30 to 80
	GW-GM, GP-GM, or GM	150 to 200	Medium	4,000 to 5,700	20 to 60
Sand	SW or SP	150 to 200	Medium	4,000 to 5,700	10 to 40
	SM	100 to 150	Medium-Low	2,700 to 4,000	to 30
Silt	ML or LL < 50 and PI < 10	50 to 100	Very Low	1,000 to 2,700	0 to 15
Clay	CL or LL > 50 and PI > 10	50 to 100	Very Low	1,000 to 2,700	0 to 15

References: Rollings and Rollings (1996), Iowa Statewide Urban Design and Specifications (2013), Pavement Interactive, American Concrete Pavement Association, Asphalt Paving Association, and the State of Ohio.

Harison (1986) would have been used for the CBR correlation because of its use in all soil types. Additionally, it is a widely used equation and rather reliable. Chen, Lin, Liau, and Bilyeu (2005) would have been used for the resilient modulus correlation. It is considered useful for all soil types. Lastly, to find the k-value of soil subgrade, the equation presented by AASHTO (1993) would have been used. It is based off of the resilient modulus from Chen, Lin, Liau, and Bilyeu (2005). It is useful for all soil types.

To find these parameters, a DCP was chosen for the present research. Several reviews have produced detailed equations for DCP-CBR and DCP-M_R relationships, which can be seen in Table 4.2 and Table 4.3 below, where the penetration index (PR) from DCP readings is in mm/blow.

Table 4.2 CBR equations based off of DCP tests

Literature Review	CBR Estimation Equations	For Soil Type
Harison (1986)	$\log(CBR) = 2.81 - 1.32(\log PR)$	All Soil Types
Harison (1989)	$\log(CBR) = 2.54 - 1.12 \log(PR)$	$PR < 10$
	$\log(CBR) = 2.56 - 1.16 \log(PR)$	$PR \geq 10$
Webster, Grau, and Williams (1992)	$\log(CBR) = 2.465 - 1.12 \log(PR)$	All Soil Types
	$CBR = 292/PR^{1.12}$	All Soil Types Except (CL) or (CH)
Webster, Brown, and Porter (1994)	$CBR=(1/0.017PR)^2$	Low Plasticity Clay (CL)
	$CBR=(1/0.0029PR)$	High Plasticity Clay (CH)

Table 4.3 MR equations based off of DCP tests

Literature Review	M_R Estimation Equations (psi)	For Soil Type
George and Uddin (2000)	$M_R = 77174.72(PR)^{-0.492}$	Fine-Grained Soils
	$M_R = 34127.44(PR)^{-0.475}$	Course-Grained Soils
Chen, Lin, Liau, and Bilyeu (2005)	$M_R = 78050(PR)^{-0.6644}$	All Soil Types
Mohammad et al. (2008)	$M_R = 151800(PR)^{-1.096}$	Fine-Grained Soils
	$M_R = 56730(PR)^{-0.23}$	Course-Grained Soils
AASHTO (1993)	$M_R = 19.4(k)$	All Soil Types

4.4 Large-Scale Tracking Wheel (LSTW) Test

4.4.1 Apparatus Set-up

A large-scale tracking wheel (LSTW) testing apparatus was designed and built by the research team at the University of Nebraska-Lincoln for the proposed project. Through this test, the mechanical performance of geosynthetic-reinforced pavement was evaluated. The condition of the test is close to the field condition in terms of the dimensions and the number of cyclic loadings. To investigate the long-term performance of the pavement in terms of permanent deformation (rutting), strength/stiffness and pressure reduction, the team conducted tests by applying rolling wheel loading on the pavement layer and measured how these properties within the pavement layers changes.

The design of the box was taken in part from research performed by Bagshaw et al. (2015) and the Kim et al. (2018) in conjunction with the Georgia Department of Transportation.

The test was conducted for soil-geosynthetic interaction under a base layer. The box was one steel piece with additional ribs on the sides to help provide reactionary stiffness. The interior of the box was cleaned and spray-painted with a black gloss to minimize friction and to prevent rust.

The large-scale box was constructed with 5.5-foot wide, 5.5-foot long, and 2.0-foot tall (1.67 m × 1.67 m × 0.61 m) internal dimensions. A better understanding of the layout and the entire assembly is shown in Appendix C. The box was placed atop a track that was doweled into the floor. The track was made from c-channel steel. The track had four outer plate extensions with holes in them for the dowels to pass through. These extensions were bolted to the inner track at one end and doweled into place on the other stabilizing the track. The box was attached to a pulley frame. This frame was connected to a motor, gearbox and the crank arm to push and pull the box in a unidirectional motion. Ten wheels were attached to the bottom of the box to aid with this movement. These wheels were greased to reduce the heat generated from friction during testing. The tire used during testing to apply rolling wheel loading on the base course surface had a 30-inch diameter with a 7.5-inch width (Figure 4.30). It holds a maximum load of 3000 lbs (1360 kg) at 80 psi (550 kPa) tire pressure. A two-bolt flange bearing was placed in the wheel and connected to the setup frame by a 6-feet high strength carbon steel rod. This enabled the tire to rotate freely in place. This bearing was greased as well to reduce the friction during testing. A hydraulic actuator was used to apply a load of approximately 10 kN through the rectangular steel frame to the tire. The test was run at an approximate speed of 1mph (0.447 m/s). The complete set-up is shown in Figure 4.31.

Figure 4.30 Tire used for LSTW test

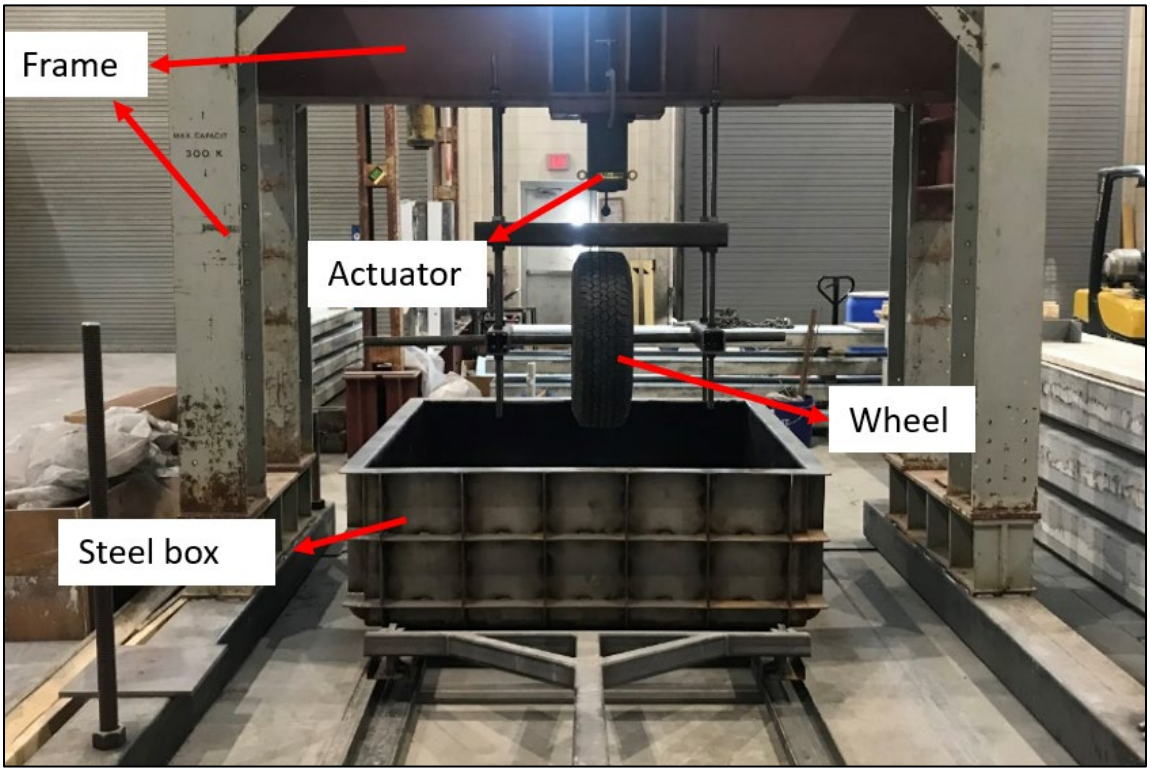

Figure 4.31 Complete set-up of the large-scale tracking wheel

4.4.2 Testing Matrix

Three different cases were evaluated for the Large-Scale Tracking Wheel Test to evaluate the extent to which the permanent deformation would be reduced, the pressure reduction effects and change in strength/stiffness of the pavement layer with the use of geosynthetics. The testing matrix is shown in Table 4.4.

Table 4.4 Large Scale Tracking Wheel Testing Plan

Case	ID	Condition	Base course thickness (in.)	Subgrade thickness (in.)
1	Control	No Geosynthetics	12 in	12 in
2	GG1 – 12 in	Geosynthetic reinforced (GG1)	12 in	12 in
3	GG1 – 9in	Geosynthetic reinforced (GG1)	9 in	12 in

4.4.2.1 Case 1 – Control Test Preparation

Sand was selected as the subgrade layer for this test. The sand was first air-dried before used. The steel box was filled with air dried sand and compacted with a heavy-duty plate compactor as shown in Figure 4.32 to a relative density of approximately 80% in two lifts approximately 6 in thick. The compacted sand layer can be seen in Figure 4.33. The total thickness of the sand layer was approximately 12 in.

The aggregates used for the base course were prepared at OMC (2.75%) using a concrete mixer (Figure 4.35). The base course layer was then placed in two lifts approximately 6 in thick and compacted with a heavy-duty place compactor to a relative density of approximately 95%. The compacted aggregate base course layer can be seen in Figure 4.36.

4.4.2.2 Case 2 – GG1 – 12 in Test Preparation

This case involved the use of geogrid (GG1) between the subgrade and base interface. The sand subgrade layer was approximately 12 in. thick with a base layer of 12 in. directly on top of the geogrid. The compaction of the sand and base layers was completed in a similar manner as the control case to the respective relative densities. Steel plates were used to fasten the geogrid onto the top of the sand subgrade layer to ensure the geogrid was flat and stretched out as shown in Figure 4.34.

4.4.2.3 Case 3 – GG1 – 9 in Test Preparation

This case involved the use of geogrid (GG1) between the subgrade and base interface. The sand subgrade layer was approximately 12 in. thick. The thickness of the base layer was reduced for this case to assess performance of a reinforced pavement with a reduced base layer. Steel plates were also used to fasten the geogrid onto the top of the sand subgrade layer to ensure the geogrid was flat and stretched out. The compaction of the sand and aggregate layers was compacted in two lifts each to relative densities approximately 80% and 95% respectively.

Figure 4.32 Heavy duty plate compactor

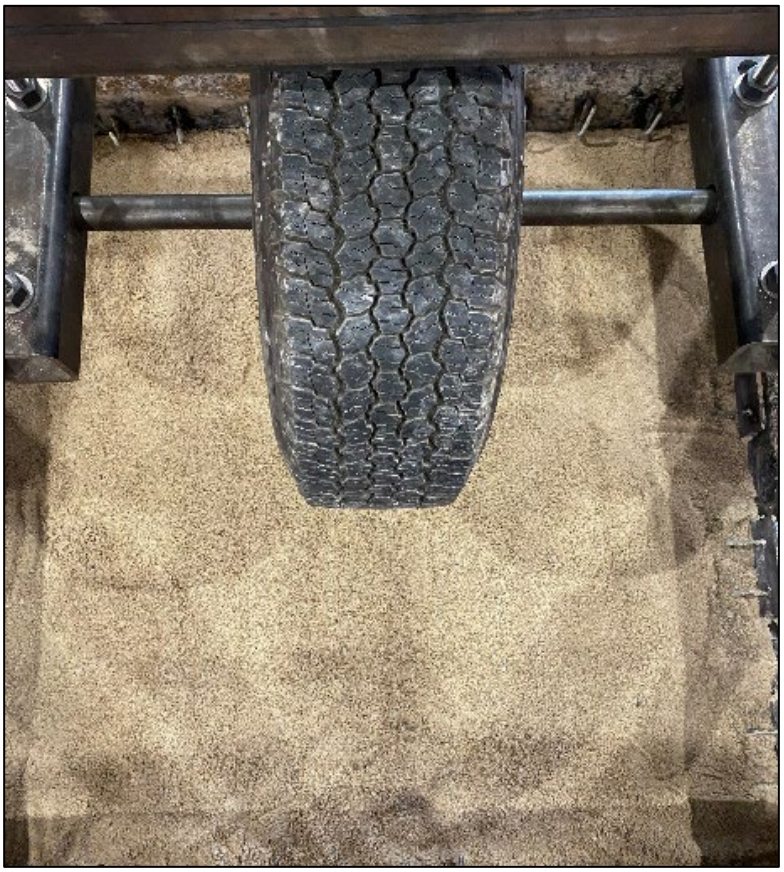

Figure 4.33 Compacted sand subgrade layer

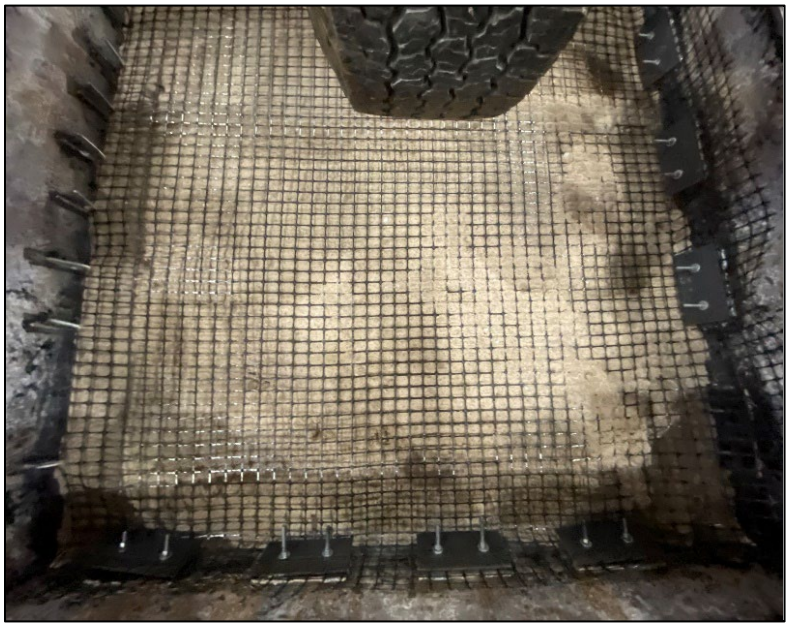

Figure 4.34 Installed geogrid on sand subgrade layer

Figure 4.35 Aggregate mixing at OMC using concrete mixer

Figure 4.36 Compacted aggregate base course layer

4.4.3 Large Scale Tracking Wheel Test Instrumentation

4.4.3.1 Linear Variable Displacement Transducer

Six LVDTs from Harold G. Schaevits Industries with a measuring range of 2 in. were used to record the vertical deformation of the base layer. These were made from industrial duty material for resistance to dust, temperature, shock, and variable. The vertical deformation recorded showed how rutting progressed during the test. These were fixed along a wooden beam held in place by a threaded rod on the two sides of the steel box with bolts at the top and bottom to prevent movement during testing. The LVDTs were installed at the center of the steel box at equal intervals approximately six inches along the wooden beam as shown in Figure 4.37. All LVDTs were calibrated before usage. The coefficient of determination (R^2) for LVDTs, representing the linear relationship between the voltage and calibrated readings, ranges from 0.9979 to 1.0, as highlighted in Table 4.5. This range signifies the accuracy and precision of the LVDTs readings. The LVDTs were connected to a Keysight DAQ970A 20-channel data logger using the Benchvue software.

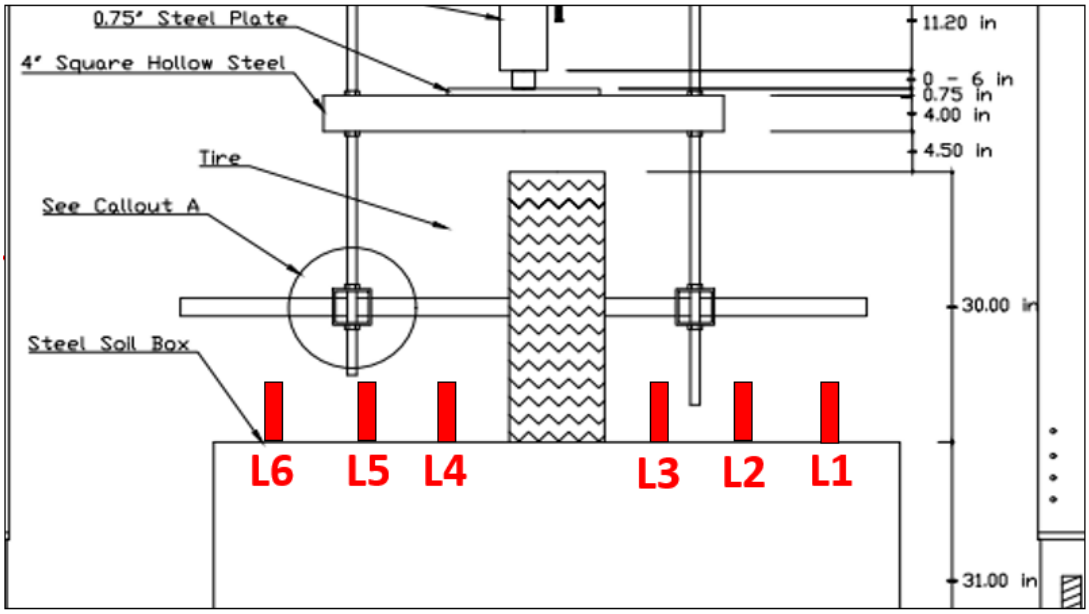

Figure 4.37 LVDT positions in steel box

Table 4.5 LVDT R2 Summary

LDVT	R^2
1	0.9996
2	0.9996
3	0.9996
4	0.9979
5	0.9982
6	1.0

4.4.3.2 Pressure Cells

Three pressure cells were used for this test. They were stainless steel with excellent corrosion resistance from Tokyo Measure Instrument Lab. They have a 50 mm in outer diameter and a dual diaphragm structure (Figure 4.38). The pressure cells were calibrated by applying different loads with the help of a calibrated actuator. A linear trend was established from which

an equation was obtained for the relationship between the pressure and output voltage. The R^2 for the three pressure cells used are found in Table 4.6. The pressure sensors were also connected to a Keysight DAQ970A 20-channel data logger using the Benchvue software. Two pressure cells were installed on top of the compacted subgrade layer for Case 1 (Figure 4.39) and a third pressure cell installed on the top of the compacted base course layer (Figure 4.41). For Case 2 and 3, one pressure cell was installed beneath the geosynthetic at the base and subgrade interface and a second pressure cell installed on top of the geosynthetic as shown in Figure 4.40. The third pressure cell was installed on top of the base layer in a similar manner was the Control test. These pressure cells were used to monitor pressure exerted on top of the base layer and at the subgrade and base interface and during testing. The schematic of the individual pressure cell positions can be seen in Figure 4.42.

Table 4.6 Pressure Cell R2 Summary

Pressure Cell	R^2
1	0.9999
2	0.9996
3	0.9990

Figure 4.38 TML pressure cells

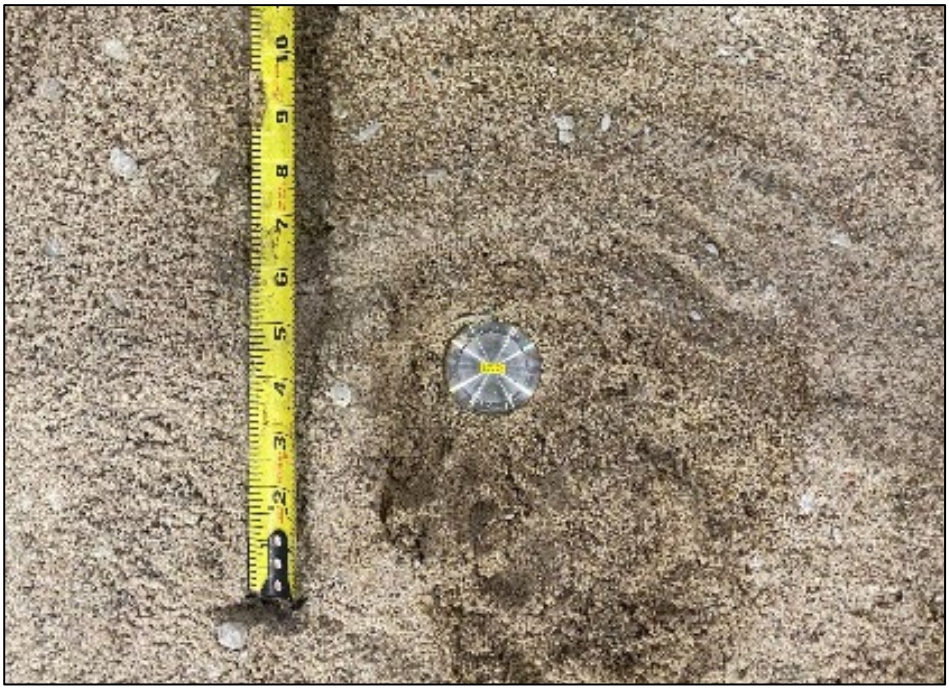

Figure 4.39 Pressure cell on compacted sand layer

Figure 4.40 Pressure cell installed on top of geosynthetic location

Figure 4.41 Pressure cell installed on top of base course

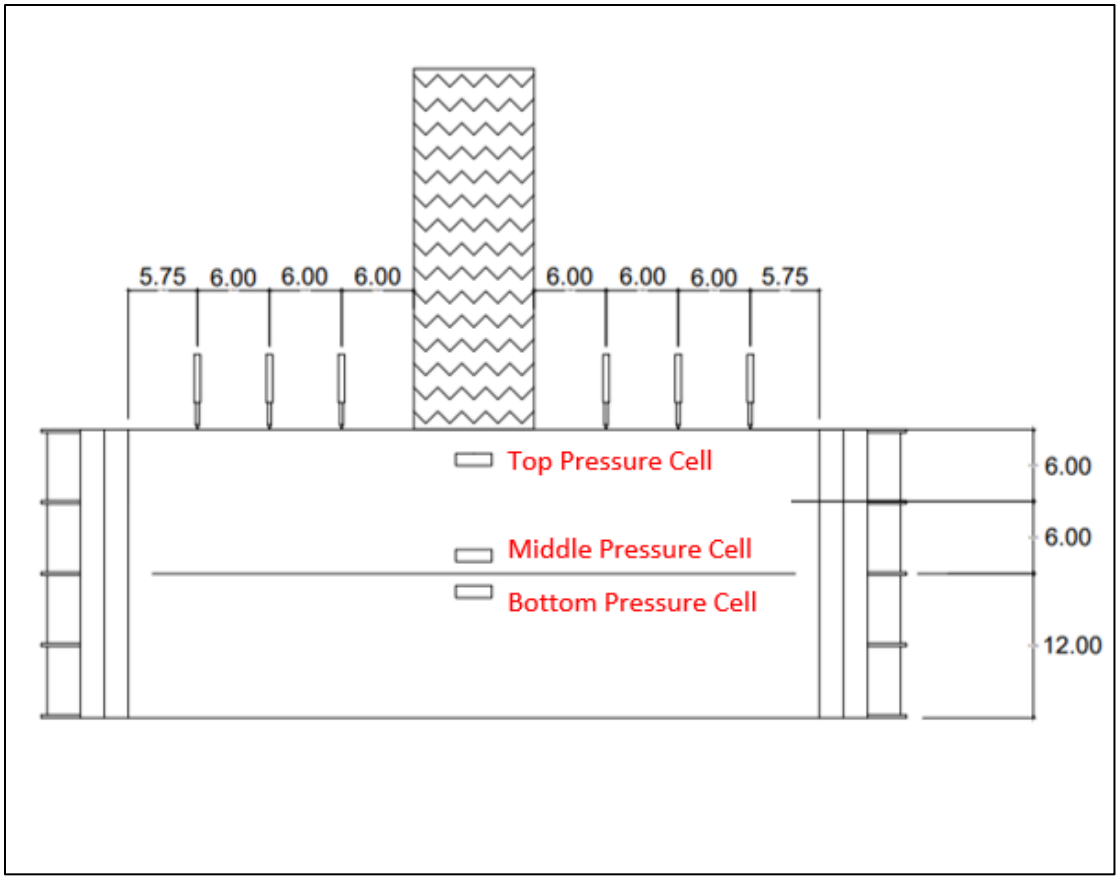

Figure 4.42 Schematic of pressure cell positions (unit, inches)

4.4.3.3 Load Cell

A load cell was installed beneath the hydraulic piston to measure the load that would being applied during the test as shown in Figure 4.43 and Figure 4.44. Assisted by an electric hydraulic pump system, an approximate load of 10 kN was applied through the actuator. The applied load was continuously monitored using a load cell and adjusted throughout testing.

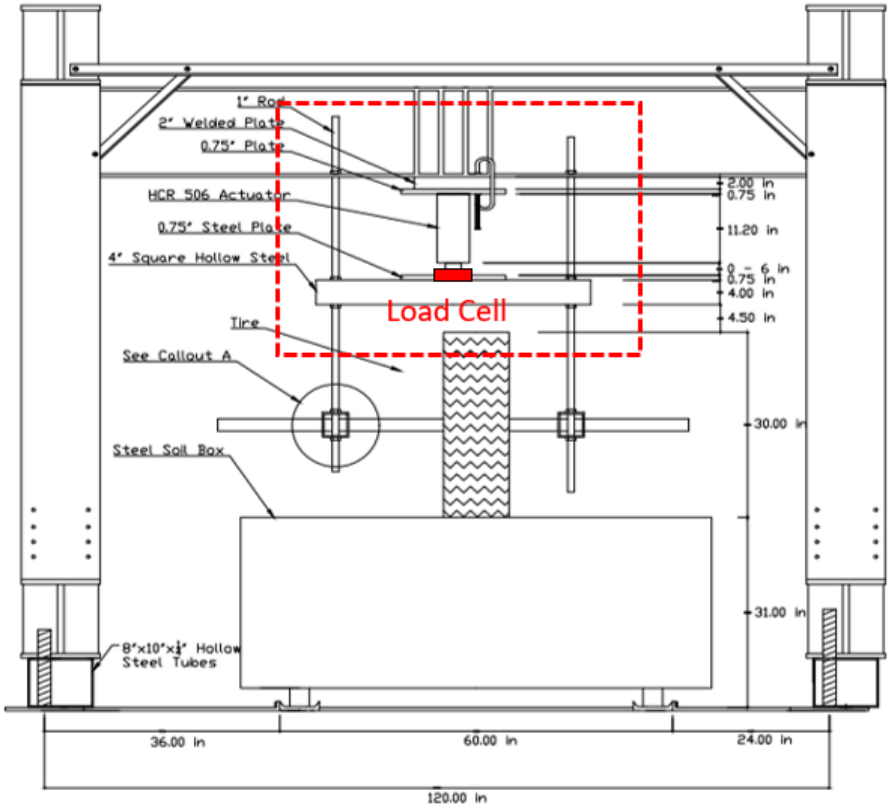

Figure 4.43 Schematic of load cell position (unit, inches)

Figure 4.44 Load cell positioned beneath actuator

4.4.4 Test Run

The load cell, linear vertical displacement transducers (LVDTs) and pressure cells were connected to their respective power supply units and then to the data acquisition box. The data acquisition box was then connected to a laptop to record the data during testing. The wheel was gently lowered onto the surface of the steel box by freeing up the nuts at the top of the steel frame. The test setup was turned on from the control unit. The unidirectional motion was initiated with the test run at a speed of approximately 1 mph. The complete testing setup in shown in Figure 4.45. Results for each case are discussed further in Section 5.7.

Figure 4.45 LSTW complete test setup

4.5 FLAC Simulation

The term FLAC stands for “Fast Lagrangian Analysis of Continua” and it is a numerical modeling software for advanced geotechnical analysis of soil, rock, and groundwater in a two-dimensional plane. It utilizes an explicit finite difference formulation that can model complex behaviors, such as problems that consist of several stages, large displacements, or even non-linear material behavior. Materials are represented by zones, known as elements, which form a grid, or a mesh. Each element, in turn, follows a prescribed linear or non-linear stress-strain law in response to the applied force and boundary restraints. Often, a higher force will cause the meshed diagram to deform and shows the applicable movement of the deformation (FLAC, 2022).

Structures such as tunnels, sheet piles, or roads can be modeled. In this regard, it is possible to examine the effects of instability with concrete, steel, or soils. The simulation investigation tried to find the surface settlement of different soil types against different geosynthetics, similar to the research properties in the present study. The interlocking and junction effect of the soil-reinforcement was considered by adapting a composite stiffness that was comprised of the soil and geosynthetic in the simulation (Eun et al. 2017). The model was validated with existing cases in literature (Kim et al. 2021) as well as the Direct Shear and Pullout tests. Table 4.7 and Table 4.8 show the input parameters for the simulation cases obtained from the literature. The cable element in FLAC has been shown to provide a good representation of geosynthetic materials in the literature (Holtz and Lee 1998, Vulova and Leshchinsky 2003, Ebrahimian 2011, and Zheng and Fox 2017).

FLAC requires the user to first establish the model type as well as the parameters for the materials that will be used. A Mohr model was used with the given parameters. A grid was created and then the mesh was applied across the grid. The mesh was generated into smaller trapezoidal elements per grid element, that way when the figure deformed, it would show a clearer settlement. A cross-section of the road was developed with the grid, specifically looking at an asymmetrical layout. Hence, smaller grids were generated under the tire load to create a more accurate simulation. The simulation further broke the cross-section into three parts, which became the asphalt roadway, the aggregate base layer, and the subgrade soil. The asphalt was determined to be half a foot in depth while the base layer was a foot deep. The subgrade soil constituted the rest of the layout, and it was 20 feet in depth – more than enough to negate the boundary effect from the bottom.

As it stood in the simulation, the cross-section was “floating” in space, meaning that if a load were applied at this time, the whole grid would shift down together and there would be no conclusive settlement. The boundaries, therefore, needed to be fixed. The sides of the cross-section were fixed in the horizontal direction, representing roller connections. The simulation was still free to move in the vertical direction. The base of the model was fixed in both the horizontal and vertical directions. The properties of the three layers were applied. These properties were taken largely in part from the direct shear and pullout tests, as previously mentioned. Once the properties were in place, geosynthetic was added. The simulation made a biaxial geogrid, a triaxial geogrid, and a geotextile. The properties were representative of current research. The geosynthetics were placed at a different depth for each individual soil case to correspond with the same 13 kPa confining stress. The sand had an assumed density of 1900 kg/m^3, so its depth was concluded at 0.70-meter depth. The clay had an assumed density of 1600 kg/m^3, so its depth was concluded at 0.83-meter depth. The soft soil had an assumed density of 1360 kg/m^3, so its depth was concluded at 0.98-meter depth. The 40,000 Newton load was then applied to the cross-section shown in Figure 4.46.

Table 4.7 Layer type parameters used in study

Parameter	Layer Type				
	Asphalt	Granular Aggregate	Louisville Sand	Clay	Soft Soil
Modulus of Elasticity (psi)	174,100	4,800	7,300	4,300	2,200
Density (pcf)	144	133	118	100	85
Poisson's Ratio (-)	0.25	0.30	0.25	0.30	0.25
Cohesion (psi)	0	0	0	500	360
Friction Angle (°)	0	65	30	0	0
Dilatancy Angle (°)	0	6	0	0	0

References: Hatami and Bathurst (2001), Iowa DOT (2015), Lambe and Whitman (1969), NDOT (1990), Radhakrishna and Klym (1974), Rajagopal et al. (2014), Subramanian (2006), Song et al. (2019), Tan et al. (2017), and Zheng et al. (2014).

Table 4.8 Cable element parameters used in study

Parameter	Sand		
	Biaxial Geogrid	Triaxial Geogrid	Geotextile
Modulus of Elasticity (psi)	150,000	120,000	70,000
Bond Stiffness, kbond (psf)	36,600	33,400	20,000
Bond Strength, sbond (lbf/ft)	560	450	320
Bond Friction Angle, sfriction (°)	35	37	30
Parameter	Clay and Soft Soil		
	Biaxial Geogrid	Triaxial Geogrid	Geotextile
Modulus of Elasticity (psi)	150,000	120,000	70,000
Bond Stiffness, kbond (psf)	70,000	60,000	100,000
Bond Strength, sbond (lbf/ft)	150	120	350
Interface friction angles considering Bond friction, sfriction (°)	30	29	25

References: Abdi and Arjomand (2001), Iowa DOT (2015), and Zheng et al. (2014).

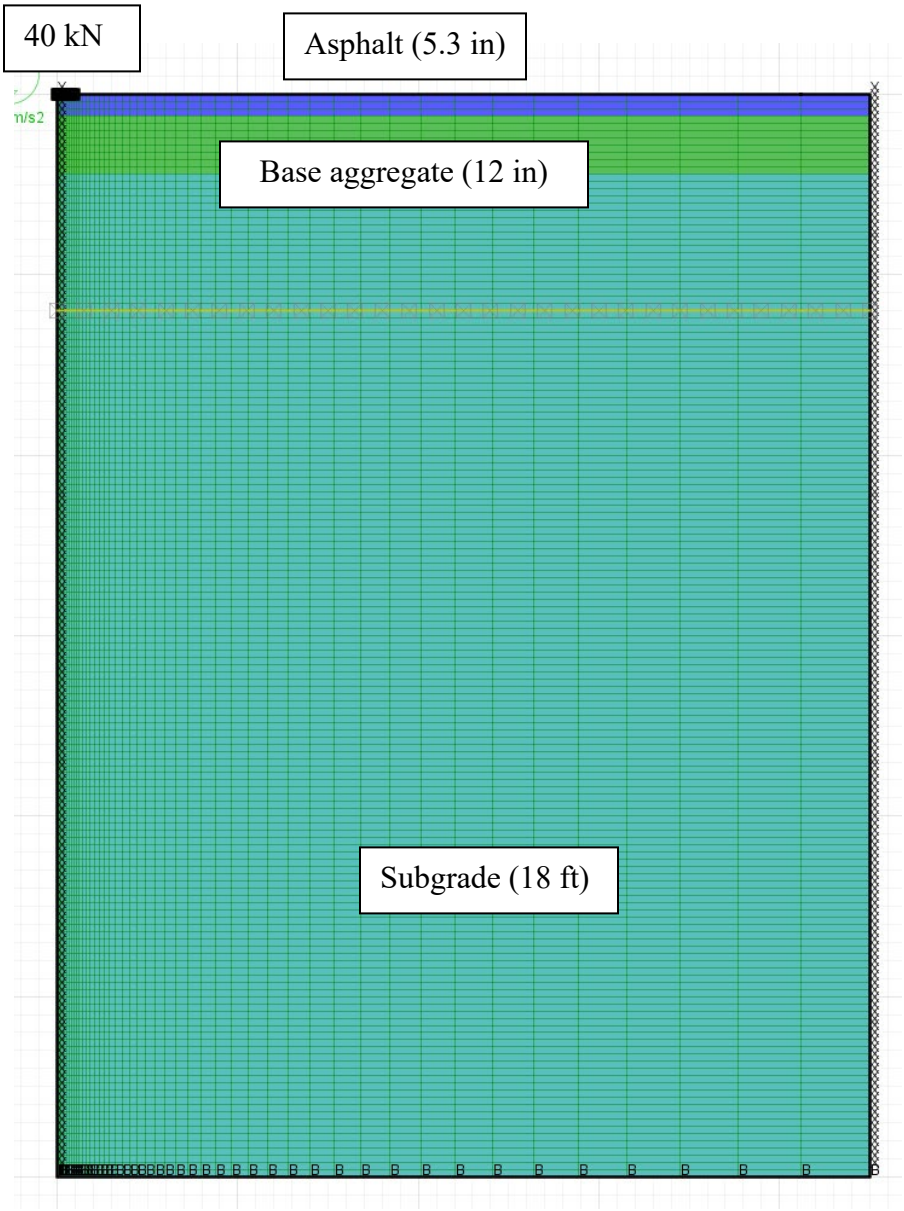

Figure 4.46 Cross-section of the asymmetric roadway with the geosynthetic and load

Chapter 5 Results and Discussion

5.1 Large Direct Shear Box

The sand, clay, and red shale soils were tested under the three various normal pressures. The clay test was run twice to compare and verify the results, as the large-scale direct shear over a clay soil is not a common test. The friction angle was found using Mohr-Coulomb. There have been several literature papers that have discussed direct shear with various soils. Sakleshpur et al. (2017) performed large-scale direct shear tests with several types of biaxial geogrids at optimum moisture contents. The research also tested at higher compaction levels and the interface shear resistance was conducted using the peak shear stress. Meanwhile Athanasopoulous (1997) conducted a direct shear test with geotextile-reinforced clay at a rate recommended by Smith and Criley (1995) and Ingold (1994) for cohesive soils. The rate, similar to the one used in the present study, was 0.4 mm/min. The study used a silt-heavy material, and results showed a 15° friction angle while unreinforced. Shear stress proved greater with the addition of a geotextile. Tiwari and Marui (2005) concluded that liquid limit of a soil can influence the residual friction angle; the lower the liquid limit, and the higher the residual friction angle. Some clay-like samples saw angles as high as 30°.

The soils performed well in the direct shear. For a given soil, each test was run incrementally, that is, each test was run with different geosynthetics but at the same normal pressure before moving to the next round of tests under the new normal pressure. The tests were conducted at optimum moisture content. When water is added to the clay past optimum, it gradually moves from a semi-solid to a liquid state. It loses strength in the process. It would be believable that the friction angle would be higher for a soil presented at optimum rather than one 50% saturated. The added water makes it so there is hardly any friction, and soil particles are

allowed to "glide over" the apertures. It was believed that the friction angles were reliable because of this fact. The friction angles were collected and the data was normalized with their peak shear stresses to create the interfacial shear resistance, given as

$$\alpha = \frac{\tau_{soil-geosynthetic}}{\tau_{soil-soil}} \tag{5.1}$$

where α is the interfacial shear resistance coefficient, and τ is the peak shear stress for both geosynthetic-reinforced and unreinforced cases. This parameter shows whether the addition of a geosynthetic is beneficial for a given soil. If the alpha value is above 1, then the geosynthetic helps under the applied pressure. The graphs showed that each increase in confining pressure increased the shear stress. All the graphs looked to be satisfactory and were consistent with one another. The trends in each graph showed that there was fairly loose soil, as was consistent with the 75% compaction. Only at high pressure in the original clay was there some densified soil, which is one reason for the verification when the test was run again.

5.1.1 Sand Direct Shear Soil Results

The graphs shown for the cases of sand were subjected to three confining pressures. The higher the confining pressure, the higher the shear stress of the graph. The general shape of these graphs indicates a loose soil compaction, consistent with the 75% desired compaction. The reinforced cases show a consistent initial modulus and then a leveled residual line as the displacement is carried on. The shape of each graph is very consistent with one another, as seen in Figure 5.1 through Figure 5.5 below. The peak shear stresses are commonly seen around the same displacement and the graphs follow a good slope stiffness before they yield.

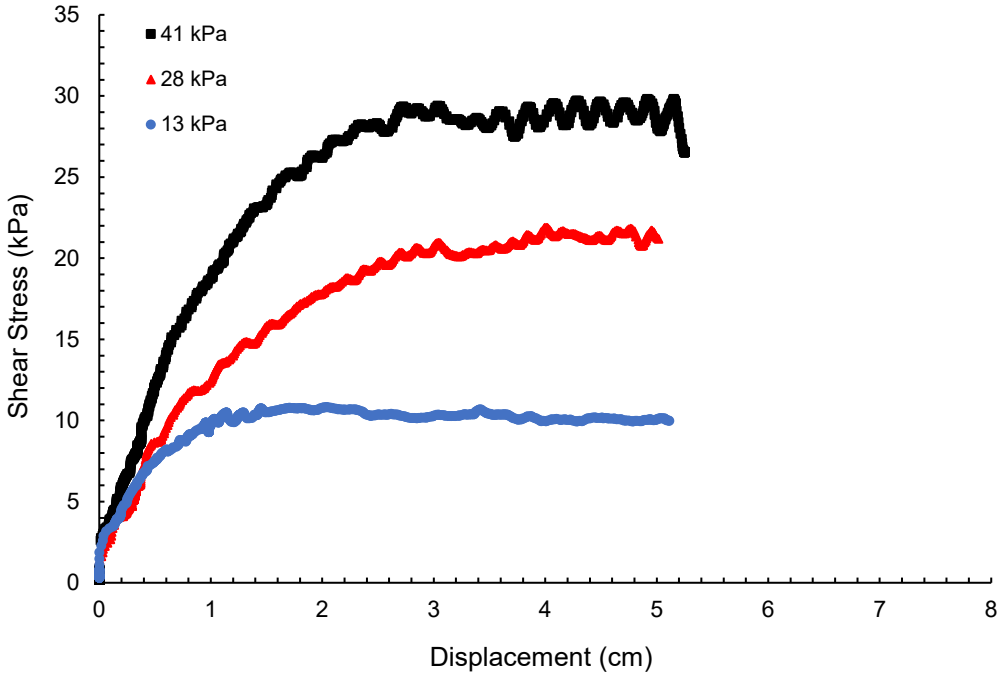

Figure 5.1 Unreinforced sand

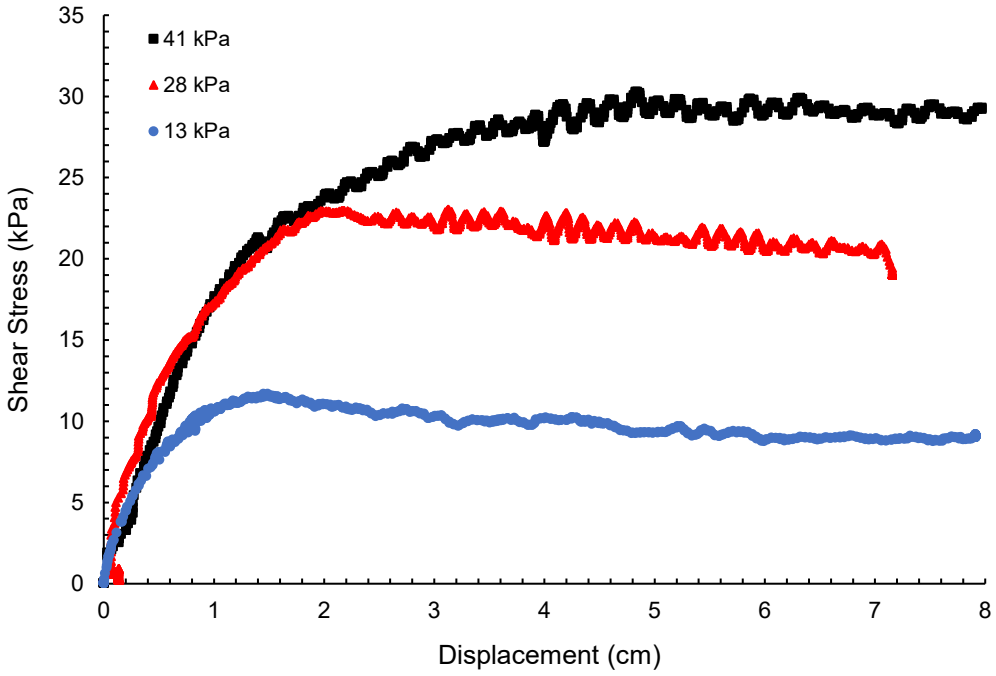

Figure 5.2 GG1 reinforced sand

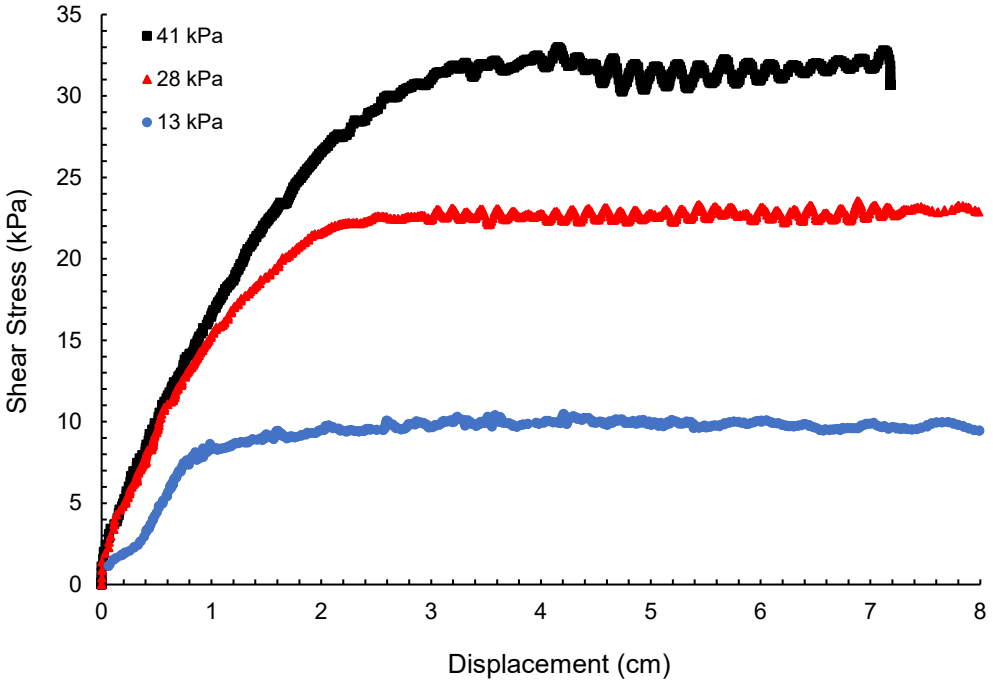

Figure 5.3 GG2 reinforced sand

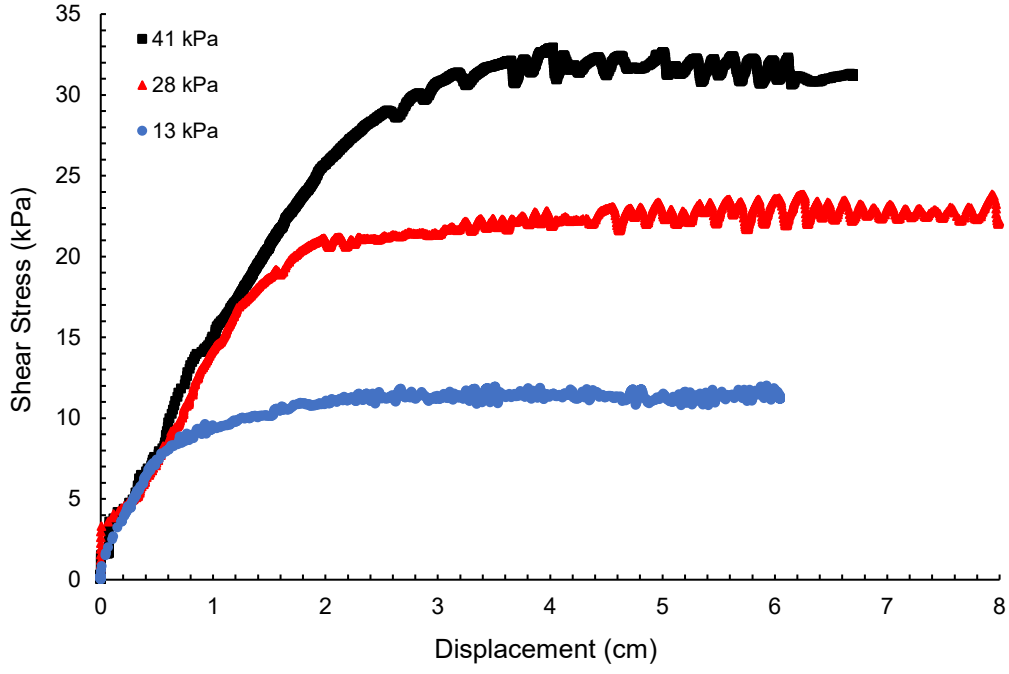

Figure 5.4 GG3 reinforced sand

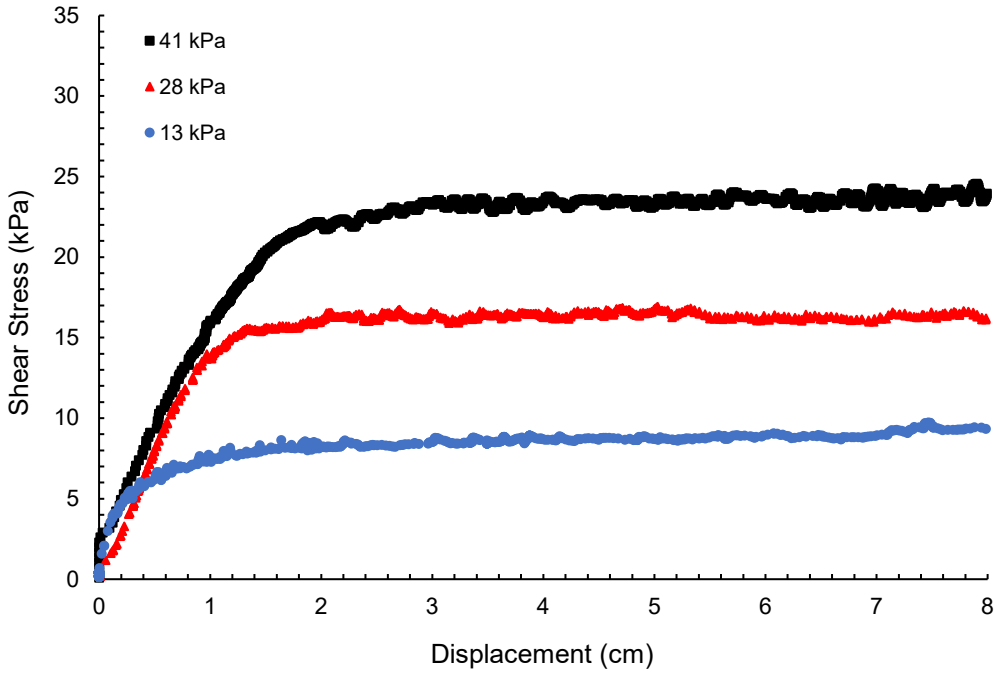

Figure 5.5 GT reinforced sand

Figure 5.6 shows the interface friction angle trendlines for the sand. The unreinforced case did not do well, as it produced a lower friction angle. The GT also showed that the friction angle is lower than the unreinforced case. This can simply be explained by the fact the geotextile does not allow for the particles to interact, as expected. The three geogrids, and specifically GG2 and GG3, showed higher friction angles (Table 5.1).

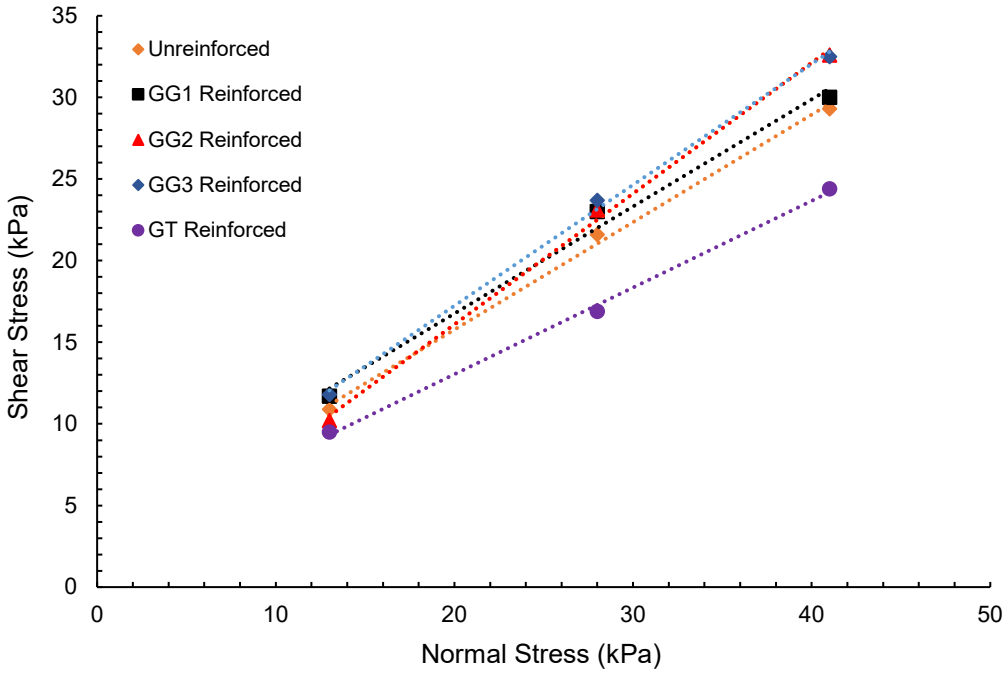

Figure 5.6 Shear stress versus normal stress for sand

The data shows that the normalized interfacial shear resistance increases as normal pressure increases for sand. This may be due to the fact that an individual soil particle has a very high bulk modulus. This is evidenced in Table 5.2 and visually seen in Figure 5.7, where there is a general upward trend. All the geogrids performed well and stayed above 1 when pressurized at 28 kPa and 41 kPa. The geotextile did not perform well, as expected, and was below 1 for all three pressures. The geotextile is contradictory to the trend, as it seems to stay pretty level in all three pressurized cases. This indicates that geotextiles do not produce much friction with sand and are more likely to slide along the surface rather than catch any particles. The geotextile has no apertures and the sand cannot interlock with one another. GG1 also seems to have a level normalized shear resistance. This may be due to its apertures being too large for the sand particle size. Its trend suggests that it would start to perform worse at higher pressure. GG2 and GG3 enjoy rises in their values as the pressure increases presumably due to their smaller aperture sizes

or the fact that GG3 has a more flexible nature and can react to the increased load more efficiently. But GG3 only sees a slight increase, whereas GG2 shows significant improvement. Its apertures are meant for interlock, which is consistent with the product's manufacturing details. Its triangular shape gives it the edge to maximize the pressure into the soil and not the ribs.

The geotextile performed poorly and the geogrids performed better in the order of increasing friction angle – GT, GG1, GG3, and GG2. The GT had a 28.0° friction angle, GG1 had a 33.3° friction angle, GG3 had a 36.5° friction angle, and GG2 had a 38.7° friction angle. For the sand, this was clear-cut evidence proven in Figure 5.8 that the higher the friction angle, the higher the normalized interfacial shear resistance.

Table 5.1 Sand friction angle and cohesion

Sand		
	Friction Angle (°)	Cohesion (kPa)
Unreinforced	33.4	2.60
GG1 Reinforced	33.3	3.63
GG2 Reinforced	38.7	0.06
GG3 Reinforced	36.5	2.42
GT Reinforced	28.0	2.42

Table 5.2 Sand normalized peak interfacial shear resistance

Geosynthetic	Normal Stress			
	13 kPa	28 kPa	41 kPa	Average
GG1 Reinforced	1.073	1.065	1.024	1.054
GG2 Reinforced	0.936	1.069	1.113	1.039
GG3 Reinforced	1.083	1.097	1.109	1.096
GT Reinforced	0.872	0.782	0.833	0.829

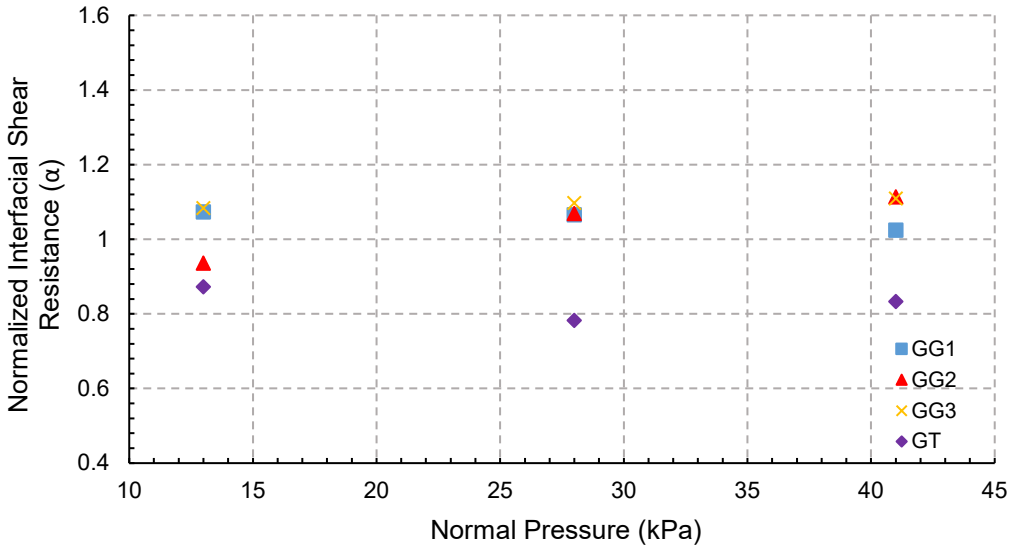

Figure 5.7 Sand normalized interfacial shear resistance versus normal pressure for all geosynthetic types

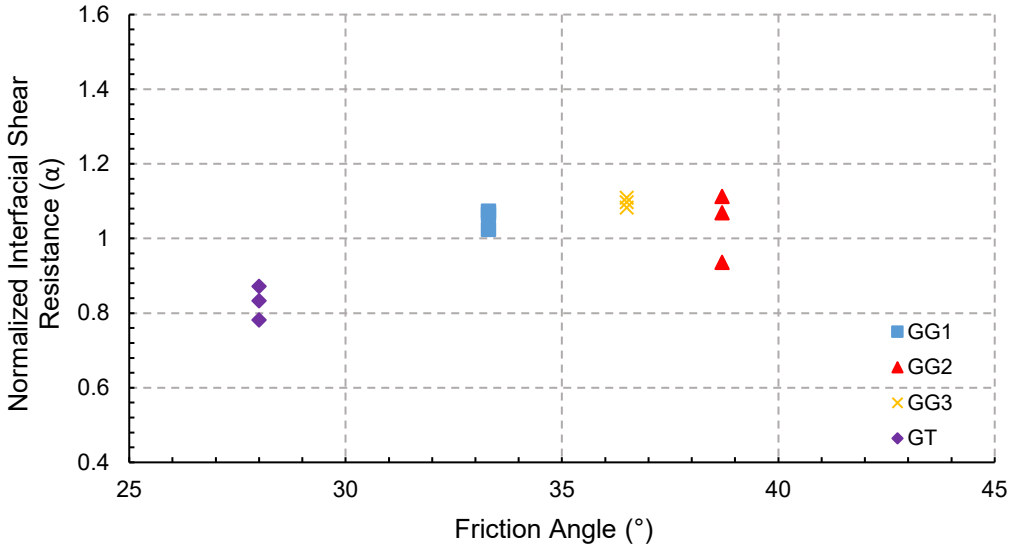

Figure 5.8 Sand normalized interfacial shear resistance versus friction angle for all geosynthetic types

5.1.2 Original Clay Direct Shear Soil Results

The graphs shown for the cases of original clay were subjected to three confining pressures. The higher the confining pressure, the higher the shear stress of the graph. The shape of each graph is very consistent with one another. The general shape of these graphs indicated a loose soil compaction for the lower confining pressure while the two higher pressures densified the clay shown in Figure 5.9 through Figure 5.13. Throughout all the graphs, the black line consistently became denser. There was some disagreement with the initial modulus for these graphs, mainly that the lower pressure jumped in shear stress and then gradually increased while the higher two pressures built into their peaks. The peak shear stresses are commonly seen around the same displacement and the graphs follow a good slope stiffness before they yield.

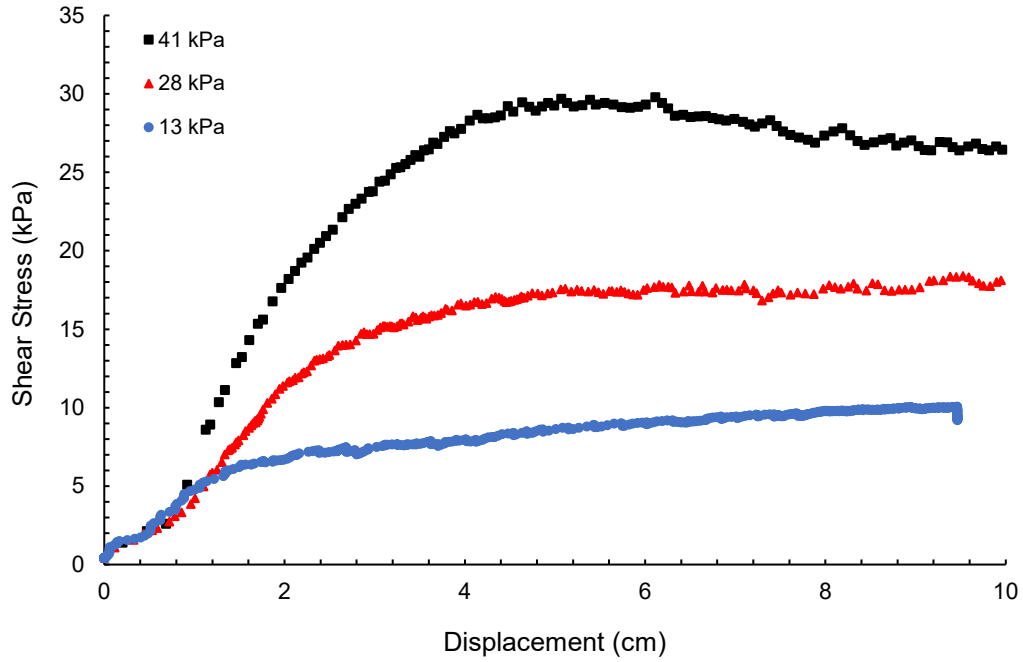

Figure 5.9 Unreinforced clay

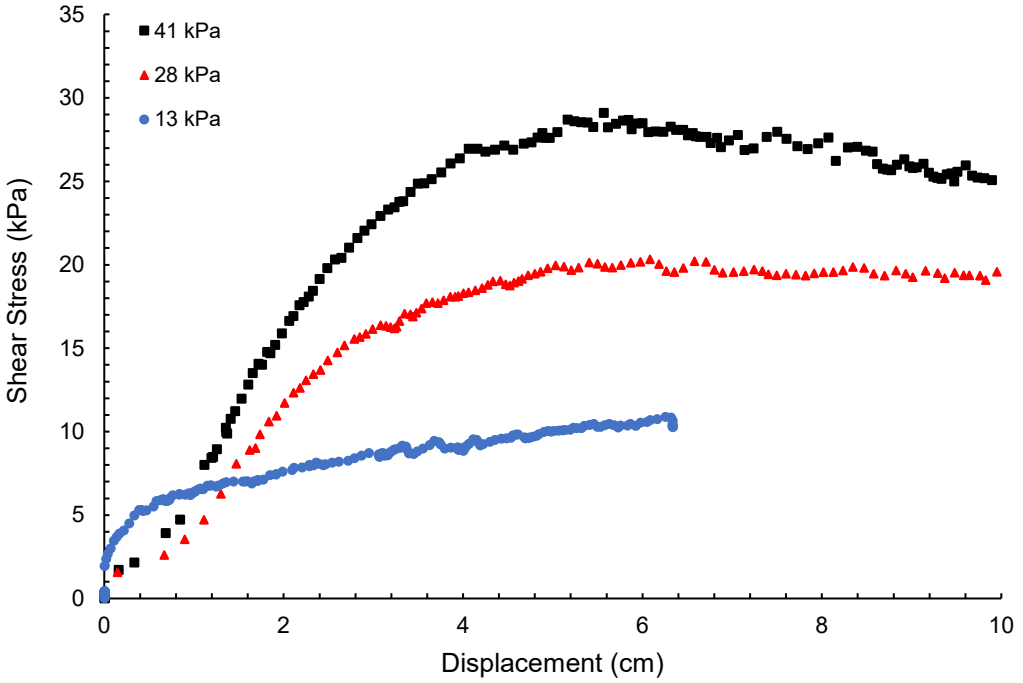

Figure 5.10 GG1 reinforced clay

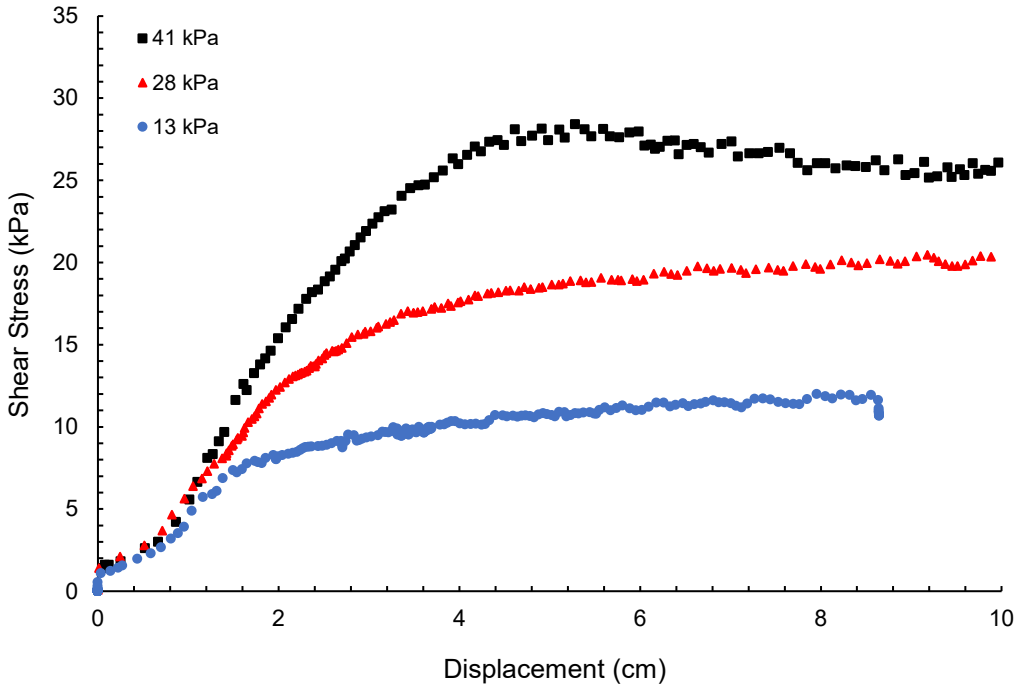

Figure 5.11 GG2 reinforced clay

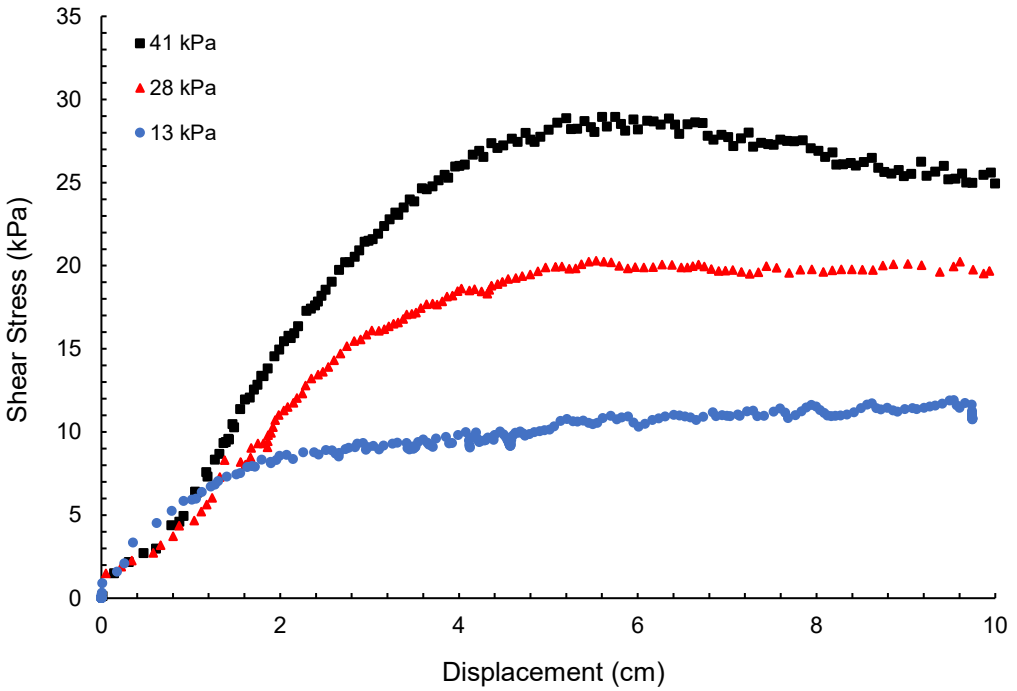

Figure 5.12 GG3 reinforced clay

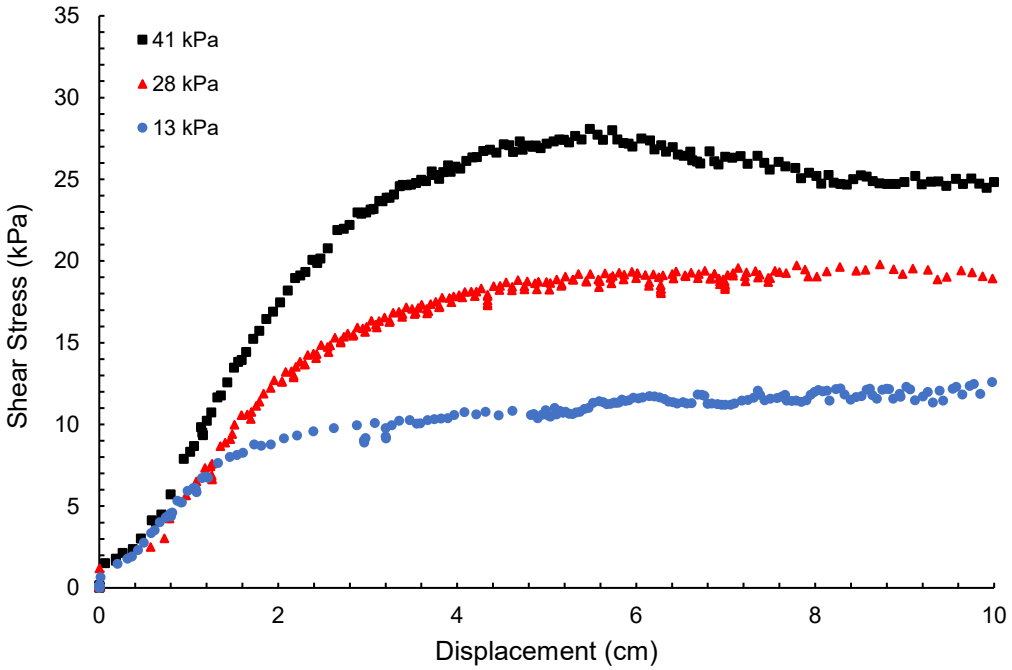

Figure 5.13 GT reinforced clay

Figure 5.14 shows the interface friction angle trendlines for the original clay. The unreinforced case was believed to be run at too high of a pressure for the black line. Its sudden jump in peak shear stress would indicate that the pressure was higher than 41 kPa. If the point was lowered, the trendline would be underneath the other reinforced cases in the Figure 5.14, and it would show the lowest friction angle rather than the highest. Cohesion would also be present. All the other geosynthetics generally show the same friction angle. The biaxial geogrids, GG1 and GG3, show the greatest friction angles. The results for the friction angles can be seen in Table 5.3.

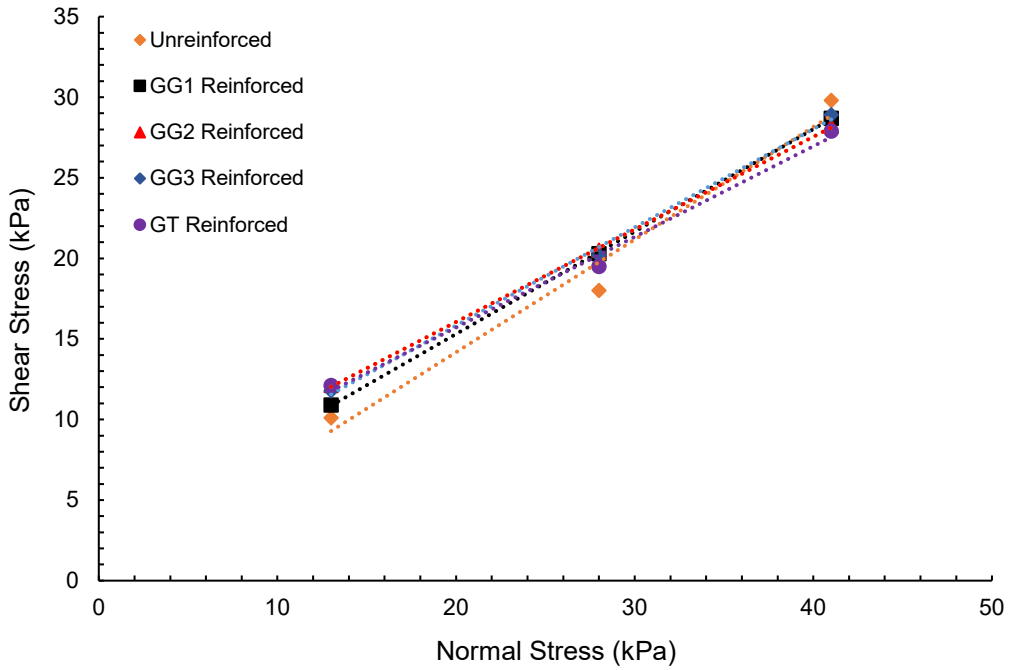

Figure 5.14 Shear stress versus normal stress for original clay

The data shows that the normalized shear resistance decreases as pressure increases, as described in Table 5.4 and Figure 5.15. In the clay case, the geosynthetic reinforced soils showed higher shear stress under both low and medium-range pressures than the unreinforced ones, while they showed lower stress at high pressure. The values for this graph have the tightest accumulation of data. The higher concentration of data indicates that using a certain geosynthetic in clay does not necessarily lead to a significant improvement over another one, as seen in Figure 5.16. This contrasts with the sand because the particles have remarkable resistance and interlocking. Despite a lower friction angle, the GT has the most significant interfacial shear resistance. Presumably, the soil clumps itself together, which results in a more significant interaction of clay soil particles instead of being “sliced” between the apertures. The fine particles do not allow the soil to interlock as well as sand, and they shear more easily.

Table 5.3 Original clay friction angle and cohesion

Original Clay		
Geosynthetic	Friction Angle (°)	Cohesion (kPa)
Unreinforced	35.0	0.19
GG1 Reinforced	32.4	2.60
GG2 Reinforced	29.9	4.56
GG3 Reinforced	31.4	3.64
GT Reinforced	29.4	4.46

Table 5.4 Original clay normalized peak interfacial shear resistance

Geosynthetic	Normal Stress			
	13 kPa	28 kPa	41 kPa	Average
GG1 Reinforced	1.079	1.128	0.963	1.057
GG2 Reinforced	1.198	1.139	0.946	1.094
GG3 Reinforced	1.168	1.122	0.970	1.087
GT Reinforced	1.198	1.083	0.936	1.072

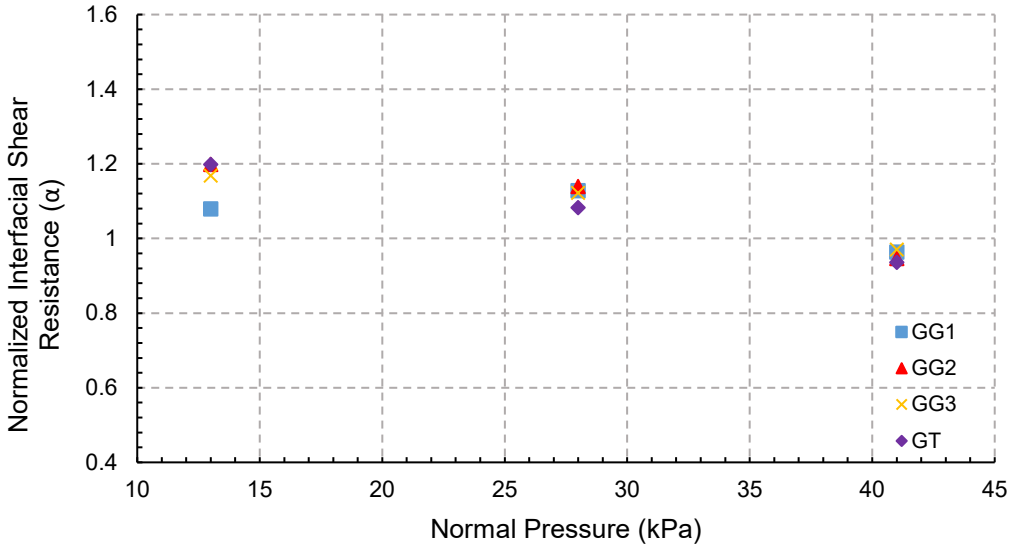

Figure 5.15 Original clay normalized interfacial shear resistance versus normal pressure for all geosynthetic types

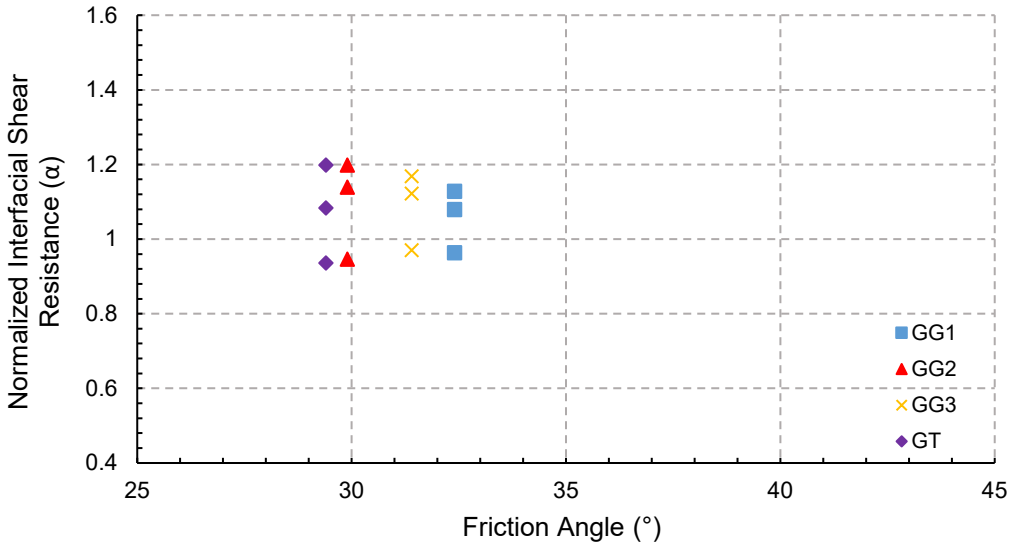

Figure 5.16 Original clay normalized interfacial shear resistance versus friction angle for all geosynthetic types

5.1.3 Repeated Clay Direct Shear Soil Results

The graphs shown for the cases of repeated clay were subjected to three confining pressures. The higher the confining pressure, the higher the shear stress of the graph. The general

shape of these graphs indicated a loose soil compaction, consistent with the 75% desired compaction. The shape of each graph was relatable to the other graphs, but the consistency in how the graphs built into the peak shear stress was a little different as shown in Figure 5.17 through Figure 5.21. It is seen that the higher pressures needed to build into their peaks after a longer amount of displacement. This caused disagreement with the initial modulus between the graphs.

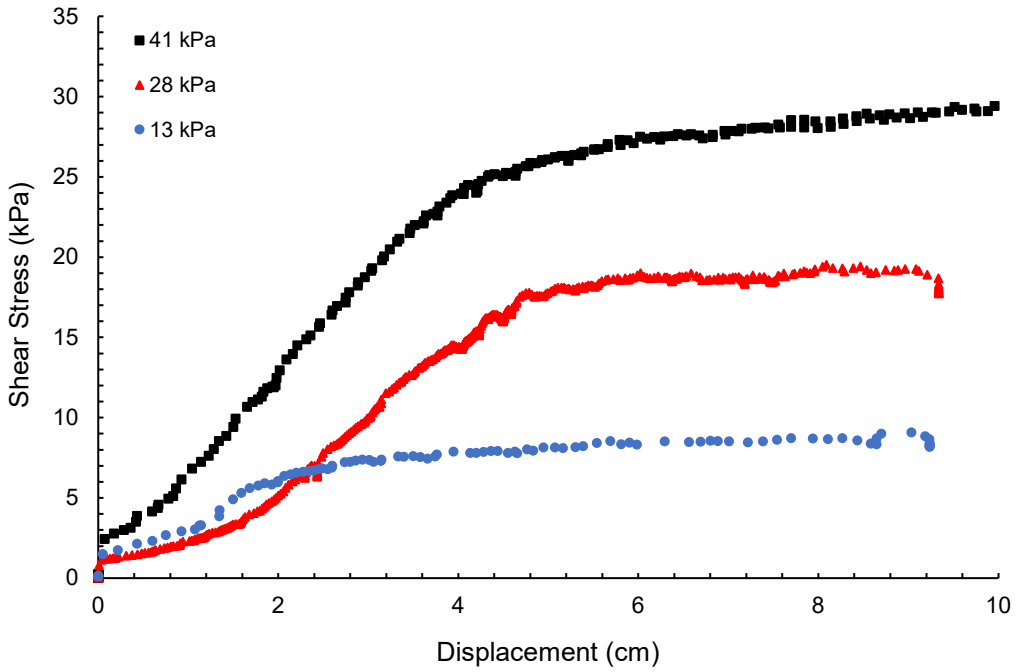

Figure 5.17 Unreinforced repeated clay

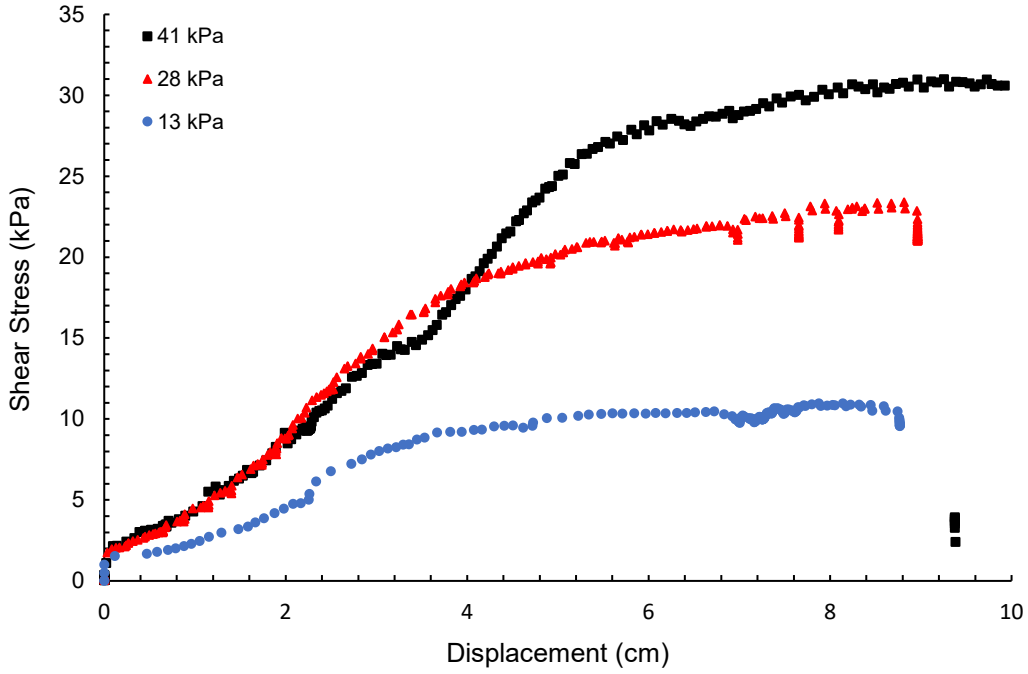

Figure 5.18 GG1 reinforced repeated clay

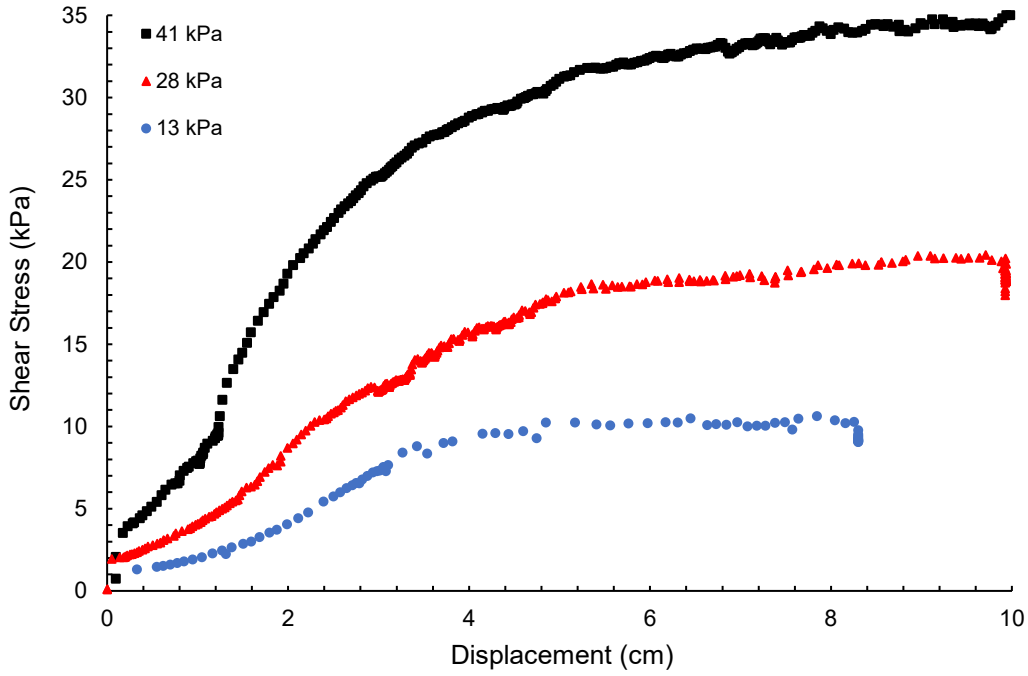

Figure 5.19 GG2 reinforced repeated clay

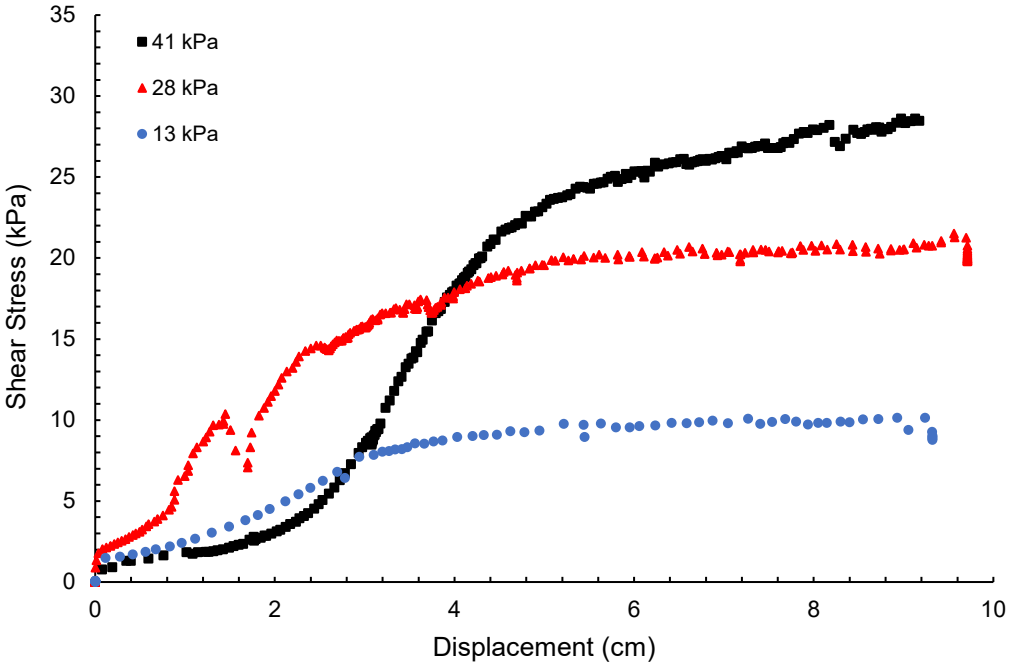

Figure 5.20 GG3 reinforced repeated clay

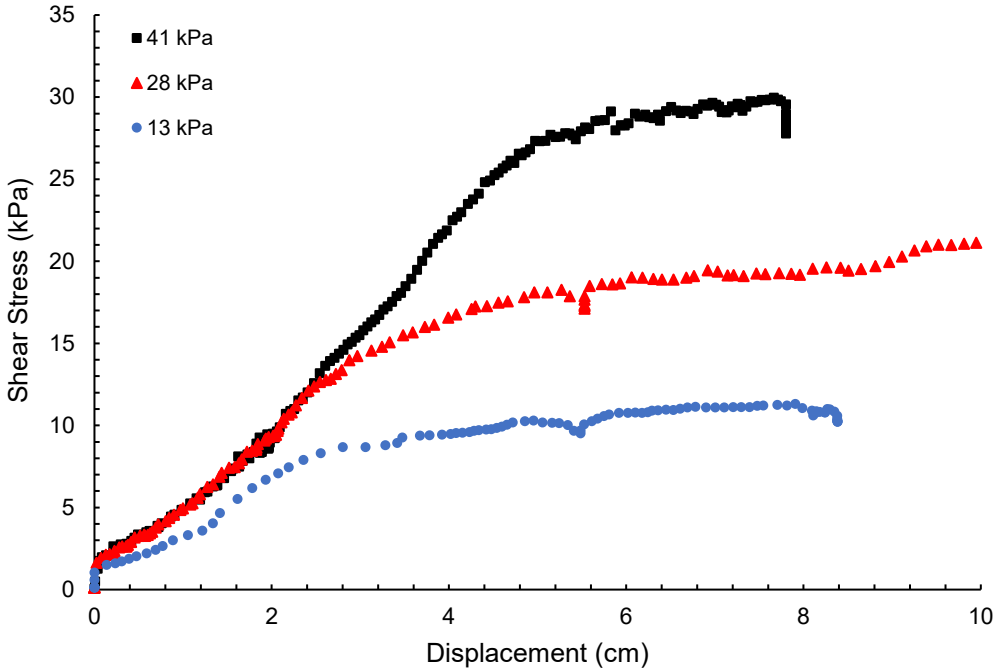

Figure 5.21 GT reinforced repeated clay

Figure 5.22 showed the shear strength versus normal stress to produce the friction angle, just like the original clay. There is one expectation, which is the GG2 trendline. It is believed that the highest-pressure value is an outlier due to such a high peak shear stress. If it were lowered, it would become more consistent with the others and produce a cohesion value. In fact, the GG2 jumps almost five degrees greater than the rest of the data. This is compounded with a 10.8° jump from its original clay value. All the friction angles for the repeated clay were higher than the original clay by an average of 5.2°, or a 3.4° higher friction angle average when excluding the outliered GG2. The results for the friction angles can be seen in Table 5.5.

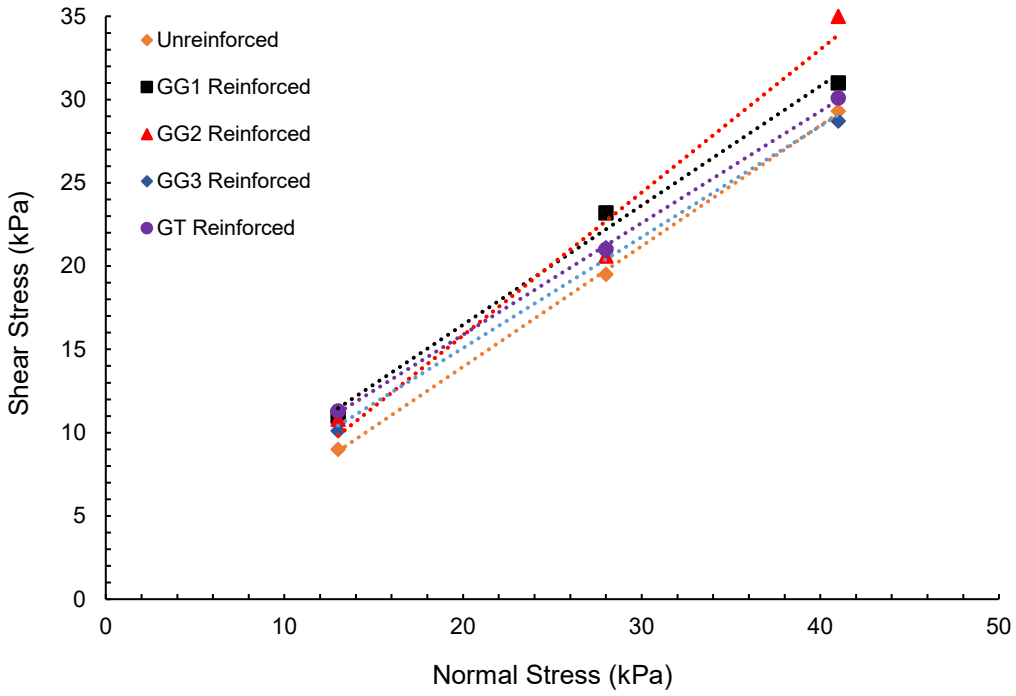

Figure 5.22 Shear stress versus normal stress for repeated clay

For the repeated clay case, it is seen that as pressure increases, the normalized shear resistance decreases. There is no leveling of any geosynthetics. Like the original clay, the graph produces concentrated values. These values are provided in Table 5.6. The clay once again does

well under the lower pressures. Figure 5.23 shows that GG2 under the highest pressure actually increased its normalized shear resistance. It is believed that this is an outlier because the other geosynthetics, including GG2 at 28 kPa, make a continuous decrease. Figure 5.24 further suggests a value that is too high when compared to its neighbors. It is evidenced again as an outlier because of such a high friction angle. One hypothesis for this occurrence is that the direct shear test was run at too high of a confining pressure resulting in a higher peak shear stress. Overall, the repeated clay tests produced higher friction angles than the original clay tests. This was believed to be due in part to an over-consolidation of the clay. The tests for the repeated clay were rerun with the original clay, so therefore the clay had already been subjected to a much higher pressure when it was rerun at the lower pressures. Unfortunately, there was not enough virgin material to be used, and so the same soil was again dried, ground, and prepped for the repeated clay tests. Despite the limitations imposed by the unavailability of virgin material, the congruence between the tests is noteworthy. The dataset exhibits a concentration of values, maintaining consistency within the same range of alpha values for both iterations. At the lower pressures, both clays stayed above 1. At the highest 41 kPa pressure, the geosynthetics floated just above and below 1. The original clay saw the geosynthetics below 1, while the repeated clay saw most of the geosynthetics above 1.

Table 5.5 Repeated clay friction angle and cohesion

Repeated Clay		
Geosynthetic	Friction Angle (°)	Cohesion (kPa)
Unreinforced	35.9	-0.53
GG1 Reinforced	35.6	2.14
GG2 Reinforced	40.7	-1.34
GG3 Reinforced	33.7	1.76
GT Reinforced	33.9	2.46

Table 5.6 Repeated clay normalized peak interfacial shear resistance

Geosynthetic	Normal Stress			
	13 kPa	28 kPa	41 kPa	Average
GG1 Reinforced	1.222	1.190	1.058	1.157
GG2 Reinforced	1.200	1.056	1.195	1.150
GG3 Reinforced	1.122	1.082	0.980	1.061
GT Reinforced	1.256	1.077	1.027	1.120

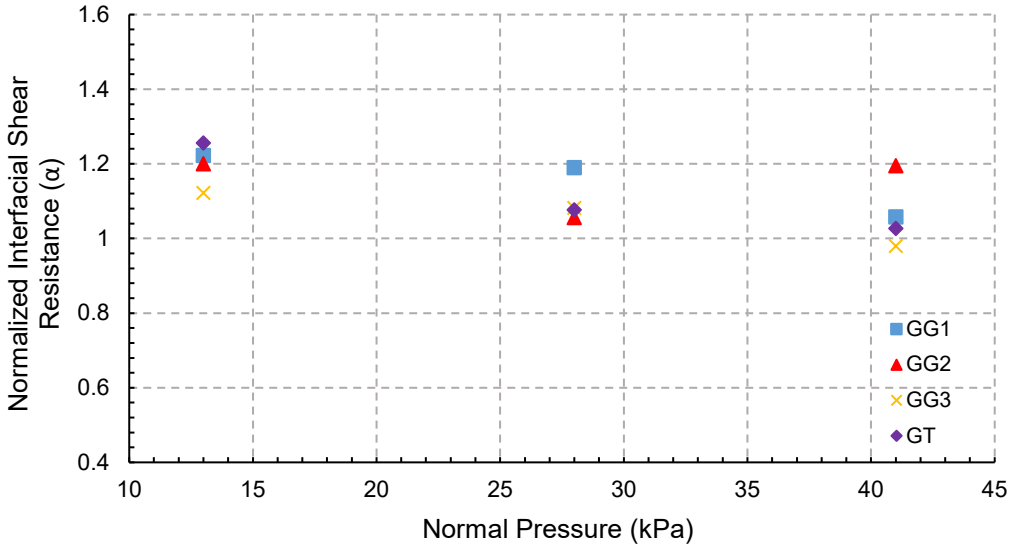

Figure 5.23 Repeated clay normalized interfacial shear resistance versus normal pressure for all geosynthetic types

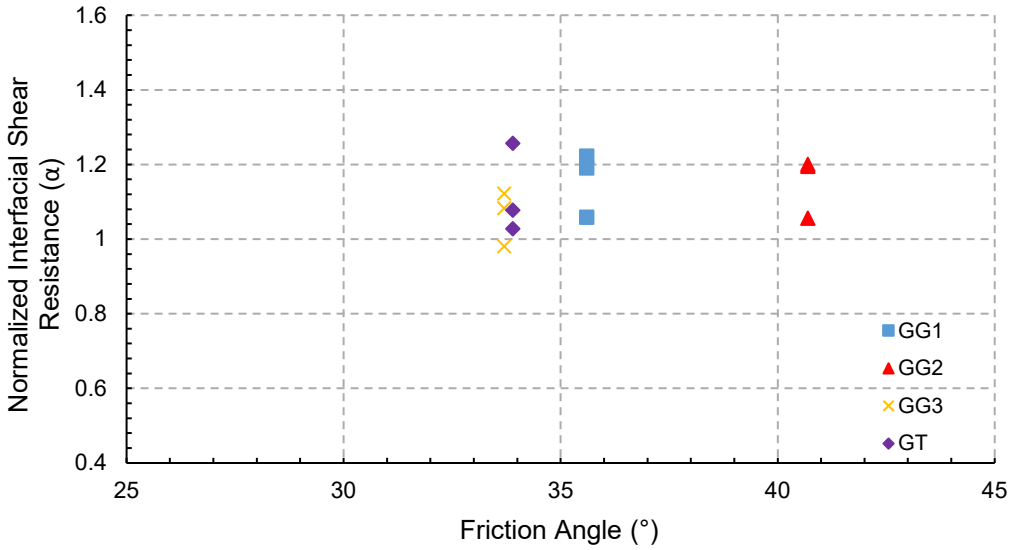

Figure 5.24 Repeated clay normalized interfacial shear resistance versus friction angle for all geosynthetic types

5.1.4 Red Shale Direct Shear Soil Results

The graphs shown for the cases of red shale were subjected to three confining pressures. The higher the confining pressure, the higher the shear stress of the graph. The general shape of

these graphs indicates a loose soil compaction, consistent with the 75% desired compaction. The higher pressures had a gradual build-up to their peaks and then like the lower pressure, had a steady slope shown in Figures 5.25 through 5.29. The 41 kPa confining pressure saw a rise after it leveled out. The shape of each graph is very consistent with one another. The peak shear stresses are generally seen a little later for the highest pressure and sooner for the lowest pressure.

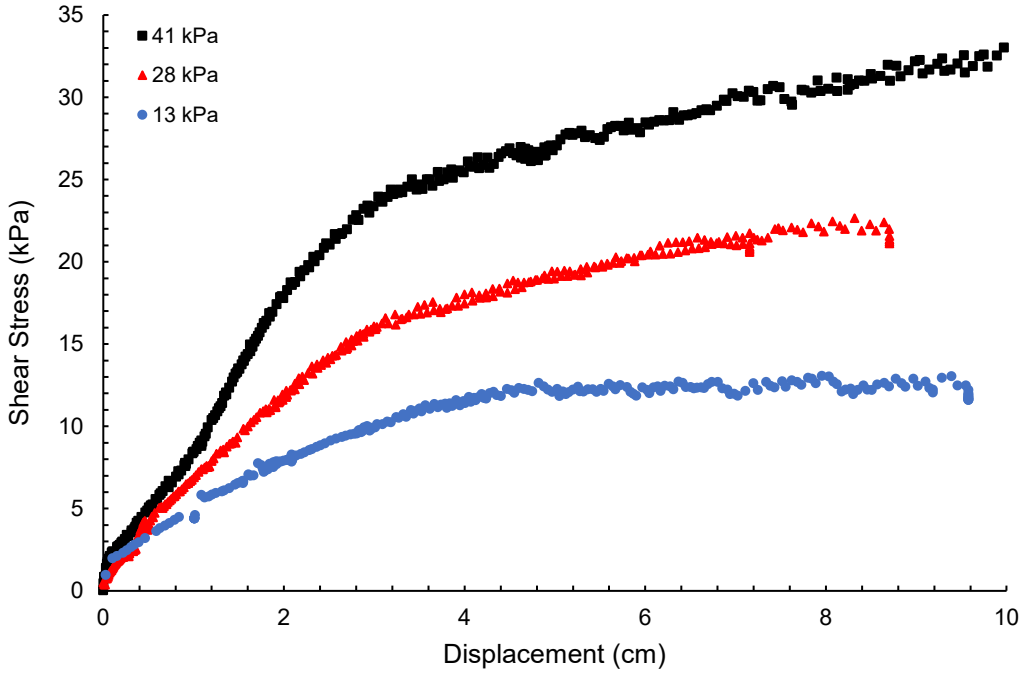

Figure 5.25 Unreinforced red shale

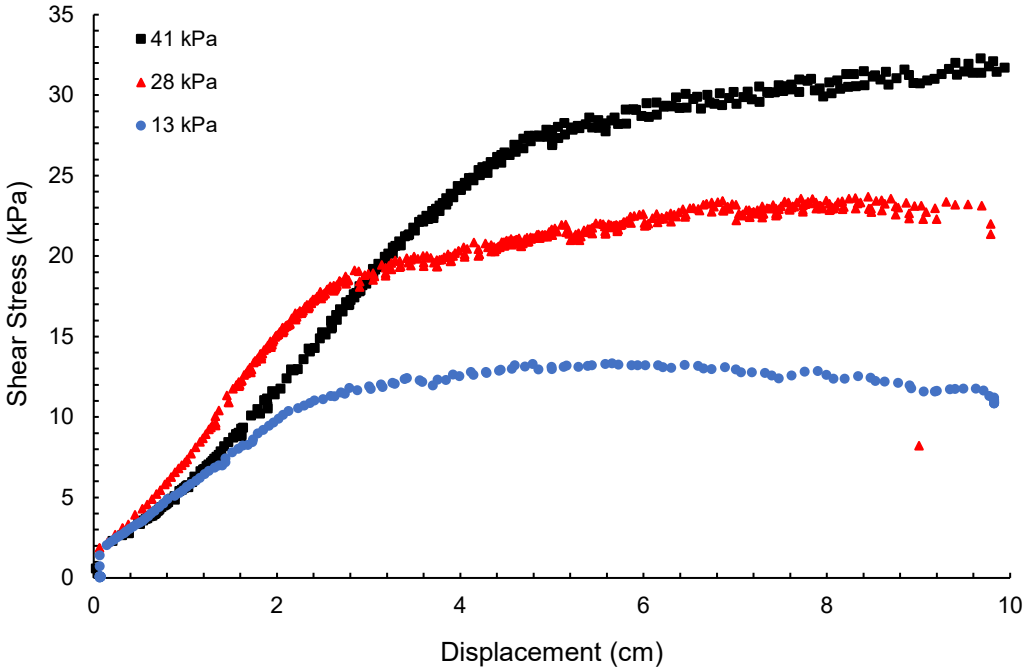

Figure 5.26 GG1 reinforced red shale

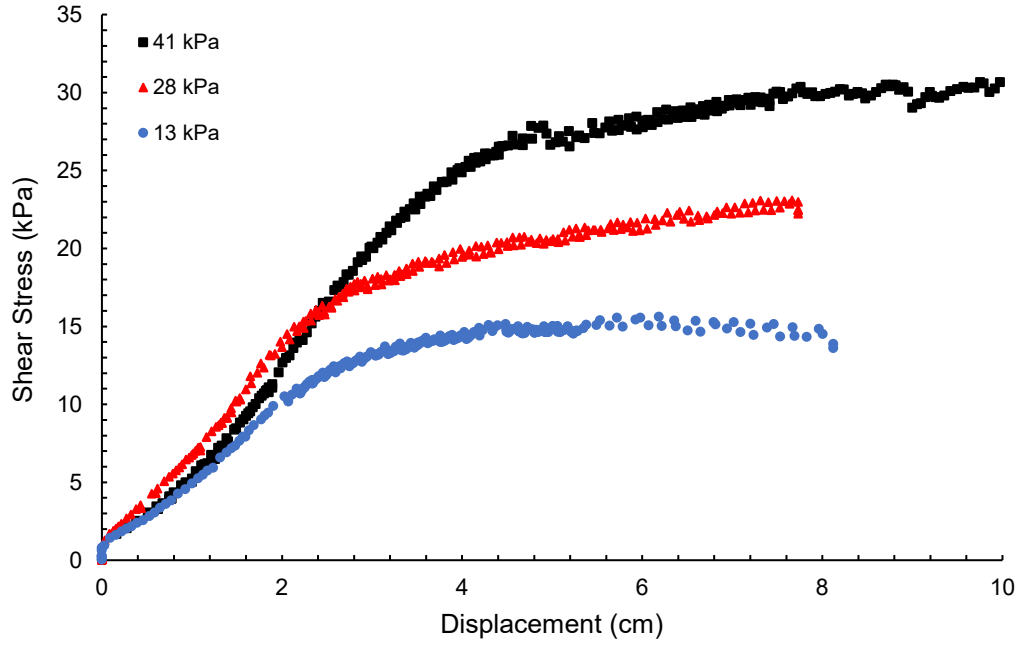

Figure 5.27 GG2 reinforced red shale

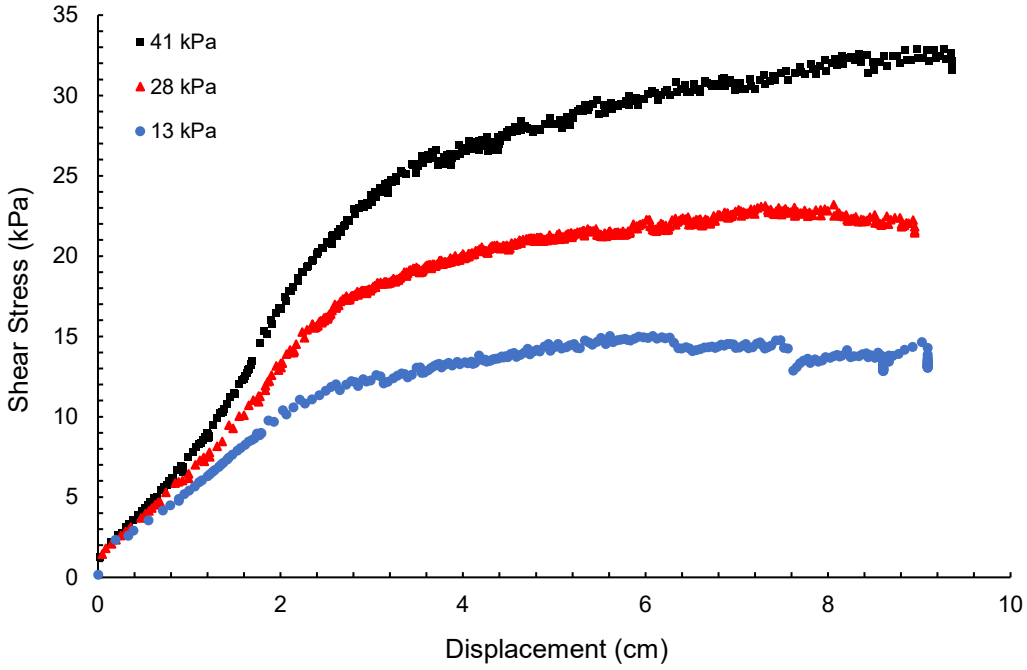

Figure 5.28 GG3 reinforced red shale

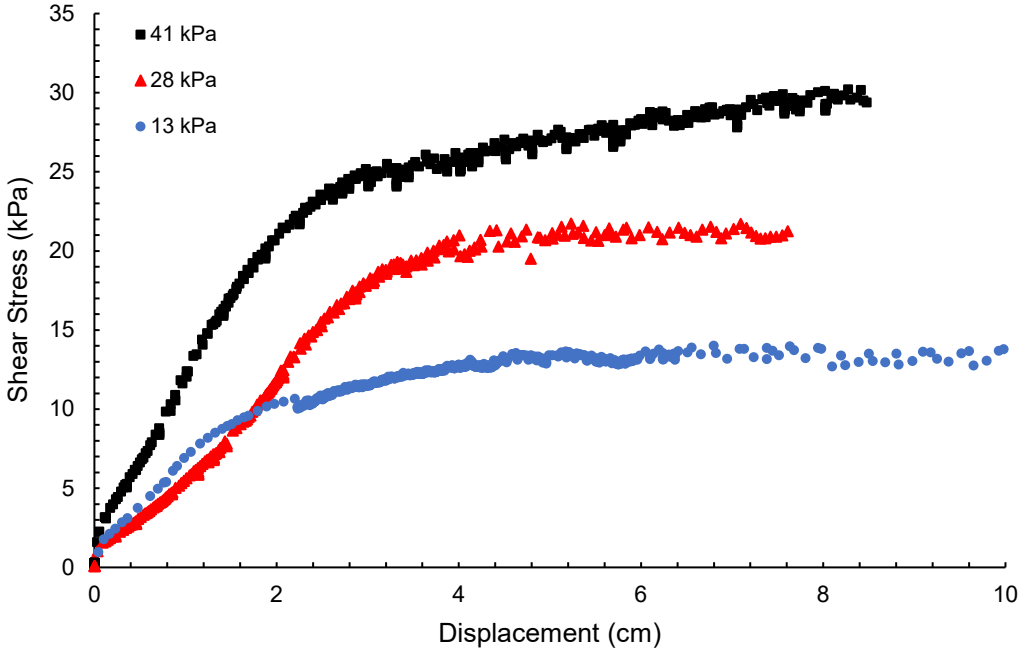

Figure 5.29 GT reinforced red shale

The interface friction angle trendlines are shown in Figure 5.30 below. The unreinforced trendline showed the friction angle is higher, and the cohesion is lower, which makes it inconsistent with the rest of the data. It is not believed to be a fair representation of the data because if the trendline had a less steep slope, it would result in a lower friction angle and a higher cohesion like the rest of the data. GG2 and GG3 show the greatest friction angles for the reinforced trendlines, similar to the sand. The results for the friction angles can be seen in Table 5.7.

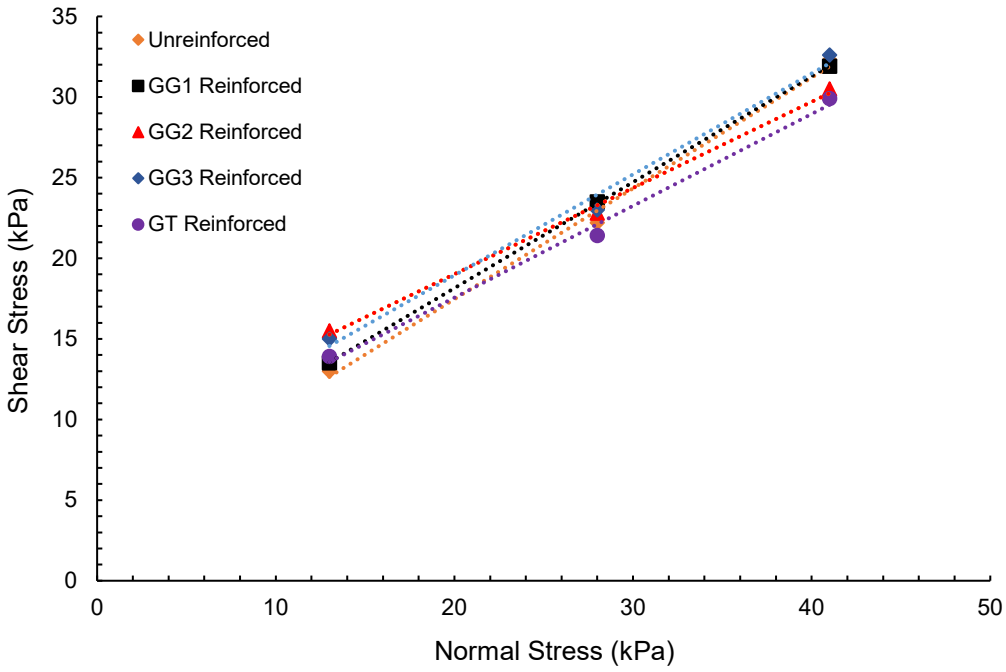

Figure 5.30 Shear stress versus normal stress for red shale

The red shale showed similar trends to the clay. As the pressure increased, the normalized shear resistance also decreased, as indicated in Table 5.8 and shown visually in Figure 5.31. All the geosynthetics stayed above 1 at the lower pressure, but systematically dipped beneath the threshold at the higher pressures. The red shale is a moderate between the two graphs. Sand had

more dispersed data and clay was more concentrated, while red shale was in between, with data not too dispersed and not too concentrated. The red shale is classified as clay, but the soil consistency retains some coarse-grained like properties. It showed the moderation of the other three graphs and rightfully so. Red shale can be seen as a median for both clay and sand. Consequently, the outcomes depicted across all graphs exhibit a considerable degree of mutual congruence. The original clay and red shale both float around the same friction angles and keep each other composed staying around 29° – 32°. They suggested that the repeated clay is probably too high in its friction angles.

Only under lower pressures is the red shale effective for interfacial shear resistance. Every geosynthetic stayed above 1. In the test, the GT was at or near the bottom for all three pressures, leading to the fact that geotextile should not be used with red shale. GG1 fluctuated the most throughout the three pressures. It is believed that it underperformed due to the greater aperture size. GG3 showed consistent results and continually stayed above 1 for all three pressures because it had the smallest aperture size among the three geogrids. Perhaps one of the most interesting conundrums of the red shale testing was the fact that triaxial GG2 had the lowest friction angle, seen in Figure 5.32. However, even with a low friction angle, it still showed the highest normalized interfacial shear resistance at the lowest pressure. To be fair, its values had the greatest rate decrease along the three pressures.

Table 5.7 Red shale friction angle and cohesion

Red Shale		
	Friction Angle (°)	Cohesion (kPa)
Unreinforced	34.5	3.71
GG1 Reinforced	33.3	5.00
GG2 Reinforced	28.1	8.32
GG3 Reinforced	32.1	6.42
GT Reinforced	29.7	6.16

Table 5.8 Red shale normalized peak interfacial shear resistance

Geosynthetic	Normal Stress			
	13 kPa	28 kPa	41 kPa	Average
GG1 Reinforced	1.038	1.059	0.988	1.028
GG2 Reinforced	1.192	1.027	0.944	1.054
GG3 Reinforced	1.154	1.036	1.009	1.066
GT Reinforced	1.069	0.964	0.926	0.986

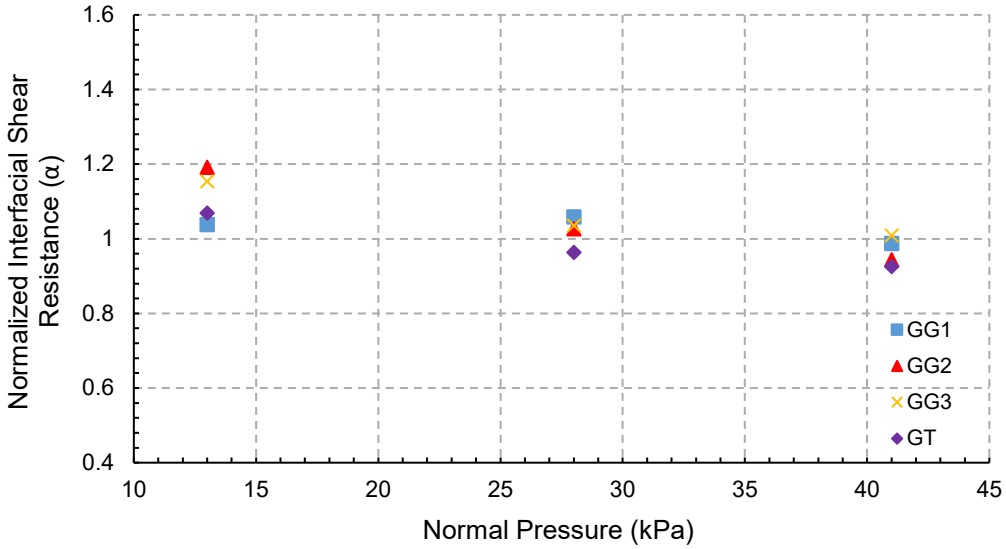

Figure 5.31 Red shale normalized interfacial shear resistance versus normal pressure for all geosynthetic types

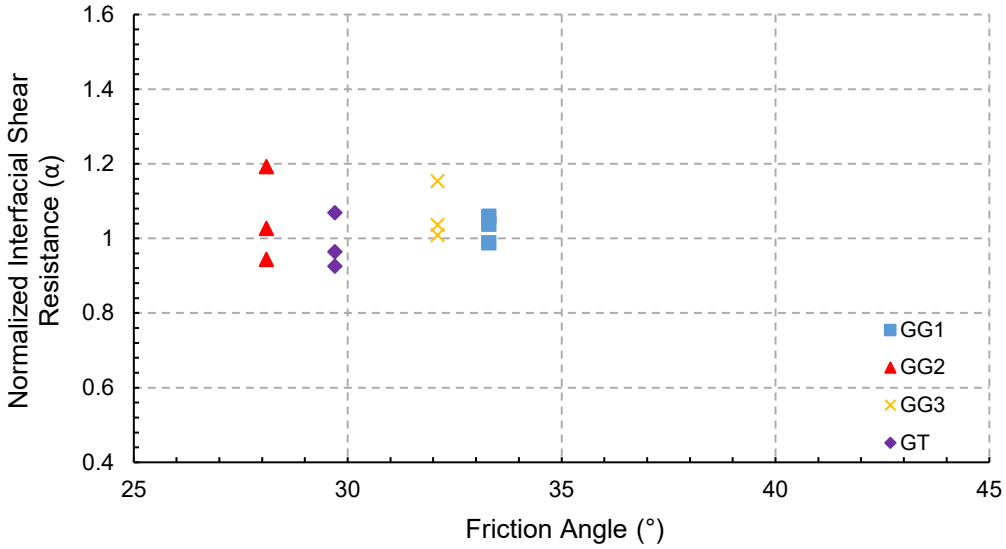

Figure 5.32 Red shale normalized interfacial shear resistance versus friction angle for all geosynthetic types

5.1.5 Overall Direct Shear Analysis

Geosynthetics perform better at lower confining pressures for the clay and red shale. Every geosynthetic, when run under a 13 kPa pressure, saw values above 1 for the normalized

shear resistance. For example, GG2 had a 19.8% increase under 13 kPa pressure for original clay or GG3 had a 15.4% increase under 13 kPa pressure in the red shale. This is compared to GG2 having a 5.4% decrease under 41 kPa pressure for original clay and GG3 having only a 0.9% increase under 41 kPa pressure for red shale. This may be an indication that a geosynthetic should be placed at a shallower depth rather than a deeper one. Geosynthetics may not be as effective in higher pressures because the particle-to-particle interlock is diminished. Sand shows that geosynthetics are better under higher confining pressures rather than low ones. All the geogrids tested proved that frictional resistance is improved under a larger force, presumably due to better interlock between sand particles as opposed to finer particle soils. The geotextile in this study proved that they should not be used with sand because of their low frictional resistance.

Under clay conditions, the friction angle becomes rather irrelevant when determining the best geosynthetic. All the angles were too close together to make an accurate prediction. While there was a high concentration of the friction angles for the clay, the sand shows more dispersed data and how that dispersion could be aptly applied to predict the normalized shear resistance. Clearly with the lowest friction angle, the geotextile performed the worst, whereas GG2 or GG3 performed the best and had the highest friction angles.

When looking at the red shale and clay, it is evident that the type of geosynthetic does not make too much of a difference. GT has the highest values, but not by a large margin. Sand shows more variance. All the geogrids did significantly better than the geotextile, but the smaller aperture-sized geogrids performed best. Therefore, it is important to select the correct size.

The averaged values of the normalized interfacial shear resistance were compared to individual geosynthetic types, and a trend developed showing how virtually all reinforcement helped the soil resistance. Shown in Figure 5.33, GG1, GG2, and GG3 (denoted as 1, 2, and 3)

all stayed above the 1 threshold for any soil type. GT (denoted as 4) was the exception showing a decrease in productivity for sand and red shale. This means that geosynthetics provide improvement for all the clay soils. It also shows, more practically, that any of the geogrids provide improvement. Figure 5.34 shows the friction angle against the geosynthetic type and there was no clear trend.

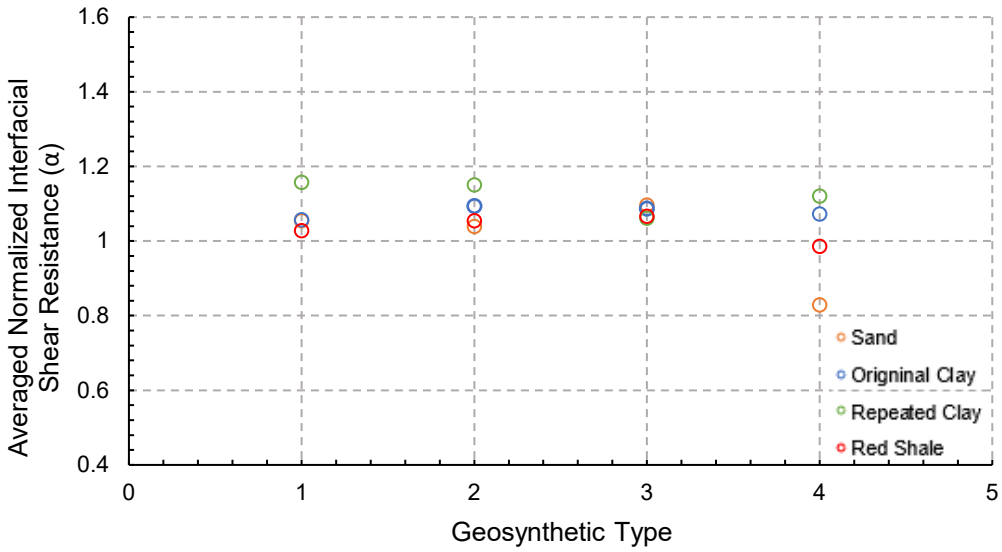

Figure 5.33 Averaged normalized interfacial shear resistance versus geosynthetic types for all soils

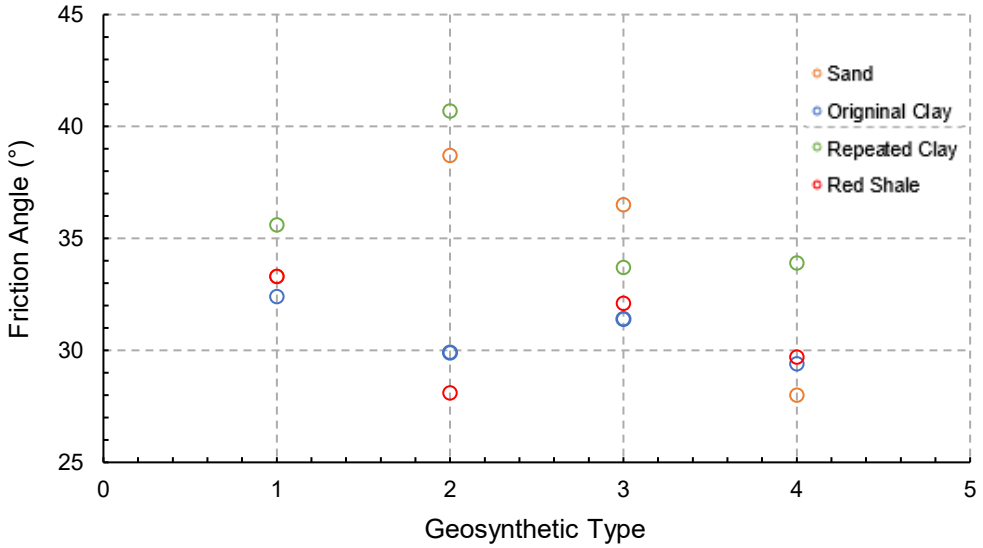

Figure 5.34 Friction angle versus geosynthetic types for all soils

5.2 Large-Scale Pullout Box

The four geosynthetics were tested for the three soil cases. Sand was trialed first under the three confining pressures of 10 kPa, 25 kPa, and 38 kPa. GG1 and GG2 were the only geosynthetics tested with sand. It was determined, further, that the middle confining pressure could be dropped from the pool of tests since the middle pressure was not needed to achieve a steady supply of data, unlike the direct shear where the middle pressure was needed for the friction angle. For the clay and red shale, only two confining pressures of 10 kPa and 38 kPa were tested. The confining pressures for the pullout tests were almost the same as those of the direct shear. Each test was run incrementally, that is, each test was run at the same normal pressure before moving on to the next round of higher pressure. The tests were conducted at optimum moisture content.

Once a test was completed, the initial modulus (or stiffness) of the material was determined. The secant modulus was determined and taken at a 2% displacement of the geosynthetic. This, of course, was at the 2 centimeter mark. The Interaction Ratio, based off the

friction coefficient, was determined. As defined by Ingold (1983), Moraci et al. (2014), and Hegde et al. (2017), the interaction ratio is expressed with maximum pullout resistance per unit width (P_{max}), as

$$C_i = \frac{P_{max}}{2\ l\ \sigma_n\ tan\varphi} \tag{5.2}$$

where l is the length of the embedded geosynthetic, σ_n is the normal force exerted on the specimen, and φ is the friction angle taken from the large-scale direct shear apparatus results. If the graph shows continuous pullout with no residual pullout force, it is recommended by ASTM 6706 that the maximum pullout force be taken at 7.62 centimeters (3 inches). When soil acts on both sides of the geosynthetic, there is a subsequent shear on both sides, but in the same direction. It requires a strong tensile force to take it from the soil. This is known as anchorage reinforcement (Koerner 2005). From the plots, the ultimate pullout resistance can be found for different geosynthetic materials. It was expected that there would be an increase in the pullout resistance with increasing confinement pressure, and the initial (stiffness) modulus would vary between the soil-composite materials and soil type. Stiffness was deemed a more reliable measure of the geosynthetic in pullout due to the tensile nature of the test. The maximum pullout resistance, meanwhile, was not considered for the design criteria of subgrade pavement reinforcement (Abdi and Arjomand 2001, Hatami and Bathurst 2001, Iowa DOT 2015, Rajagopal et al. 2014, and Zheng et al. 2014).

As mentioned earlier, seven linear variable differential transformers were attached to the box, five in the back and two in the front along the hydraulic pistons where they measured pullout displacement. The two front LVDTs were averaged to create the displacement, and

thusly the following graphs show their greater movement. Unfortunately, LVDT 5 was lost during testing. The normal pressure from the pneumatic pistons on top of the tested samples was applied. This pressure was kept on the tested sample for 20 minutes to insure a uniform pressure distribution across the sample and a stable environment before testing. Three tests were conducted under various normal pressures of 10 kPa, 25 kPa, and 38 kPa (i.e., 1.45 psi, 3.60 psi and 5.50 psi), respectively.

Based on the pullout testing results, the Interaction modulus of the material was determined. The secant modulus was determined and taken at a 2% displacement of the geosynthetic. This, of course, was at the 2 centimeter mark. The Interaction Ratio, (WI DOT 2005) is expressed with maximum pullout resistance per unit width (F_p or P_{max}), as

$$M_i = \frac{F_p / W\, L_g}{\Delta_f / L_g} \tag{5.3}$$

where Mi is an interaction modulus (an index of in-situ extensibility), F_p is maximum pullout force, and W is width of the geosynthetic. Δ_f is front displacement of the geosynthetic. According to Figure 5.35, we also determined the initial pullout modulus and secant modulus. The secant modulus can be defined as the slope of plots at a 2% strain level between pullout stress and pullout strain obtained from the pullout test. The initial modulus is defined as the initial slope of plots between pullout force and displacement, which is obtained from the pullout test.

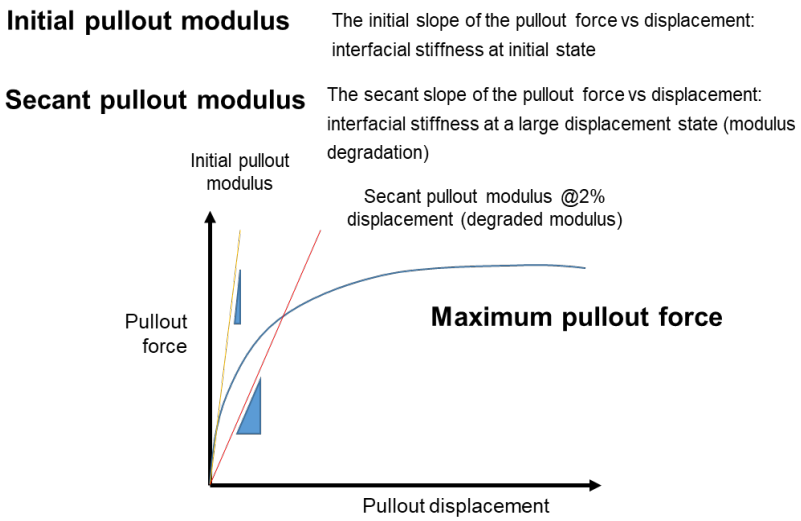

Figure 5.35 Determination of initial pullout modulus and secant pullout modulus

5.2.1 Pullout Repeatability

To ensure the accuracy of the testing equipment, the pullout test was conducted twice in the beginning under 10 kPa confining pressure to check the repeatability of the results as shown in Figure 5.36. It was also coincidentally checked again with GG2 under a 38 kPa confining pressure as shown in Figure 5.70 to verify the Figure 5.67 graph. The two tests show a good agreement in the results. Moreover, the results generally show that maximum pullout forces increase as confining pressure is increased, though it is not necessarily linear.

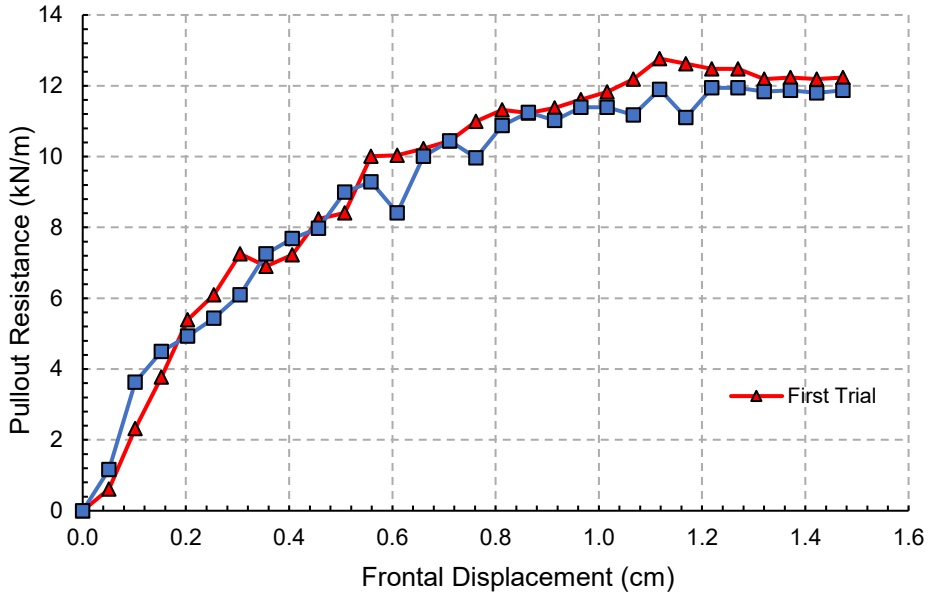

Figure 5.36 Repeatability check under the same confinement pressure of 10 kPa

5.2.2 Reinforced Sand

5.2.2.1 Normal Pressure of 10 kPa

Both GG1 and GG2 experienced a pullout failure represented by a plateau of the data. The graphs in Figure 5.37 and Figure 5.38 show that the sand had a slope that was consistent with a Mohr-Coulomb failure line. The pullout forces increased at a high rate at the beginning of each test and then the rate decreased until there was no change in the pullout force. This indicated that the interface between the geogrid and the soil had yielded. The gradual mobilization of the pullout force across the sample was captured with the internally attached telltales. The telltales closer to the source of the pullout were triggered first and the last telltales to be triggered were the ones that were deeply embedded in the soil. There was good movement of all the LVDTs. The displacements for both GG1 and GG2 ended early due to the residual.

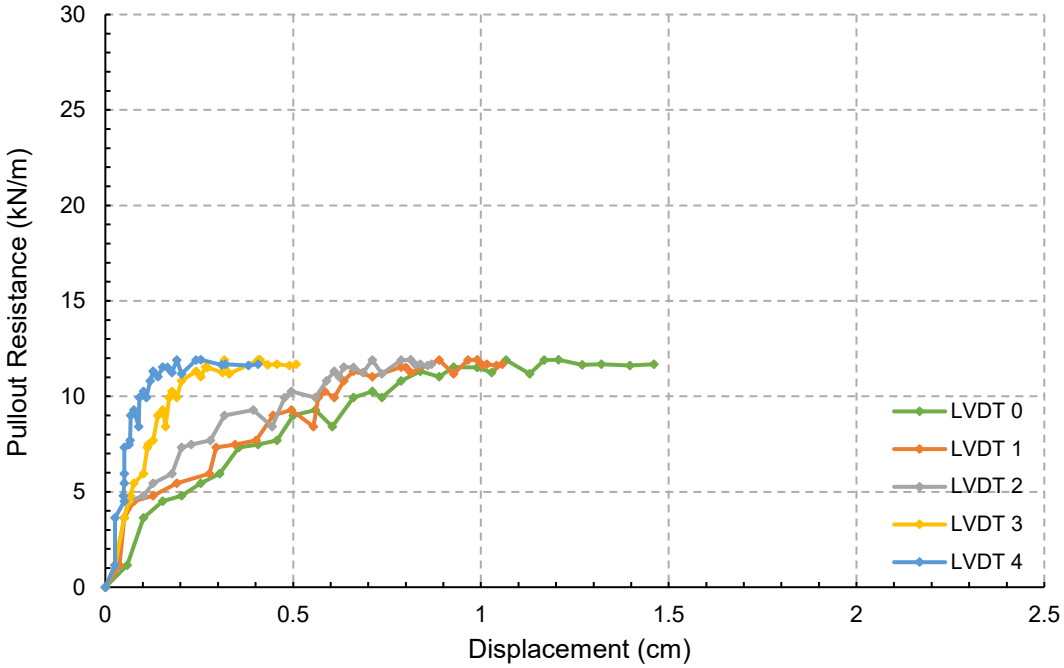

Figure 5.37 GG1 reinforced sand at 10 kPa

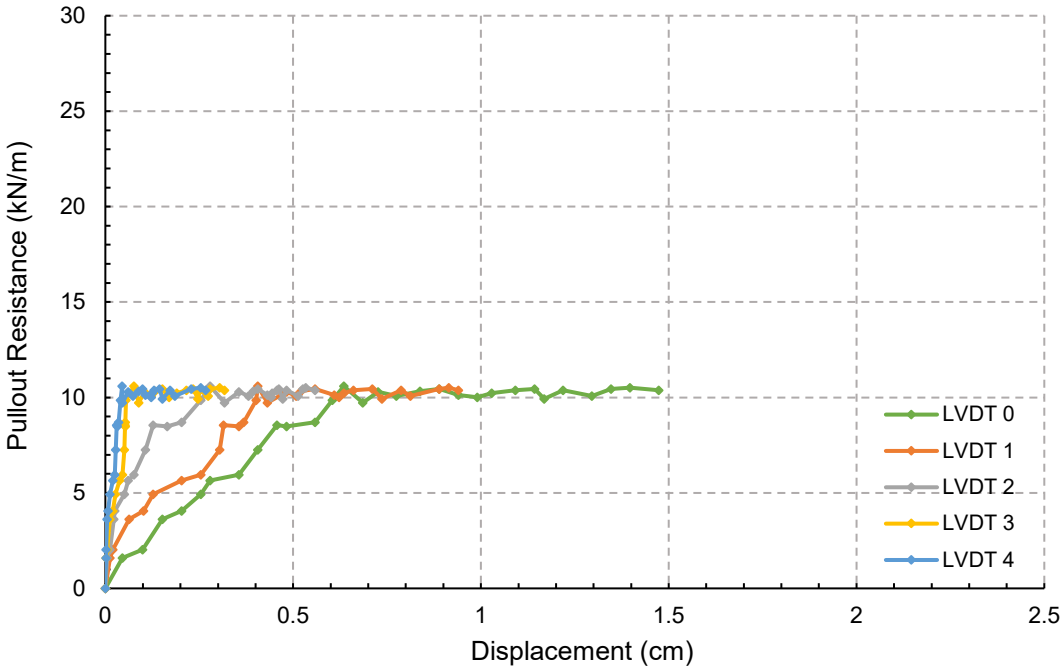

Figure 5.38 GG2 reinforced sand at 10 kPa

5.2.2.2 Normal Pressure of 25 kPa

Both GG1 and GG2 experienced a pullout failure. The graphs in Figure 5.39 and Figure 5.40 show that the sand had a slope that was consistent with a Mohr-Coulomb failure line. The pullout forces increased at a high rate at the beginning of each test which was in attune with the lower pressure. There was an indication that the soil had yielded between the interface with a clear residual line. The gradual mobilization of the pullout force across the sample was captured with the internally attached telltales. The telltales closer to the source of the pullout were triggered first and the last telltales to be triggered were the ones that were deeply embedded in the soil. There was good movement of all the LVDTs. The test ended due to a residual displacement. The biaxial had a greater displacement before the residual took place. The peaks showed significant improvement as pressure increased. The increase in GG1 from 10 kPa to 25 kPa was 95.8%. GG2 increased 119.0% from 10 kPa to 25 kPa.

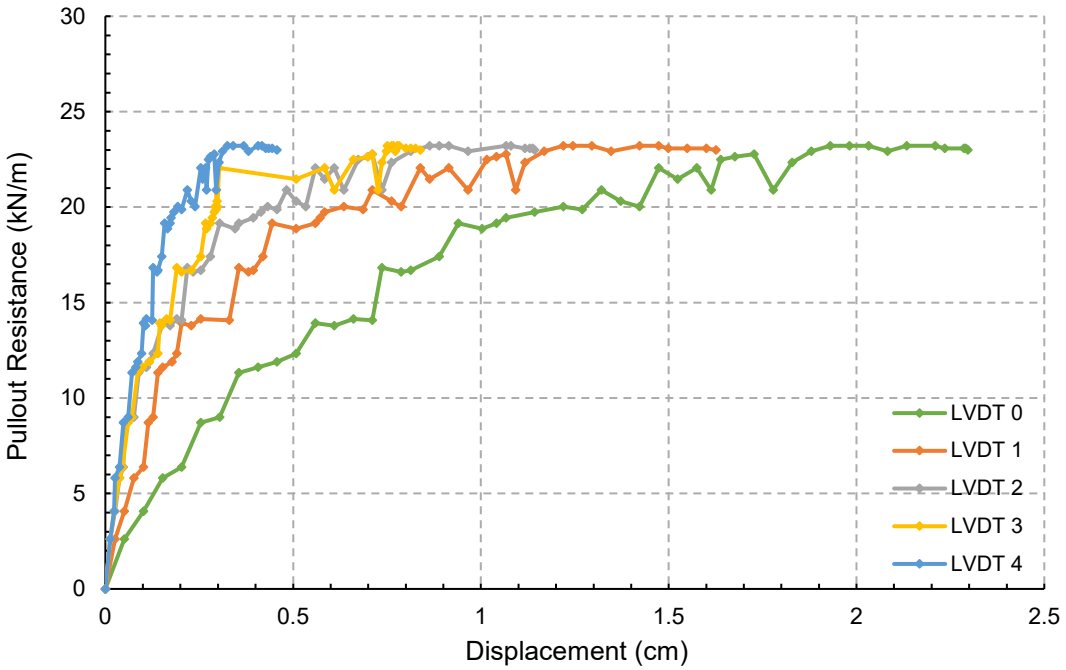

Figure 5.39 GG1 reinforced sand at 25 kPa

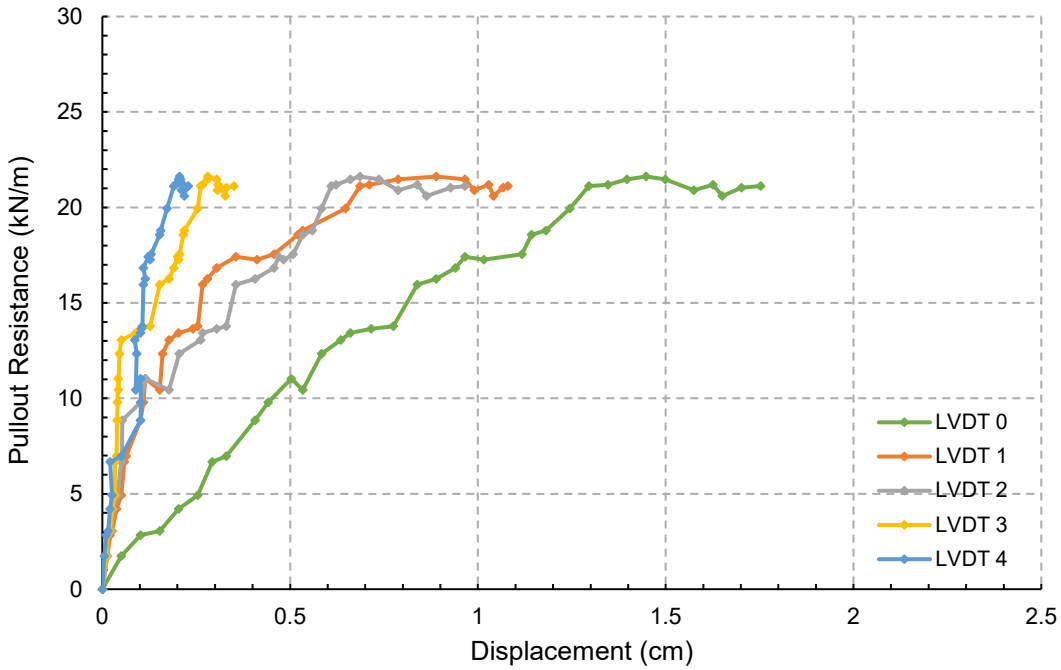

Figure 5.40 GG2 reinforced sand at 25 kPa

5.2.2.3 Normal Pressure of 38 kPa

Both GG1 and GG2 experienced a pullout failure. The graph in Figure 5.41 and Figure 5.42 show that the sand had a slope that was consistent with a Mohr-Coulomb failure line. The pullout force for GG1 increased to the highest peak of all the sand tests. The rate leveled out until there was no change in the pullout force. This indicated that the interface between the geogrid and the soil had yielded. The gradual mobilization of the pullout force across the sample was captured with the internally attached telltales. From the data, the telltales closer to the source of the pullout were triggered first and the last telltales to be triggered were the ones that were deeply embedded in the soil. There was good movement of all the LVDTs. The test ended early due to the residual displacement. The peaks showed improvement as pressure increased. The increase of GG1 from 25 kPa to 38 kPa was 21.3%. GG2 increased 13.6% from 25 kPa to 38 kPa.

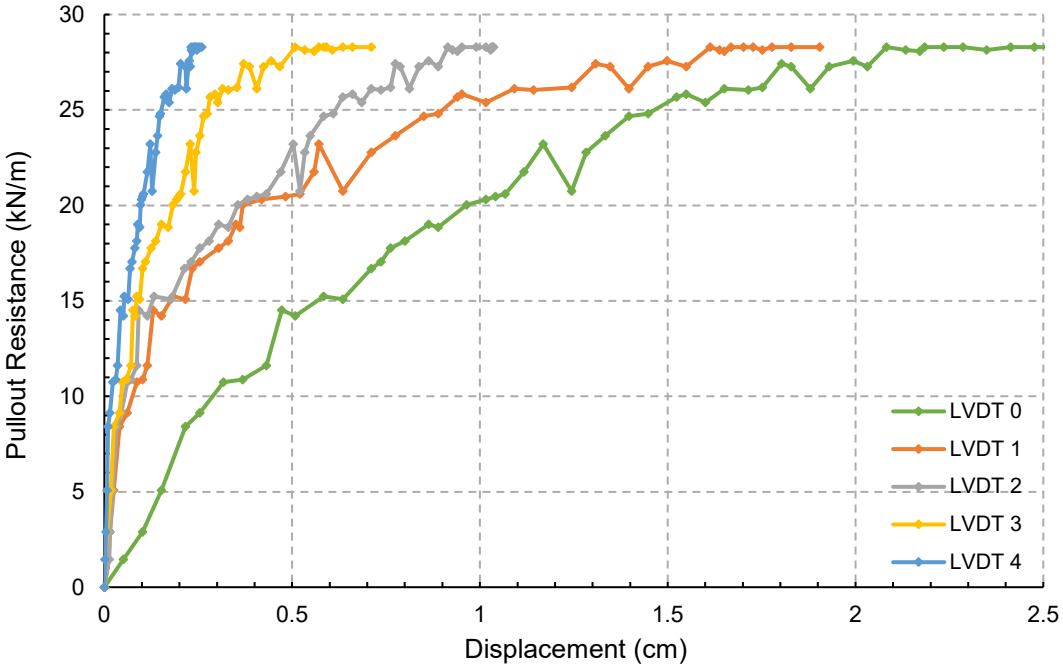

Figure 5.41 GG1 reinforced sand at 38 kPa

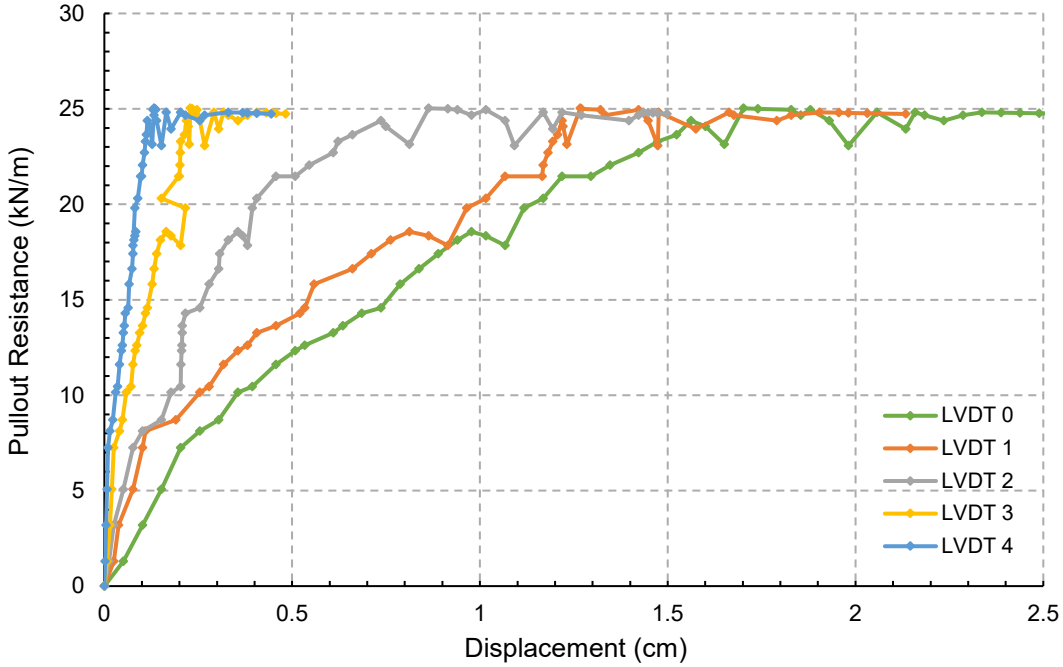

Figure 5.42 GG2 reinforced sand at 38 kPa

The initial modulus and secant modulus reflected the data quite well in Table 5.9. The sand provided the highest initial modulus and secant modulus values. This is because sand can interlock better than clay. Sand produces higher peak values than clay or red shale and reaches its peak values much quicker than the clay or red shale. It also has a more defined residual. There is one instance, for reinforced clay at 10 kPa confining pressure, where the peak value is not higher for sand. However, with sand, the rate of increase in pullout resistance is greater as confining pressure gets higher. This would indicate that not only is sand more useful at higher pressure, but it also is still valuable at lower pressures. This phenomenon is also reflected in the direct shear tests with the interfacial shear resistance value. However, while GG1 showed a high modulus that was higher than both clay and red shale, GG2 had a lower modulus by 15.0% on average as compared to GG1. Figure 5.43 and Figure 5.44 show the geosynthetic difference in initial modulus. The secant modulus, depicted in Table 5.10, was also higher than the clay or red shale, but its values were not as domineering as the initial modulus. Not all secant values were able to be recorded. Figure 5.45 and Figure 5.46 show the results. The friction angle might suggest that the higher it is, the lower the modulus would be. However, the interaction ratio was small for all three pressures. Thus, the values are significantly lower because their values at the lower pressures were smaller than the other soils. Its rate of decrease was not as rapid as either the clay or red shale, though. The results are depicted in Table 5.11 and Figure 5.47 and Figure 5.48. The interaction ratio shows that both geogrids are better at the lower pressures.

Table 5.9 Initial modulus (kPa) for sand pullout testing.Initial modulus (kPa) for sand pullout testing

Sand			
Geosynthetic	Normal Stress		
	10 kPa	25 kPa	38 kPa
GG1 Reinforced	2200	3000	3300
GG2 Reinforced	2000	2200	3000

Table 5.10 Secant modulus (kPa) at 2% for sand pullout testing

Sand			
Geosynthetic	Normal Stress		
	10 kPa	25 kPa	38 kPa
GG1 Reinforced	-	1150	1375
GG2 Reinforced	-	-	1200

Table 5.11 Interaction ratio (Ci) for sand pullout testing

Sand			
Geosynthetic	Normal Stress		
	10 kPa	25 kPa	38 kPa
GG1 Reinforced	0.913	0.706	0.571
GG2 Reinforced	0.655	0.549	0.411

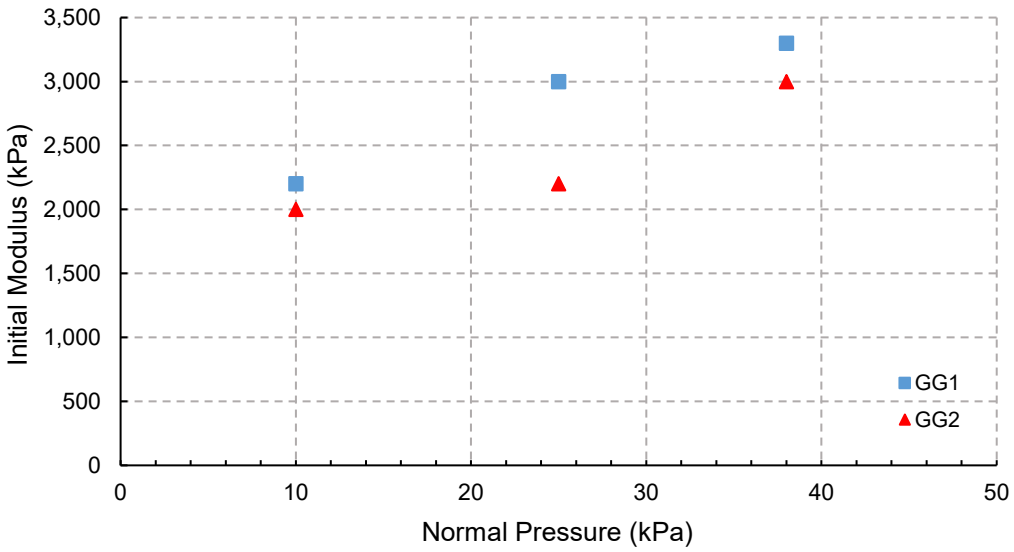

Figure 5.43 Sand initial modulus versus normal pressure for GG1 and GG2

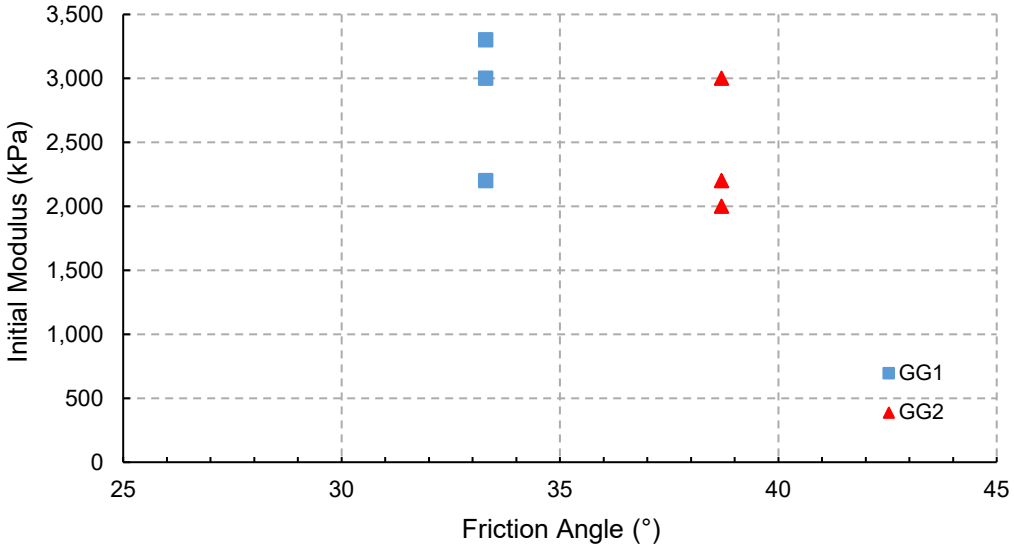

Figure 5.44 Sand initial modulus versus friction angle for GG1 and GG2

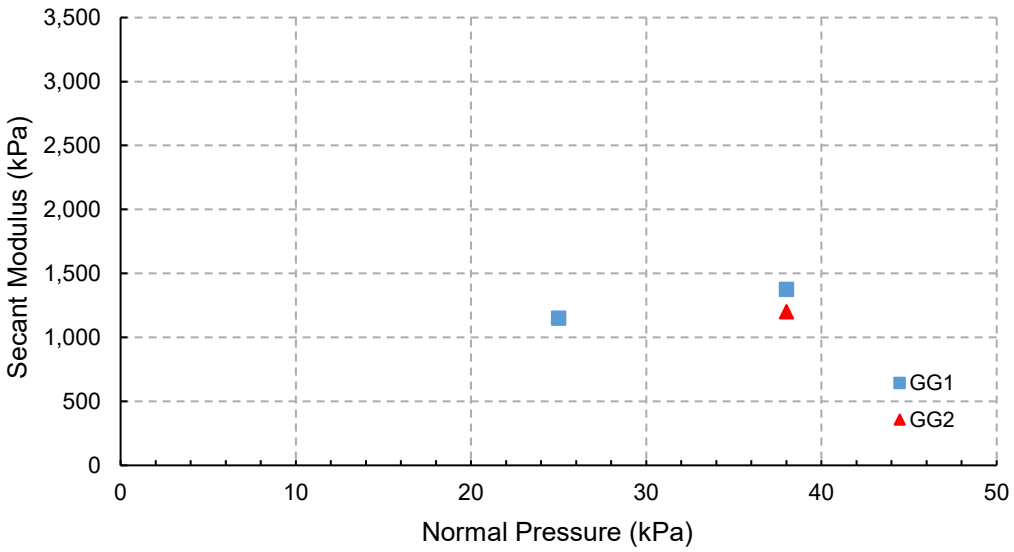

Figure 5.45 Sand secant modulus versus normal pressure for GG1 and GG2

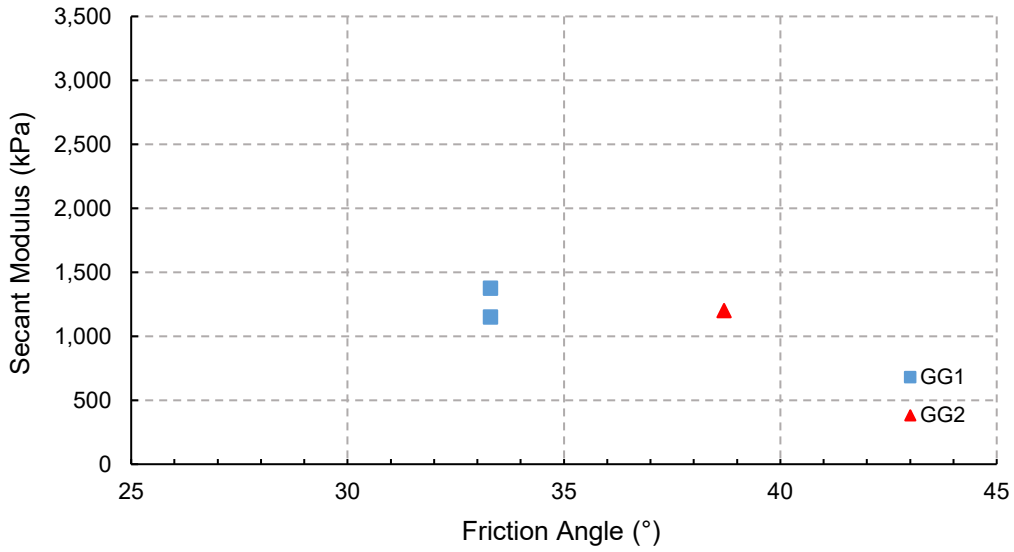

Figure 5.46 Sand secant modulus versus friction angle for GG1 and GG2

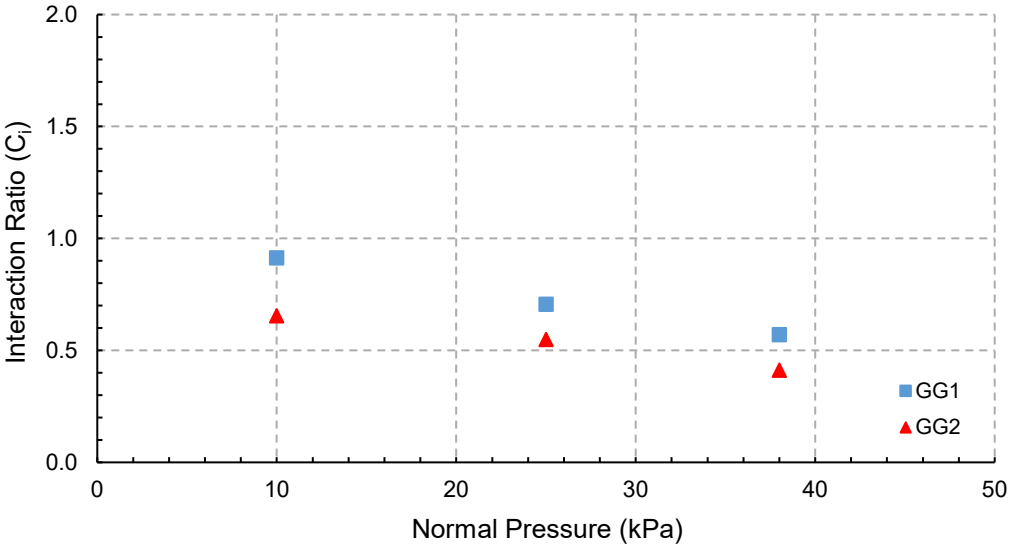

Figure 5.47 Sand interaction ratio versus normal pressure for GG1 and GG2

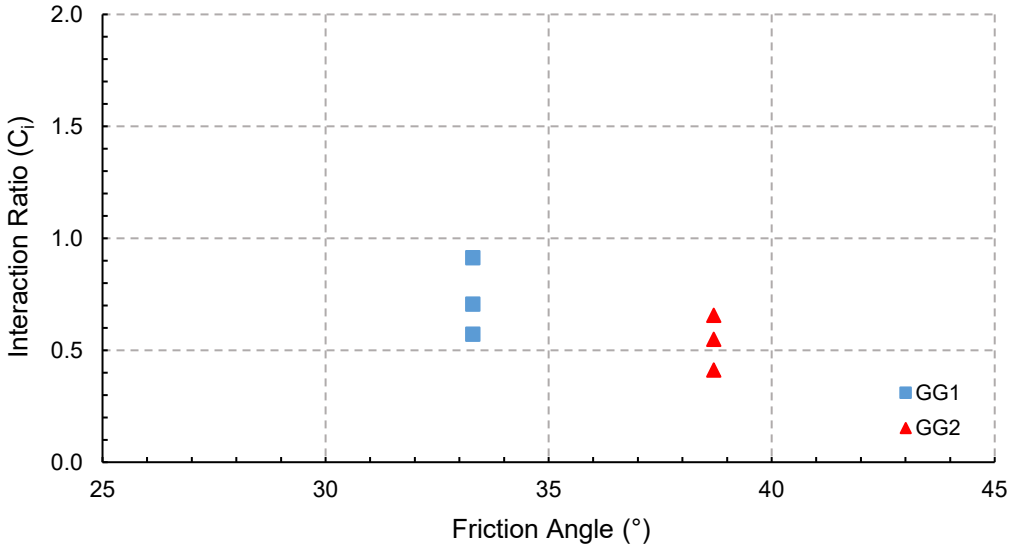

Figure 5.48 Sand interaction ratio versus friction angle for GG1 and GG2

5.2.3 Reinforced Clay

5.2.3.1 Normal Pressure of 10 kPa

The graphs shown in Figure 5.49 through Figure 5.52 indicated a low rate of increase for the pullout. The residual line was more apparent for GG1, GG3, and GT because they had

pullout failures. They all showed gradual displacements ending around 8 centimeters. The peaks of these three graphs were remarkably similar, peaking around 15 kN/m pullout resistance. There were no ruptures, though GG1 had a fracture in two of its apertures. The test continued to run since this did not qualify as a rupture. The LVDTs moved with the geosynthetics. The LVDTs also moved together rather than one at a time in gradual succession, as evidenced by Roodi (2016) or as the previous reinforced sand case. Still, it took time for the LVDTs to activate. GG2 resulted in a rupture. Its modulus at 1 centimeter was similar to the other graphs, but it did not show a residual in the pullout resistance, but rather a steady rise until the geosynthetic abruptly snapped.

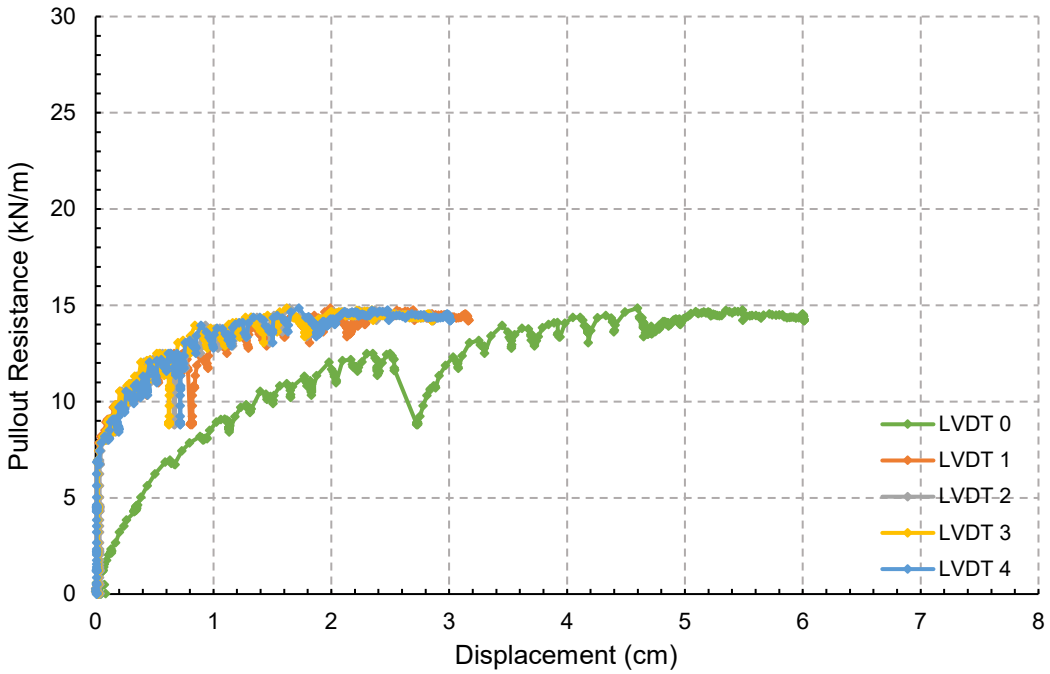

Figure 5.49 GG1 reinforced clay at 10 kPa

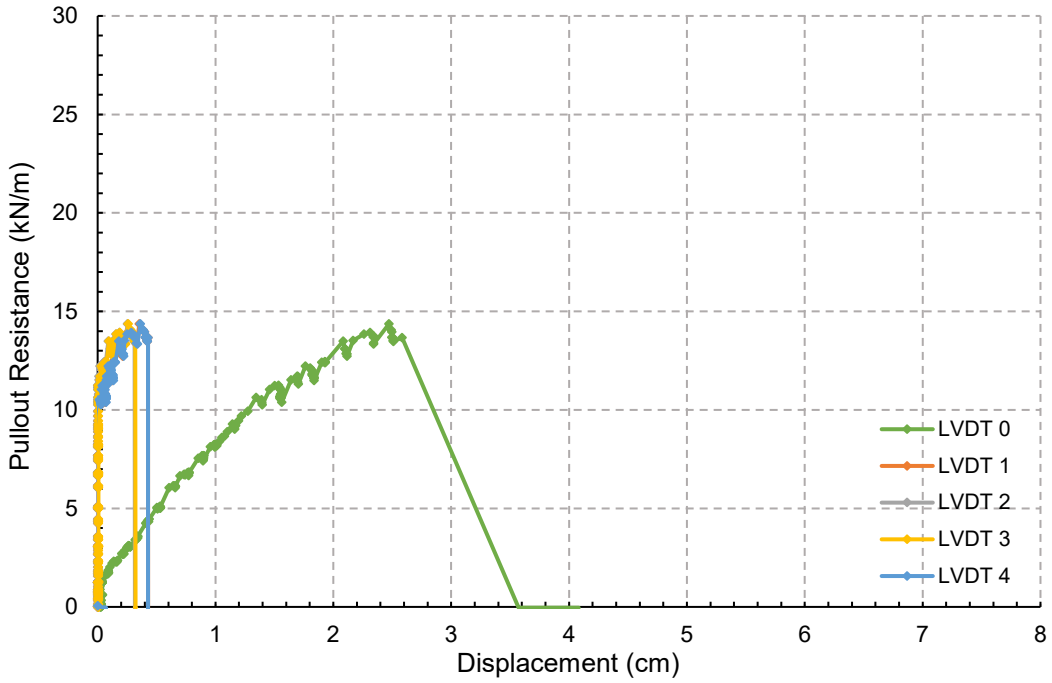

Figure 5.50 GG2 reinforced clay at 10 kPa

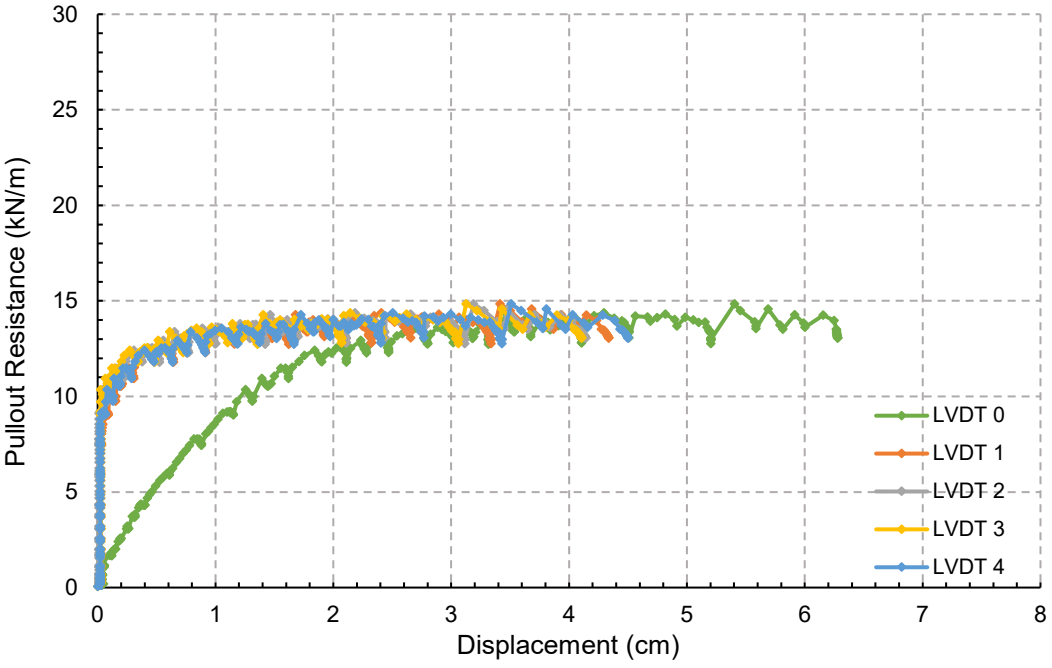

Figure 5.51 GG3 reinforced clay at 10 kPa

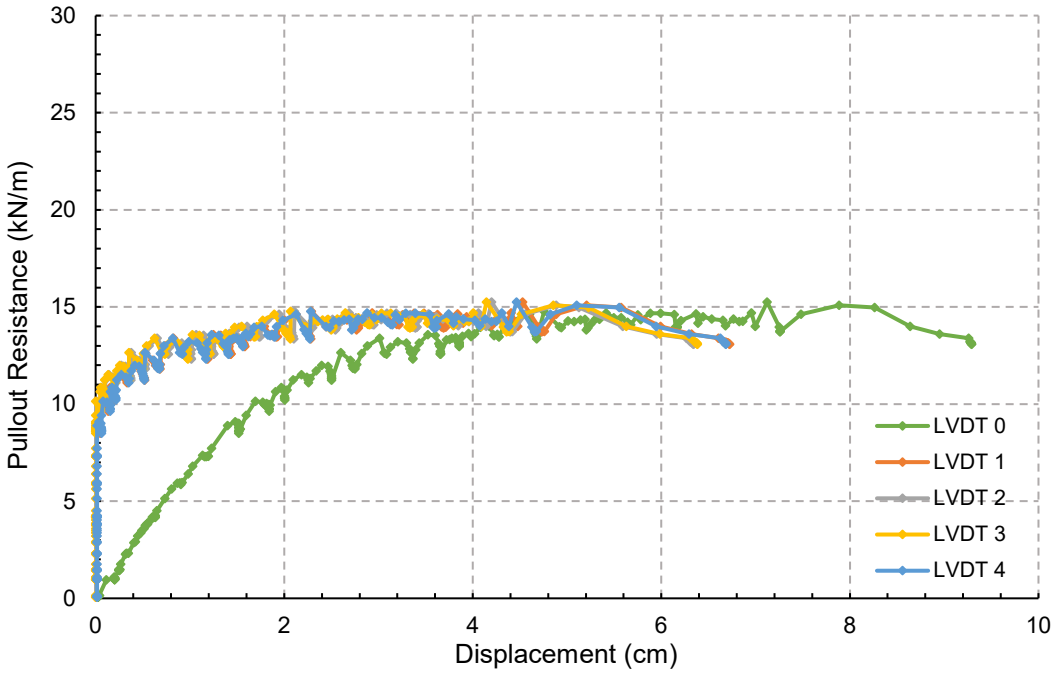

Figure 5.52 GT reinforced clay at 10 kPa

5.2.3.2 Normal Pressure of 38 kPa

At higher pressures, all four geosynthetics ruptured, which means the pullout behavior of the reinforcement was not fully developed and the pullout force and displacement curves were not observed, as shown in Figure 5.53 through Figure 5.56. The three geogrids ruptured quite suddenly and completely. There is a noise that is made beforehand when the geosynthetic is about to rupture, similar to crackling. This is the only indication that rupture is about to occur. GT had more of a pullout-rupture combination in that it was pulled until the stitching gradually came apart. It was still strong enough to be ejected from the box as it tore. This is why Figure 5.56 shows a smaller dip and a greater displacement than the rest. Further, it showed improvement in pullout resistance versus its lower pressure with 18.0 kN/m, resulting in a 21.6% overall increase. The two biaxial geogrids saw the most significant pullout resistance values, around 21.8 kN/m. Their overall improvement was roughly 45.3% and 46.1%, respectively. This

is compared to GG2, which witnessed a 12.9 kN/m pullout resistance. Not only was this smaller than either of the biaxial, but this was also smaller than the geotextile and a 12.8% decrease compared to its lower confining pressure. The confining pressure is too high for GG2, as evidenced further by the lack of LVDT movement. This is true of all cases. Since none of the LVDTs moved, all of the resistance was in the frontal portion of the embedded geosynthetic. This small area deformed while the rest of the embedded area did not displace or deform.

Figure 5.53 GG1 reinforced clay at 38 kPa

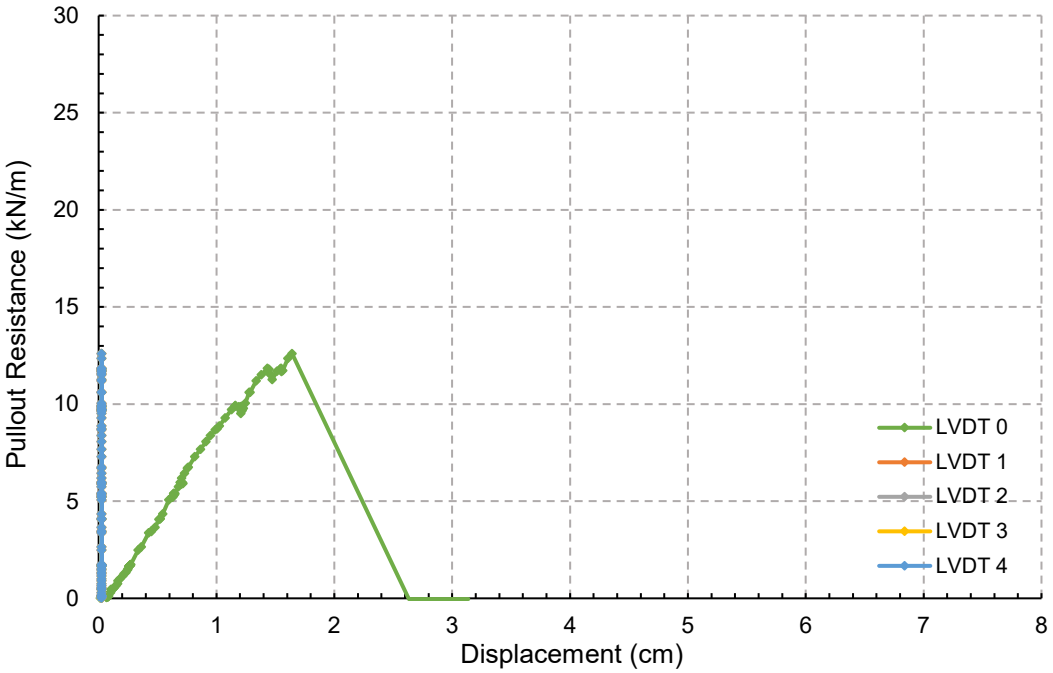

Figure 5.54 GG2 reinforced clay at 38 kPa

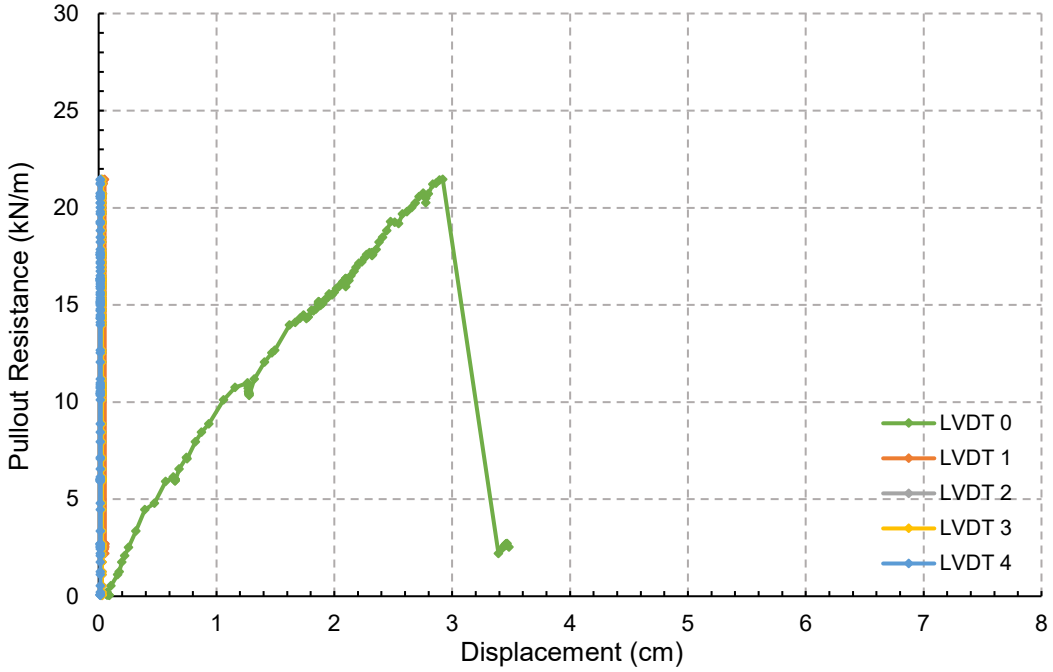

Figure 5.55 GG3 reinforced clay at 38 kPa

Figure 5.56 GT reinforced clay at 38 kPa

The initial modulus of these geosynthetics reflects the data quite well. Of course, the modulus was taken from the data, but the point being that as higher normal stress increased from 10 kPa to 38 kPa, so did the initial modulus of the geosynthetic, as indicated in Table 5.12. This is true of all cases, save GG2 where the initial modulus stayed the same. Figure 5.57 also supports this theory from a graphical perspective. GG1, GG3, and GT see an averaged 32.0% gradual rise in initial modulus. This is coupled with the secant modulus, depicted in Table 5.13, where again there is a steady rise in value except for GG2. It was unable to be computed, but its trend suggested a similar number to the 10 kPa confining pressure, shown in Figure 5.58. In other words, it would have leveled off here too. What is also interesting to infer about the clay is how the friction angles seem to have a direct impact on predicting the initial modulus and secant modulus. Figure 5.59 and Figure 5.60 show that as the friction angle gets higher, so do the initial and secant moduli. However, in direct contrast to the modulus, the interaction ratio saw a

significant decrease in value when subjected to higher confining pressure, as shown in Table 5.14. Its values suggest a loss of 66.4% on average; this results from the reduction of internal friction angle with increasing confining pressure. Figure 5.61 shows the decline in value. The original and repeated clay values from the direct shear were averaged together for C_i in the pullout. There is seemingly no correlation between interaction ratio and friction angle, as shown in Figure 5.62.

Table 5.12 Initial modulus (kPa) for clay pullout testing

Clay		
Geosynthetic	Normal Stress	
	10 kPa	38 kPa
GG1 Reinforced	1140	1400
GG2 Reinforced	820	800
GG3 Reinforced	930	1350
GT Reinforced	675	865

Table 5.13 Secant modulus (kPa) at 2% for clay pullout testing

Clay		
Geosynthetic	Normal Stress	
	10 kPa	38 kPa
GG1 Reinforced	575	1055
GG2 Reinforced	650	-
GG3 Reinforced	615	785
GT Reinforced	540	690

Table 5.14 Interaction ratio (Ci) for clay pullout testing

Clay		
Geosynthetic	Normal Stress	
	10 kPa	38 kPa
GG1 Reinforced	1.093	0.421
GG2 Reinforced	1.052	0.245
GG3 Reinforced	1.099	0.444
GT Reinforced	1.207	0.383

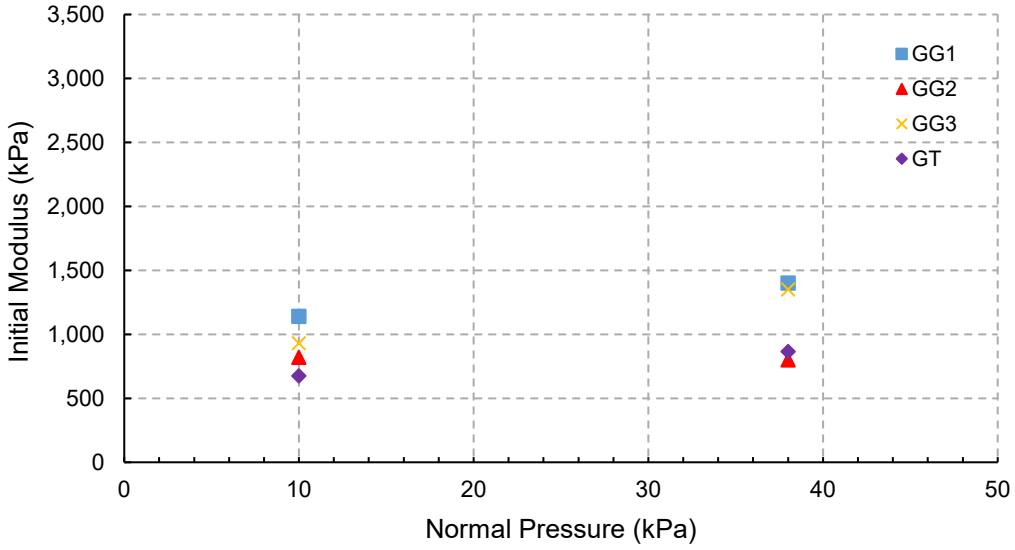

Figure 5.57 Clay initial modulus versus normal pressure for all geosynthetic types

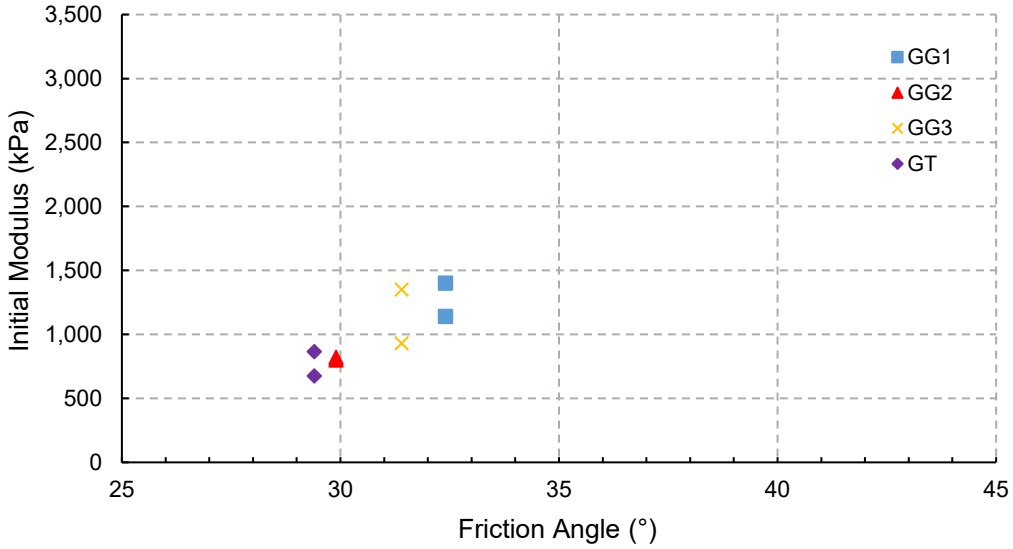

Figure 5.58 Clay initial modulus versus friction angle for all geosynthetic types

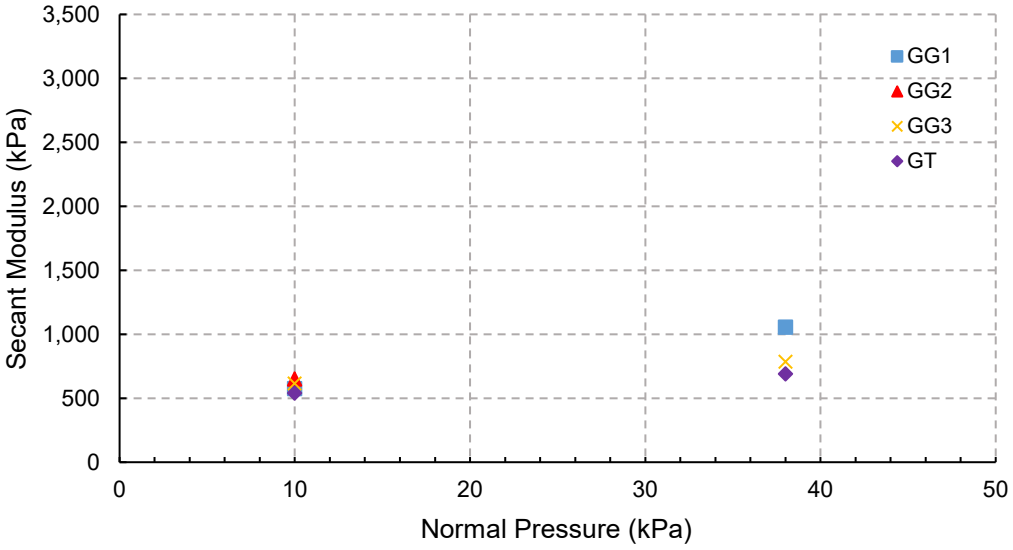

Figure 5.59 Clay secant modulus versus normal pressure for all geosynthetic types

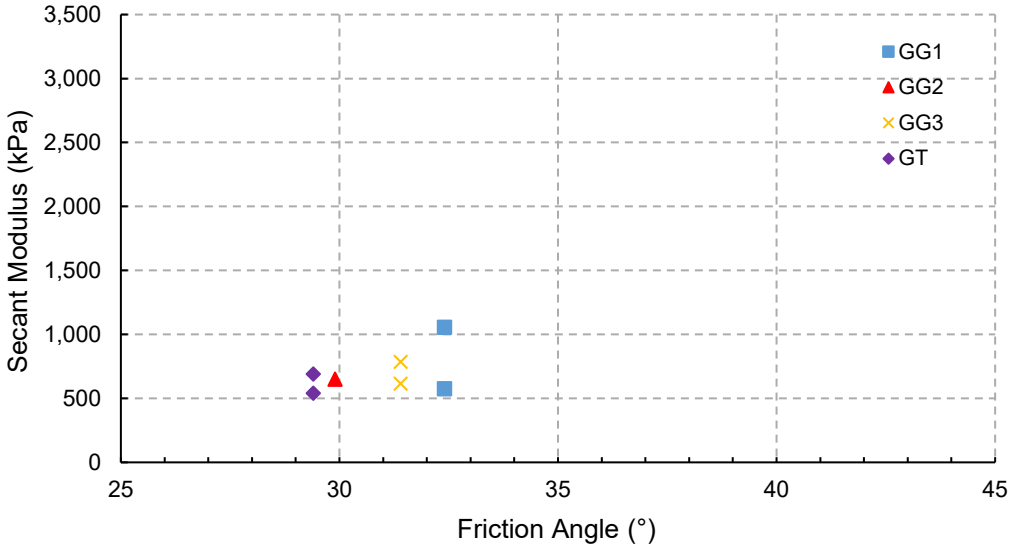

Figure 5.60 Clay secant modulus versus friction angle for all geosynthetic types

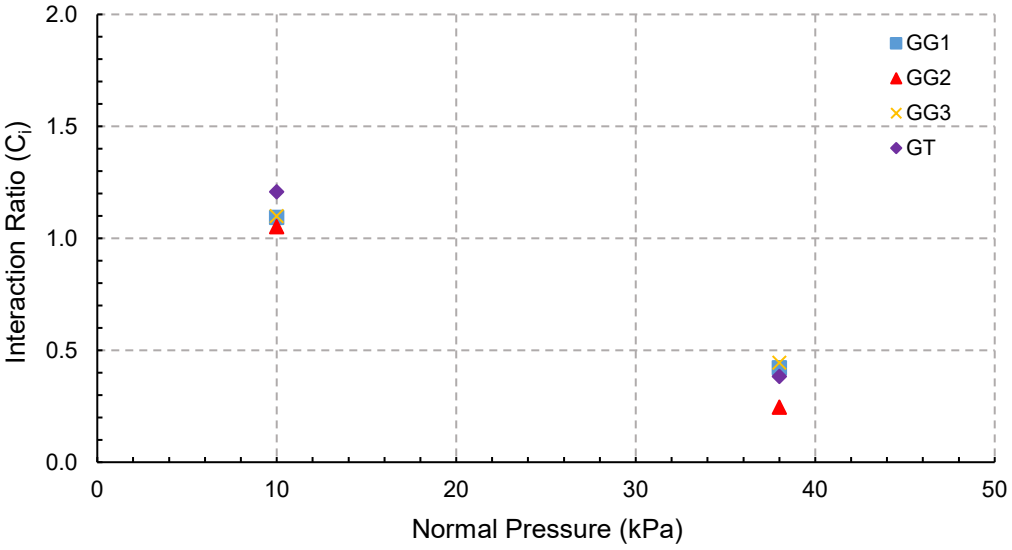

Figure 5.61 Clay interaction ratio versus normal pressure for all geosynthetic types

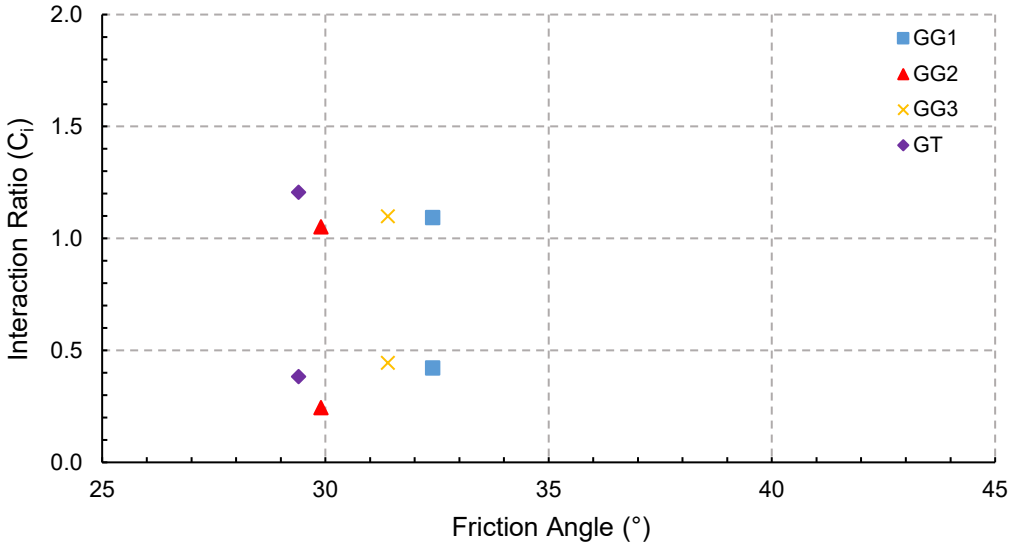

Figure 5.62 Clay interaction ratio versus friction angle for all geosynthetic types

5.2.4 Reinforced Red Shale

5.2.4.1 Normal Pressure of 10 kPa

For the red shale results at lower pressure, shown in Figure 5.63 through Figure 5.66, GG1 had a pleasant pullout with a slight rupture on one of its sides. It would still be classified as a pullout failure, but the fracture did affect the pullout resistance. GT also had a pullout failure. GG2 and GG3 resulted in a rupture. The peak was highest with GG3 at around 19.5 kN/m followed by GG1 at around 17.8 kN/m. The LVDTs were engaged with these geosynthetics indicating good uniform pullout. They were pulled together and not one at a time. The GT had the most uniform pull, as the telltales overlap one another quite closely. GG2 did not show much movement of its LVDTs, though it was clear that the front ribs were elongating as a point of compensation before it ruptured. The biaxial geogrids showed the highest pullout resistance and covered a fair distance. They had roughly a 75% greater pullout resistance than GG2 or GT. GG2 had a steady increase in its modulus, again like the lower pressure clay, and did not taper. It had

a quick rupture that was nearly complete. Its peak value was seen around 12.0 kN/m. GT had the lowest peak around 8.3 kN/m and had great specimen displacement.

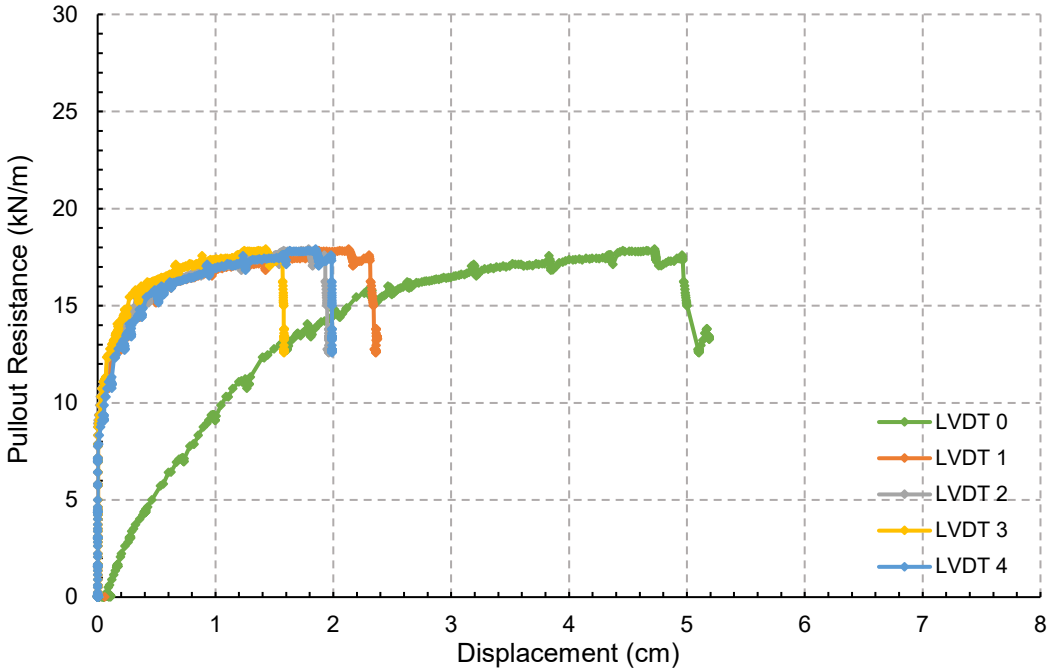

Figure 5.63 GG1 reinforced red shale at 10 kPa

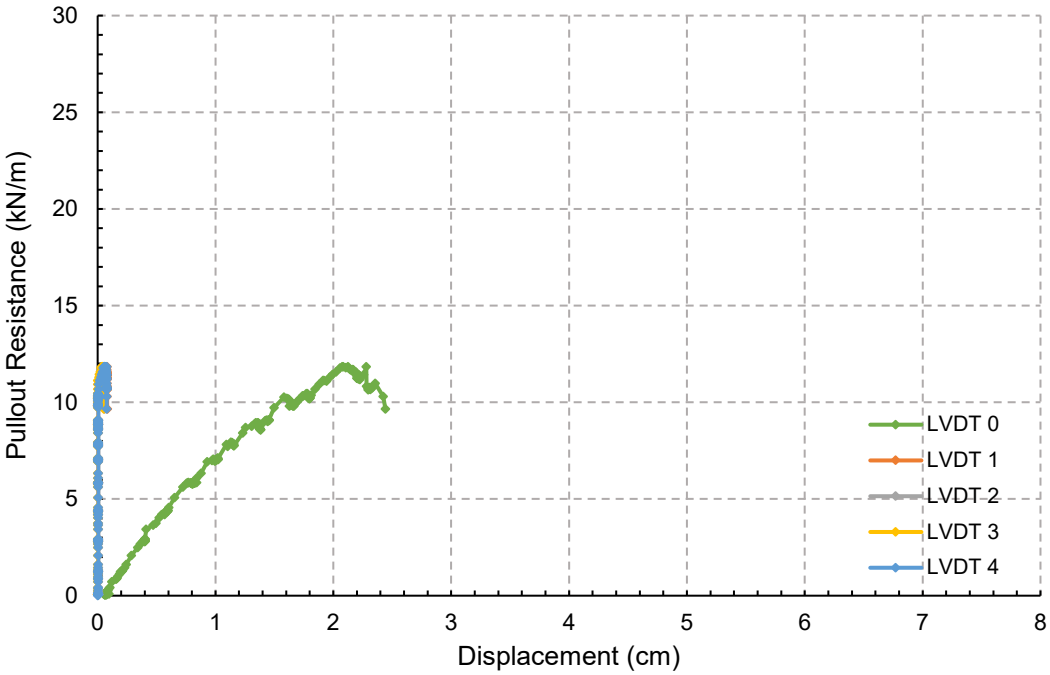

Figure 5.64 GG2 reinforced red shale at 10 kPa

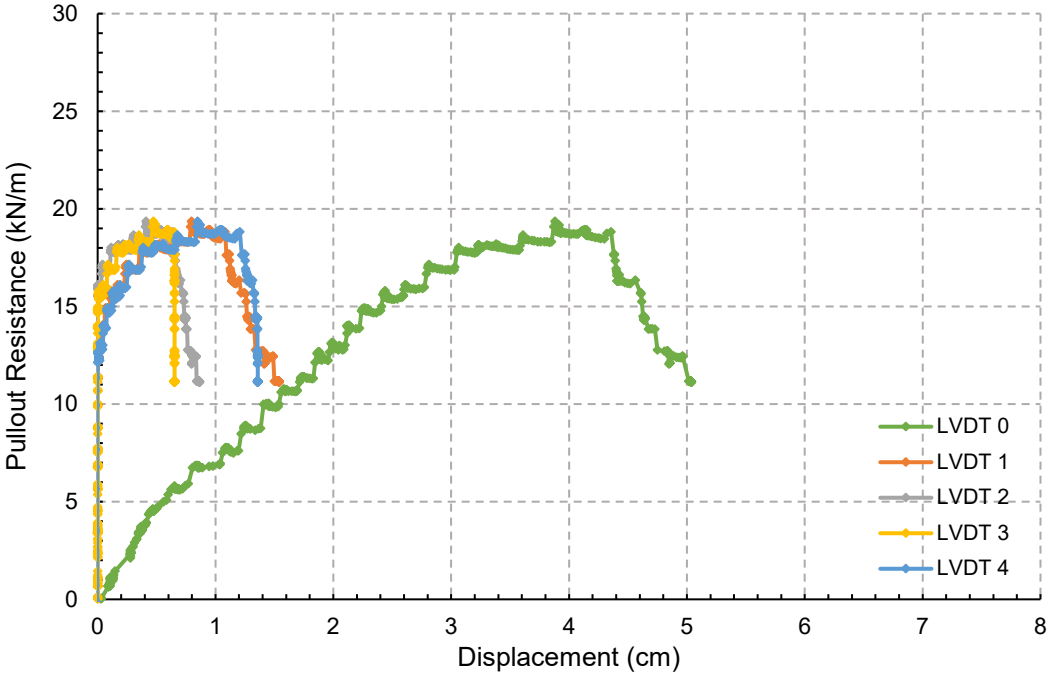

Figure 5.65 GG3 reinforced red shale at 10 kPa

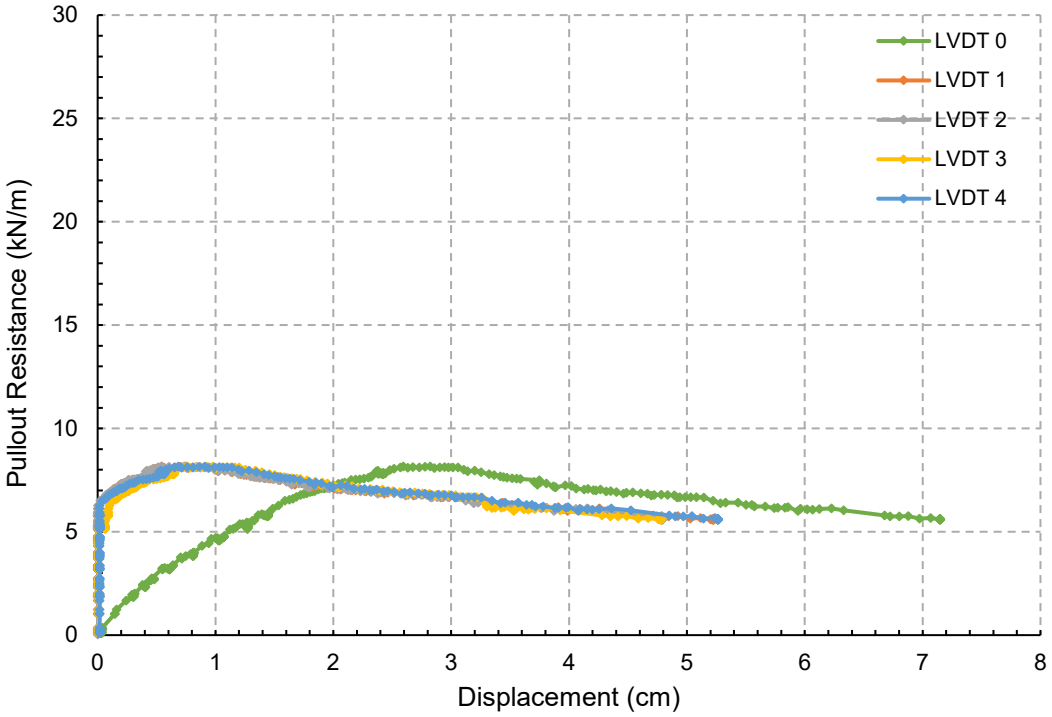

Figure 5.66 GT reinforced red shale at 10 kPa

5.2.4.2 Normal Pressure of 38 kPa

At higher pressures, all four geosynthetics ruptured again, shown in Figure 5.67 through Figure 5.70. The three geogrids were quite sudden and complete. This proved that the embedded geosynthetic was not engaged, as indicated by no movement of the back LVDTs. This is due to the efficient clamping efficiently at the front of the box and both hydraulic pistons moving together. Hence, only the frontal portion of the geosynthetic bore the brunt of the tension. The geotextile had a pullout-rupture combination, similar to the clay case, where the stitching was eventually pulled apart. This is indicated by the similar graphs of Figure 5.56 and Figure 5.70. In the cases of GG1, GG3, and GT, there were increases in their pullout resistance as compared to the lower confining pressure. Again, the biaxial geogrids saw better strains than the triaxial. Biaxial GG1 had a 25.9 kN/m peak, resulting in a 45.5% increase while biaxial GG3 had an increase of 14.4% as compared to their lower pressures. GT had an astounding increase of

140.0%. However, even with this increase, the overall performance was lower than either GG1 or GG3. GG2, meanwhile, at a higher pressure again saw a decrease in its pullout resistance. It was a 16.7% decrease. There was no movement of the back LVDTs which indicated that it was secure in place, so it did not adapt well to tensile force. The test was run twice to confirm this phenomenon. The second test, indicated in Figure 5.71 as a repeated check, showed that indeed the pullout resistance was nearly identical. Figure 5.71 shows that there was a partial rupture, but the test was continued until there was complete rupture. It is believed the triaxial GG2 ruptured both times, even under low pressure, due to the smaller rib dimension. The geosynthetic is made for interlock and lateral confinement, not necessarily tensile resistance. Even in the product manual, the tensile strength is not stated, but rather its radial stiffness (Tensar).

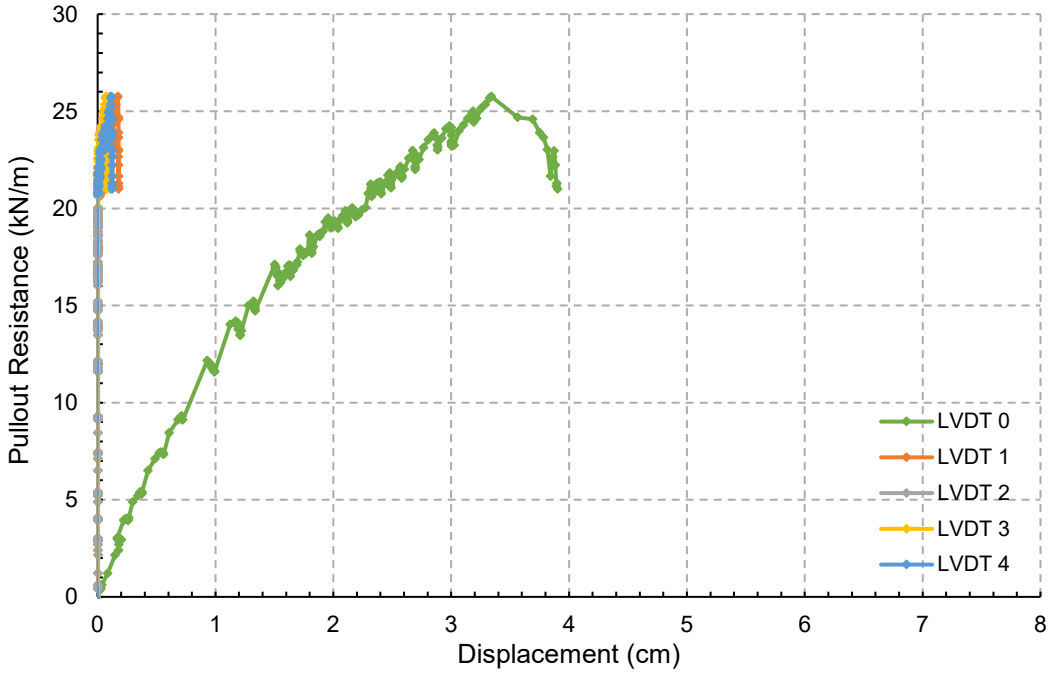

Figure 5.67 GG1 reinforced red shale at 38 kPa

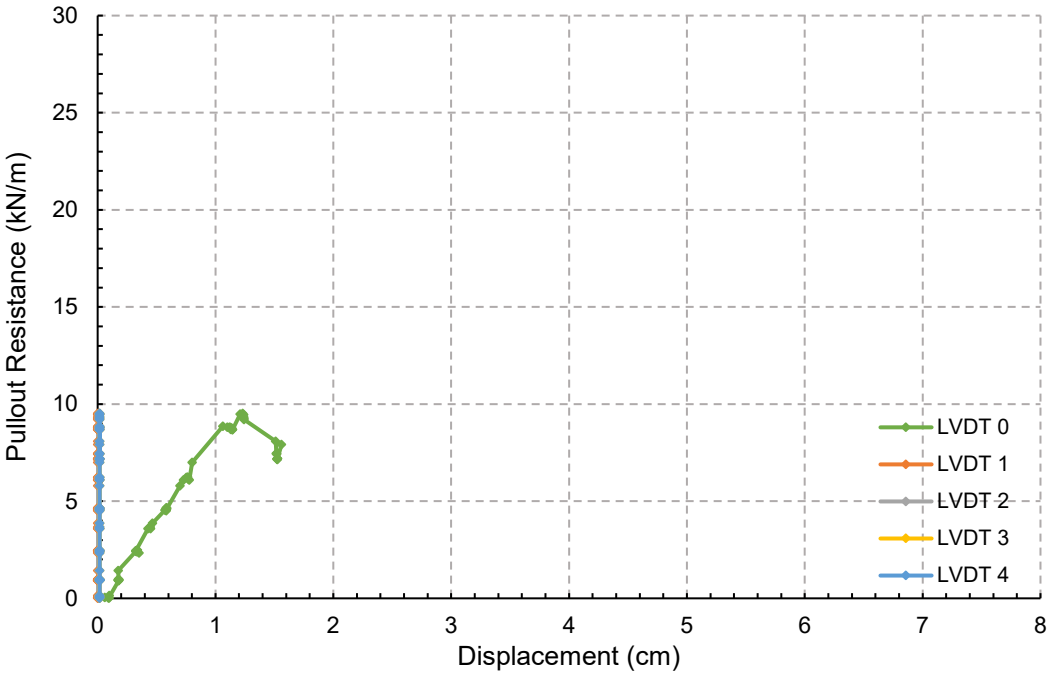

Figure 5.68 GG2 reinforced red shale at 38 kPa

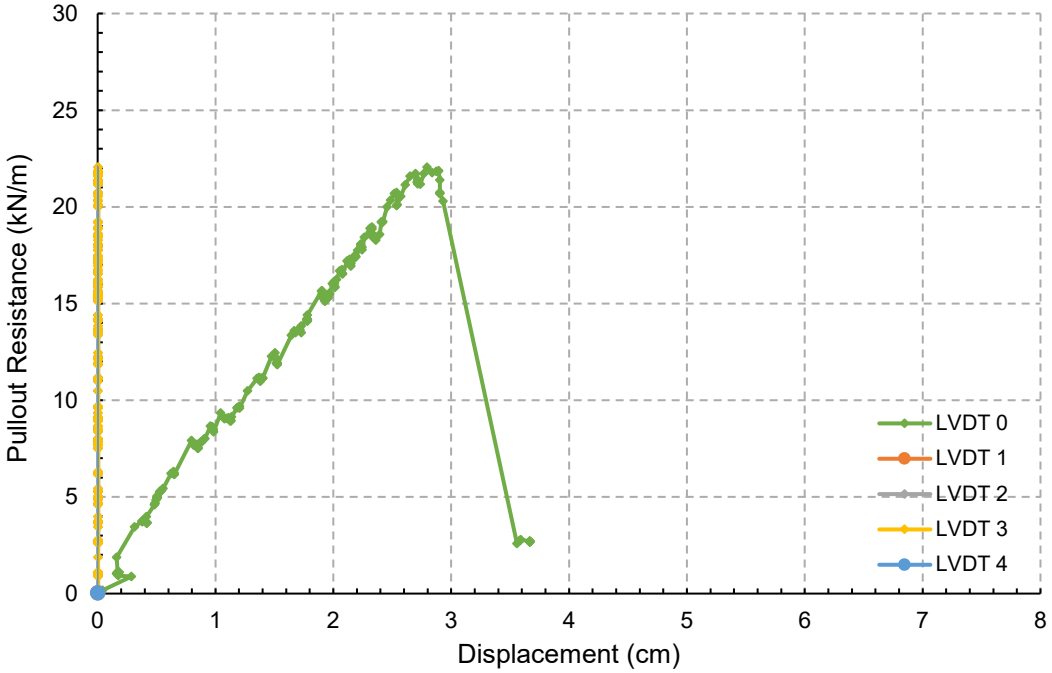

Figure 5.69 GG3 reinforced red shale at 38 kPa

Figure 5.70 GT reinforced red shale at 38 kPa

Figure 5.71 Repeated check of GG2 reinforced red shale at 38 kPa

The initial modulus of these geosynthetics can reflect the increases and decreases of the pullout resistances. Table 5.15 shows the initial modulus. GG1, GG3, and GT saw an averaged 42.4% improvement in their resistances at the higher pressure for the initial modulus, shown in Figure 5.72. GG2 sees a steadier level with the initial modulus. The reason that GG2 had a lower stiffness modulus than the rest of the geogrids in red shale was because the embedded portion of the geosynthetic did not move. The material elongated and ruptured in the section that was outside of the box and clamped around the front roller. It is precisely due to this reason that for both confining pressures, the GG2 had nearly identical stiffnesses. It simply had to use the same area of free geosynthetic to withstand the tensile force. As shown in Figure 5.73, friction angle can be a way to predict the initial modulus. The secant modulus is also quite similar to the initial modulus. GG1, GG3, and GT all saw a rise in the secant modulus, shown in Table 5.16 and Figure 5.74. Similar to the clay and shown in Figure 5.75, the friction angle can be a way to predict the initial modulus and secant modulus. As the friction angle gets higher, so does the modulus. The interaction ratio values are depicted in Table 5.17. It is evident that as the normal pressure increases, the interaction ratio decreases drastically, as shown in Figure 5.76. There is seemingly no correlation between interaction ratio and friction angle, as shown in Figure 5.77. Hegde et al. (2017) also found in his case study that as the normal pressure increased, the interaction ratio decreased. This reduction of friction coefficient was also true of Prashanth et al. (2016). The stiffness and interaction ratio (C_i) seem to have no direct correlation. They are inversed, to be sure, because while the stiffness gets larger at higher pressures, the C_i gets lower. There is no direct correlation, however.

Table 5.15 Initial modulus (kPa) for red shale pullout testing

Red Shale		
Geosynthetic	Normal Stress	
	10 kPa	38 kPa
GG1 Reinforced	1300	1450
GG2 Reinforced	800	850
GG3 Reinforced	750	950
GT Reinforced	450	850

Table 5.16 Secant modulus (kPa) at 2% for red shale pullout testing

Red Shale		
Geosynthetic	Normal Stress	
	10 kPa	38 kPa
GG1 Reinforced	725	950
GG2 Reinforced	575	-
GG3 Reinforced	635	810
GT Reinforced	360	695

Table 5.17 Interaction ratio (Ci) for red shale pullout testing

Red Shale		
Geosynthetic	Normal Stress	
	10 kPa	38 kPa
GG1 Reinforced	1.363	0.519
GG2 Reinforced	1.124	0.237
GG3 Reinforced	1.546	0.464
GT Reinforced	0.719	0.457

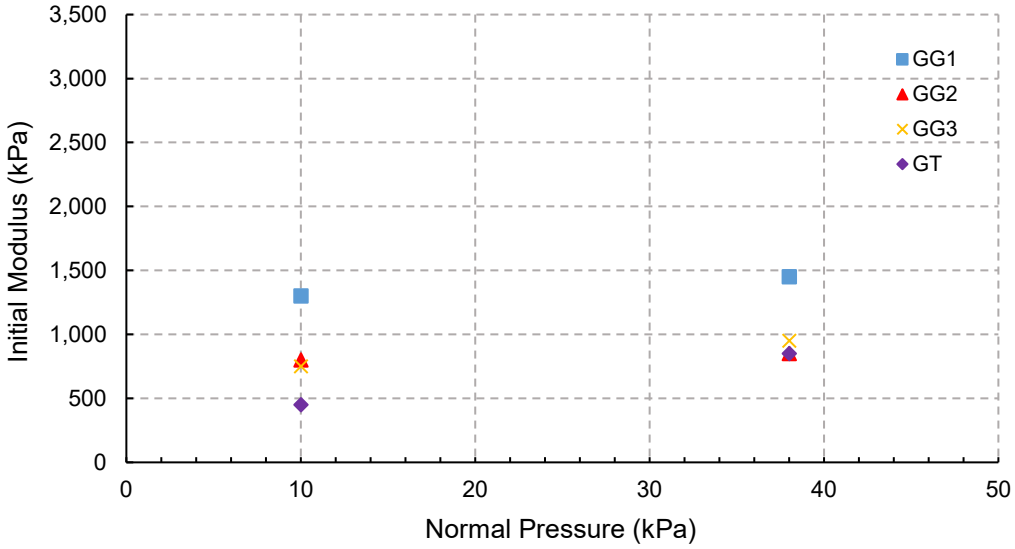

Figure 5.72 Red shale initial modulus versus normal pressure for all geosynthetic types

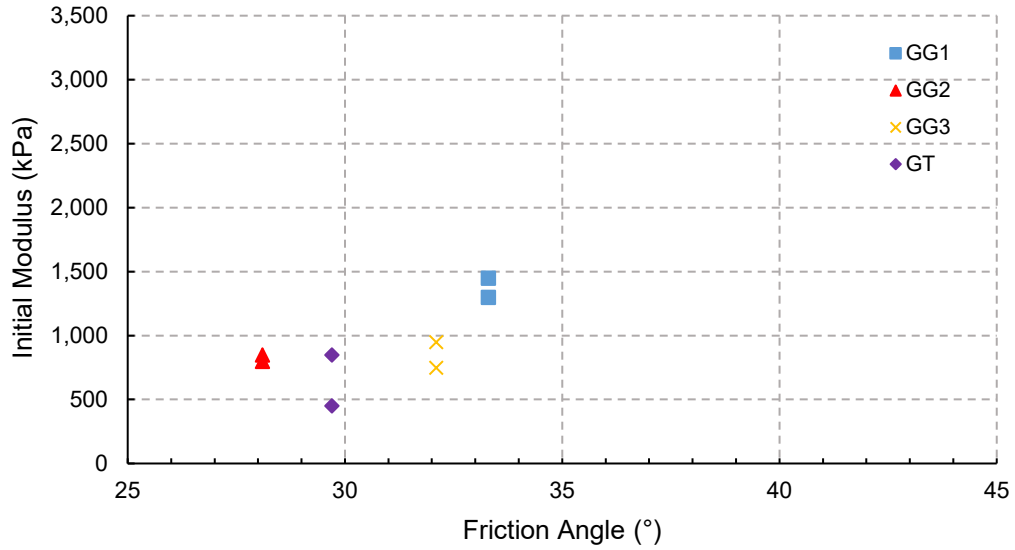

Figure 5.73 Red shale initial modulus versus friction angle for all geosynthetic types

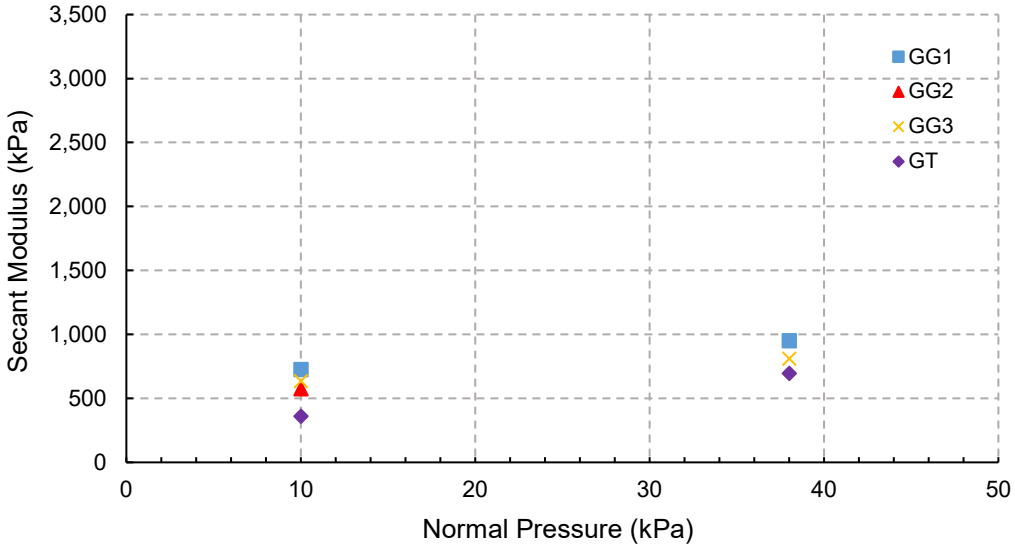

Figure 5.74 Red shale secant modulus versus normal pressure for all geosynthetic types

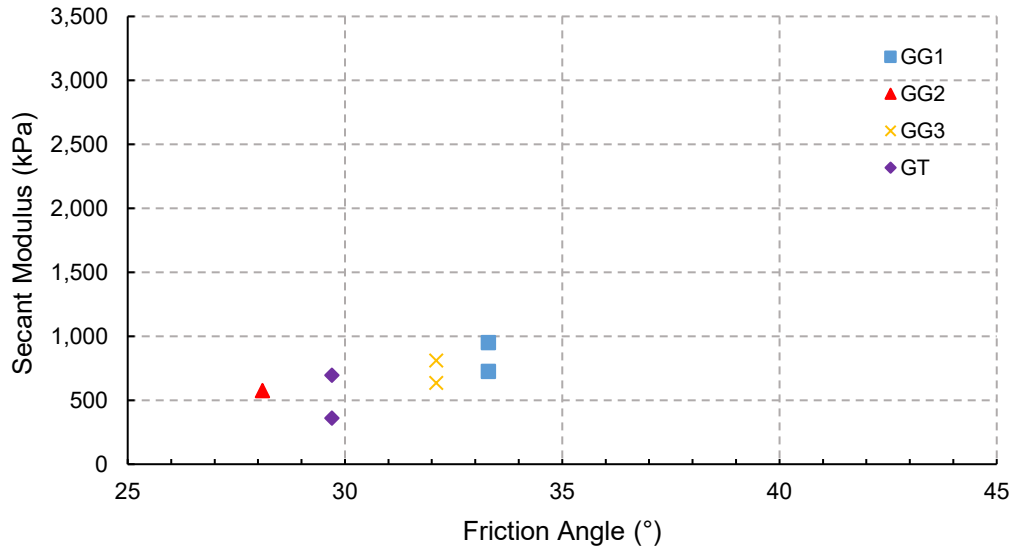

Figure 5.75 Red shale secant modulus versus friction angle for all geosynthetic types

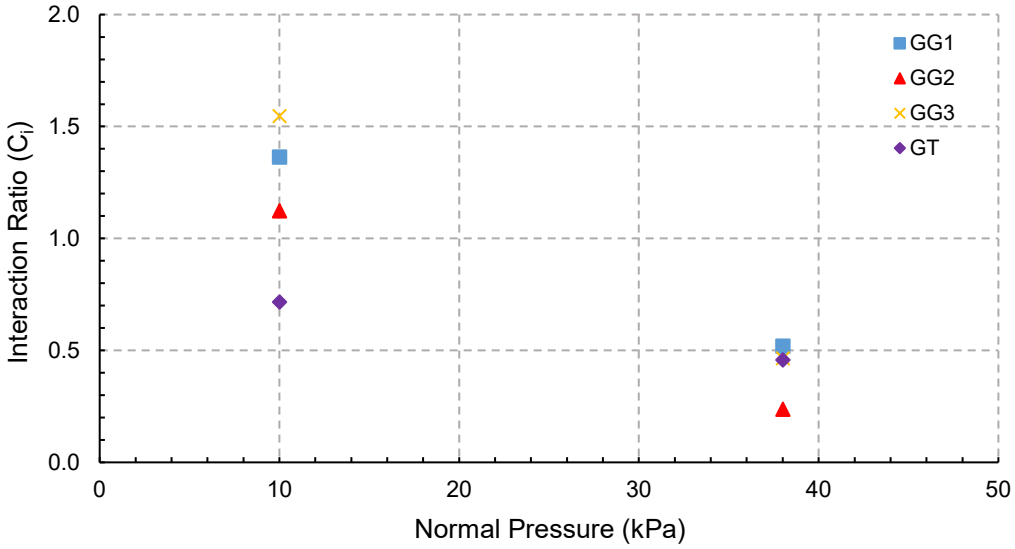

Figure 5.76 Red shale interaction ratio versus normal pressure for all geosynthetic types

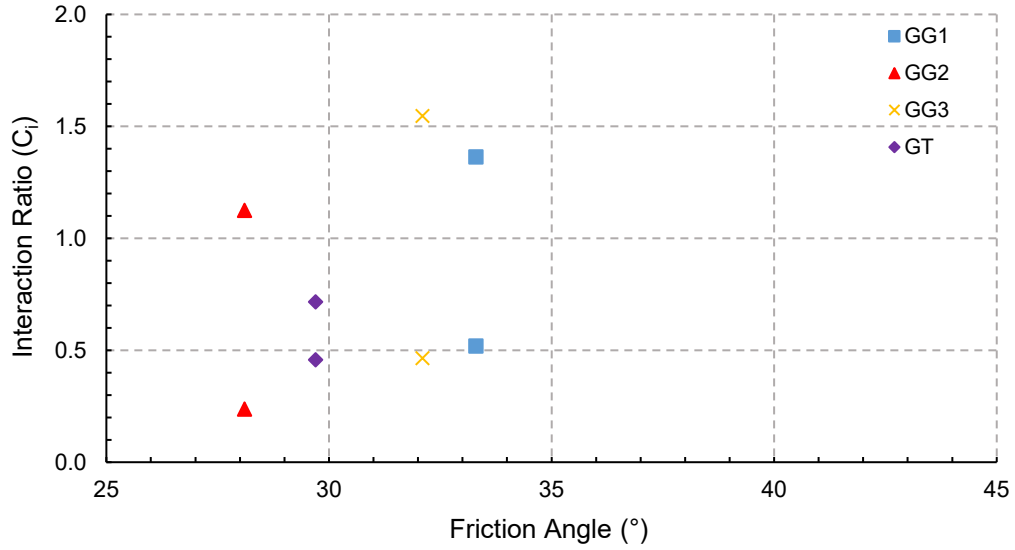

Figure 5.77 Red shale interaction ratio versus friction angle for all geosynthetic types.Red shale interaction ratio versus friction angle for all geosynthetic types

5.2.5 Overall Pullout Results Analysis

Clay particles are smaller and do not have the same bulk modulus, leaving the simple truth that the higher confining pressure might result in crushing the soil particles, which would explain why they lose the interaction at higher confinement. This is the same reason that lower pressure allows for better values. The geotextile at lower pressures for both clay and red shale saw slightly different graphs. While both had pullout failures, the GT in clay produced a higher pullout resistance and did not relinquish its peak value whereas the GT in red shale had a much smaller pullout resistance and came down from its peak. The geotextile at higher pressures for both the clay and red shale saw a pretty similar trend. It resulted in a gradual hump succeeded by a gradual tear and subsequent rip. GG2 at higher pressure decreased its pullout resistance in both the clay and red shale. The values were similar, as in clay the decrease was 12.8% and in the red shale it was 16.7%. GG2 had similar pullout resistance values for both clay and red shale. The triaxial geogrid is not good in tension. This is presumably why it is neglected on the manufacturer's product specifications.

The clay at lower pressure saw very similar peak pullout resistance for all four cases. This may have been due to a low confining stress acting upon a fine particle-sized soil. When the confining pressure was increased, the pullout resistance saw different changes in that the densified clay packed well with the geosynthetics and caused ruptures for every case. Under the lower pressure, the triaxial geogrid had more movement of its LVDTs, indicating that the whole geosynthetic was being moved. It is clear takes a little while for the back LVDTs to activate. For a certain time, if not the whole time, the extruded part of the geosynthetic at the front takes the bulk of the tensile force.

The initial stiffness of the material from pullout proved to tell a different story. While the productivity of the geosynthetic can be read from the interaction ratio, their elongation can be reliable for other matters. Specifically, that as confining pressure increases, the values also increase. For all soil types, there was a general increase in the stiffness modulus. The geosynthetics readily increased their stiffnesses, showing greater tensile resistance. The GT greatly improved both the clay and red shale soils, nearly doubling under higher pressure for red shale. GG1 showed improvement, as did GG3 in the clay. But for the red shale case, GG3 did not see any increase and virtually stayed the same, which was the same story for GG2 in both the clay and red shale. When GG2 was subjected to the lower 10 kPa confining pressure, it showed a nearly identical stiffness while under the higher 38 kPa confining pressure. This indicates that the lower pressure is in fact quite high enough to rupture the geosynthetic and makes it useless under anything greater. At the lower pressures, for both clay and red shale, GG2 is able to hold out until at least 2 centimeters, but with higher pressures, it cannot. In both cases for clay and red shale, the stiffness is around 820 kPa for all four cases, proving that it does not exhibit any significant tensile resistance qualities.

The productivity of the C_i values went down for the clay tests. It was highest overall for the red shale, excluding the geotextile. Since the GT did not perform well in the red shale soil, it is presumed it would have also done poorly in sand. This is in reference to the direct shear test and how much closer in relation to sand the red shale is versus its relation to clay. However, when looking at the clay results, the geotextile did well; it had the highest interaction ratio among all of the geosynthetics. It is also noteworthy, though, that all of the geosynthetics were very close in their values, indicating, again, that clay concentrates its values because of the fine particle size. It seems that with clay, it does not matter which geosynthetic is used. In both the

direct shear and the pullout, the results were concentrated and similar. The geotextile made the greatest edge for both the normalized interfacial shear resistance and the interaction coefficient, so it would be preferred with this soil type.

Looking at the geogrids, their interaction ratios were higher in the red shale versus the geotextile. This is presumed to be because of the courser soil material. The biaxial geosynthetics, GG1 and GG3, showed higher interaction ratios than the triaxial. This is also true of the interfacial shear resistance for sand, where the biaxials GG1 and GG3 outmatched the triaxial GG2. Even so, all three geogrids performed well under the sand and red shale conditions. The higher stiffness of a geogrid leads to greater active zones with sand particles, which increases resistance. Since geogrid reinforcement is mobilized by the interaction between geosynthetics and soil, it proves that geogrid stiffness plays a foremost role in reinforcement application.

5.3 Comparative Analysis of Pullout and Direct Shear Testing Results

In this section, we conducted a comparison of the outcomes derived from both pullout and direct shear testing methods. Through this analysis, we assessed and scrutinized the parameters gathered from these tests across various soil and geosynthetic types.

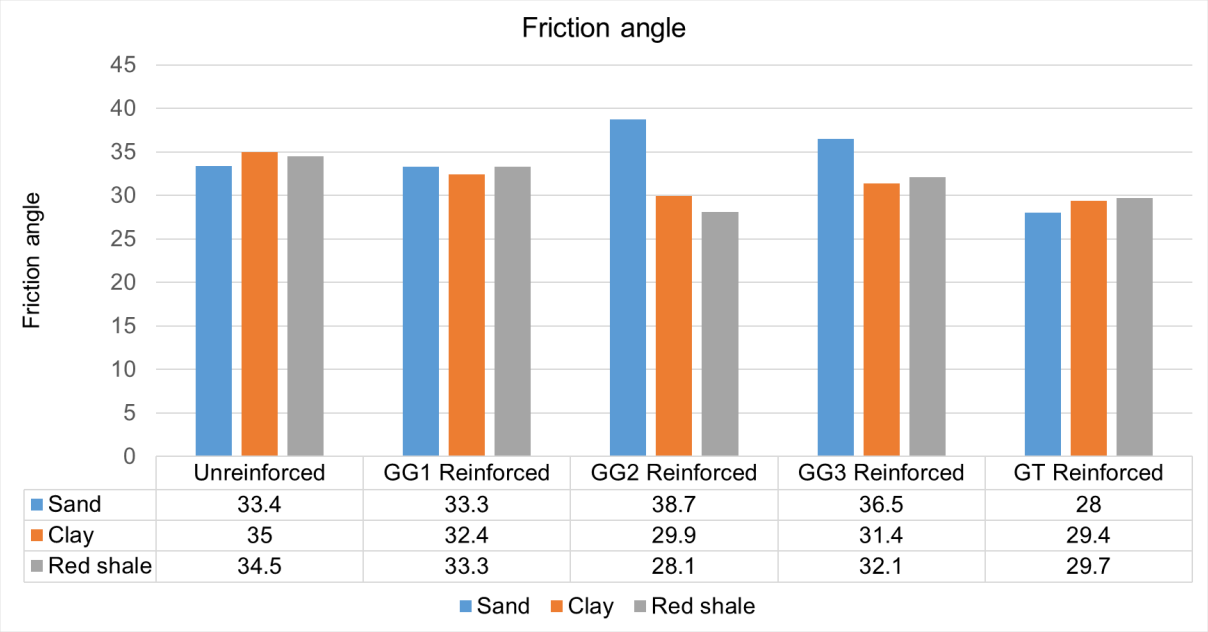

Figure 5.78 Summary of direct shear testing results: interface friction angle

The interface friction angles between different geosynthetics and soils were comparatively evaluated. For poor-quality subgrade, including clay and red shale, GG1 and GG3 show higher friction angles than GG2 and GT, as shown in Figure 5.78. This might be because the material properties of the geosynthetic itself and the geometric shape of the aperture of the geosynthetic influence the friction angle. GG2 is a triangular shape and consists of relatively thin rods, which can be improper for clay and red shale materials.

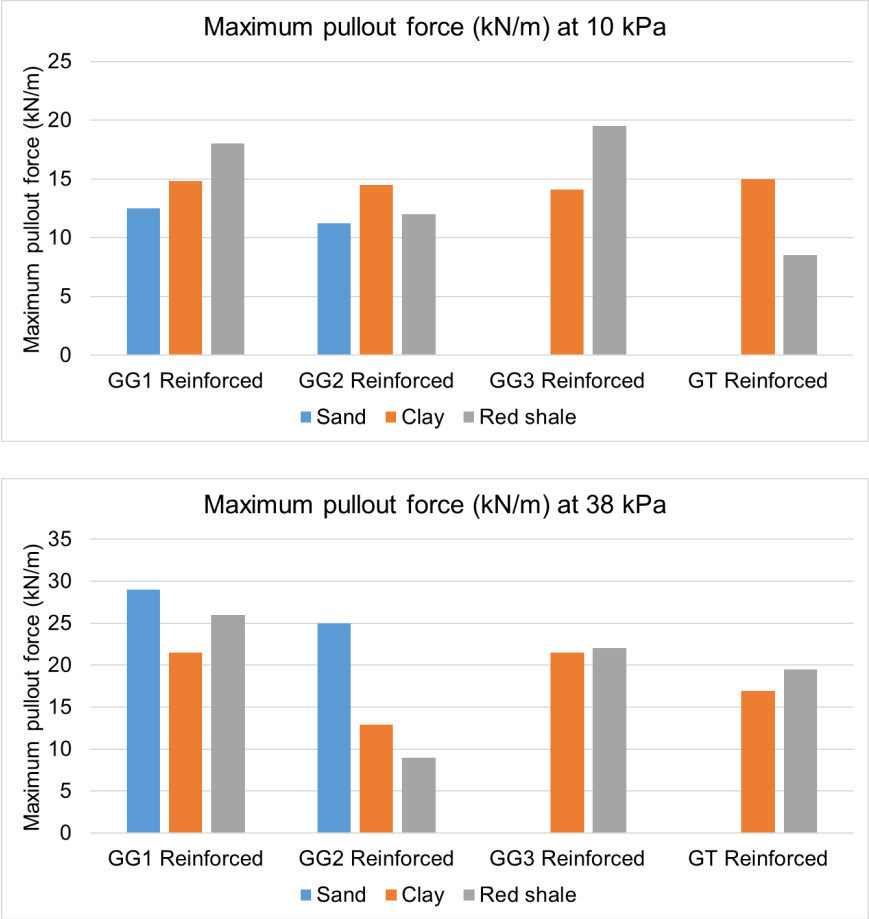

Figure 5.79 Summary of maximum pullout force (PF)

The maximum pullout force for different geosynthetics and soils were comparatively evaluated. The maximum pullout force is the highest value in the pullout force during the pullout test. The maximum pullout force is higher at higher confining pressure because confinement and interaction effects can be more dominant than those at lower confining pressure. Since sand is a good quality soil, the force is highest. For poor quality subgrade, including clay and red shale, GG1 and GG3 show higher maximum pullout force than GG2 and GT, as shown in Figure 5.79. This is also related to a similar reason in the previous case, the interface friction angles. Since the geosynthetic material properties and the aperture's geometric shape influence the pullout force,

GG2 is a triangular shape and relatively thin grid, which might not be for clay and red shale materials.

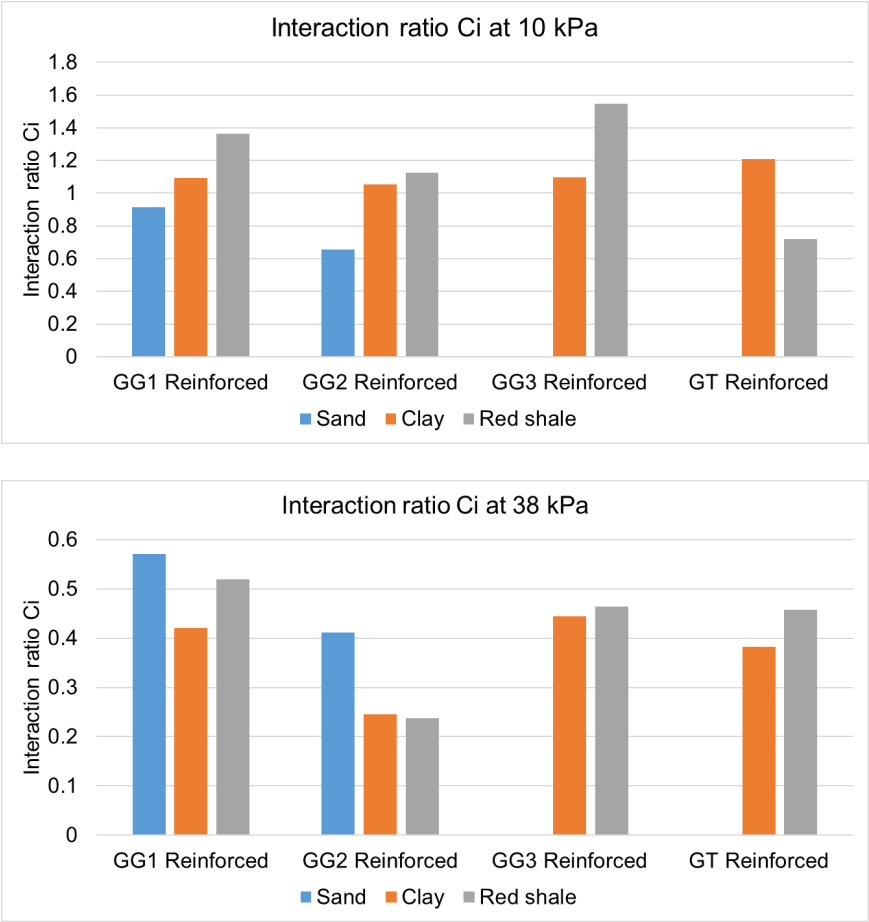

Figure 5.80 Summary of pullout box testing results: Ci

A comparative evaluation of the interaction ratio, or pullout coefficient (Ci), for various geosynthetics and soils was conducted. The interaction ratio, which is defined as the maximum pullout force divided by both the shear resistance and the geosynthetics' up and downside, was analyzed in detail. It is found that Ci tends to be higher at lower confining pressures, primarily due to the increased significance of the junction rib and geosynthetic reinforcing effect. The results showed that sand, a high-quality soil, generally exhibits the highest interaction ratio.

However, for poor-quality subgrades, such as clay and red shale, GG1 and GG3 displayed higher Ci than GG2 and GT, as shown in Figure 5.80. This difference could be attributed to the interface friction angle and interlocking, as was the case with sand. Furthermore, the material properties of the geosynthetic itself and the geometric shape of the aperture were found to influence the interaction ratio. We observed that GG2, which has a triangular shape and relatively thin grid, may not be suitable for clay and red shale materials due to its specific properties.

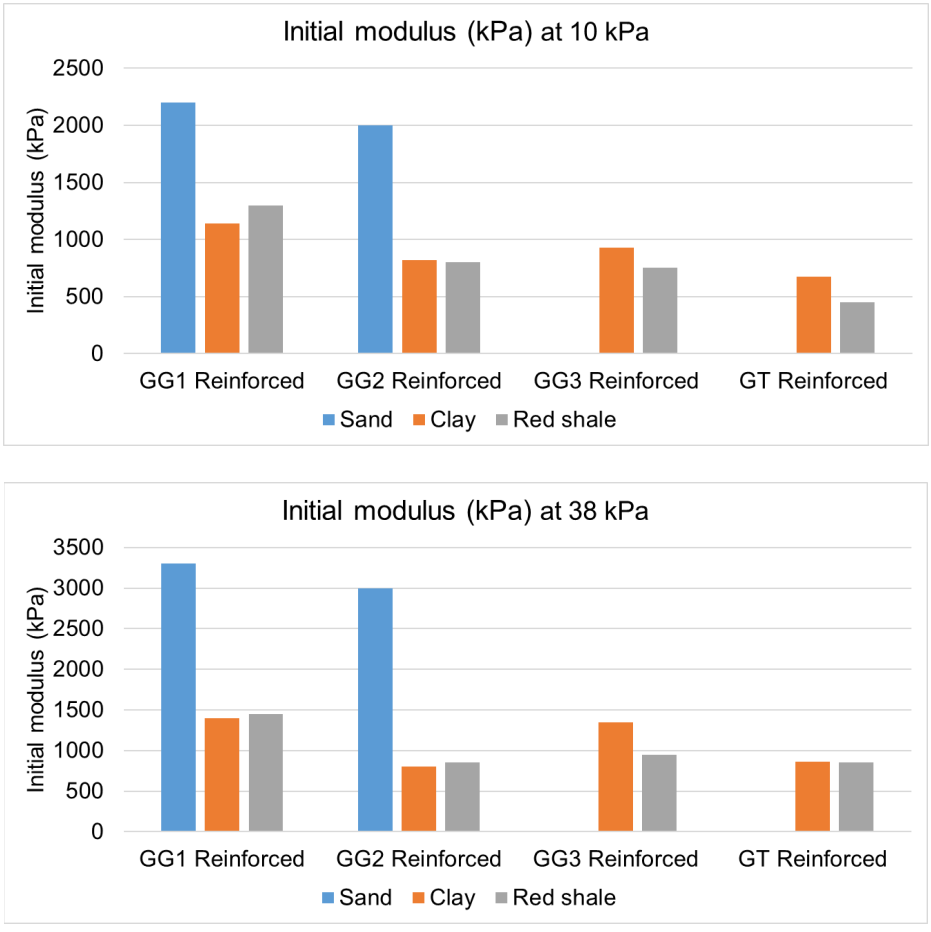

Figure 5.81 Summary of pullout box testing results: In. Mod

A comparative evaluation of the initial modulus for various types of geosynthetics and soils was conducted. The initial modulus is defined as the initial slope of plots between pullout force and displacement, which are obtained from the pullout test. We found that the initial modulus is higher when the confining pressure is lower because the junction rib and geosynthetic reinforcing effect are more significant at lower pressure. Additionally, we observed that the initial modulus is highest for sand, which is a high-quality soil. We also examined the performance of different geosynthetics on poor-quality subgrade soils, including clay and red shale. In this case, GG1 and GG3 showed higher initial modulus values than GG2 and GT, as shown in Figure 5.81. This difference can be attributed to the interface friction angle and interlocking, which are crucial factors in determining the initial modulus. Furthermore, we identified that the material properties of the geosynthetic and the geometric shape of its aperture could affect the interaction ratio. Specifically, GG2, which is a triangular shape with a relatively thin grid, may not be suitable for use with clay and red shale materials due to their properties.

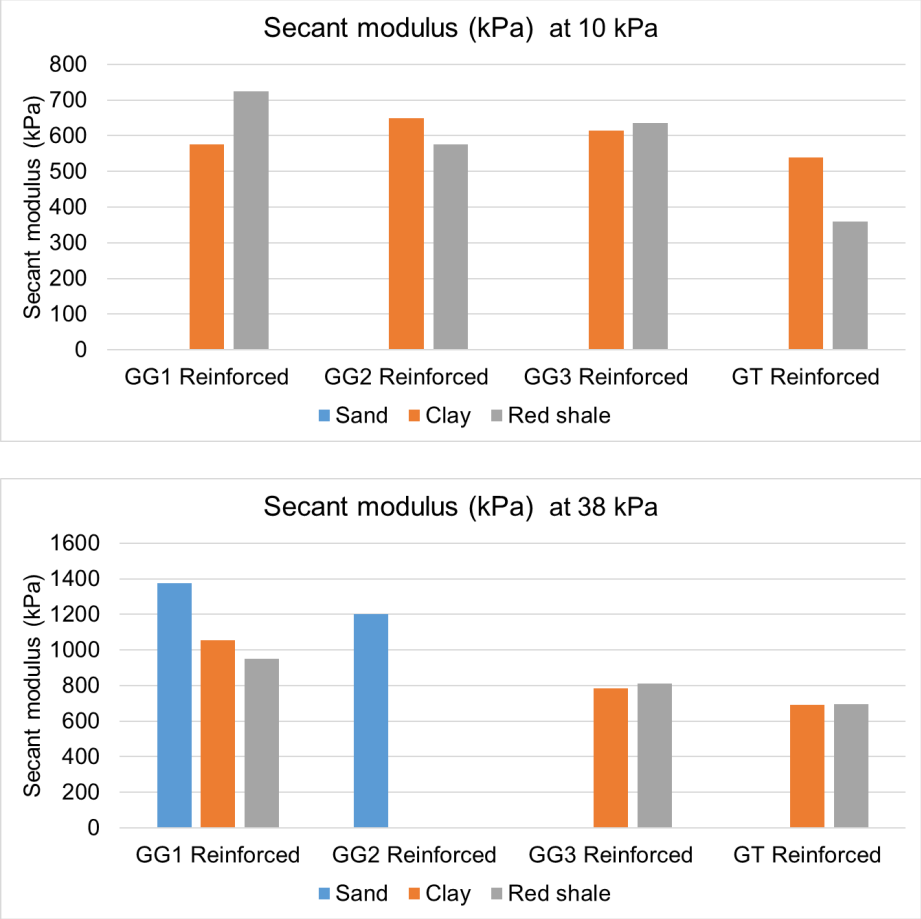

Figure 5.82 Summary of pullout box testing results: Sec. Mod

A comparative evaluation of the secant modulus for various geosynthetics and soils was conducted. The secant modulus, which can be defined as the slope of plots at a 2% strain level between pullout stress and pullout strain obtained from the pullout test, was analyzed. Our results indicate that the secant modulus tends to be higher at lower confining pressure due to the significant reinforcing effect of junction rib and geosynthetics. Specifically, the secant modulus was found to be highest for sand, which is considered to be a good quality soil. For poor-quality subgrades such as clay and red shale, we observed that GG1 and GG3 geosynthetics displayed higher secant modulus values than GG2 and GT, as shown in Figure 5.82. It should be noted that GG2 failed under high confining pressure in clay and red shale, which may be attributed to the

material properties of the geosynthetic itself and the geometric shape of its aperture. In particular, the triangular shape and relatively thin grid of GG2 were found to be unsuitable for clay and red shale materials. These findings suggest that the material properties and geometric characteristics of the geosynthetic influence the interaction ratio between the geosynthetic and the soil. Thus, considering these factors is necessary when selecting geosynthetics for reinforcement applications in different soil types.

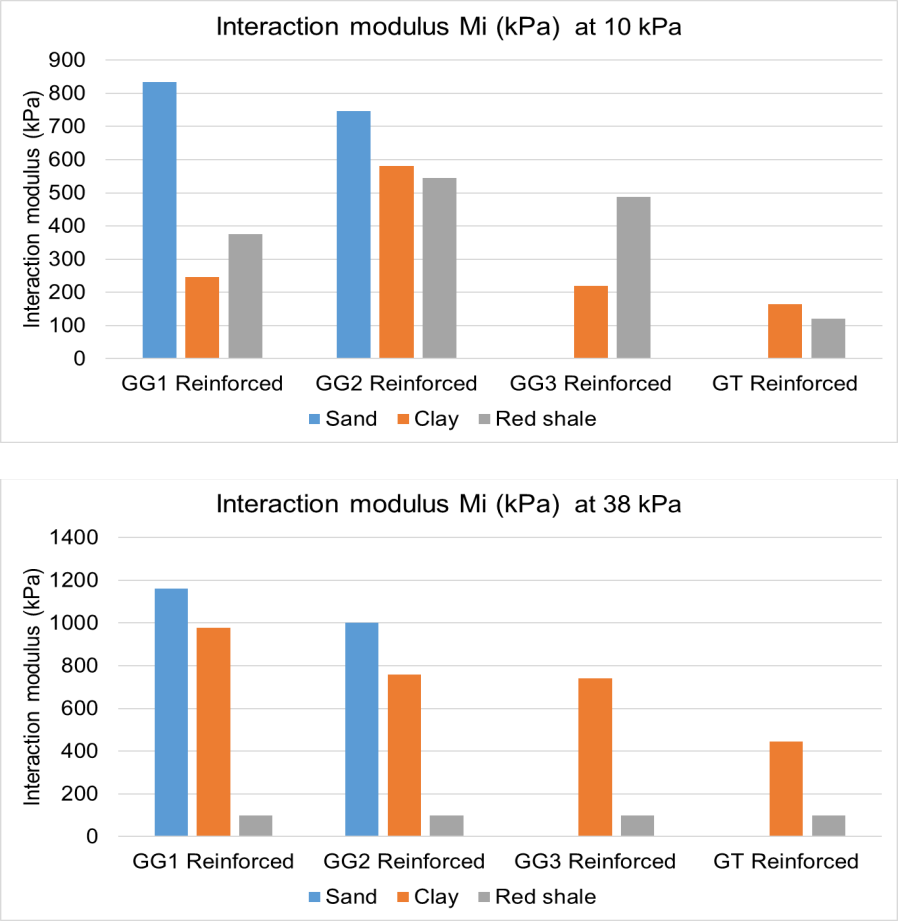

Figure 5.83 Summary of pullout box testing results: Mi

The interaction modulus (Mi) for different geosynthetics and soils was comparatively evaluated. According to WISDOT (2005), the interaction modulus is a ratio of maximum pullout stress over unit displacement at maximum pullout force. At lower confining pressure, Mi is higher because junction rib and geosynthetic reinforcing effect are more significant than at higher pressure. Similar to other cases, since sand is a good quality soil, the interaction modulus is highest. For poor-quality subgrade, including clay and red shale, GG1 and GG3 apparently show higher maximum pullout force than GG2 and GT, as shown in Figure 5.83. This is also related to a similar reason in the previous case, interface friction angle. Since the material properties of the geosynthetic itself and the geometric shape of the aperture of the geosynthetic influence the interaction ratio, GG2 is a triangular shape and relatively thin grid, which is not proper for clay and red shale materials.

5.4 FLAC Simulation

We conducted the simulation because the effect of geosynthetic reinforcement on the response of the pavement layers in the full scale. Also, we wanted to evaluate various cases including different soils and location of geosynthetic. The laboratory testing results were compared to the simulation results to confirm the trend and consistency of the outcome for both.

The input parameters for the simulation come from the evaluation of the direct shear and pullout boxes, specifically utilizing the soil-geosynthetic interface, friction angles, and tensile strengths of the geosynthetics.

5.4.1 Modeling setup

A numerical modeling was conducted to investigate the behavior of a typical roadway consisting of asphalt surface layer, aggregate base, and subgrade. The geometric representation of the modeling is illustrated in Figure 5.84. Our modeling geometry was based on axi-

symmetric conditions, as described by Erickson and Drescher (2001), which allowed us to simulate the response of the pavement layer without distortion effects from the different axes. We adopted a general configuration of the pavement system, as presented in the literature and the pavement design manual of the Nevada Department of Transportation (NDOT) (NDOT Pavement Design Manual 2021).

We investigated the impact of a simulated tendon vehicle load on pavement layer response, as per the Federal Highway Administration (FHWA-HRT-13-091) report (Hallenbeck et al. 2014). To accurately capture the response of the pavement layer near the loading point, we employed a finer mesh in the modeling. The side wall was fixed to ensure boundary conditions that reflect the infinite ground assumption. Additionally, we considered the geostatic condition as the initial state to reflect gravity in the modeling. This approach aligns with previous studies that have used finite element analysis to model pavement layer response subjected to vehicle loading (e.g., Zhang et al. 2018, Sajjadi et al. 2019). FHWA-HRT-13-091 report are also consistent with other studies that have focused on simulating vehicle loads on pavement layers (e.g., Wasiuddin et al. 2017, Saleh et al. 2021).

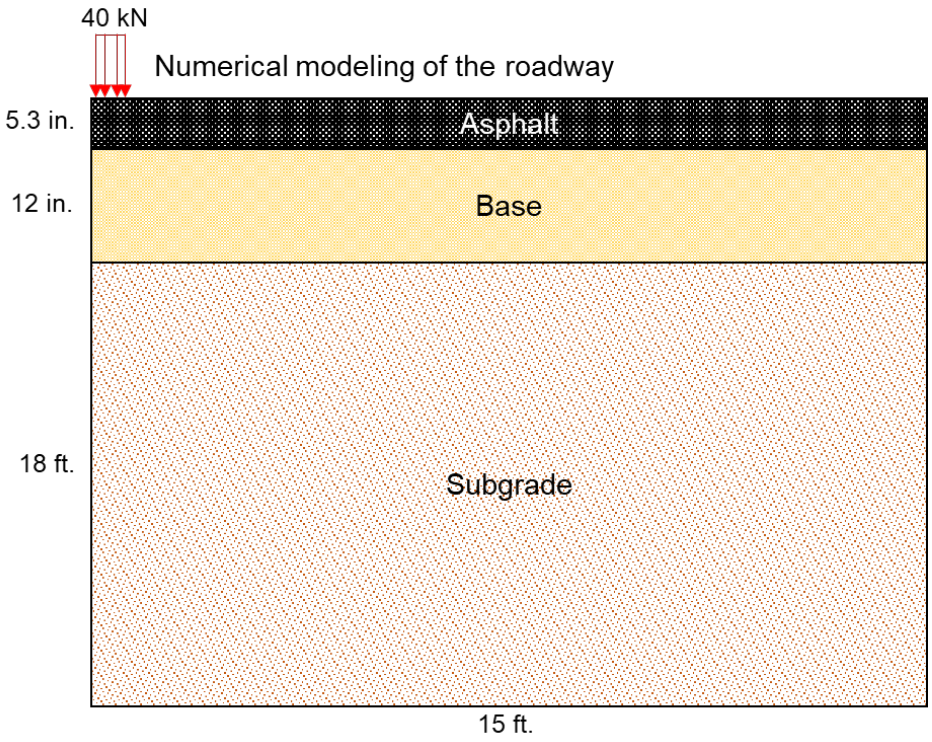

Figure 5.84 Modeling geometric condition

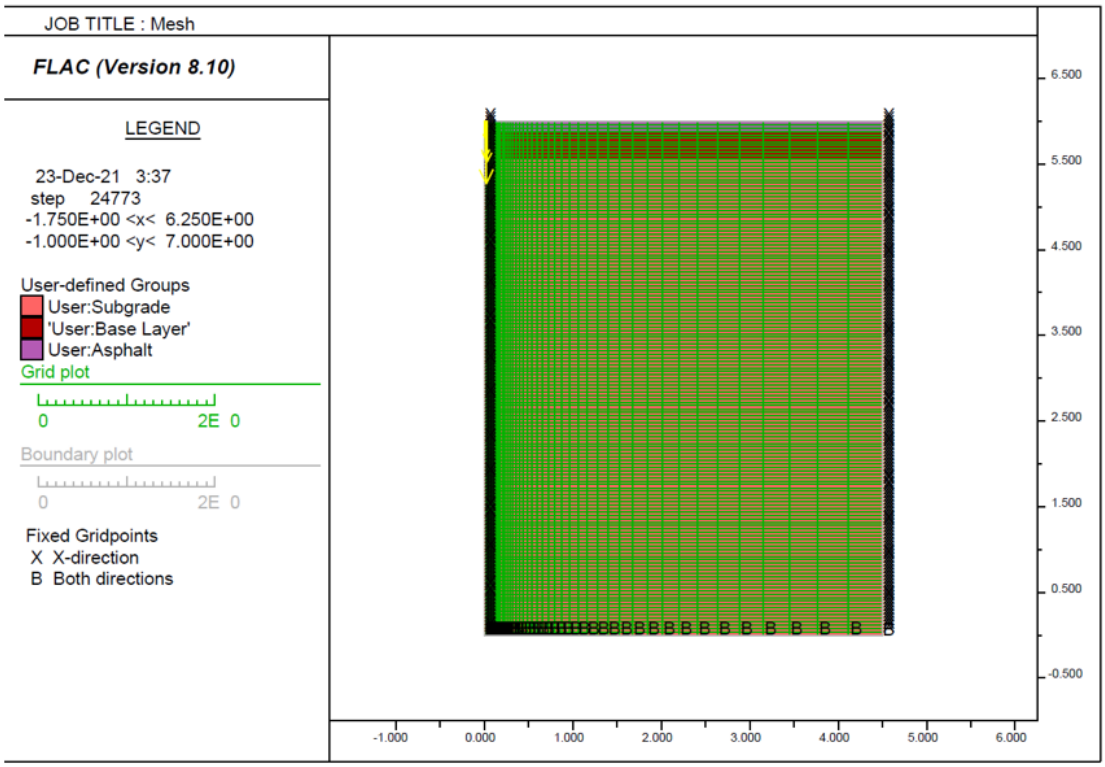

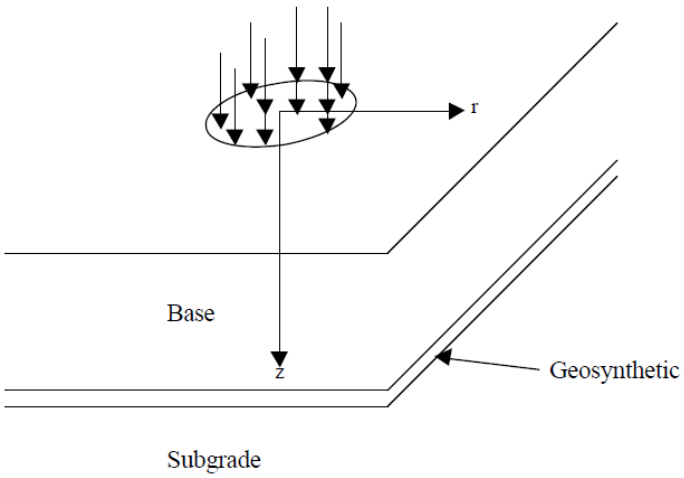

Figure 5.85 Modeling mesh and simulation condition - axisymmetric problem (Erickson and Drescher, 2001)

Table 5.18 Material properties to input the numerical model of each pavement layer

Parameter	Material				
	Asphalt [1]	Base layer [2]	Backfill		
			Sand[3,4]	Lean clay[5,6]	Soft soil[6]
Modulus of Elasticity (psi)	174.05×10^3	4,786	7,251	4300	2170
Soil density (pcf)	143.5	133	111	100	83
Poisson's ratio (-)	0.25	0.3	0.25	0.3	0.3
Cohesion (psi)	0	0	0	5.9	2.5
Friction angle (°)	0	65	30	0	0
Dilatancy Angle (°)	-	6	0	0	0

References :[1] Tan et al. (2017), [2] Karpurapu et al. (2014), [3]Hatami and Bathurst, [4]NDOT, [5] Song et al (2019), [6] Subramanian (2006)

In this study, the modeling parameters for simulating the interface behavior between geosynthetic and soil layers were obtained from both literature and the current investigation. These parameters are listed in Table 5.18. To ensure accurate simulation results, the interface properties were calibrated based on the pullout test data. A comparison was made between the modeling and testing results to parameterize the interface properties listed in Table 5.19. Among these properties, the bond stiffness and bond friction angle were calibrated with the pullout testing data. The properties were then defined to fit the modeling results to the testing results. Finally, the properties were used for simulating the pavement layer behavior. The methodology used in this study is consistent with similar studies in the field. The calibration of interface properties with pullout testing data has been widely used in pavement engineering (e.g., Wang et al. 2020, Xiao et al. 2019). Additionally, the use of modeling parameters obtained from literature and experimentation is a common practice in engineering simulations (e.g., Han et al. 2018, Zhang et al. 2021).

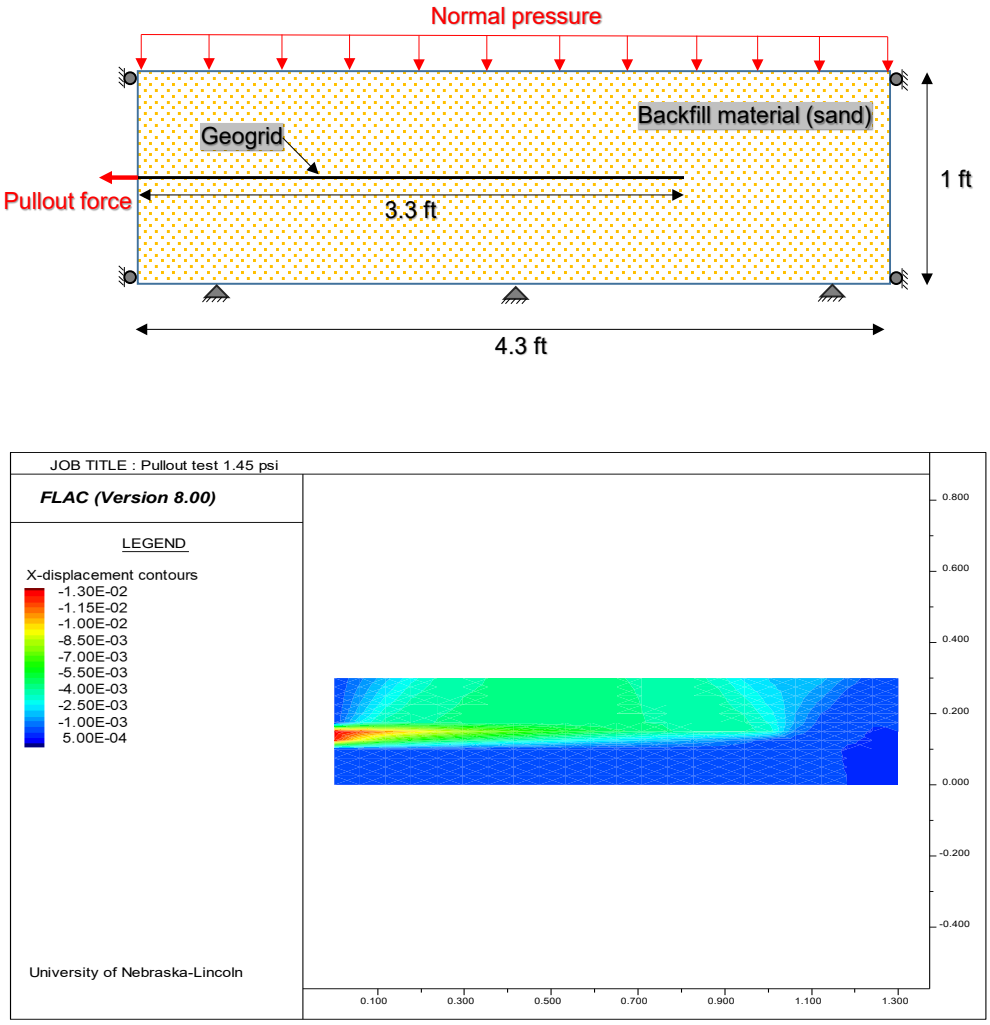

Figure 5.86 Modeling schematic and FLAC modeling example

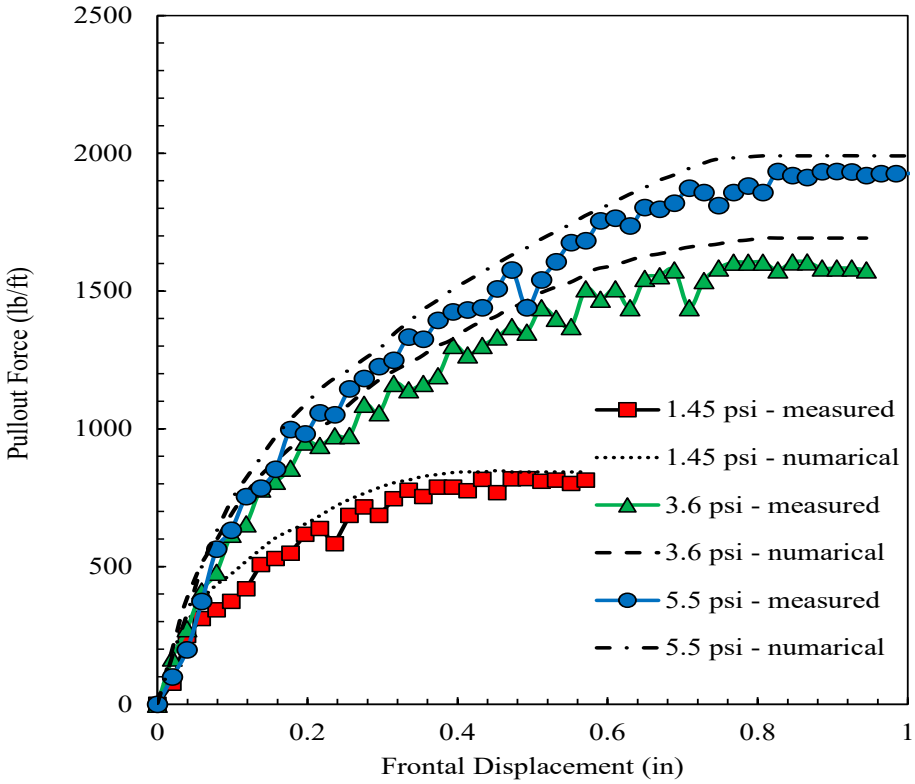

Figure 5.87 Match between pullout testing data and numerical simulation for parameter calibration

Table 5.19 Parameter for geosynthetic soil composite

Parameter	Biaxial geogrid	Triaxial geogrid	Geotextile
Elasticity modulus (psi)	150×10^3	120×10^3	70×10^3
Bond stiffness, kbond (psf)	36,600	33,400	20,000
Bond friction angle, sfriction (°)	43	39	30
Bond strength, sbond (lb/ft)	560	450	320

*Modified after Abdi and Arjomand (2011) and experimental direct shear tests

5.4.2 Simulation Cases

We conducted a series of simulation to evaluate how the geosynthetic work on reinforcing different types of subgrades such as sand, lean clay, and soft soils. Also, we tested the location of geosynthetic in the different pavement layers. We installed geosynthetic beneath the asphalt surface layer, middle of base layer and interface between base and subbase. All cases of the simulation are shown in Figure 5.88. Table 5.20 describe the modeling cases associated with soil type.

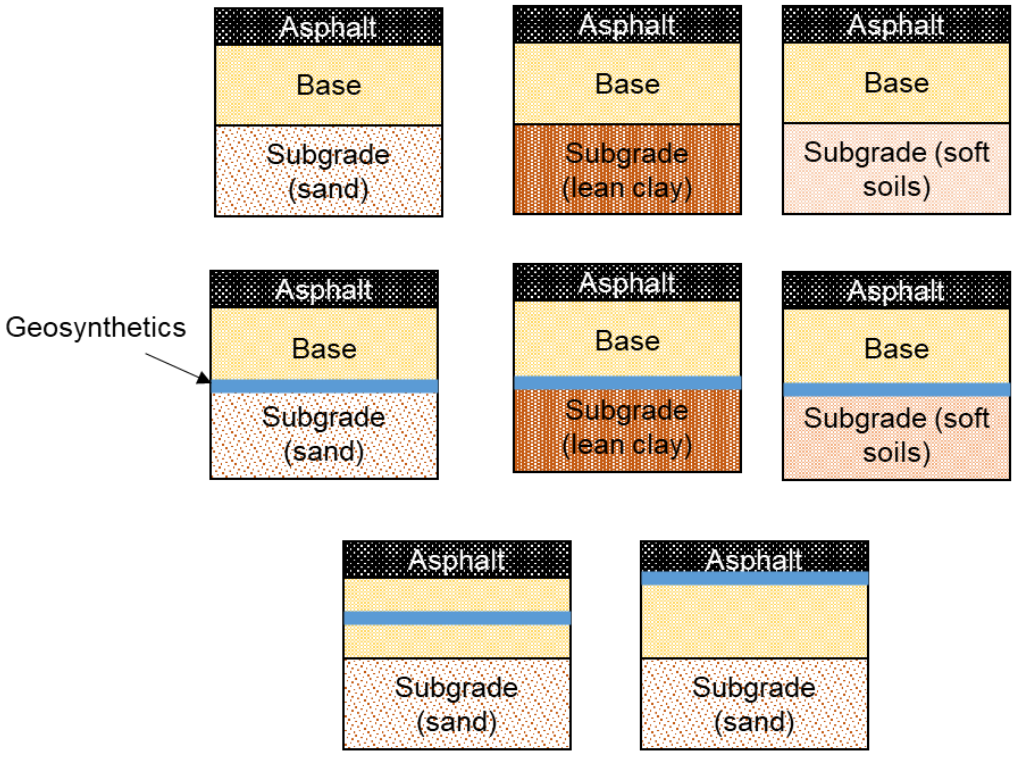

Figure 5.88 Simulation cases

Table 5.20 Number of simulation cases

Soil type (subgrade)	Cases modeled	Number of cases
Sand	Change in reinforcement type	4
	Change in reinforcement location	2
Lean clay	Change in reinforcement type	4
Soft soil	Change in reinforcement type	4

5.4.3 Simulation Results for Reinforcement in Sand

Figure 5.89 shows the surface displacement or settlement for sand along to distance from the center of the pavement modeling. The modeling results showed that the displacement was highest for the unreinforced case, followed by the geotextile, triaxial, and biaxial geogrids. While the direct shear tests showed that the geotextile could perform poorly in sand, the simulations concluded that it performed better than the unreinforced case. This was presumed to be because the geotextile was not subjected to resistive shear and was subjected to more bearing load. In the sand-based test, the geotextile with the lowest confinement increased its performance by 9.02% compared to the unreinforced case. Meanwhile, the biaxial showed an 18.0% reduction in settlement in the simulation and the triaxial showed a 14.8% reduction. The simulations showed that for sand conditions, the biaxial was better than the triaxial and the geotextile was the worst, which is consistent with the collected data.

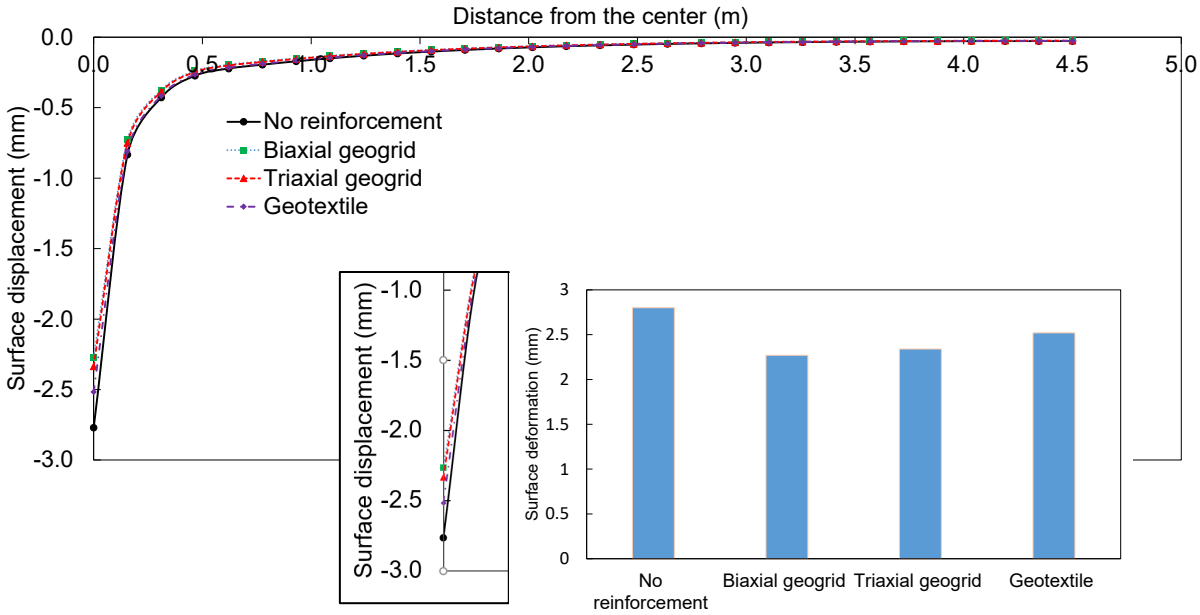

Figure 5.89 Displacement in san

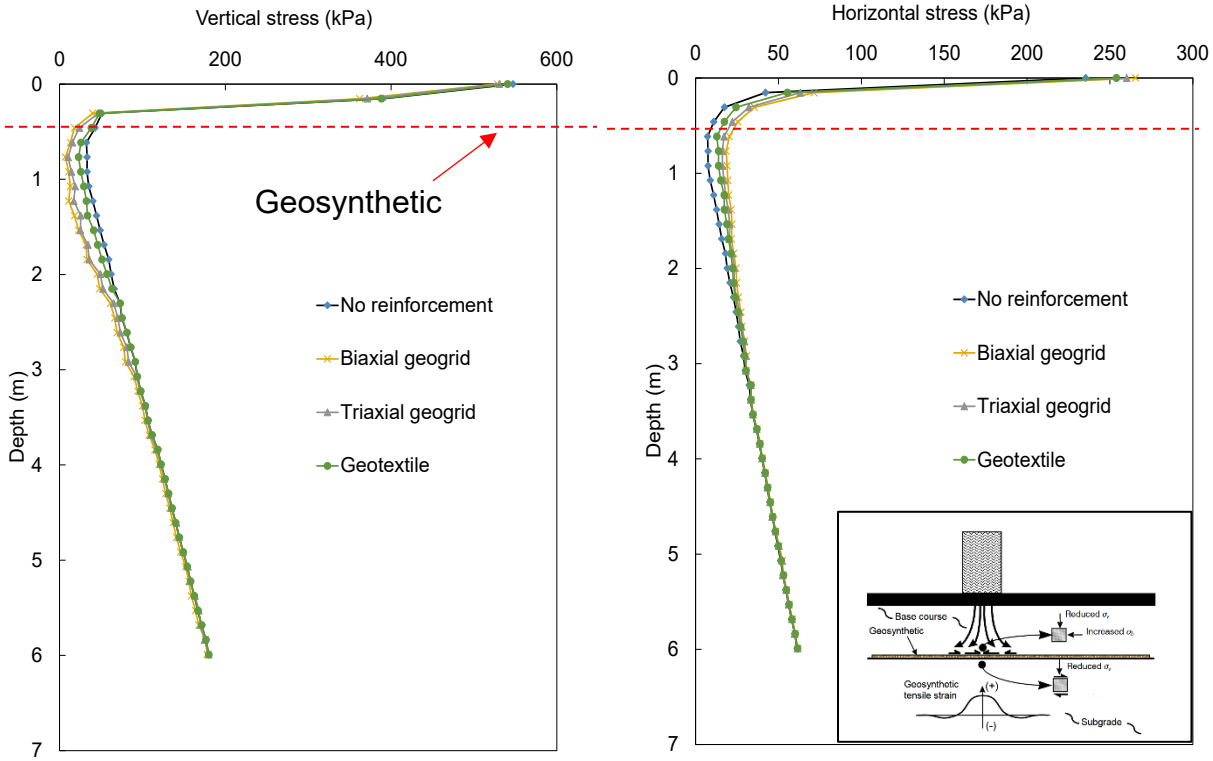

Figure 5.90 Vertical and horizontal stress in sand

Figure 5.90 shows the vertical and horizontal stresses as a function of depth. The axial loading applied on the surface is significantly reduced along with the base layer. At the base and subbase interlayers, there is a stress dispersion due to the reinforcement. It can be seen the vertical stress decreases when the geosynthetic reinforcement layer is present, which is believed to be because the vertical stress caused by the axial load is transferred to the horizontal stress through the geosynthetic reinforcement. In the foundation aggregate, the horizontal stresses also increased with the reinforcement layer compared to the case without reinforcement. Furthermore, the stress distribution is matched well to the order of settlement occurrences. The case of no reinforcement shows the highest vertical and lowest horizontal stress. Also, to the settlement occurrence, the biaxial and triaxial show relatively lower vertical and higher horizontal stress than other cases. This result means the reinforcement is working adequately matched with the settlement results. The stress transfer mechanism illustrates this process well as shown in Figure 5.90. This result confirms the reinforcement function of geosynthetics.

5.4.4 Simulation Results for Reinforcement in Clay

Figure 5.91 shows the surface displacement or settlement for clay. The settlement in the clay is significantly reduced compared to the no-reinforcement case when geosynthetics were installed. The input parameters for the clay corresponded nicely to the normalized interfacial shear resistance values of red shale. To this end, the red shale also falls into the clay-simulated category. The clay shear resistance had the greatest increases in their values, ranging from 6.9% - 25.6% for the direct shear test. It showed improvement in all cases for the direct shear, similar to the simulation. In the direct shear, the geotextile had the greatest values for the interfacial shear resistance followed closely behind by the geogrids. The simulation also reflected those increases. The geotextile provided the least amount of settlement, and it had the highest shear resistance

values for clay. Its settlement was improved by 41.8%. The biaxial and triaxial also had great improvements of 37.2% and 27.5%.

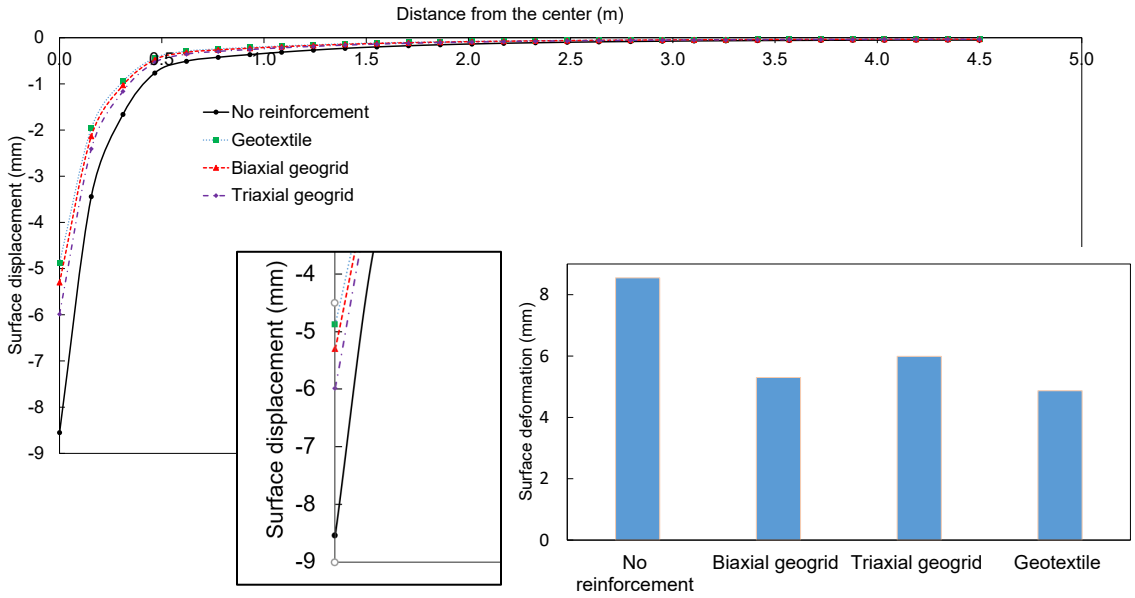

Figure 5.91 Displacement in clay

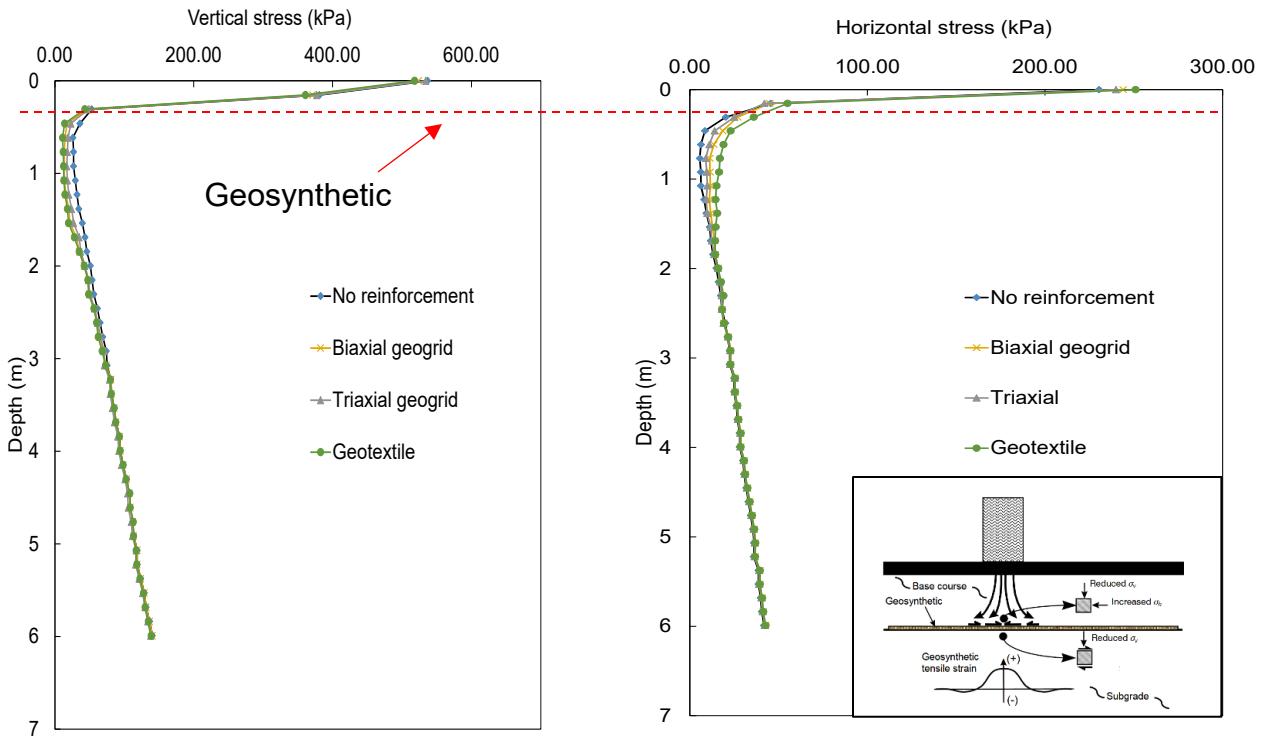

Figure 5.92 Vertical and Horizontal Stress in Clay

Similar to sand subgrade, Figure 5.92 shows the vertical and horizontal stresses as a function of depth in clay. The axial loading applied on the surface is significantly reduced along with the base layer. At the base and subbase interlayers, there is a stress dispersion due to the reinforcement. It can be seen the vertical stress decreases when the geosynthetic reinforcement layer is present, which is believed to be because the vertical stress caused by the axial load is transferred to the horizontal stress through the geosynthetic reinforcement. In the foundation aggregate, the horizontal stresses also increased with the reinforcement layer compared to the case without reinforcement. Furthermore, the stress distribution is matched well to the order of settlement occurrences. When there was no reinforcement there was the highest vertical and lowest horizontal stress. Also, the biaxial and triaxial show relatively lower vertical and higher horizontal stress than other cases during the settlement occurrence. This result means the

reinforcement is working adequately matched with the settlement results. The stress transfer mechanism illustrates this process well in Figure 5.92. This result confirms the reinforcement function of the geosynthetics.

5.4.5 Simulation Results for Reinforcement in Soft Soil

Figure 5.93 shows the surface displacement or settlement for soft soil. The soft soil simulation represents sensitive subgrade soils, and it saw the most significant increases in productivity with the addition of geosynthetics. Though the geotextile did not improve as well as the geogrids, this might have been due to the geogrids being stiffer in the soft surrounding and provided more of a reactionary force than the geotextile. The geotextile still had a good improvement with 41.9% while the biaxial and triaxial had a 62.0% and 57.5% decrease in settlement.

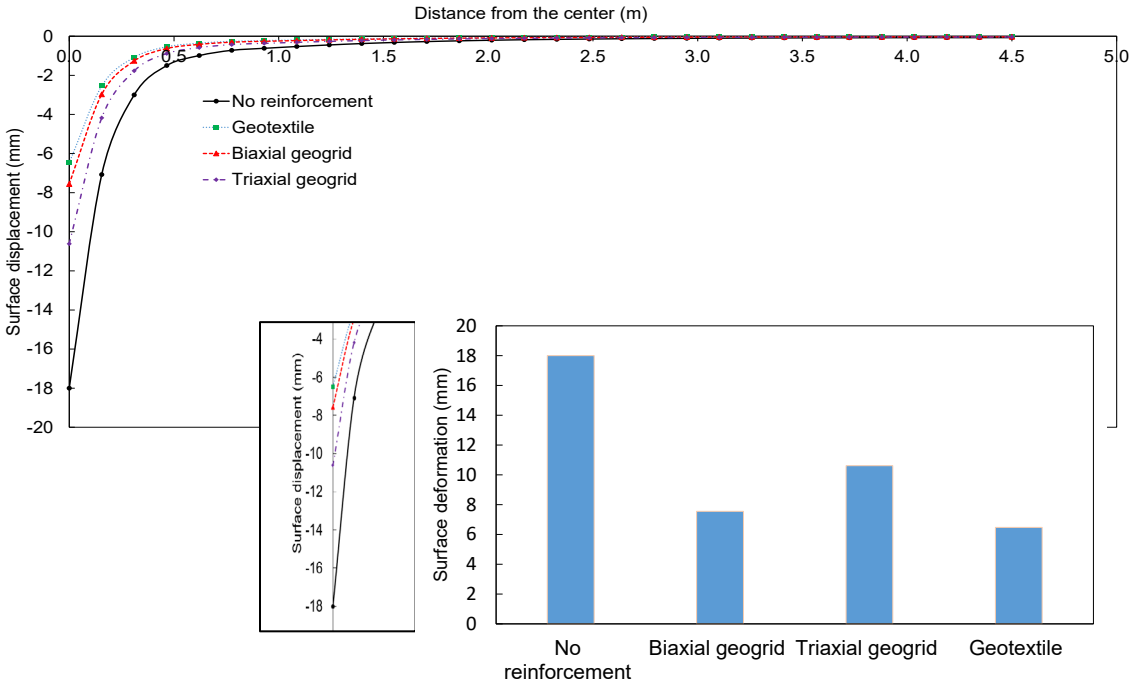

Figure 5.93 Displacement in soft soils

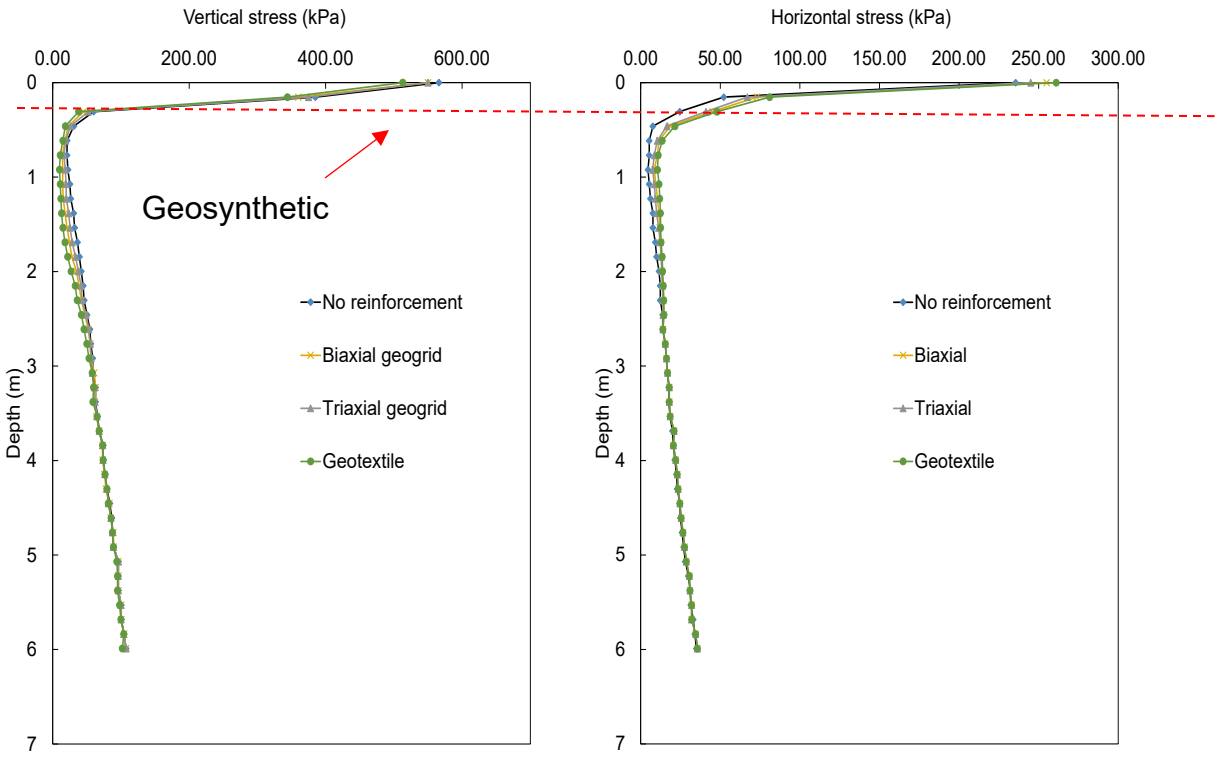

Figure 5.94 Vertical and horizontal stress in soft soils

According to a study by Wu et al. (2019), the use of geosynthetic reinforcement in foundation aggregates can significantly affect the stress distribution and settlement occurrence in soft soil subgrade Figure 5.94 shows the vertical and horizontal stresses as a function of depth in the soft soil subgrade with and without geosynthetic reinforcement. The study found that the geosynthetic reinforcement layer reduces the axial loading applied on the surface and in the base layer, which leads to stress dispersion in the subbase interlayers. The presence of the geosynthetic reinforcement layer causes a decrease in the vertical stress due to the transfer of the axial load to the horizontal stress through the reinforcement layer. In addition, the study found that the horizontal stresses in the foundation aggregates increase with the use of geosynthetic reinforcement. The stress distribution was observed to be well-matched with the order of settlement occurrences. The case with no reinforcement showed the highest vertical and lowest

horizontal stress, while the biaxial and triaxial cases showed relatively lower vertical and higher horizontal stress than other cases. Overall, the study confirmed the effectiveness of geosynthetic reinforcement in reducing the vertical stress and improving the horizontal stress distribution in foundation aggregates. The stress transfer mechanism was illustrated in Figure 5.94 provided further evidence of the reinforcement function of geosynthetics.

5.4.6 Simulation Results for Sand Subgrade-Different Reinforcement Location

In this section, we evaluated the effect of different geosynthetic locations on the response of the pavement layers in the modeling. Figure 5.89 shows the surface displacement or settlement for different geosynthetic location in the pavement layers. All three cases showed better performance compared to the no reinforcement in reducing the settlement. In particular, when the geosynthetic is located at the bottom at the interface between base and subgrade layers, the settlement shows the least compared to two other locations, however the difference is slight. This result would be different when the soil is not sand because sand subgrade is stronger than other soils.

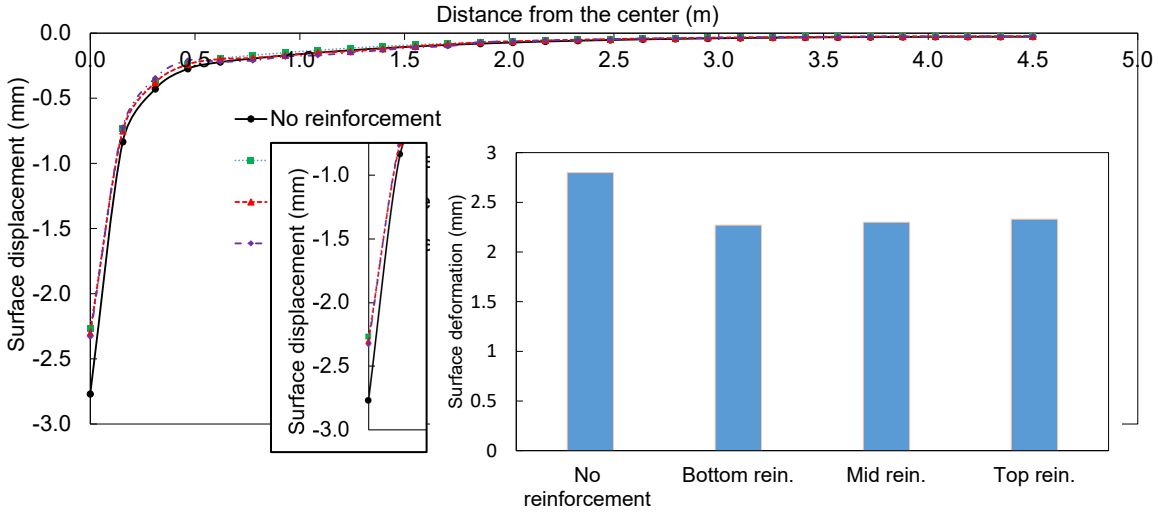

Figure 5.95 Displacement for different location of geosynthetics

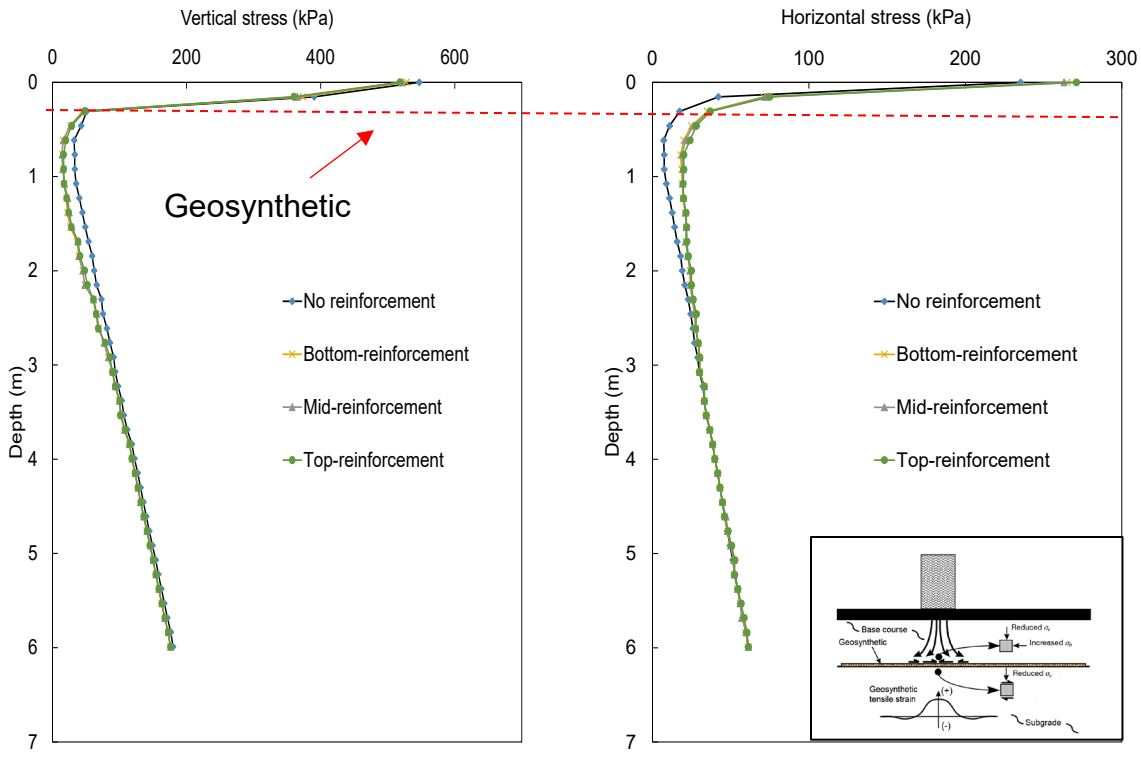

Figure 5.96 Vertical and horizontal stress for different location of geosynthetics

Similar to other cases, Figure 5.96 shows the vertical and horizontal stresses as a function of depth when the geosynthetics are installed at different depths. The axial loading applied on the surface is significantly reduced along with the base layer. At the base and subgrade interlayers, there is a stress dispersion due to the reinforcement. It can be seen the vertical stress decreases when the geosynthetic reinforcement layer is present, which is believed to be because the vertical stress caused by the axial load is transferred to the horizontal stress through the geosynthetic reinforcement. Similar to the settlement analysis, all three cases show similar vertical and horizontal stresses.

5.5 Dynamic Cone Penetrometer (DCP) Test

The outcomes of the soil chamber test for DCP were presented using the dynamic cone penetration index (DPI, mm/blow), which measures how deep the cone penetrates the soil with

each hammer blow. The DCP tests were conducted with three different subgrade materials namely Sand, Red Shale, and Clay, which are the same as the materials used in the direct shear and pullout tests. Gravel was used as the base course material in both cases. DPI was then used in estimating the CBR for the Sand subgrade and Gravel base course layer based on the US Army Corps of Engineers equations below.

$$CBR = \frac{292}{DCP^{1.12}} \; for \; DCP \; in \; mm/blow \tag{5.4}$$

$$CBR = \frac{1}{(0.017019 \; x \; DCP)^2} \; for \; DCP \; in \; mm/blow \tag{5.5}$$

Equation (5.1) can be used in estimating the CBR for all soils except CL soils below CBR 10 and CH soils whiles Equation (5.2) applies for CL with a CBR less than 10. This is because the surface is exposed to the atmosphere and subjected to low confining pressure. For this analysis the first 100 mm base course layer was neglected.

The CBR for Red Shale soil at optimum moisture content were higher than the expected range for clayey soil as such CBR results for clayey soil were not included in the result discussion.

5.5.1 Results of Sand Subgrade

Figure 4.18 shows the case of a compacted sand subgrade layer where the sand was used as a subgrade material for the DCP test. Tests were conducted firstly with no geosynthetic and subsequently with different geosynthetics to evaluate the performance and improvement in the soil layer with the geosynthetic addition. The four different geosynthetic material used for the test here are GG1, GG2, GG3, and GT. Figure 5.97 shows the cumulative blows against the

depth from the surface for the various geosynthetic material. The change in slope at 300 mm shows the boundary between the gravel base course material and the sand layer. Figure 5.98 and Figure 5.99 show the varying DPI, which is the penetration per blow and CBR against the depth from the surface of the barrel respectively. A summary of the average DPI across the sand subgrade layer is found in Table 5.21. Results from Table 5.21 show the improvement in the sand subgrade layer for the cases where geosynthetic material was placed between the base and subgrade layer. GG2 had the best performance in terms of the improvement in the sand subgrade layer with a DPI of 5.4 mm/blow as against a DPI of 8.6 mm/blow for the unreinforced case. This represents an estimated CBR of 44.2%, representing a 68.7% increase in the CBR of the sand layer. GG1 and GG3 showed similar performance with DPIs of 6.1 mm/blow and 6.2 mm/blow with an estimated CBR of 38.5% and 37.8%, respectively. This represents 46.9% and 44.3% increase in CBR respectively for the sand layer. The improvement in the sand subgrade reading was least in the case for GT with a DPI of 7.4 mm/blow and an estimated CBR of 31%. This represents an 18.3% increase in the CBR of the sand layer. It is found that the DPI can provide a way to estimate the strength of soil with depth through the test.

Table 5.21 Average DPI reading for reinforced and unreinforced sand layer

Type	DPI (mm/blow)	CBR (%)	Percentage increase in CBR (%)
Sand without reinforcement	8.6	26.2	-
GG1 Reinforced Sand	6.1	38.5	46.9
GG2 Reinforced Sand	5.4	44.2	68.7
GG3 Reinforced Sand	6.2	37.8	44.3
GT Reinforced Sand	7.4	31.0	18.3

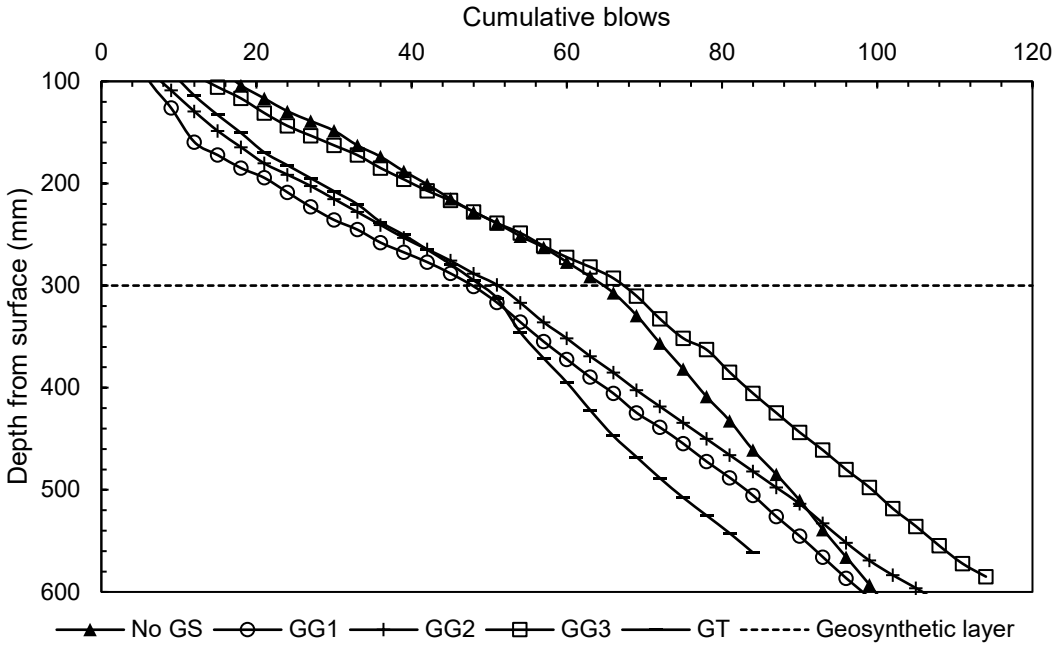

Figure 5.97 Cumulative blows against depth from surface - gravel base course with sand. subgrade

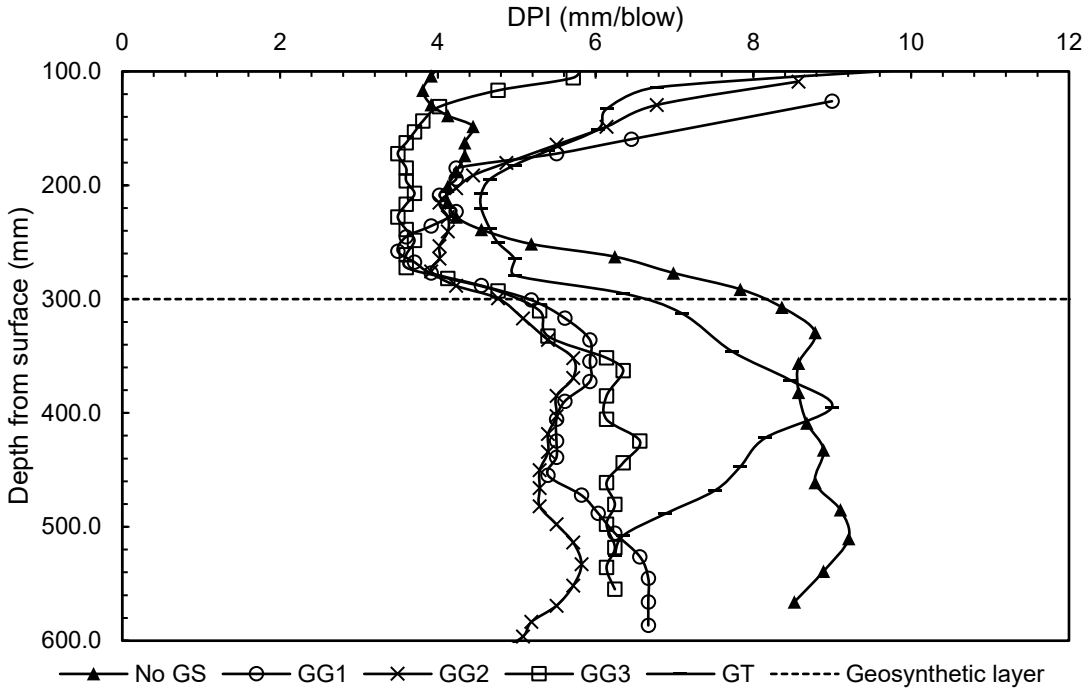

Figure 5.98 DPI against depth from surface - gravel base course with sand subgrade

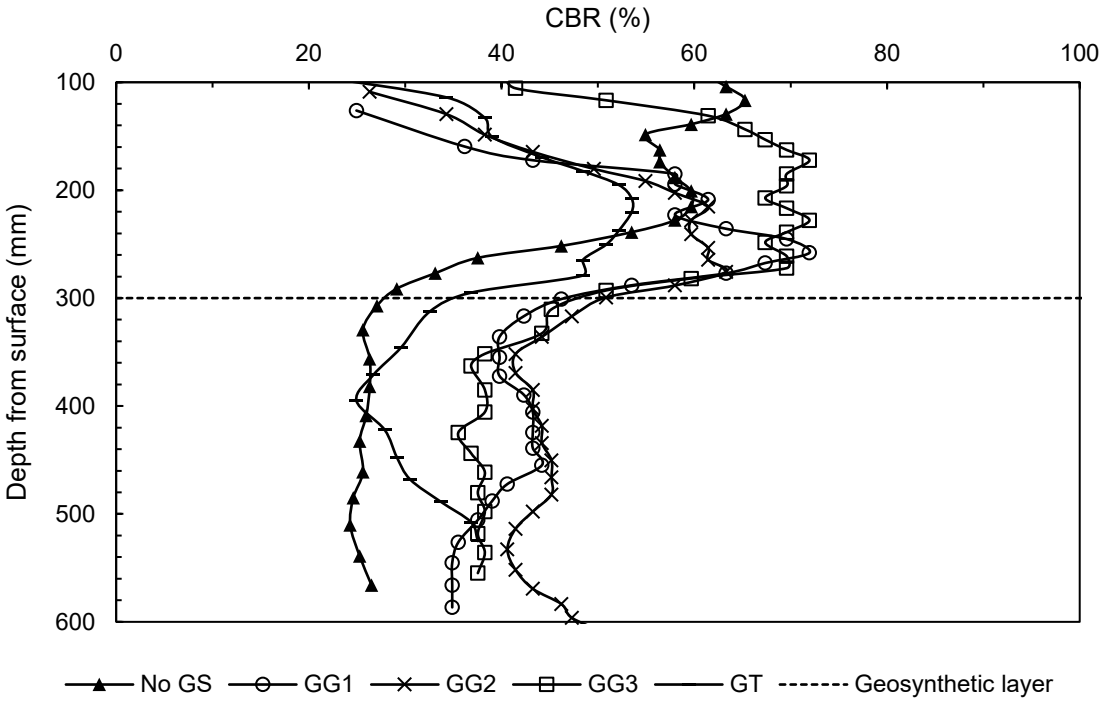

Figure 5.99 CBR against depth from surface for gravel base course with sand subgrade

Also, there was improvement in the soil packing structure approximately 70 mm above the geosynthetic layer highlighted as the confinement zone in Figure 5.100. Table 5.22 highlights the average DPI of the gravel base course layer 70 mm above the sand layer for both reinforced and unreinforced cases. The average DPI for the base course layer 70 mm above the subgrade layer was approximately 5.8 mm/blow, representing an estimated CBR of 41%. The use of GG3 resulted in the best soil packing structure above the sand subgrade layer as shown in Table 5.22 with an estimated CBR increase of 70.7%. GG1 and GG2 had a similar trend with DPI of 3.9 mm/blow and 3.6 mm/blow which gives an estimated CBR of 64% and 62% respectively. The CBR increase in the GG1 and GG2 reinforced base course layer 70 mm above the subgrade layer is 56.1% and 51.2% respectively. From these results, the confined zone due to the geosynthetic

reinforcement can be observed and the effect of the reinforcement in the layer was proved clearly.

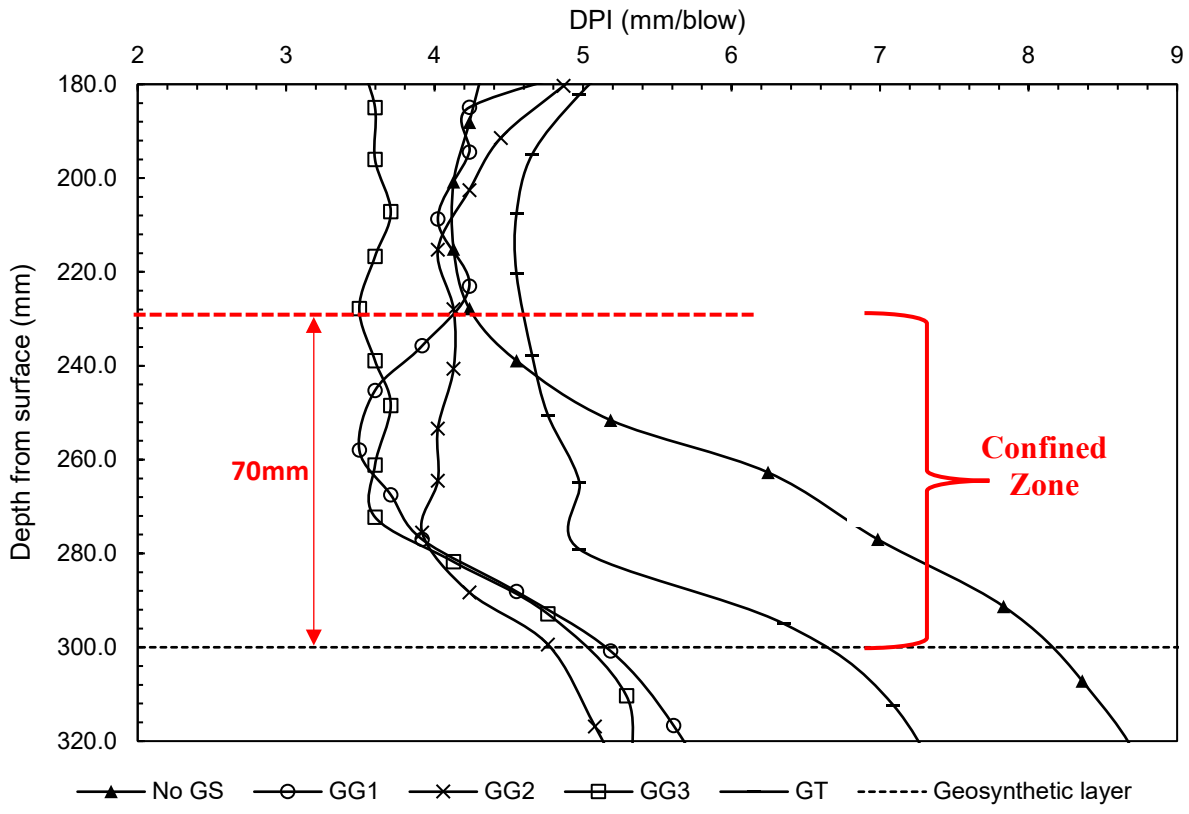

Figure 5.100 Confinement zone above geosynthetics – sand subgrade

Table 5.22 Average DPI reading and corresponding estimated CBR for confinement zone

Type	DPI (mm/blow)	CBR (%)	Percentage increase in CBR (%)
No Reinforcement	5.8	41	-
GG1 Reinforced	3.9	64	56.1
GG2 Reinforced	4	62	51.2
GG3 Reinforced	3.6	70	70.7
GT Reinforced	5	48	17.0

5.5.2 Results of Red Shale Subgrade

Figure 4.25 shows the case where Red Shale was used as a subgrade material for the DCP test. Tests were conducted firstly with no geosynthetic and subsequently with GG1 and GG2 geosynthetics to evaluate the performance and improvement in the soil layers with the geosynthetic addition. Figure 5.101 shows the cumulative blows against the depth from the surface for both reinforced and unreinforced cases. The change in slope at 300 mm shows the boundary between the gravel base course material and the Red Shale layer. Figure 5.102 shows the varying DPI, which is the penetration per blow against the depth from the surface of the barrel.

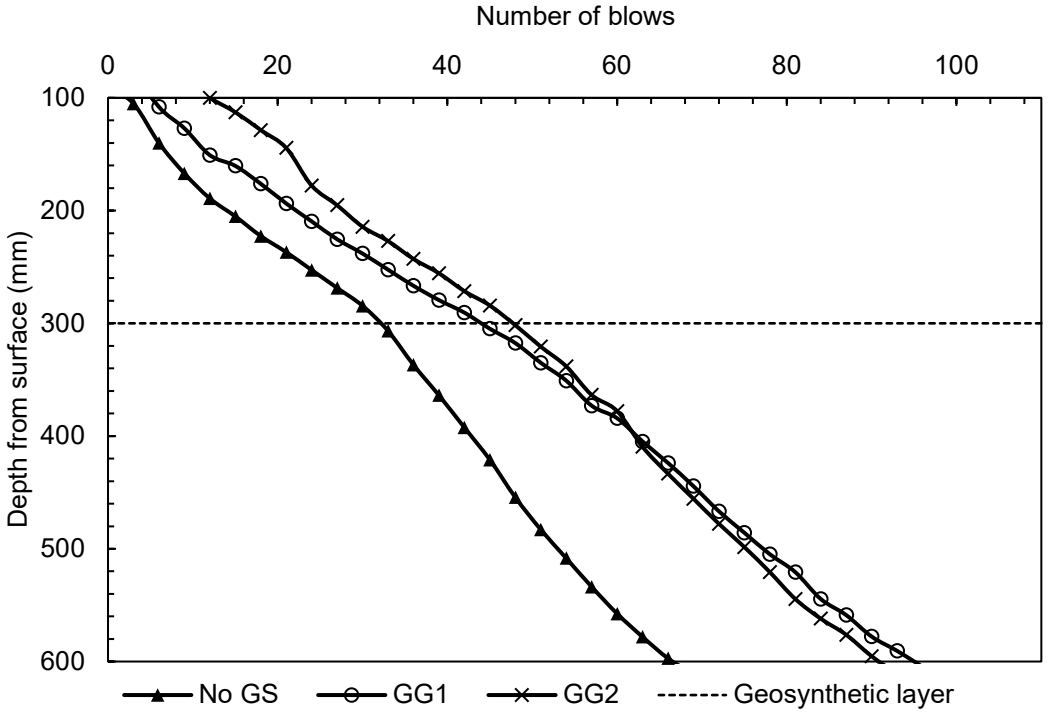

Figure 5.101 Cumulative blows against depth from surface – gravel base course with red shale subgrade

A summary of the average DPI across the Red Shale layer is found in Table 5.23. These results show the improvement in the Red Shale subgrade layer for the geosynthetic reinforced case. GG1 had the best performance regarding the improvement in the Red Shale subgrade layer with the DPI of 6.0 mm/blow and a corresponding decrease in the penetration index by 35.5% while GG2 had a DPI of 7.1 mm/blow and a corresponding decrease by 23.6 % in the penetration index compared to the case where no geosynthetic material was placed between the base and subgrade layer. The confined zone was generated in the subgrade from the interface to around 400 mm depth. The thickness of the zone is approximately 100 mm, which is thicker than that in sand subgrade. The decrease in the DPI from 450 mm downwards can be attributed to the sand layer below the Red Shale layer which increased the stiffness of the Red Shale layer at the lower half of the Red Shale layer. This sand layer was put in place to reduce the effect of boundary condition on the Red Shale layer.

Table 5.23 DPI index of Red Shale subgrade for reinforced and unreinforced cases

Type	DPI (mm/blow)
No Reinforcement	9.3
GG1 Reinforced	6
GG2 Reinforced	7.1

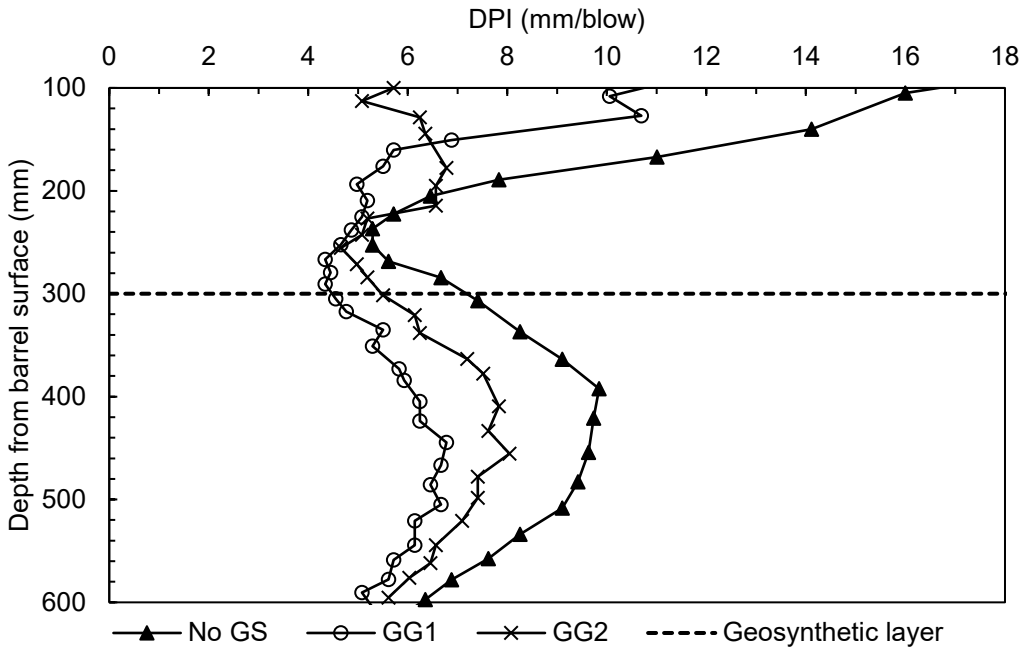

Figure 5.102 DPI against depth from surface - gravel base course with red shale subgrade

A similar situation of improvement in the base course layer was observed in the case of the Red Shale subgrade as well. There was an improvement in the soil packing structure just above the geosynthetic reinforcement. The thickness of this observed area was approximately 60 mm for this case (Figure 5.103). From these results, the confined zone due to the geosynthetic reinforcement can be observed and the effect of the reinforcement in the layer was proved clearly.

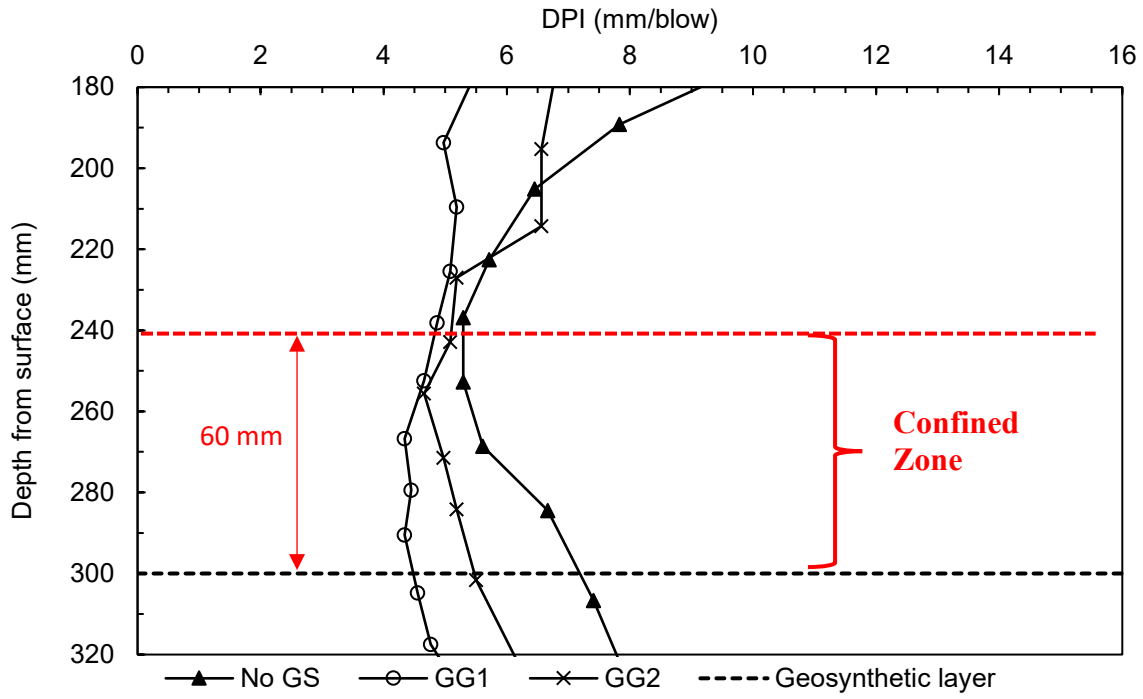

Figure 5.103 Confinement zone above geosynthetics – red shale subgrade

5.5.3 Results of Clay Subgrade

In Table 5.24, Figure 5.104 and Figure 5.105, GG2 and GT had the best performance regarding the improvement in the clay subgrade layer with the DPI of approximate 15.0 mm/blow and a corresponding decrease in the penetration index by 34.7% whiles GG1 had a DPI of 16.0 mm/blow and a corresponding decrease by 30.4% in the penetration index compared to the case where no geosynthetic material was placed between the base and subgrade layer. The confined zone was generated in the subgrade from the interface to around 400 mm depth as shown in Figure 5.106. The thickness of the confined zone in the base is approximately 120 mm, which is thicker than that in sand subgrade. The decrease in the DPI from 450 mm downwards can be attributed to the sand layer below the Clay layer which increased the stiffness of the Clay

layer at the lower half of the Clay layer. This sand layer was put in place to reduce the effect of boundary condition on the Clay layer.

Table 5.24 DPI index of Clay subgrade for Reinforced and Unreinforced cases

Type	DPI (mm/blow)
No Reinforcement	23
GG1 Reinforced	16
GG2 Reinforced	15.5
GT reinforced	15

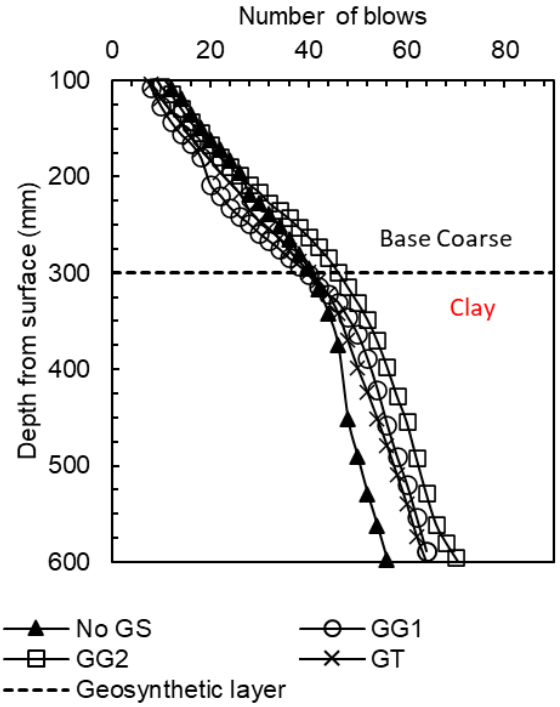

Figure 5.104 Cumulative blows against depth from surface – gravel base course with clay subgrade

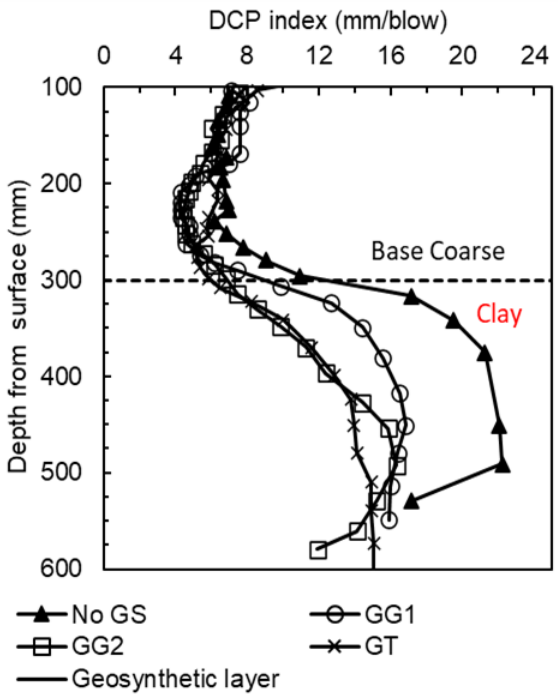

Figure 5.105 DPI against depth from surface - gravel base course with clay subgrade

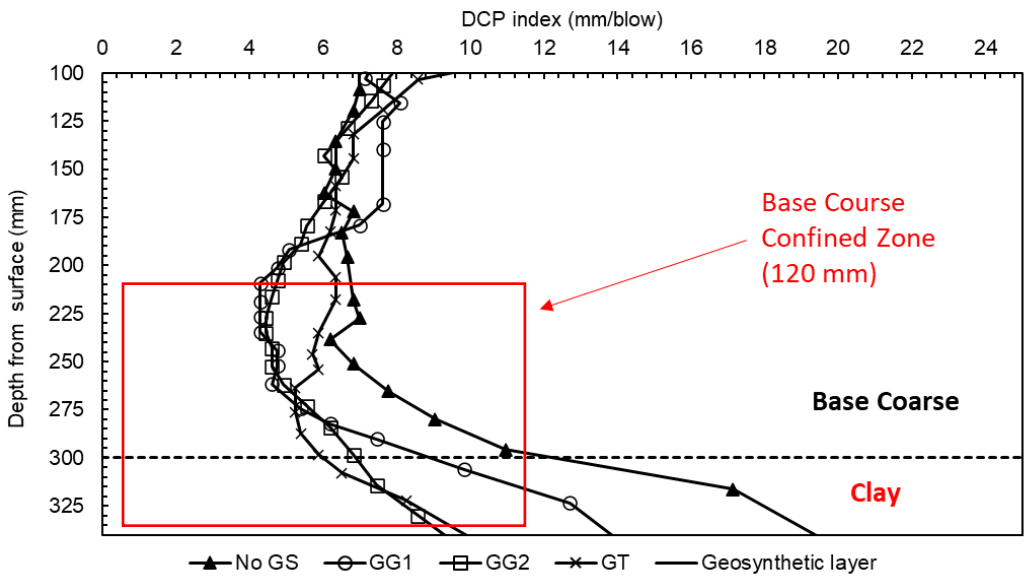

Figure 5.106 Confinement zone above geosynthetics – clay

5.5.4 DCP Result Evaluation

The results shown in Figure 5.107 show reduction in the DPI for the various cases where geosynthetic was applied in the chamber implying an improvement in the strength of the subgrade (clay, red shale and sand) for different geosynthetic types. Comparison of DPI profiles with depth for different geosynthetic and soil types can also be found in Figure 5.108 Using correlation from Lin et al (2005), The resilient modulus of the different soil subgrades was computed as shown in Table 5.25 showing the percentage increases in the resilient moduli compared with the control for each soil type.

Table 5.25 DPI and Resilient Modulus correlation

Soil Type	Type	DPI (mm/blow)	Mr (psi)	% increase
Sand	Control	8.6	18701	-
	GG1	6.1	23491	25.6
	GG2	5.4	25472	36.2
	GG3	6.2	23239	24.3
	GT	7.4	20663	10.5
Red shale	Control	9.3	17754	-
	GG1	6	23751	33.8
	GG2	7.1	21239	19.6
Clay	Control	23	9731	-
	GG1	16	12383	27.2
	GG2	15.5	12647	30.0
	GT	15	12925	32.8

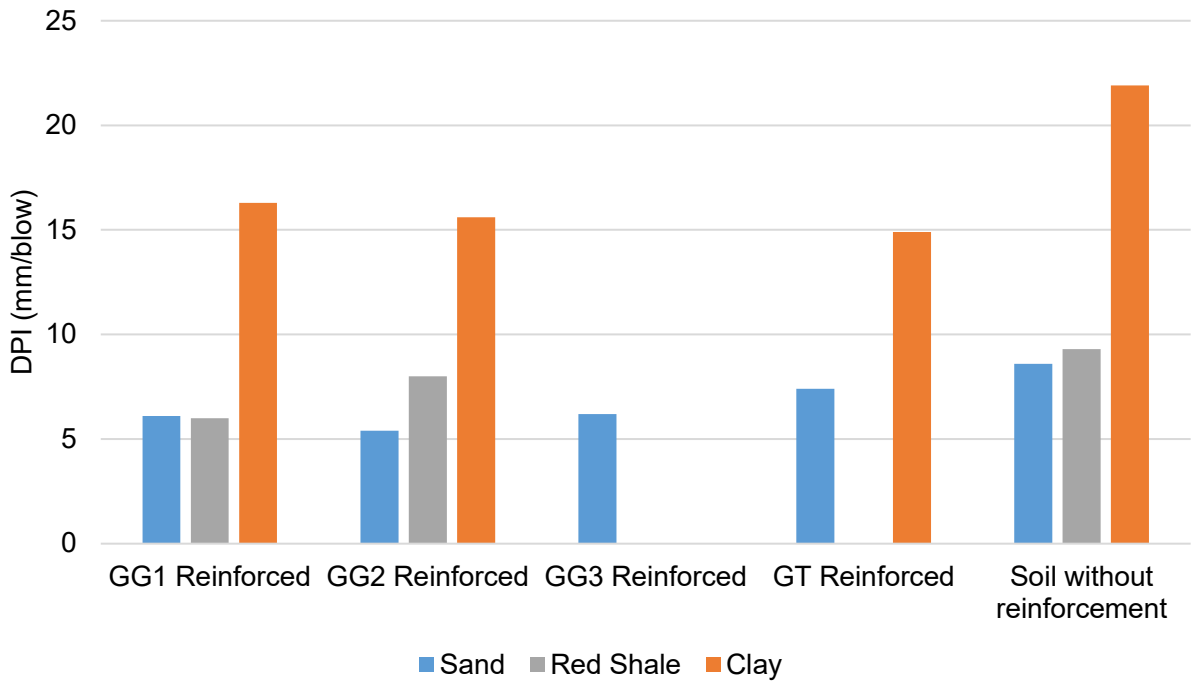

Figure 5.107 Comparison of DPI for different geosynthetics and soil type

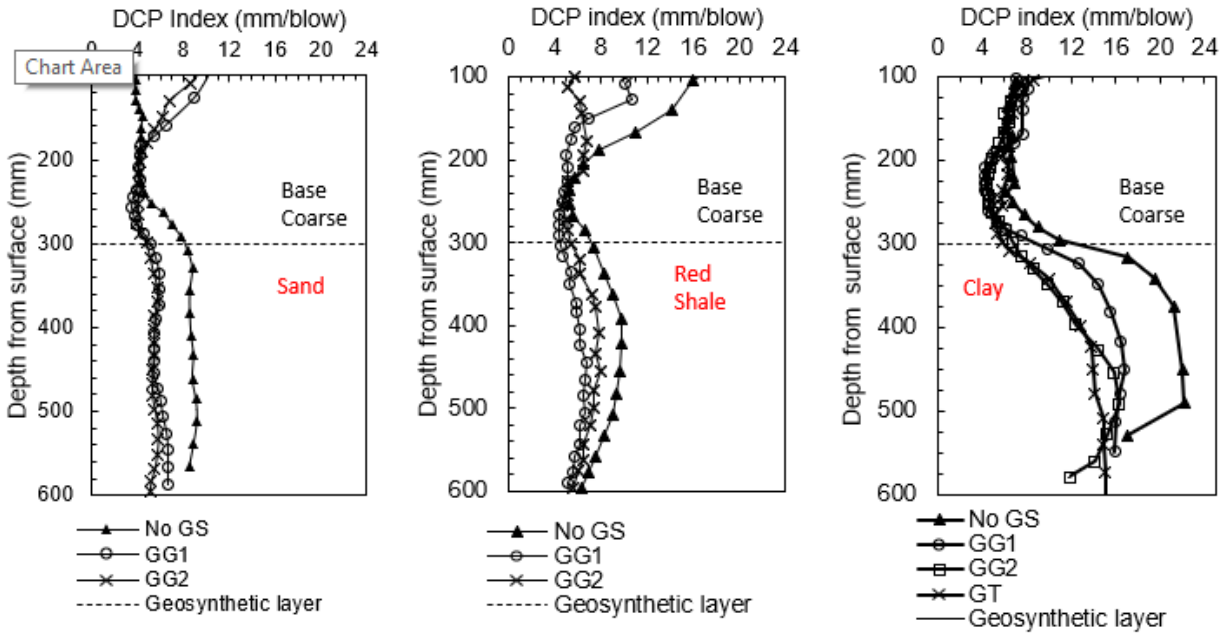

Figure 5.108 Comparison of DPI profiles with depth for different geosynthetic and soil types

5.6 Relationship between pull-out, direct shear and DCP in Chamber

Table 5.26 summarizes the parameters obtained from the pull-out and direct shear tests and the DPI from the soil chamber test. Both DPI and CBR are correlated with different parameters obtained in laboratory experiments. Figure 5.109 highlights the relationship between DPI and pullout coefficient (or interaction coefficient) for red shale. Relationship between DPI and interface friction angle for sand can be seen in Figure 5.110.

Table 5.26 Summary of results for both reinforced and unreinforced cases

Geosynthetic type	Friction angle(deg)	Interaction ratio (Ci)	Initial modulus (kPa)	DPI (mm blow)	CBR
GG1 Reinforced	33.3	0.913	2200.0	6.1	38.5
GG2 Reinforced	38.7	0.655	2000.0	5.4	44.2
GG3 Reinforced	36.5	NA	NA	6.2	37.8
GT Reinforced	28	NA	NA	7.4	31.0
Sand without reinforcement	30	NA	NA	8.6	26.2

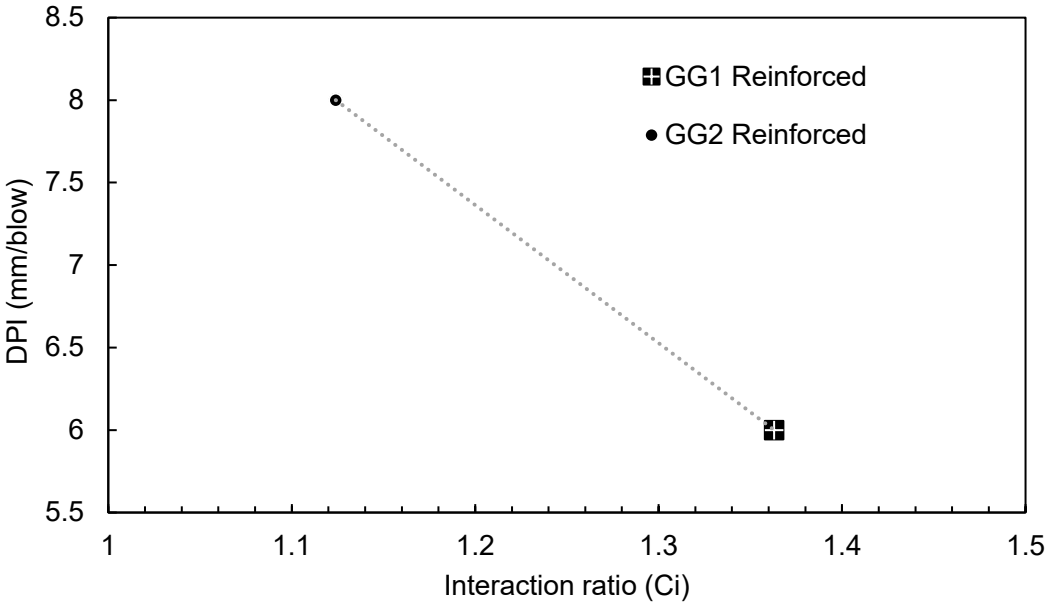

Figure 5.109 Relationship between DPI and pullout coefficient (or interaction coefficient) for red shale

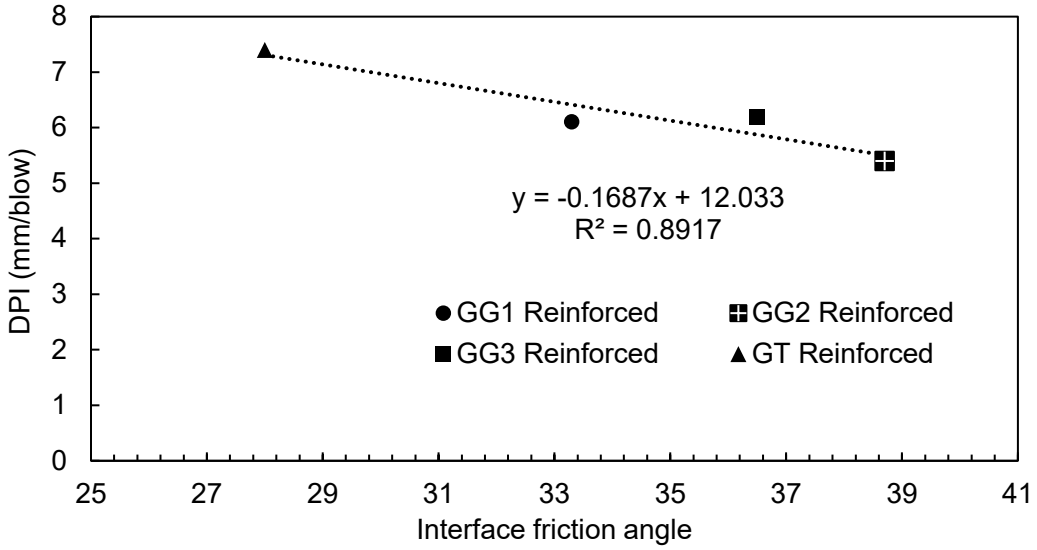

Figure 5.110 Relationship between DPI and interface friction angle for sand

5.7 Large Scale Tracking Wheel Test

Three parameters namely strength/stiffness as indicated by DCP indices, permanent deformation and pressure reduction effects were evaluated for the three cases to understand how the use of geosynthetic influences theses parameters in a pavement layer.

5.7.1 Evaluation of Pavement Strength/Stiffness

DCP tests were conducted before and after the LSTW test to evaluate the increase in strength of the pavement layer after the LSTW test. 1 shows the cumulative blows against depth for the three cases. GG1-12 in. showed the best performance in terms of increase in strength/stiffness of the entire pavement layer after the LSTW test. GG1–9 in. also showed a relatively better performance in terms of increase in base course layer strength compared with the control.

Figure 5.112 shows the cumulative blow against depth for the three cases. The profile of DPI with depth for the three cases can be found in Figure 5.112. The confining zone above the geogrids due to interlocking effect about the geosynthetic was identified and was more profound in the GG1-12 in. A as against GG1 – 9 in. A and the Control A. GG1 – 12 in. A also showed the highest level of improvement in both the base course and the subgrade strength/stiffness. GG1 – 9 in. A showed a relative increase in the base course strength/stiff but a reduction in the subgrade strength as compared to Control A. This can be attributed to the reduced confining stress acting on the pavement layer with the reduction in the pavement thickness. The reduction in the base course thickness resulted in a reduction in the subgrade restraint which is primarily affected by the confining stress acting on top of the geogrids. Figure 5.113 and Figure 5.114 shows the percentage reduction in the layer DCP indices for the three cases for both the base and subgrade.

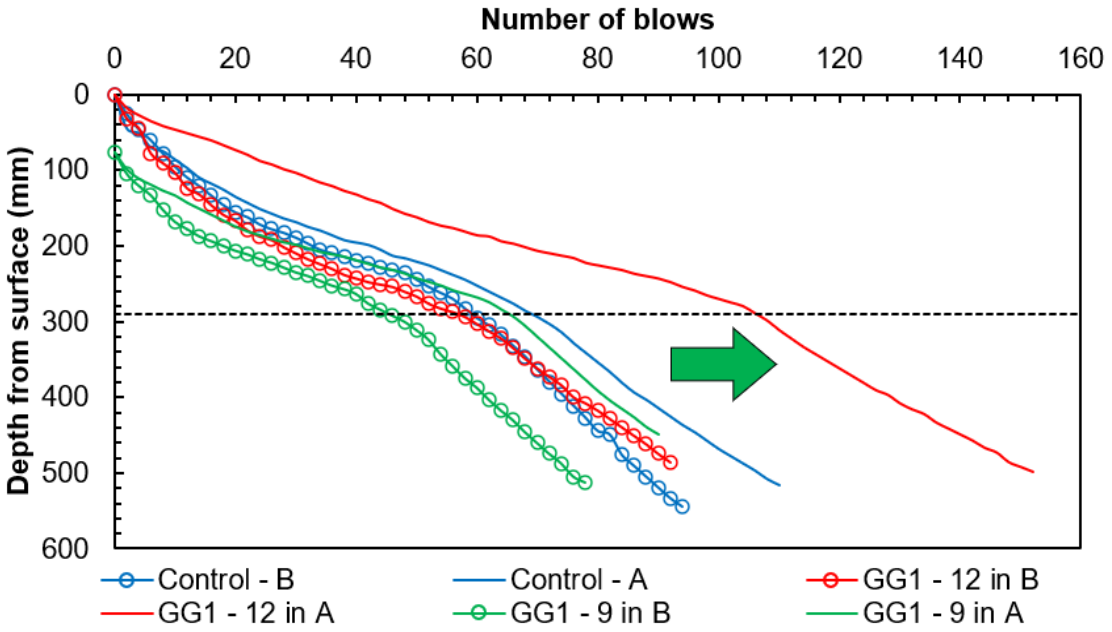

Figure 5.111 Cumulative blows vs Depth – LSTW

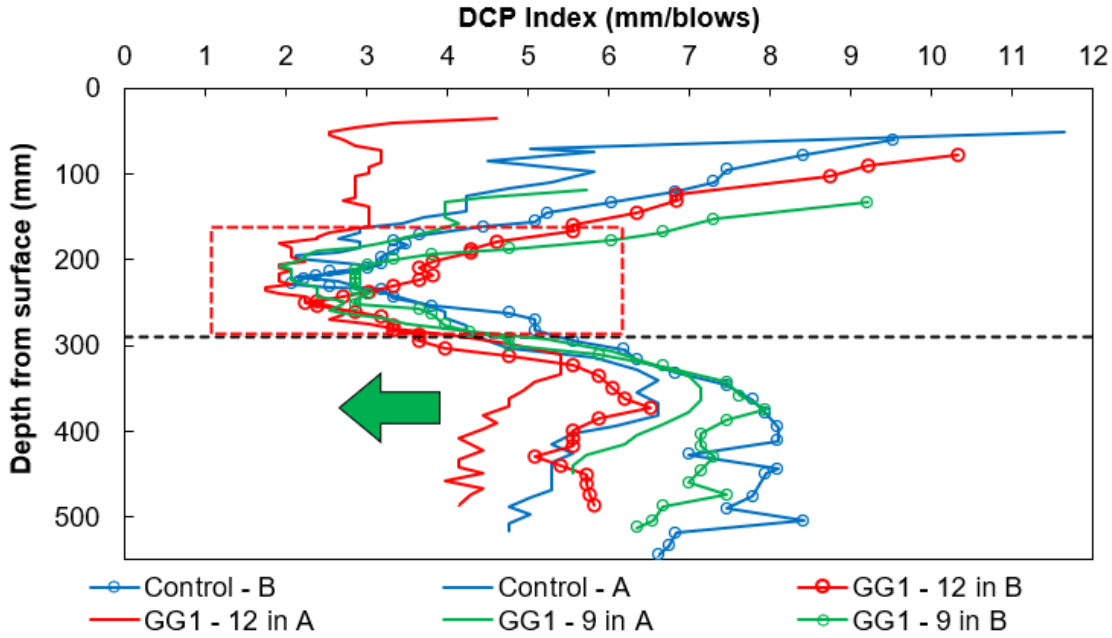

Figure 5.112 DPI vs Depth – LSTW

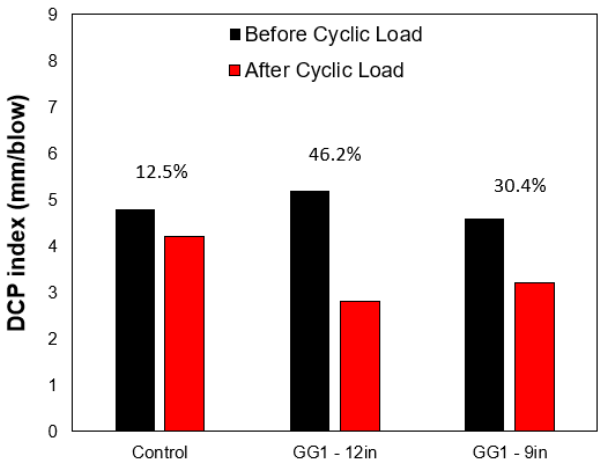

Figure 5.113 Base Course DPI comparison

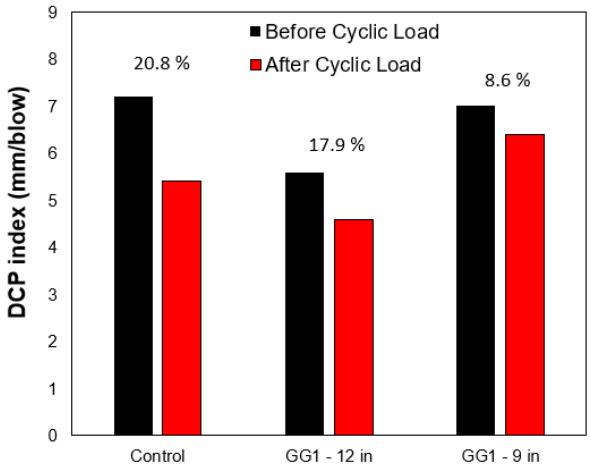

Figure 5.114 Sand subgrade DPI comparison

Using correlation by Lin et. Al 2005, Harison 1986 and Mohammed et al. 2008, the Resilient Modulus, CBR and Subgrade modulus of reaction were computed from the DPI as shown in Figure 5.27. Figure 5.114 and Figure 5.115highlight the increase in resilient modulus for the 3 different cases and layers both before and after the rolling wheel loading using the correlation by Lin et. al. 2005. Case 2 showed the highest increase in resilient modulus of the base layer after the LSTW test with a 50.8% increase while Case 3 showed a 27.2% increase in the resilient modulus. For the sand subgrade, Case 2 showed the highest increase in the resilient modulus of 14% followed by the Control with an increase of 21% and a 6% increase in the resilient modulus of Case 3.

Table 5.27 Correlations Between DPI and Strength Parameters

Correlation	DPI (mm/blow)		Mr (psi) (Lin et. al. 2005)		CBR (%) (Harison 1986)*		Ks (MN/m3) (Mohammad et. al. 2008)	
Case:1	Control							
Layer	B	A	B	A	B	A	B	A
Base course	4.8	4.2	27544	30098	50	58	218.82	246.79
Subgrade	7.2	5.4	21043	25472	32	44.14	151.85	196.79
Case:2	GG1-12 in							
Layer	B	A	B	A	B	A	B	A
Base course	5.2	2.8	26118	39396	46	92	203.59	355.62
Subgrade	5.6	4.6	24864	28334	42	53	190.44	227.37
Case: 3	GG1-9 in							
Layer	B	A	B	A	B	A	B	A
Base course	4.6	3.2	28334	36053	53	79	227.37	315.31
Subgrade	7	6.4	21440	22754	33	37	155.76	168.85

Table 5.28 Resilient Modulus Evaluation before Rolling Wheel Load Application

Case	DPI Before	Mr (psi)	% increase
Control	7.2	21042.8292	-
GG1-12 in	5.6	24864.2897	33.0
GG1-9 in	7	21440.1495	14.6

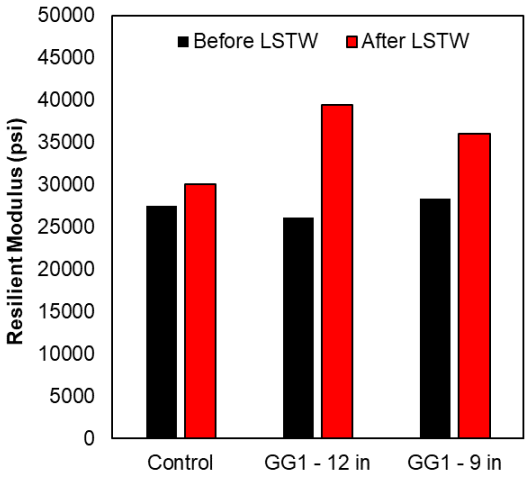

Figure 5.115 Resilient modulus estimate – base

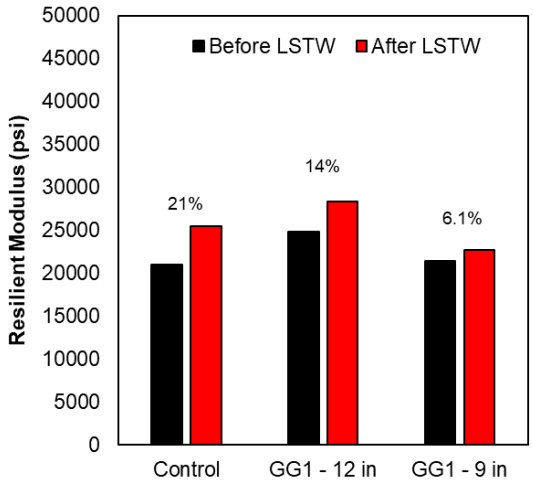

Figure 5.116 Resilient modulus estimate – subgrade

5.7.2 Evaluation of Permanent Deformation (Rutting)

The total vertical deformation (rutting) that occurred beneath the tire at the top surface of the base course layer was measured after the Large-Scale Tracking Wheel Test for the three cases using tape measurement. Figure 5.117 shows the total deformation recorded for the three cases. With the use of geogrid, the total permanent deformation reduced from 44mm for the Control to 29 mm which represents a 34.1% reduction for Case 2. Comparing the Control and Case 3, the total permanent deformation reduced from 44mm to 31mm which represents a 29.5% reduction.

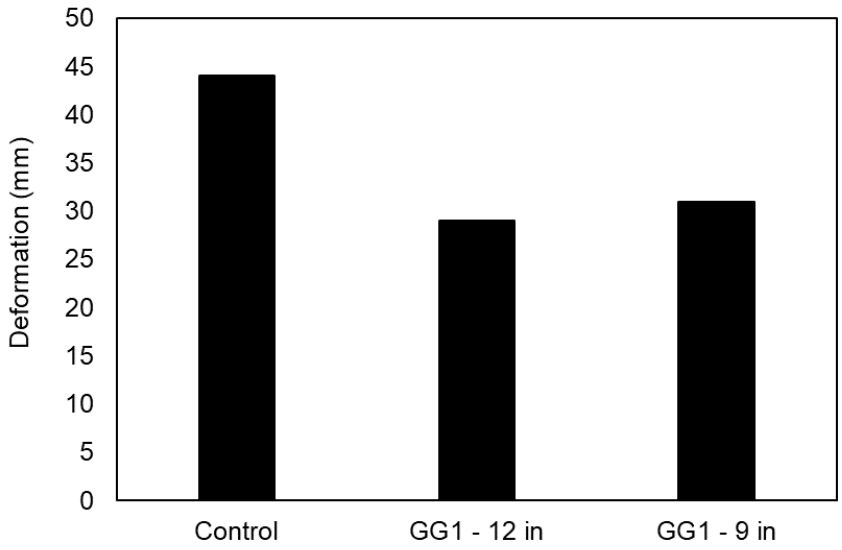

Figure 5.117 Deformation comparison for 3 Cases

The 6 LVDT installed on the sides of the wheel also recorded the total deformation for Case 1 and Case 2. Figure 5.118 to Figure 5.124 show the total deformation recorded by the six LVDTs. Comparing the deformation measured for the Control to Case 2, a significant reduction in the total deformation was observed in the use of geogrids. This can primarily be attributed to the geogrids lateral restraint effect which provided more resistance to deformation. The deformation reduction with the use of geosynthetic is more prominent in LVDT 3 and LVDT 4 which are the closest to the point of application of the wheel loading.

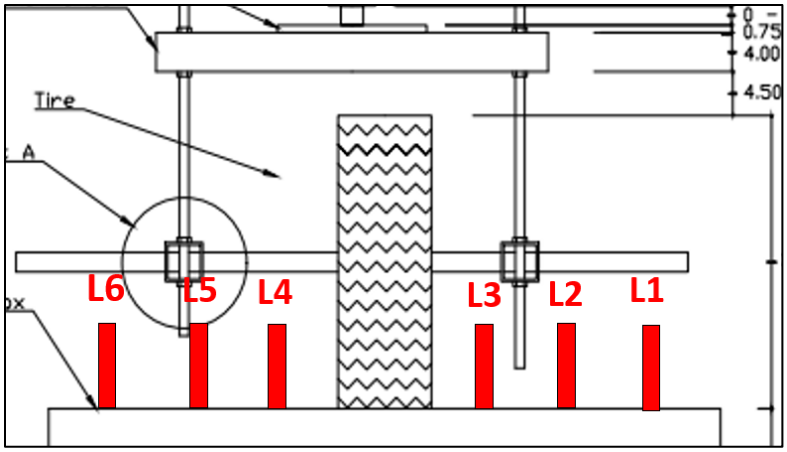

Figure 5.118 LVDT positions in LSTW setup

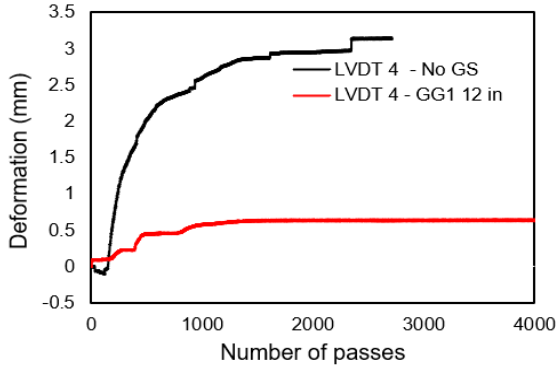

Figure 5.119 LVDT 4 deformation readings

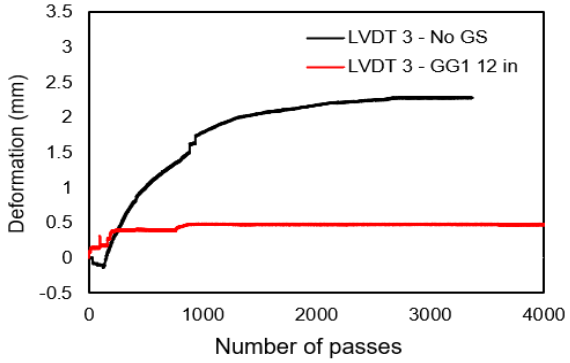

Figure 5.120 LVDT 3 deformation readings

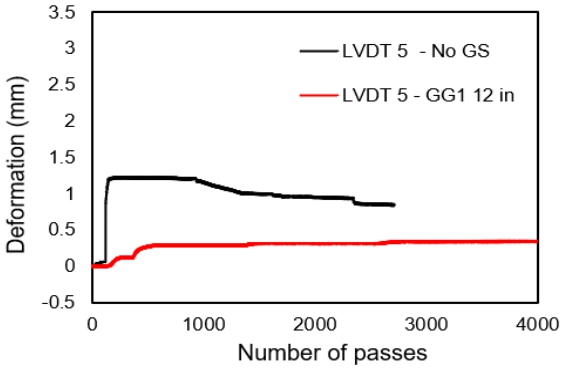

Figure 5.121 LVDT 5 deformation readings

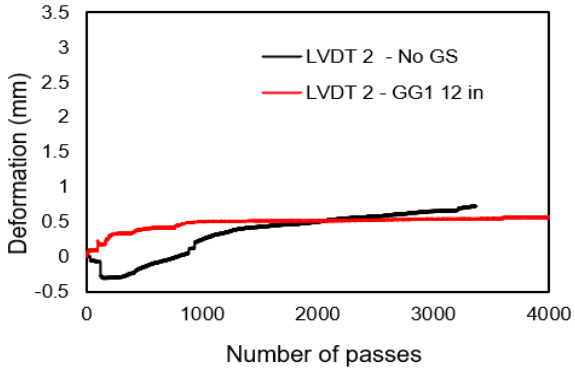

Figure 5.122 LVDT 2 deformation readings

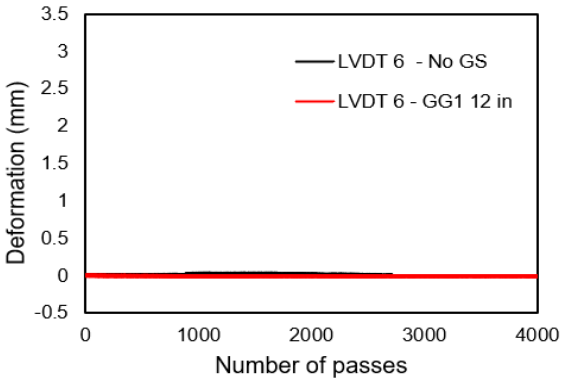

Figure 5.123 LVDT 6 deformation readings

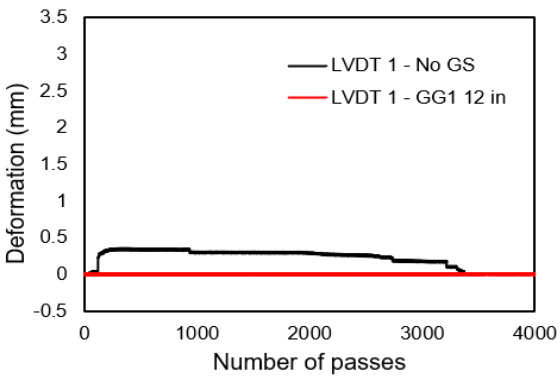

Figure 5.124 LVDT 1 deformation readings

5.7.3 Pressure Reduction Effect

Figure 5.125 shows the typical rolling wheel loads applied on the pavement surface taken over a 1-minute period. The pressure cell reading recorded by the top, middle and bottom pressure cell taken over a 1-minute period are shown in Figure 5.126, Figure 5.127 and Figure 5.128 respectively.

The pressure distribution within the pavement layer for the three cases were analyzed to show how the pressure reduction occurs at the subgrade/base interfaces. Figure 5.127 shows the pressure acting at the middle and bottom pressure cells for all three cases. The reduction in pressure from the middle to the bottom pressure cell is highlighted in Figure 5.129. The Control test had the least reduction in the pressure between the middle and bottom pressure cell. The pressure acting on the subgrade/base interface decreases by 13.2% and 19.5% for Case 2 and 3 respectively which highlights the significant effect geogrid has in pavement shown in Figure 5.130.

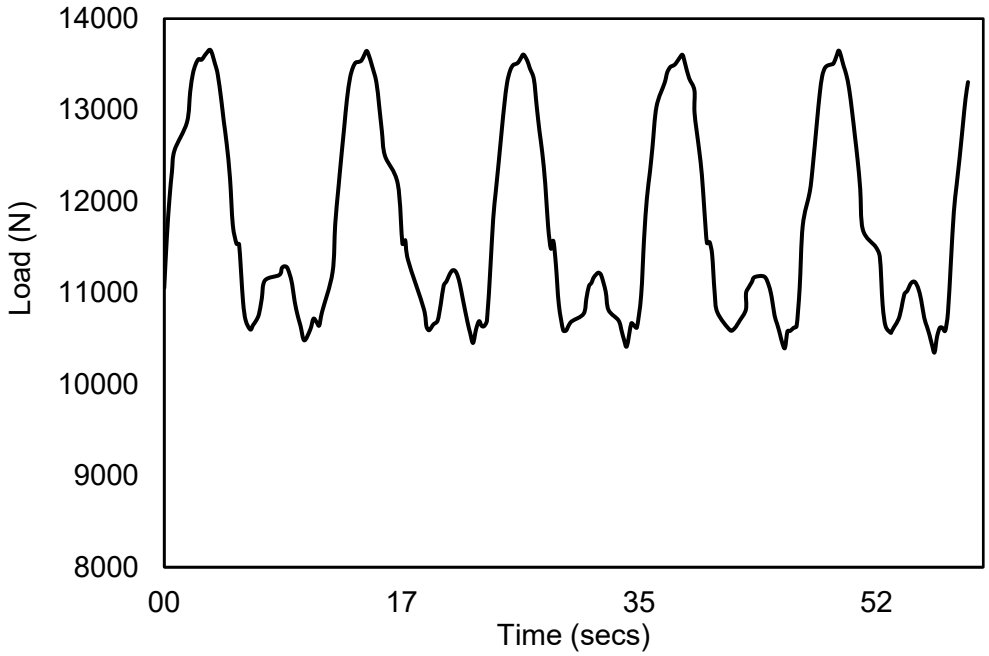

Figure 5.125 Load cell reading taken over 1-minute period

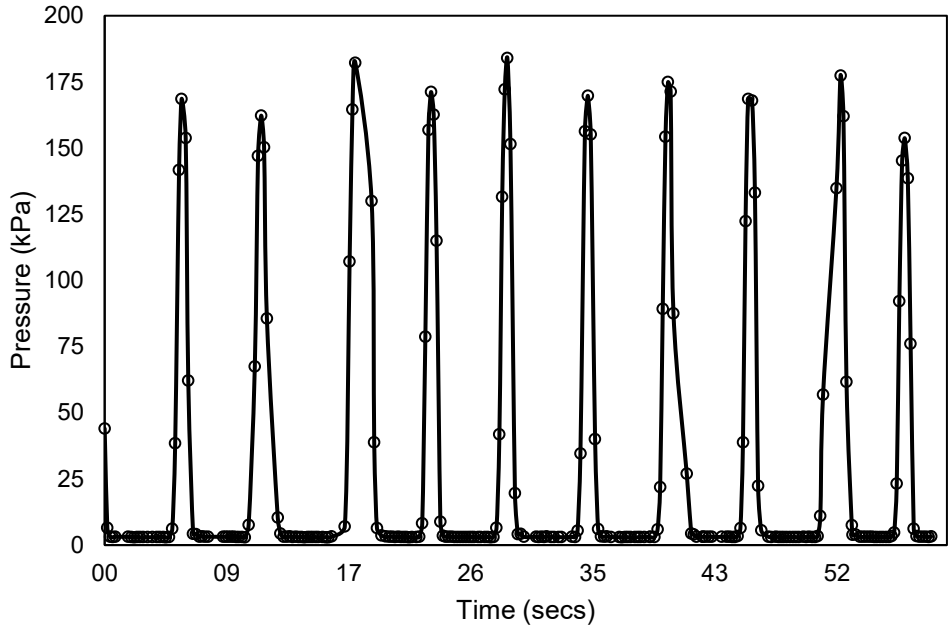

Figure 5.126 Top pressure cell reading taken over a 1-minute period

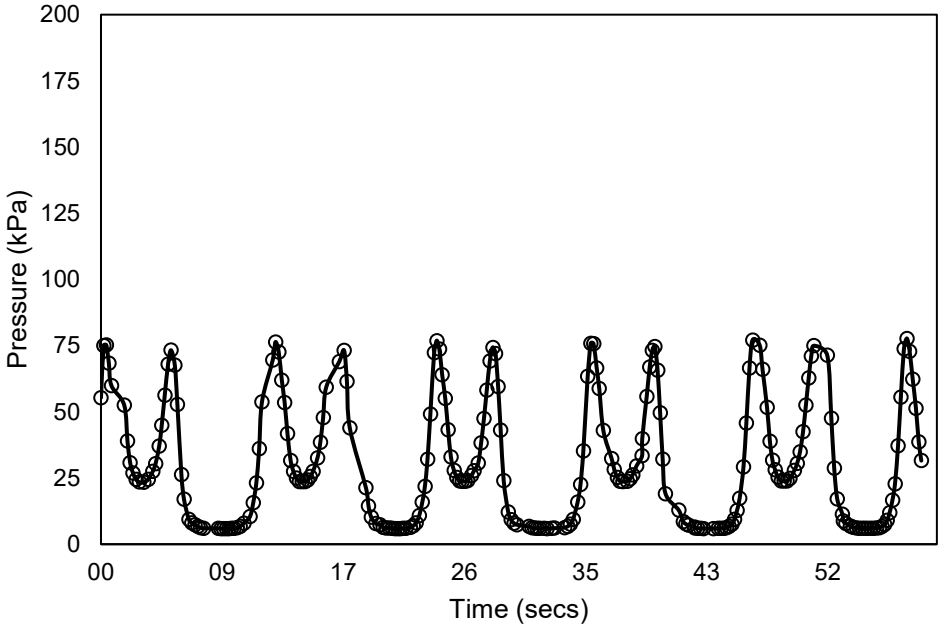

Figure 5.127 Middle pressure cell reading taken over a 1-minute period

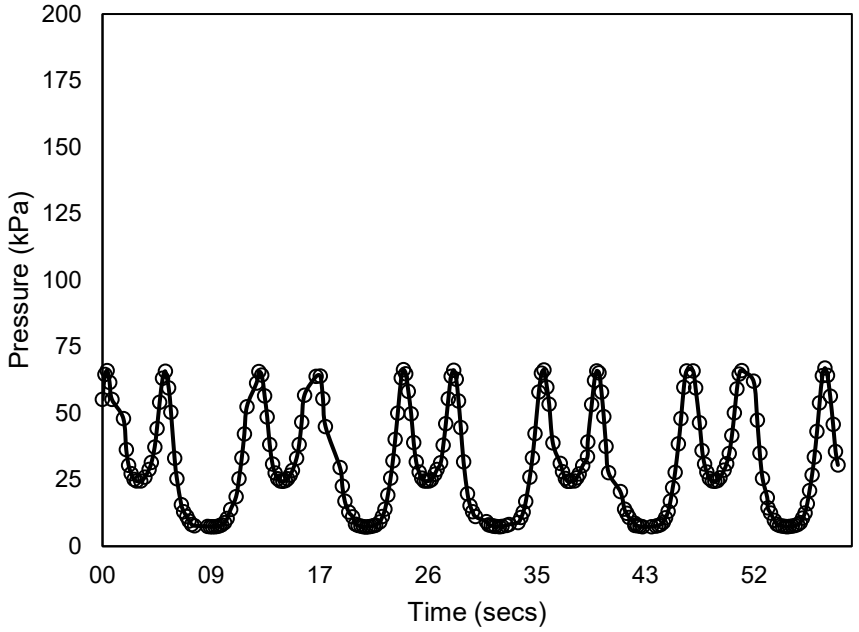

Figure 5.128 Bottom pressure cell reading taken over a 1-minute period

Table 5.29 Pressure reduction at base/subgrade interface

Case	Middle Pressure Cell (kPa)	Bottom Pressure cell (kPa)
Control	74	71
GG1 – 12 in	76	66
GG1 – 9 in	118	95

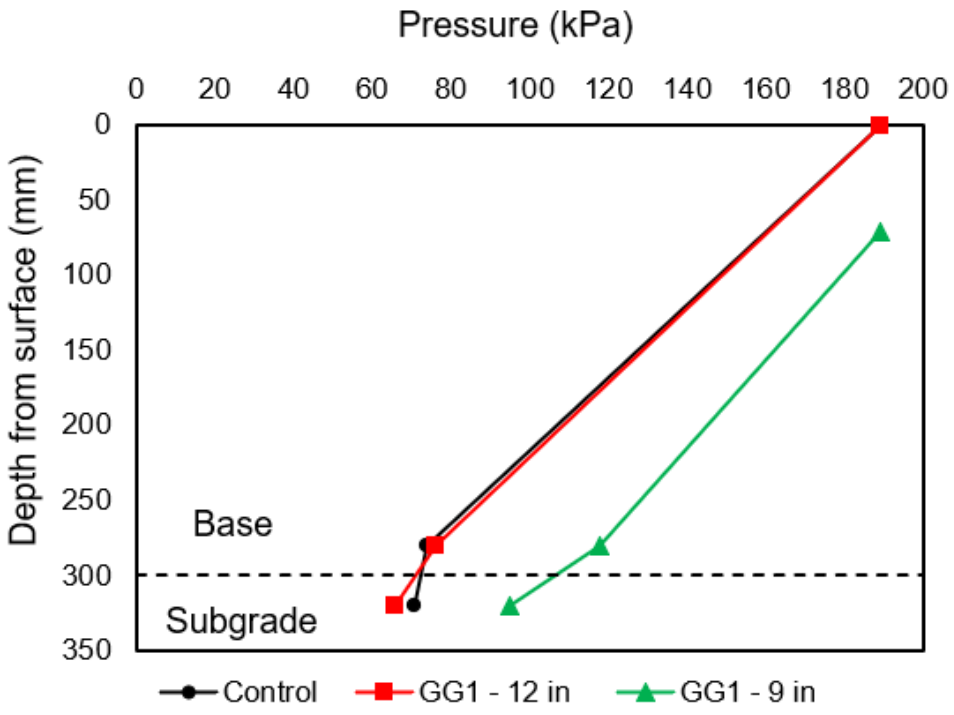

Figure 5.129 Pressure reduction through pavement layer – 3 cases

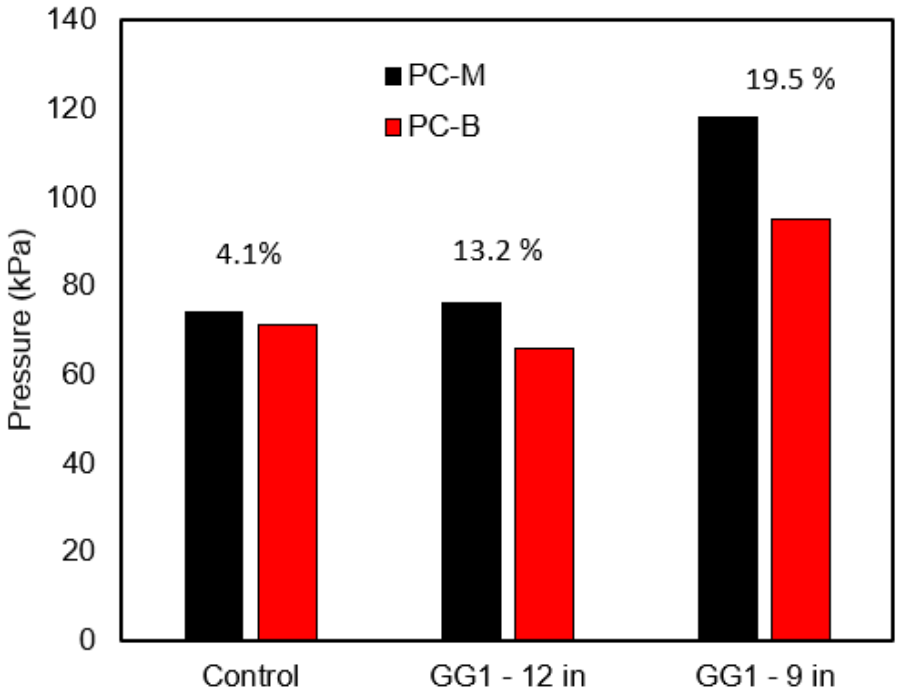

Figure 5.130 Pressure reduction at base/subgrade interface – 3 cases

Chapter 6 Conclusion

This study was conducted to evaluate the design properties of the geosynthetic reinforced soils for the roadway pavement layers and based on the results, to compare the performance of the geosynthetic reinforced soils to implement to a roadway pavement system, in particular, subgrade layers. Other states in the United States have used geosynthetics to help rehabilitate and elongate the life of their subgrades. They are more formally used to protect against the underlying damage by stabilizing the subgrade and base layers under the flexible pavement. The benefits of the geosynthetic application incorporate longer serviceability and slower deterioration. However, the geosynthetic application should be a case-by-case study because of the variable site conditions and soil types. Thus, in this study, extensive experimental work through a pullout test, a large direct shear test, a soil chamber with Dynamic Cone Penetrometer (DCP) and Large-Scale Tracking Wheel (LSTW) Test were performed to evaluate various parameters and the performance of the geosynthetic reinforcement for three different soils, including sand, clay, and red shale. The parameters include interface friction angle, normalized shear resistance, pullout interaction coefficient, maximum pullout force, initial modulus, and secant modulus, Dynamic Cone Penetrometer Index (DPI), strength/stiffness improvement, deformation reduction and pressure reduction effects. These parameters were explained and graphed to compare their effectiveness to the controllable variables.

For the sand case, in most testing results, geogrids show better performance than sand alone or GT. All geogrids produced better friction angles and normalized shear resistance values in the direct shear tests than GT and sand alone. Among them, GG1 showed slightly better performance than others regarding pullout and interface shear resistance, but the difference was not statistically significant. In the pullout or tension phase, it was seen that GG1 produced more

beneficial values for the interaction coefficient and its initial modulus. This was believed to be due to its greater tensile properties. The results of the pullout and direct shear tests subjected to lower confining pressure showed that biaxial geogrids GG1 or GG3 work best for use in the sand application in shallow depth (< 3 ft). However, if high normal pressure is applied to the roadway, GG2 would be a good choice because of its interlock and ability to transfer stress into the soil, not its ribs.

For the clay case, all the friction angles of tested geogrids show similar values and the difference in the values was not statistically significant when analyzing the direct shear. However, in most cases, the geosynthetic reinforced soils performed better in the clay than the unreinforced. The results of the direct shear tests showed that the friction angle does not have a relationship with the normalized shear resistance. However, the higher the friction angle, the slightly higher the pullout and shear resistance parameters. For clay, GG1 consistently showed slightly better performance than other geogrids in terms of the pullout and interface resistance-related parameters. However, at low pressure the geotextile does not show meaningful enhancement when applied for the direct shear and the interaction ratio. GT had the lowest stiffness, which was expected.

The red shale showed that generally, the three geogrids worked better, specifically GG2 and GG3. Friction angle, for the geogrids, could be used as an indication for initial modulus. GG1 and GG3 had the best results for the interaction ratio, and they were slightly higher for the initial modulus as well. For the shearing and tensile properties, GG3 seemed to be the most consistent in the red shale.

From the DCP test, it is clearly found the improvement of strength and bearing resistance in terms of DPI and CBR values for different subgrade layers reinforced with geosynthetics. The

test results demonstrated a higher resistance to penetration through the geosynthetic-reinforced soils in the chamber. The larger penetration resistance was observed when the geosynthetic is applied showing the significance of geosynthetics in enhancing the performance of the test area. The GG1 and GG3 geosynthetics showed a relatively remarkable improvement compared to others. Based on the results, it is concluded that the DCP can be used to verify the effect of geosynthetic reinforcement along the depth. The confined zone was obviously generated around 60-70 mm above and 100 mm below at the interface layer installing geosynthetics. For all the cases, the improvement with GT was detected a bit but was not significant compared to other GGs.

In the LSTW test, the use of biaxial geogrid at the subgrade and base interface was effective in reducing the total permanent deformation (rutting) of a pavement system by 34.1% and 29.5% with the same base course aggregate thickness and a reduced base layer of 3 inches, respectively as compared to the control case. The resilient modulus of base course after the LSTW test increased by 30.9% and 19.8% with the same base course aggregate thickness and a reduced base layer of 3 inches, respectively as compared to the control case as well. The intensity of stress acting on the subgrade layer reduced by 13.2% and 19.5% with the same base course aggregate thickness and a reduced base layer of 3 inches respectively as compared to the control case. These results highlight the benefit of using a biaxial geogrid (GG1) in a pavement layer.

Furthermore, numerical modeling through FLAC employing the input parameters obtained from the laboratory test to simulate practical pavement layers with and without geosynthetic application proved a significant enhancement to apply geosynthetic in reducing settlement and vertical stress. Based on the modeling results, it is found that the stress transfer

mechanism through geosynthetics is clearly generated, and the confined zone of the layer is established, which shows good agreement with DCP data obtained from the soil chamber test. Also, it is effective to install geosynthetic at the interface between base and subgrade among the tested soils in reducing vertical stress and deformation of the soil layers.

In short, the results obtained from a large direct shear test, pullout test, soil chamber test using DCP in the laboratory and LSTW test show that geosynthetic improves soil properties associated with the pullout, interface shear resistance-related parameters, strength/stiffness, deformation, and pressure reduction. Also, numerical modeling employing the input parameters obtained from the test to simulate practical pavement layers with and without geosynthetic application proved to be a significant enhancement to apply geosynthetic in reducing settlement and vertical stress. Among the geosynthetic, three geogrids consistently show better enhancement than GT and significantly improve than all soils, including sand, red shale, and clay. In most cases, GG1 consistently performs slightly better than other geogrids in terms of the pullout and interface resistance-related parameters.

Chapter 7 Recommendations

Based on the comprehensive literature review, the description of the geosynthetic installation, storage, etc. can be addressed in the NDOT manual. The following description can be examples.

"Geosynthetic Specifics: Geosynthetics are synthetic materials made of a minimum of 85% polyester, polyolefin, or polyamide by weight. Geosynthetics, including Geotextiles, Geogrids, Geomembranes, Geocomposites, and so on, are used to provide multiple functions such as filtration and drainage or reinforcement and separation in applications such as road construction and landfills."

"Construction Practices: When working with geosynthetics:

- Avoid placing construction equipment or machinery directly on top of them.
- Store them in a way that protects them from sunlight and UV rays and keeps them away from mud, dirt, and debris.
- Follow ASTM D4873 guidelines for proper wrapping during storage.
- Refer to FHWA HI-95-038 (2008) or AASHTO M288 guidelines (2006) for proper application and construction of geosynthetics."

Based on the evaluation of various parameters for different soils obtained from the field sites in Nebraska through the pullout test, direct shear test, Dynamic Cone Penetrometer (DCP) test, Large-Scale Tracking Wheel (LSTW) test and numerical simulation, it is found that all tested geogrids showed great outcomes for different soils. Overall, GG1 consistently performs slightly better than other geogrids associated with the pullout and interface resistance-related parameters and strength/stiffness improvement, deformation reduction and pressure reduction for the LSTW test. The FLAC model successfully identified the ideal location for a geosynthetic as

the base and subgrade interface. For a crushed stone base and sand subgrade a biaxial geogrid was identified as the ideal geosynthetic type. The LSTW test conducted based on these findings successfully identified a 25% base course reduction potential for a biaxial geogrid (GG1) with a sand subgrade and a crushed stone base. This potential reduction is in line with works of other research works as highlighted in Table 7.1.

Table 7.1 Design Approaches and Procedures for Base/Subbase Reinforcement

Developer/ Organization	Geosynthetic Type	Maximum Range of Improvement	Design Method and Basis
This study	Biaxial Geogrid	25% reduction in base	Large scale tracking wheel test
Mirafi, 1982	Specific geotextile	7% to 18% reduction in base thickness	Empirical/Modified AASHTO ‘72
Penner et al. 1985	Specific geogrid	30 to 50% reduction in base thickness	Empirical/modified AASHTO ‘81
Barksdale et al. 1989	Generic geosynthetic	4% to 18% reduction in base thickness	FEM

Other geogrids have some superior performance for specific soils. However, depending on the soil types, the performance of geosynthetic can be varied. This is because geosynthetic has a different configuration, like the aperture size and rib thickness of the geogrid, and has different integrity with soils. Thus, it is recommended to conduct pullout, direct shear tests, and an LSTW test to evaluate the parameters for other subgrade and base configurations before applying geosynthetics. The DPI values obtained from the DCP test successfully identified the depth of the geosynthetic installation, the confined zone enhanced by the geosynthetic, and significant variations in the strength compared with that of and unreinforced test area. The resilient modulus computed from the DCP in chamber and Large Wheel test showed comparable

performance in terms of percentage increase in the Subgrade Resilient Modulus compared with the control of these two sets of tests as shown in Table 5.25, Table 5.26, Table 5.27 and Table 5.28. From these results, the percentage increase ranged between 25% to 33% for the biaxial geogrid (GG1) and 19.6% to 36.2% for the triaxial geogrid (GG2). A conservative percentage increase of 20% in Resilient Modulus is proposed when a biaxial geogrid (GG1) is used in pavement design and evaluation purposes while a 15% conservative increase is proposed for the triaxial geogrid (GG2) as no test data is available pertaining to the use of triaxial geogrid (GG2) in the Large-Scale Tracking Wheel test for this project. Future works would explore the effects of the geosynthetic types, including GG2, in the LSTW test.

Based on the experimental testing data, several correlations were proposed which includes relationship between DPI and interface friction angle. This showed good agreement, particularly for the sand subgrade case. Also, selected parameters, such as the pullout interaction coefficient (Ci) and DPI, show a good agreement but need more cases. However, the relationship between DPI and interface friction angle does not match well for the clay case.

The results of these tests can be utilized to make informed decisions regarding the design properties of roadway pavement. The shear strength obtained from direct shear testing can be utilized to determine the bearing capacity of soil, while the pullout strength can be used to evaluate the effectiveness of geosynthetics in reinforcing soil.

References

AASHTO Standard M288, 2017. “Standard Specification for Geosynthetic Specification for Highway Applications.”

Abdi, M. and Arjomand, M., 2011. “Pullout Tests Conducted on Clay Reinforced with Geogrid Encapsulated in Thin Layers of Sand.” *Geotextiles and Geomembranes,* 29(6), 588-595.

Abu-Farsakh, M., Souci, G., Voyiadjis, G.Z., and Chen, Q., 2012. “Evaluation of Factors Affecting the Performance of Geogrid-Reinforced Granular Base Material Using Repeated Load Triaxial Tests.” *American Society of Civil Engineers,* 24(1), 72-83, https://doi.org/10.1061/(ASCE)MT.1943-5533.0000349.

Adams, C., Apraku, E., and Opoku-Boahen, R., 2015. “Effect of Triaxial Geogrid Reinforcement on CBR Strength of Natural Gravel Soil for Road Pavements.” *Journal of Civil Engineering Research*, 5(2), 45-51. https://doi.org/10.5923/j.jce.20150502.05.

Al-Refeai, T. and Al-Suhaibani, A., 1996. “Prediction of CBR Using Dynamic Cone Penetrometer.” *J. King Saud University*, 9(2), 191-204.

Al-Qadi, I.L., Dessouky, S., Tutumluer, E., and Kwon, J. “Geogrid Mechanism in Low-Volume Flexible Pavements: Accelerated Testing of Full-Scale Heavily Instrumented Pavement Sections.” *International Journal of Pavement Engineering,* 121-135, https://doi.org/10.1080/10298436.2010.535534.

American Association of State Highway and Transportation Officials, 2000. “Standard Specifications for Transportation Materials and Methods of Sampling and Testing,” Washington, D.C.

Appea, A.K., 1997. “In-Situ Behavior of Geosynthetically Stabilized Flexible Pavement,” Virginia Polytechnic Institute and State University.

ASTM Standard D1195, 2021. “Standard Test Method for Repetitive Static Plate Load Tests of Soils and Flexible Pavement Components, for Use in Evaluation and Design of Airport and Highway Pavements.”

ASTM Standard D1196-93, 2017. “Standard Test Method for Nonrepetitive Static Plate Load Tests of Soils and Flexible Pavement Components, for Use in Evaluation and Design of Airport and Highway Pavements.” 1997.

ASTM Standard D1557-12, 2021. “Standard Test Methods for Laboratory Compaction Characteristics of Soil Using Modified Effort (56,000 ft-lbf/ft^3 (2,700 kN-m/m^3)).”

ASTM Standard D1883-21, 2021. “Standard Test Method for California Bearing Ratio (CBR) of Laboratory-Compacted Soils.”

ASTM Standard D2487-17, 2020. “Standard Practice for Classification of Soils for Engineering Purposes (United Soil Classification System).”

ASTM Standard D3080-04, 2012. “Standard Test Method for Direct Shear Test of Soils Under Consolidated Drained Conditions.”

ASTM Standard D4318-17, 2018. “Standard Test Methods for Liquid Limit, Plastic Limit, and Plasticity Index of Soils.”

ASTM Standard D4491, 2020. “Standard Test Methods for Water Permeability of Geotextiles by Permittivity.”

ASTM Standard D4751-21, 2021. “Standard Test Methods for Determining Apparent Opening Size of a Geotextile.”

ASTM Standard D5321, 2021. “Standard Test Method for Determining the Shear Strength of Soil-Geosynthetic and Geosynthetic-Geosynthetic Interfaces by Direct Shear.”

ASTM Standard D6706-04, 2021. “Standard Test Method for Measuring Geosynthetic Pullout Resistance in Soil.”

ASTM Standard D6951, 2018. “Standard Test Method for Use of the Dynamic Cone Penetrometer in Shallow Pavement Applications.”

Athanasopoulos, G.A., 1996. “Results of Direct Shear Tests on Geotextile Reinforced Cohesive Soil.” *Geotextiles and Geomembranes,* 14(11), 619-644, https://doi.org/10.1016/s0266-1144(97)00002-2.

Bagshaw, S. A., Herrington, P. R., Kathirgamanathan, P., and Cook-Opus International Consultants LTD, 2015. “Geosynthetics in Basecourse Stabilization.” Research Report 574, Wellington, New Zealand: New Zealand Transportation Agency.

Bakeer, R.M., Sayed, S.M., Cates, P., and Subramanian, R., 1998. “Pullout and Shear Tests on Geogrid Reinforced Lightweight Aggregate.” *Geotextiles and Geomembranes*, 16(2), 119-133.

Baker, T.L. and Marienfeld, M.L., 1999. “Paving Fabric Interlayer System as a Pavement Moisture Barrier,” pp. 13, *Transportation Research Board Circular #E-C006*.

Barksdale, R. D., Brown, S. F., and Chan, F., 1989. “Potential Benefits of Geosynthetics in Flexible Pavement Systems,” pp. 56, *Transportation Research Record #315*, Washington, D.C.

Barr, M., 2001. Pulse Width Modulation. *Embedded Systems Programming*, 103-104.

Basu, G., Roy, A.N., Bhattacharyya, S.K. and Ghosh, S. K., 2009. “Construction of Unpaved Rural Road Using Jute–Synthetic Blended Woven Geotextile–A Case Study,” *Journal of Geotextiles and Geomembranes*, 27(6), 506-512.

Biczysko, S.J., 1996. “Long-Term Performance of Lime Stabilized Road Subgrade,” pp. 62-71, Thomas Telford Publisher, London, England.

Caltrans, 2018. “Standard Specifications,” California Department of Transportation.

Caltrans, 2013. “Subgrade Enhancement of Geosynthetic Design and Construction Guide,” California Department of Transportation.

Carmichael, R.F. and Marienfeld, M.L., 1999. “Synthesis and Literature Review of Nonwoven Paving Fabrics Performance in Overlays,” pp. 112-124, *Transportation Research Record #1687*, Washington, D.C.

Chen, D. H., Lin, D. F., Liau, P. H., and Bilyeu, J., 2005. “A Correlation Between Dynamic Cone Penetrometer Values and Pavement Layer Moduli,” *Geotechnical Testing Journal*, ASTM International, 28(1), West Conshohocken, Pennsylvania.

Chen, W., Zhou, W., and Jing, X., 2019. “Modeling Geogrid Pullout Behavior in Sand Using Discrete-Element Method and Effect of Tensile Stiffness.” *American Society of Civil Engineers,* 19(5), 04019039, https://doi.org/10.1061/(ASCE)GM.1943-5622.0001424.

Christopher, B.R., 2014. “Cost Savings by Using Geosynthetics in the Construction of Civil Works Projects,” Proceedings of the 10th International Conference on Geosynthetics, Berlin, Germany.

City of Louisville. “We’re Closer Than You Think,” Louisville, Nebraska, https://louisvillene.gov/.

Colorado Department of Transportation, 2019. “Standard Specifications for Road and Bridge Construction,” Colorado Department of Transportation.

Cuelho, E. and Perkins, S., 2009. “Field Investigation of Geosynthetics Used for Subgrade Stabilization,” U.S. Department of Transportation, Federal Highway Administration in cooperation with the State of Montana Department of Transportation, Report Number: FHWA/MT-09-003/8193.

Ebrahimian, B., 2011. “Numerical Analysis of Strip Footing Resting on Geosynthetic-Reinforced Sand Bed Over Soft Soil,” pp. 993-1000, In Deformation Characteristics of Geomaterials, IOS Press.

El-Maaty, A.E., 2016. “Improving Rutting Resistance of Flexible Pavement Using Geosynthetics.” *Open Access Library Journal,* 3(5), 1-11. https://doi.org/10.4236/oalib.1102655.

Emergen Research, 2021. “Geosynthetics Market by Type (Geogrids, Geotextiles, Geonets, Geomembranes, Geofoam, Others), by Material (Polyethylene, Polypropylene, Polyester, PVC, Others), by Functions (Separation, Filtration, Drainage, Others), by Application, and by Region Forecast to 2028,” Geosynthetics Market Growth, Geosynthetics Industry Report, https://www.emergenresearch.com/industry-report/geosynthetics-market.

Ese, D., Myre, J., Noss, P., and Vaernes, E., 1994. "The Use of Dynamic Cone Penetrometer (DCP) for Road Strengthening Design in Norway," Proceedings from the 4th International Conference on the Bearing Capacity of Roads and Airfields.

Eun, J., Gupta, R., and Zornberg, J.G., 2017. "Effect of Geogrid Geometry on Interface Resistance in a Pullout Test," pp. 236-246, ASCE Geo-Frontier, Orlando, Florida.

Fannin, R.J. and Sigurdsson, O., 1996. "Field Observations on Stabilization of Unpaved Roads with Geosynthetics." *Journal of Geotechnical Engineering*, 122, 544-553, http://dx.doi.org/10.1061/(ASCE)0733-9410(1996)122:7(544).

Freedonia, 2002. "Geosynthetics to 2006 – Market Size, Market Share, Demand Forecast and Sales," pp. 203, Freedonia Group, Study #1621.

George, K.P. and Uddin, W., 2000. "Subgrade Characterization for Highway Pavement Design," The Federal Highway Administration, The Mississippi Department of Transportation in conjunction with the University of Mississippi.

Ghaaowd, I. and McCartney, J.S., 2020. "Pullout of Geogrids from Tire-Derived Aggregate Having Large Particle Size." *Geosynthetics International*, 27(6), 671-684.

Giroud, J.P., 1986. "From Geotextiles to Geosynthetics: A Revolution in Geotechnical Engineering," pp. 1-18, Proceedings on the 3rd International Conference on Geotextiles, Vienna, Austria.

Giroud, J.P. and Han, J., 2004. "Design Method for Geogrid-Reinforced Unpaved Roads I," *Journal of Geotechnical and Geoenvironmental Engineering,* 130(8), 775-786.

Giroud, J.P. and Han, J., 2004. "Design Method for Geogrid-Reinforced Unpaved Roads II," *Journal of Geotechnical and Geoenvironmental Engineering,* 130(8), 787-797.

Haliburton, T.A., Fowler, J., and Langan, J.P., 1980. "Design and Construction of a Fabric Reinforced Test Section at Pinto Pass, Mobile, Alabama," *Transportation Research Record #79,* Washington, D.C.

Hassan, A.B., 1996. "The Effects of Material Parameters on Dynamic Cone Penetrometer Results for Fine-Grained Soils and Granular Materials," Oklahoma State University.

Hatami, K. and Bathurst, R. J., 2001. "Modeling Static Response of a Segmental Geosynthetic Reinforced Soil Retaining Wall Using FLAC," pp. 223-231, Proceedings from the 2nd International FLAC Symposium, Numerical Modeling in Geomechanics, Lyon.

Hayden, S.A., Humphrey, D.N., Christopher, B.R., Henry, K.S. and Fetten, C., 1999. "Effectiveness of Geosynthetics for Roadway Construction in Cold Regions: Results of a Multi-Use Test Section", pp. 847-862, Proceedings of the 1999 Conference on Geosynthetics, Boston, Massachusetts.

Hegde, A. and Roy, R., 2017. "A Comparative Numerical Study on Soil-Geosynthetic Interactions Using Large Scale Direct Shear Test and Pullout Test." *International Journal of Geosynthetics and Ground Engineering,* 4(2), 1-11, https://doi.org/10.1007/s40891-017-0119-1.

Heerten, G., 2015. "History and Current State of Geosynthetic Applications in Germany," pp. 30, Proceedings on the 10th International Conference on Geosynthetics, Berlin, Germany.

Heukelom, W. and Klomp, A.J., 1962. "Dynamic Testing as a Means of Controlling Pavements During and After Construction," Proceedings on the 1st International Conference on Structural Design of Asphalt Pavements, Ann Arbor, Michigan.

Hallenbeck, M. E., Selezneva, O. I., and Quinley, R., 2014. "Verification, refinement, and applicability of long-term pavement performance vehicle classification rules" (No. FHWA-HRT-13-091). United States. Federal Highway Administration. Office of Infrastructure Research and Development.

Holtz, R.D., 2001. "Geosynthetics for Soil Reinforcement," The 9th Spencer J. Buchanan Lecture, University of Washington, Seattle, Washington.

Holtz, R.D., 2004. "Geosynthetics R & D: The Early Days," pp. 91-108, Proceeding Symphonic on Research, Philadelphia, Pennsylvania.

Holtz, R.D., 2017. "46th Terzaghi Lecture: Geosynthetic Reinforced Soil: From the Experimental to the Familiar." *American Society of Civil Engineers,* 143(9), 03117001, https://doi.org/10.1061/(ASCE)GT.1943-5606.0001674.

Holtz, R.D. and Lee, W.F., 1998. "Geosynthetic-Reinforced Wall Analysis Phase II: Use of In-Soil Geosynthetic Behavior to Predict Deformations, Volume 2: Implementation — Computer Codes and Files," No. WA-RD 452.2.

Holtz, R.D., Christopher, B.R. and Berg, R.R., 1998. "Geosynthetic Design and Construction Guidelines," pp. 460, U.S. Department of Transportation, Federal Highway Administration, Washington, D.C., FHWA-HI-98-038.

Holtz, R.D., Christopher, B.R., and Berg, R.R. "Geosynthetic Design and Construction Guidelines: Participant Handbook," U.S. Department of Transportation, Federal Highway Administration, NHI Course No. 13213, FHWA HI-95-038.

Hoppe, E.J., Hossain, M.S., Moruza, A.K., and Weaver, C.B. "Use of Geosynthetics for Separation and Stabilization in Low-Volume Roadways," Virginia Transportation Research Council, Report Number: FHWA/VTRC 20-R8.

Illinois Department of Transportation, 2005. "Subgrade Stability Manual," Illinois Department of Transportation Bureau of Bridges and Structures.

Iowa Department of Transportation, 2015. "Engineering Properties of Soil and Rock, Design Manual," Iowa Department of Transportation Office of Design, Chapter 200.

Iowa Department of Transportation, 2013. "Iowa Statewide Urban Design and Specifications," https://iowasudas.org/manuals/design-manual/.

Imjai, T., Pilakoutas, K., and Guadagnini, M., 2019. "Performance of Geosynthetic-Reinforced Flexible Pavements in Full-Scale Field Trials." *Geotextiles and Geomembranes,* 47, 217-229.

Ingold, T. S., 1994. "The Geotextile and Geomembranes Manual," Elsevier Advanced Technology, United Kingdom.

Ingold, T.S., 1983. "Laboratory Pullout Testing of Grid Reinforcements in Sand." *Geotechnical Testing Journal,* 6(3), 101–111.

Iowa Department of Transportation, 2012. "Standard Specifications for Highway and Bridge Construction," Iowa Department of Transportation.

Itasca Consulting Group, Inc. "FLAC: Explicit Continuum Modeling of Non-Linear Material Behavior in 2D." https://itascacg.com/software/FLAC, Accessed 26 January 2022.

Jewell, R.A., 1996. "Soil Reinforcement with Geotextiles," CIRIA Special Publication 123, Thomas Telford, Westminster, London.

John, N., 1987. "Geotextiles," pp. 347, Blackie Press, Chapman and Hall, New York, New York.

Jones, C., 1982. "Practical Construction Techniques for Retaining Structures Using Fabrics and Grids," pp. 581-585, Proceedings on the 2nd International Conference on Geotextiles, Las Vegas, Nevada.

Jones, D.E. and Jones, K., 1987. "Treating Expansive Soils." *Journal of Civil Engineering,* 57(8), 62-65.

Kaswell, E.R., 1963. "Handbook of Industrial Textiles," West Point Pepperell, New York, New York.

Kazmee, H., Mishra, D., and Tutumluer, E., 2015. "Sustainable Alternatives in Low Volume Road Base Course Applications Evaluated through Accelerated Pavement Testing," International Foundations Congress and Equipment Expo, pp. 409-418.

Keller, G.R., 2016. "Application of Geosynthetics on Low-Volume Roads." *Transportation Geotechnics,* 8, 119-131.

Kelley, C.M., 1977. "A Long Range Durability Study of Lime Stabilized Bases at Military Posts in the Southwest," National Lime Association Bulletin 328, Arlington, Virginia.

Kermani, B., Xiao, M., Stoffels, S.M., and Qiu, T., 2018. "Reduction of Subgrade Fines Migration into Subbase of Flexible Pavement Using Geotextile." *Geotextiles and Geomembranes*, 46, 377-383.

Kim, S., Frost, D., Durham, S., Chorzepa, M., Wright, J., and Hanumasagar, S., 2018. "Development of Geosynthetic Design and Construction Guidelines for Pavement Embankment Construction in North Georgia." FHWA-GA-19-1611, Georgia Department of Transportation.

Kim, S., Eun, J., Alhowaidi, Y., and Robertson, D., 2021. "Feasibility Study: Alternatives to Prevent Settlements and Bumps at Bridge Approach." Nebraska Department of Transportation

Koerner, R. M., 2005. "Designing with Geosynthetics, 2nd Edition," Pearson Prentice Hall, New Jersey.

Koerner, R.M., 2012. "Designing with Geosynthetics, 6th Edition," Xlibris Corporation, 1(2).

Koerner, R.M., 2016. "Early Background and History of Geotextiles." *Geotextiles*, pp. 3-15, https://doi.org/10.1016/b978-0-08-100221-6.00001-2.

Koerner, R. M. and Te-Yang, S., 1997. "The Evolution of Geosynthetics." *Journal of Civil Engineering*, 67(7), 62-64.

Lambe, T.W. and Whitman, R. V., 1969. "Soil Mechanics," Wiley and Sons, New York, New York.

Latha, G.M. and Nair, A.M., 2014. "Geosynthetics in Unpaved Roads," *Indian Journal of Geosynthetics and Ground Improvement,* 3(2), 3-13.

Leng, J. and Gabr, M.A., 2005. "Numerical Analysis of Stress-Deformation Response in Reinforced Unpaved Road Sections," *Geosynthetics International*, 12, 111-119, http://dx.doi.org/10.1680/gein.2005.12.2.111.

Livneh, M. and Ishai, I., 1987. "Pavement and Material Evaluation by a Dynamic Cone Penetrometer," Proceedings from the 6th International Conference on Structural Design of Asphalt Pavement, Ann Arbor, Michigan.

Lopes, A.C., 2008. "Definition of Geosynthetics: Geosynthetics in Engineering," http://www.woodhe ad.com/geosynthetics/.

Louisiana Department of Transportation, 2016. "Standard Specifications for Roads and Bridges," Louisiana Department of Transportation.

Markets and Markets. "Geosynthetic Market by Type (Geotextile, Geomembranes, Geogrids, Geofoams, Geonets), by Application (Waste Management, Water Management, Transportation Infrastructure, Civil Construcion), and by Region Global Forecast to 2026," pp. 87-90, Markets and Markets Group, 2021, Report #CH2880.

Maryland Department of Transportation, 2020. "Standard Specifications for Construction and Materials," Maryland Department of Transportation State Highway Administration.

Minnesota Department of Transportation, 2018. "Standard Specifications for Construction," Minnesota Department of Transportation.

Mirafi, 1982. "Guidelines for Design of Flexible Pavements Using Mirafi Woven Geotextiles," TC Mirafi, Pendergrass, GA, 23 p

Miura, N., Sakai, A., Taesiri, Y., Yamanouchi, T., and Yasuhara, K., 1990. "Polymer Grid Reinforced Pavement on Soft Clay Grounds." *Geotextiles and Geomembranes,* 9(1), 99-123, https://doi.org/10.1016/0266-1144(90)90007-Y.

Mohammad, L.N., Herath, A., Gudishala, R., Nazzal, D., Abu-Farsakh, M.Y., and Alshibli, K., 2008. "Development of Models to Estimate the Subgrade and Subbase Layers' Resilient Modulus from In-Situ Devices: Test Results for Construction Control," Louisiana Transportation Research Center.

Montana Department of Transportation, 2020. "Standard and Supplemental Specifications for Road and Bridge Construction," Montana Department of Transportation.

Moraci, N., Cardile, G., Gioffre, D., Mandaglio, M., Calvarano, L.S., and Carbone, L., 2014. "Soil Geosynthetic Interaction: Design Parameters from Experimental and Theoretical Analysis." *Transportation Infrastructure Geotechnology,* 1(2), 165-227, https://doi.org/s40515-014-0007-2.

Motanelli, F., Zhao, A., and Rimoldi, P., 1997. "Geosynthetics-Reinforced Pavement System: Testing and Design." *Proceedings of Geosynthetics*, 97, 549-604.

Mounes, S.M., Karim, M.R., Mahrez, A., and Khodaii, A., 2011. "An Overview on the Use of Geosynthetics in Pavement Structures." *Scientific Research and Essays,* 6(11), 2234-2241, https://doi.org/10.5897/SRE10.960.

Muhmood, L., Abdu, A., and Khudhur, R.M., 2021. "Using Geotextile to Reduce the Required Thickness of Subbase Layer of the Road and Improvement in CBR Value." *Journal of Physics: Conference Series,* 1973(1), 1-14, https:// doi.org/10.1088/1742-6596/1973/1/012120.

Muhs, D.R., Bettis, E.A., Roberts, H.M., Harlan, S.S., Paces, J.B., and Reynolds, R.L., 2013. "Chronology and Provenance of Last-Glacial (Peoria) Loess in Western Iowa and Paleoclimatic Implications," *Quaternary Research,* 80, 468-481.

Myles, B. and Carswell, I., 1986. "Tensile Testing of Geotextiles," pp. 713-718, Proceedings on the 3rd International Conference on Geotextiles, Vienna, Austria.

Nevada Department of Transportation, 2020. "Standard Plans for Road and Bridge Construction," Nevada Department of Transportation.

New Jersey Department of Transportation, 2019. "Standard Specifications for Road and Bridge Construction," New Jersey Department of Transportation.

North Carolina Department of Transportation, 2018. “Standard Specifications for Roads and Structures,” North Carolina Department of Transportation.

North Dakota Department of Transportation, 2014. “Standard Specifications for Road and Bridge Construction,” North Dakota Department of Transportation.

Nunn, M.E., 1998. “Structural Design of Long-Life Flexible Roads for Heavy Traffic.” *Proceedings of the Institution of Civil Engineers – Transportation,* 129(3), 126-133, https://doi.org/10.1680/itran.1998.30858.

Ochiai, H., Otani, J., Hayashic, S., and Hirai, T., 1996. “The Pullout Resistance of Geogrids in Reinforced Soil.” *Geotextiles and Geomembranes*, 14(1), 19-42.

Ogundare, D.A., Familusi, A.O., Osunkunle, A.B., and Olusami, J.O., 2018. "Utilization of Geotextile for Soil Stabilization.” *American Journal of Engineering Research*, 7(8), 224-231.

Oliver, T., Wayne, M., and Kwon, J., 2016. “Mechanical Stabilization of Unbound Layers to Increase Pavement Performance and Incorporation of Benefits into M-E Analysis,” *Procedia Engineering: Advances in Transportation Geotechnics,* The 3rd International Conference on Transportation Geotechnics, 143, 896-910.

Pancar, E.B. and Akpinar, M.V., 2016. “Comparison of Effects of Using Geosynthetics and Lime Stabilization to Increase Bearing Capacity of Unpaved Road Subgrade.” *Advances in Materials Science and Engineering,* 1-8. https://doi.org/10.1155/2016/7129356.

Pavement Interactive, 1985. “California Bearing Ratio,” https://pavementinteractive.org.

Penner, R., Haas, R., Walls, J. and Kennepohl, G., "Geogrid Reinforcement of Granular Bases," Paper Presented at the Roads and Transportation Association of Canada Annual Conference, Vancouver, Canada, September.

Perkins, S.W., Bowders, J.J., Christopher, B.R., and Berg, R.R., 2005. “Geosynthetic Reinforcement for Pavement Systems: US Perspectives,” pp. 1-25, ASCE Geo-Frontier, Austin, Texas.

Pilarczyk, K.W., 2000. “Geosynthetics and Geosystems in Hydraulic and Coastal Engineering,” pp. 913, A. A. Balkema Publishing, Rotterdam, Netherlands.

Powell, W., Keller, G.R., and Brunette, B., 1999. “Applications for Geosynthetics on Forest Service Low-Volume Roads.” *Transportation Research Record Journal of the Transportation Research Board,* 1652(1), 113-120. https://doi.org/10.3141/1652-49.

Prashanth, V., Krishna, A. M., and Dash, S. K., 2016. “Pullout Tests Using Modified Direct Shear Test Setup for Measuring Soil–Geosynthetic Interaction Parameters.” *International Journal of Geosynthetics and Ground Engineering*, 2(2), 10.

Qubain, B.S., Seksinsky, E.J., and Li, J., 2000. "Incorporating Subgrade Lime Stabilization into Pavement Design." *Journal of the Transportation Research Board,* 1721(1), 3-8, https://doi.org/10.3141/1721-01.

Radhakrishna, H. S. and Klym, T. W., 1974. "Geotechnical Properties of a Very Dense Glacial Till." *Canadian Geotechnical Journal*, 11(3), 396-408.

Rahman, M.A., Arulrajah, A., Piratheepan, J., Bo, M.W., and Imteaz, M.A., 2014. "Resilient Modulus and Permanent Deformation Responses of Geogrid-Reinforced Construction and Demolition Materials." *American Society of Civil Engineers,* 26(3), 512-519, https://doi.org/10.1061/(ASCE)MT.1943-5533.0000824.

Rajagopal, K., Chandramouli, S., Parayil, A., and Iniyan, K., 2014. "Studies on Geosynthetic-Reinforced Road Pavement Structures." *International Journal of Geotechnical Engineering,* 8(3), 287-298.

Rankilor, P.R., 1981. "Membranes in Ground Engineering," pp. 377, Wiley and Company, London, England.

Ringler, Mike, 2021. Interview. Conducted by Daniel Robertson.

Roads and Bridges, 2000. "Defining a Geosynthetic: Type and Functions." https://www.roadsbridges.com/defining-geosynthetic-type-and-functions, Accessed 7 Jan 2022.

Rollings. M.P. and Rollings, R.S., 1996. "Geotechnical Materials in Construction." ISBN: 0070536651.

Roodi, G.H., 2016. "Analytical, Experimental, and Field Evaluations of Soil-Geosynthetic Interaction Under Small Displacements," University of Texas at Austin.

Roodi, G.H. and Zornberg, J.G., 2020. "Long-Term Field Evaluation of a Geosynthetic-Stabilized Roadway Founded on Expansive Clays." *Journal of Geotechnical and Geoenvironmental Engineering,* 146(4), 05020001. https://doi.org/10.1061/(asce)gt.1943-5606.0002206.

Roodi, G.H., Zornberg, J.G., Aboelwafa, M.M., Phillips, J.R., Zheng, L., and Martinez, J., 2018. "Soil-Geosynthetic Interaction Test to Develop Specifications for Geosynthetic-Stabilized Roadways," Transportation Research Center, University of Texas at Austin, No. FHWA/TX-18/5-4829-03-1.

Sakleshpur, V.A., Prezzi, M., Salgado, R., Siddiki, N. and Choi, Y.S., 2019. "Large-Scale Direct Shear Testing of Geogrid-Reinforced Aggregate Base Over Weak Subgrade." *International Journal of Pavement Engineering*, 20(6), 649-658, https://doi.org/10.1080/10298436.2017.1321419.

Sharbaf, M., 2016. "Laboratory Evaluation of Geogrid-Reinforced Flexible Pavements," University of Nevada Las Vegas.

Shukla, S.K. and Yin, J., 2006. “Fundamentals of Geosynthetic Engineering,” Taylor and Francis.

Smith, M.E. and Criley, K., 1995. “Effect of Particle Size on the Mechanical Behavior of Sand-Geotextile Composites,” pp. 28-31, Geotechnical Fabrics Report.

Smith, R.B. and Pratt, D.N., 1983. “A Field Study of In Situ California Bearing Ratio and Dynamic Cone Penetrometer Testing for Subgrade Investigations,” pp. 285-294, Australian Road Research Board, 13(4).

Song, C. R., Chung, R. M., Bahmyari, H., and Bitar, L., 2018. “Nebraska Specific Slope Design Manual,” Nebraska Department of Transportation, NDOT: SPR-1 (17) M061, NTC: 26-1121-4036-001).

South Dakota Department of Transportation, 2015. “Standard Specifications for Roads and Bridges,” South Dakota Department of Transportation.

Steward, J.E., Williamson, R., and Mohney, J., 1977.“Guidelines for Use of Fabrics in Construction and Maintenance of Low-Volume Roads,” pp. 172, USDA Forest Service Report PB-276 972, Portland, Oregon.

Subramanian, N., 2008. “Design of Steel Structures,” Oxford University Press.

Sutherland, R. A., and Ziegler, A. D., 2007. “Effectiveness of Coir-Based Rolled Erosion Control Systems in Reducing Sediment Transport from Hill Slopes.” *Applied Geography*, 27, 150–164.

Tan, Y., Sun, Z., Gong, X., Xu, H., Zhang, L., and Bi, Y., 2017. “Design Parameter of Low Temperature Performance for Asphalt Mixtures in Cold Regions.” *Construction and Building Materials*, 155, 1179-1187.

Tencate Geosynthetics Americas, 1982. “Guidelines for Design of Flexible Pavements Using Mirafi Woven Geotextiles,” pp. 23, Tencate Mirafi, Pendergrass, Georgia.

Tencate Geosynthetics Americas, 2020. “Miragrid 2XT.”

Tencate Geosynthetics Americas, 2020. “New and Noteworthy: Mirafi 500X and 600X.”

Tencate Geosynthetics Americas, 2018. “Seaming of Geosynthetics.” Technical Note.

Tensar International Corporation, 2017. “Accelerated Pavement Testing with Tensar Triaxial Geogrids,” Tensar International Corporation, Tensar Information Bulletin, IB/Accelerated Pavement Testing.

Tensar International Corporation, 2020. “Biaxial Geogrid BX1200,” Product Specification.

Tensar International Corporation, 1996. “Design Guideline for Flexible Pavements with Tensar Geogrid Reinforced Base Layers,” pp. 109, Tensar International Corporation, Technical Note: BR96, Atlanta, Georgia.

Tensar International Corporation, 2020. “Triaxial TX160 Geogrid,” Product Specification.

Texas Department of Transportation. “Construction and Materials Tips,” Texas Department of Transportation, https://ftp.dot.state.tx.us/pub/txdot-info/cst/tips/flex-_pave_des_faq.pdf.

Texas Department of Transportation, 2014. “Standard Specifications for Construction and Maintenance of Highways, Streets, and Bridges,” Texas Department of Transportation.

Thakur, S., Naveen, B.P., and Tegar, J.P., 2021. “Improvement in CBR Value of Soil Reinforced with Non-Woven Geotextile Sheets,” *International Journal of Geo-Engineering,* 12(1), 1-10, https://doi.org/10.1186/s40703-020-00138-9.

Thompson, M.R., 1970. “Soil Stabilization for Pavement Systems—State of the Art.” Construction Engineering Research Laboratory Technical Report, Department of the Army, Champaign, Illinois.

Thompson, M.R., 1969. “Engineering Properties of Lime-Soil Mixtures.” *Journal of Materials ASTM*, 4(4).

Tingle, J.S. and Jersey, S.R., 2005. “Cyclic Plate Load Testing of Geosynthetic-Reinforced Unbound Aggregate Roads,” pp. 60-69, *Transportation Research Record,* 1936(1), Washington, D.C.

Tiwari, B. and Marui, H., 2005. “A New Method for the Correlation of Residual Shear Strength of the Soil with Mineralogical Composition.” *Journal of Geotechnical and Geoenvironmental Engineering*, 131(9), 1139-1150.

Tiwari, N., Satyam, N., and Puppala, A.J., 2021. “Effect of Synthetic Geotextile on Stabilization of Expansive Subgrades: Experimental Study,” American Society of Civil Engineers, https://doi.org/10.1061/(ASCE)MT.1943-5533.0003901.

U.S. Fabrics. “Geotextiles.” https://www.usfabricsinc.com/products/geotextiles//?- ex=eep549-y2pe0b-0, Accessed 24 September 2020.

Virginia Department of Transportation, 2020. “Road and Bridge Specifications,” Virginia Department of Transportation.

Vulova, C. and Leshchinsky, D., 2003. “Effects of Geosynthetic Reinforcement Spacing on the Behavior of Mechanically Stabilized Earth Walls,” Federal Highway Administration, Office of Infrastructure Research and Development, No. FHWA-RD-03-048.

Wang, J.X., Khan, M.A., and Ikra, B.A., 2017. “Impact of Severe Drought on the Compacted Expansive Clays (Subgrade) in Northern Louisiana,” Southern Plains Transportation Center, SPTC 14.1-76.

Wang, Z. and Richwien, W., 2002. "A Study of Soil-Reinforcement Interface Friction." *Journal of Geotechnical and Geoenvironmental Engineering*, 128(1), 92-94.

Wasage, T.L., Ong, G.P., Fwa, T.F., and Tan, S.A., 2004. "Laboratory Evaluation of Rutting Resistance of Geosynthetics Reinforced Asphalt Pavement." *Journal of the Institute of Engineers,* 1(2), 29-44.

Webster, S.L., 1993. "Geogrid Reinforced Base Courses for Flexible Pavements for Light Aircraft: Test Section Construction, Behavior Under Traffic, Laboratory Tests, and Design Criteria," Federal Aviation Administration Technical Report GL-93-6.

Webster, S. L., Grau, R. H., and Williams, T. P., 1992. "Description and Application of Dual Mass Dynamic Cone Penetrometer," U.S. Army Engineer Research and Development Center, Waterways Experiment Station, Instruction Rep. GL-92-3, Vicksburg, Mississippi.

Webster, S. L., Brown, R. W., and Porter, J. R., 1994. "Force Projection Site Evaluation Using the Electronic Cone Penetrometer (ECP) and the Dynamic Cone Penetrometer (DCP)," U.S. Army Engineer Research and Development Center, Waterways Experiment Station, Technical Report GL-94-17, Vicksburg, Mississippi.

Wu, S., 1987. "DCP Field Application," North Carolina Department of Transportation.

Harison, J. A., "In Situ CBR Determination by DCP Testing Using a Laboratory- Based Correlation," Australian Road Research Board, 19(4), 1986.

Wu, S. and Sargand, S., 2007. "Use of Dynamic Cone Penetrometer in Subgrade and Base Acceptance," The Federal Highway Administration in conjunction with the Ohio Department of Transportation, FHWA/ODOT-2007/01.

Xu, C., Liang, C., and Shen, P., 2019. "Experimental and Theoretical Studies on the Ultimate Bearing Capacity of Geogrid-Reinforced Sand." *Geotextiles and Geomembranes,* 47, 417-428.

Yang, X. and Han, J. ,2013. "Analytical Model for Resilient Modulus and Permanent Deformation of Geosynthetic-Reinforced Unbound Granular Material." *American Society of Civil Engineers,* 139(9), 1443-1453, https://doi.org/10.1061/(ASCE)GT.1943-5606.0000879.

Yoder, E.J. and Witczak, M.W., 1975. "Principles of Pavement Design, 2nd Edition," pp. 711, Wiley and Company, London, England.

Zheng, L., Roodi, G.H., and Zornberg, J.G., 2019. "Case History of a Geosynthetic-Stabilized Base Roadway Founded Over Expansive Clay Subgrade," Geotechnical Special Publication 305, pp. 430-443, Geotechnical Materials, Modeling, and Testing, ASCE Geo-Congress, Pittsburg, Pennsylvania.

Zheng, Y. and Fox, P.J., 2017. "Numerical Investigation of the Geosynthetic-Reinforced Soil-Integrated Bridge System Under Static Loading." *Journal of Geotechnical and Geoenvironmental Engineering*, 143(6), 04017008.

Zheng, Y., Fox, P. J., and Shing, P. B., 2014. "Numerical Simulations for Response of MSE Wall-Supported Bridge Abutments to Vertical Load." *In-Ground Improvement and Geosynthetics*, 493-502.

Zofka, A., Zofka, E., Maliszewski, M., and Zalimiene, L., 2017. "Geogrid Reinforcement of Asphalt Pavements." *The Baltic Journal of Road and Bridge Engineering,* 12(3), 181-186. https://doi.org/10.3846/bjrbe.2017.22.

Zornberg, J.G., 2017. "Functions and Applications of Geosynthetics in Roadways." *Procedia Engineering,* 189, 298-306, https://doi.org/10.1016/j.proeng.2017.05.048.

Zornberg, J.G. and Gupta, R., 2010. "Geosynthetics in Pavements: North American Contributions," 1, pp. 379-400, Proceedings on the 9th International Conference on Geosynthetics, Guaruja, Brazil.

Zornberg, J.G. and Thompson, N., 2010. "Guide for the Application and Selection of Geotextiles," pp. 16, Center for Transportation Research (CTR), Document 0-5812-P1, Austin, Texas.

Zumrawi, M. and Abdalgadir, E., 2019. "Experimental Study of Geotextile Effect on Bearing Strength and Permeability of Sudanese Cohesive Soils." *University of Khartoum Engineering Journal,* 9(1), 21-26.

Appendix A The Direct Shear Box

Figure A.1 Installation of geosynthetic specimen in sand

Figure A.2 Installation of geosynthetic specimen in silt

Figure A.3 Installation of geosynthetic specimen in clay

Figure A.4 Surface of compacted soil in the box

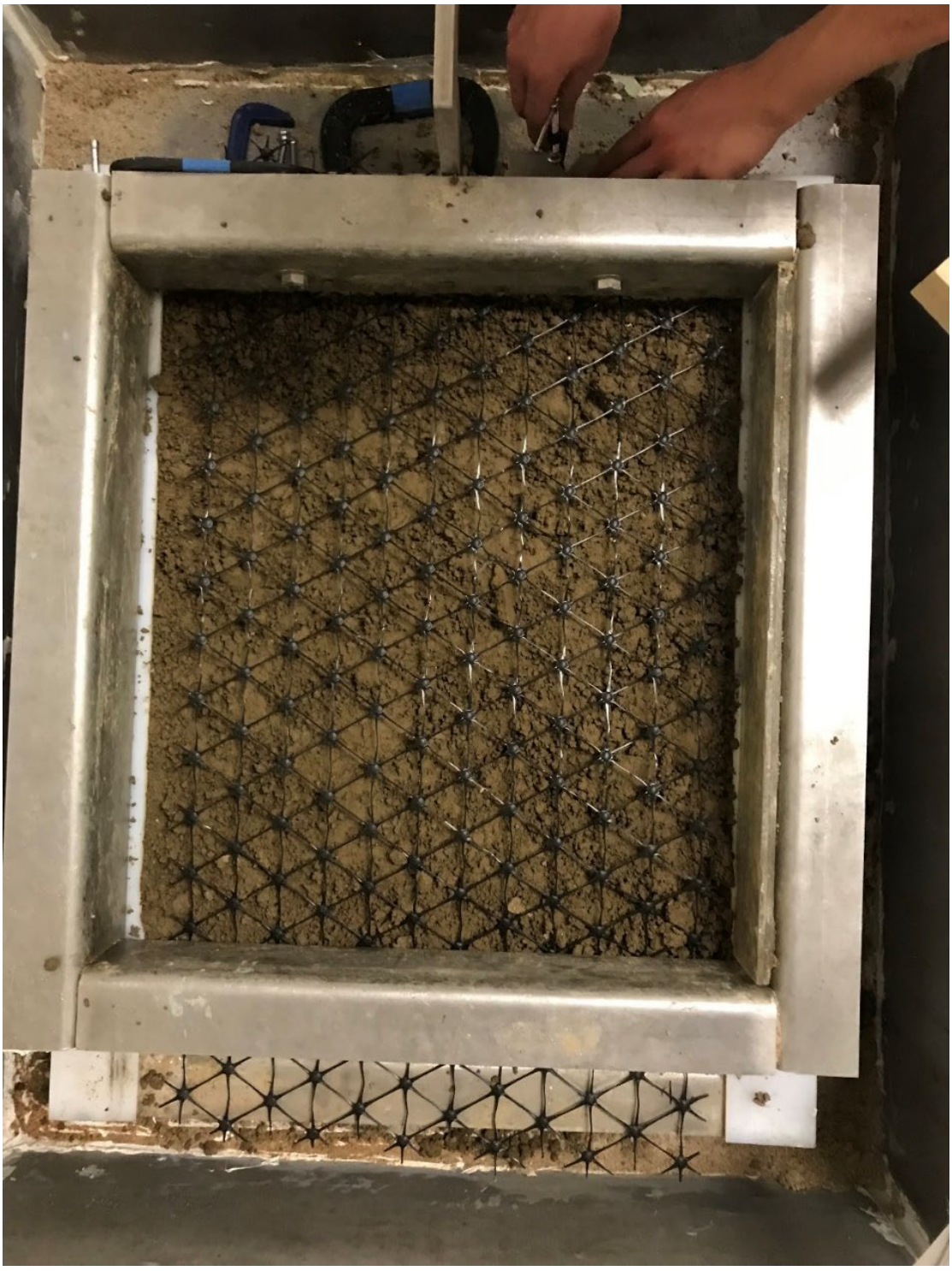

Figure A.5 Installation of geosynthetic specimen

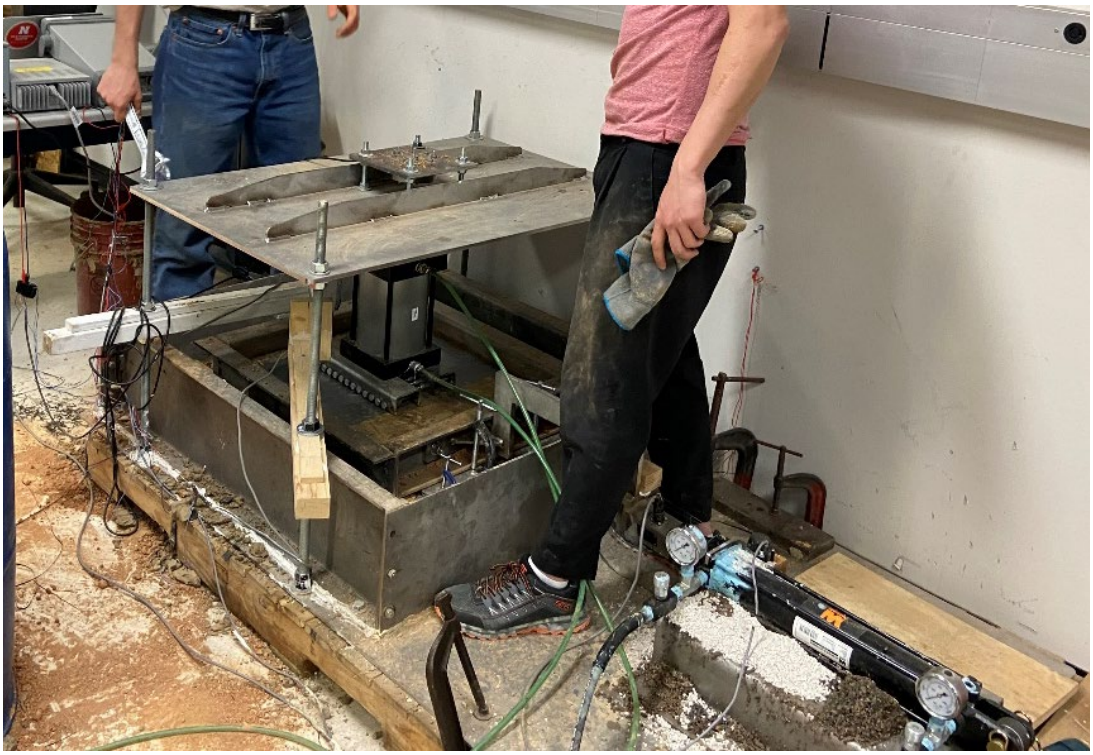

Figure A.6 A large direct shear test setup

Appendix B The Large-Scale Pullout Box

Figure B.1 A large scale pullout box

Figure B.2 LVDT cables behind the box

Figure B.3 Surface of compacted soil

Figure B.4 Fixation of frontal grip for geosynthetic

Figure B.5 Gripping for geosynthetic

Figure B.6 Gripping for geosynthetic

Figure B.7 Pull out of geogrid during the test

Figure B.8 Pull out of geogrid during the test

Figure B.9 Pull out of geotextile during the test

Appendix C The Large-Scale Tracking Wheel Test Drawings

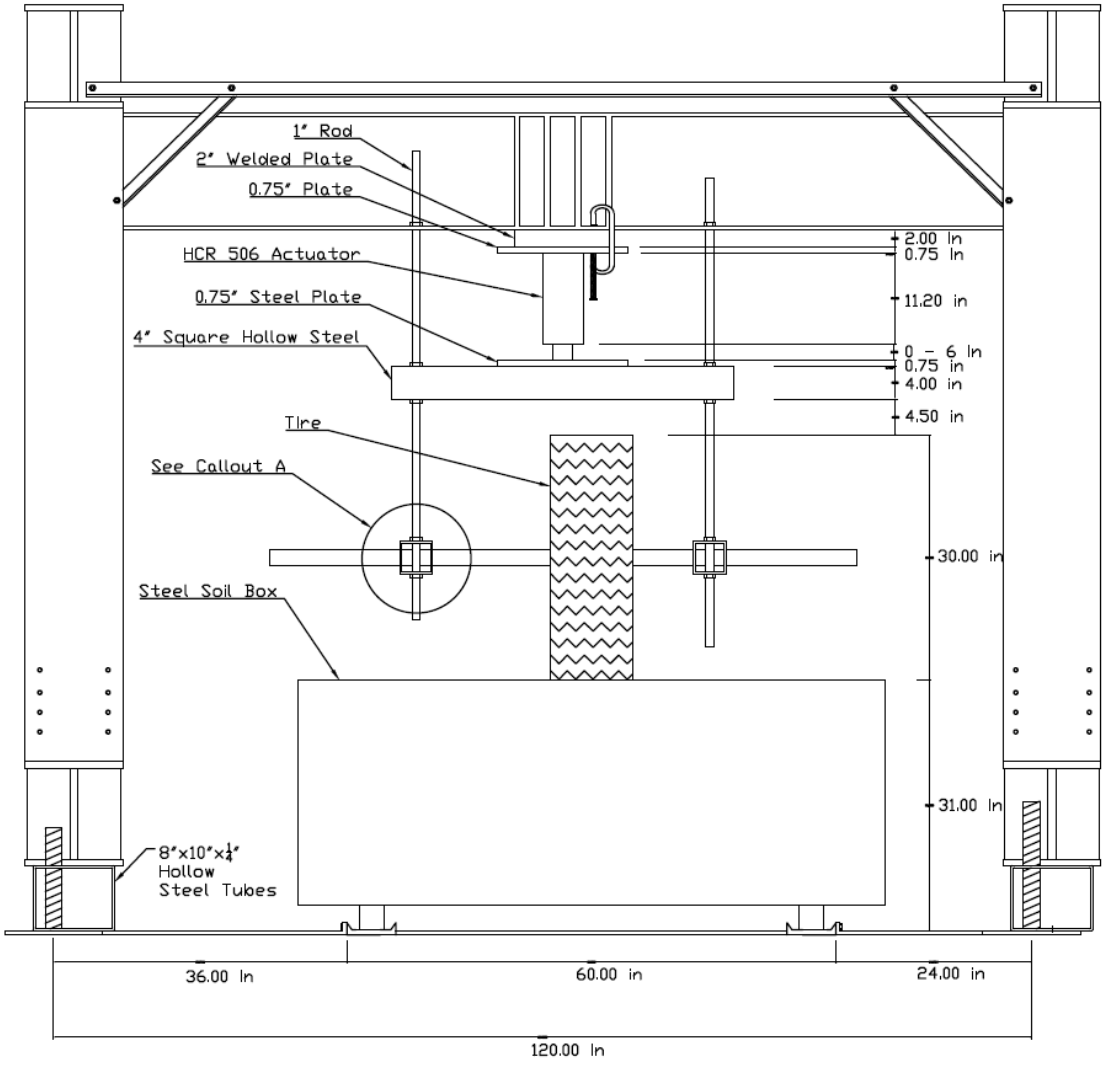

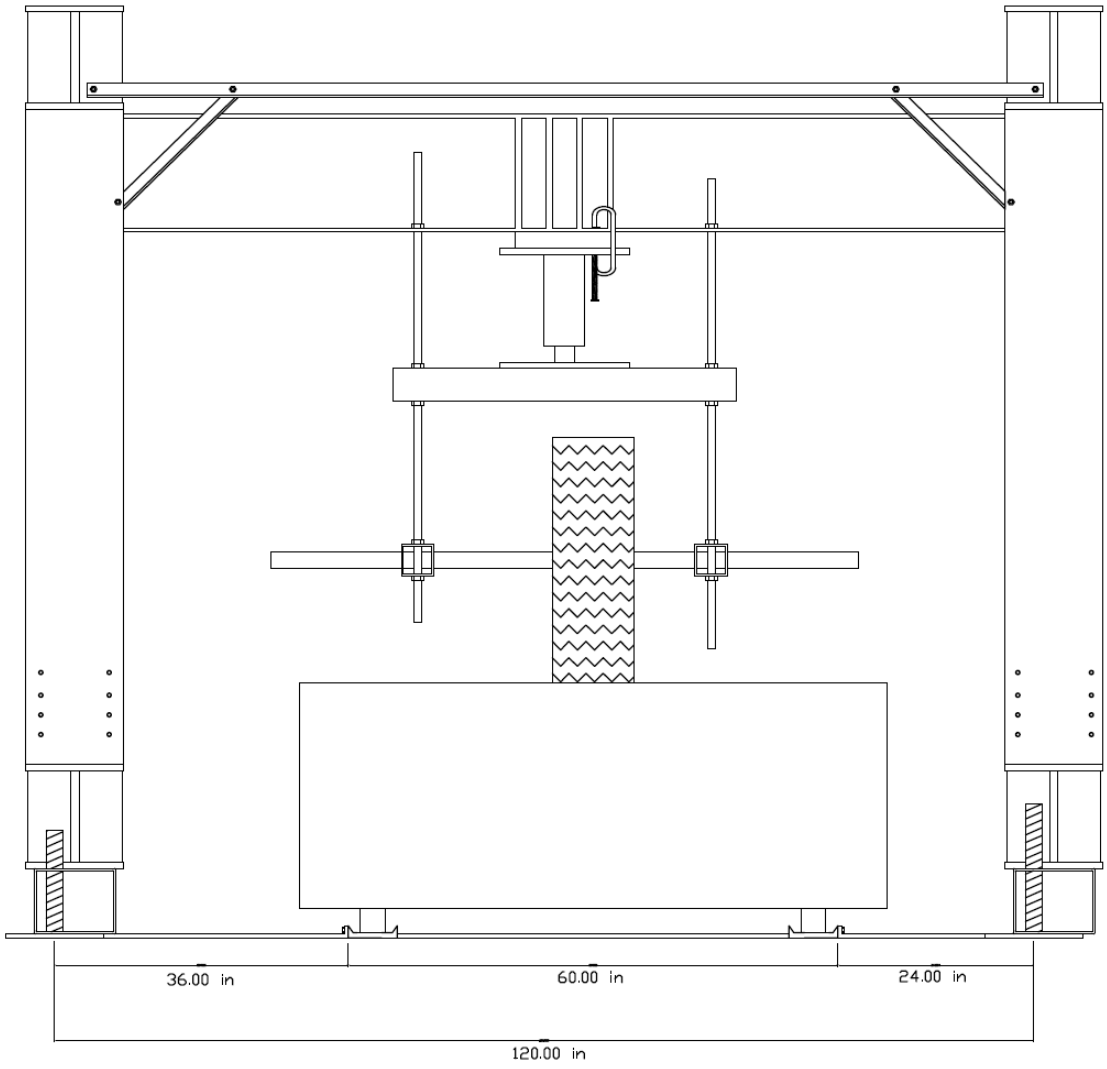
36.00 in
60.00 in
24.00 in
120.00 in

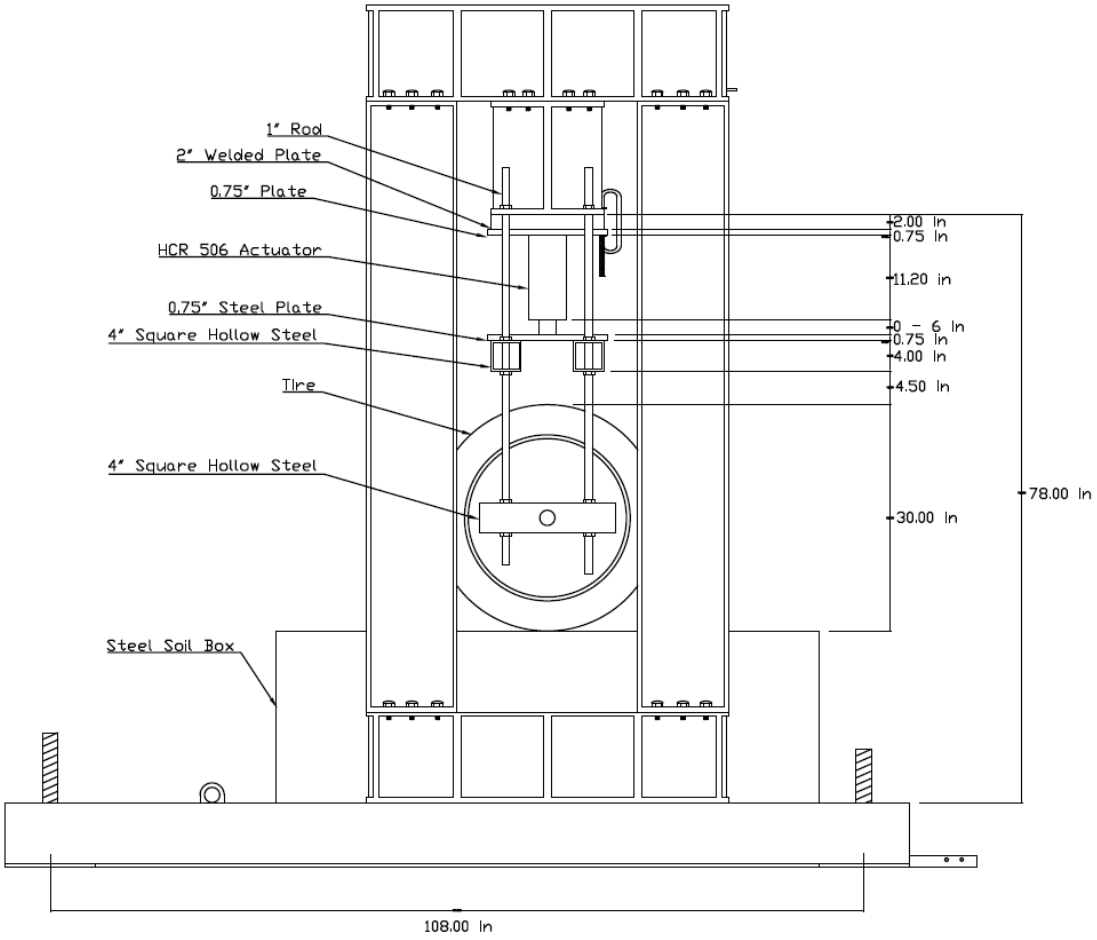
1" Rod
2" Welded Plate
0.75" Plate
HCR 506 Actuator
0.75" Steel Plate
4" Square Hollow Steel
Tire
4" Square Hollow Steel
Steel Soil Box
2.00 in
0.75 in
11.20 in
0 - 6 in
0.75 in
4.00 in
4.50 in
30.00 in
78.00 in
108.00 in

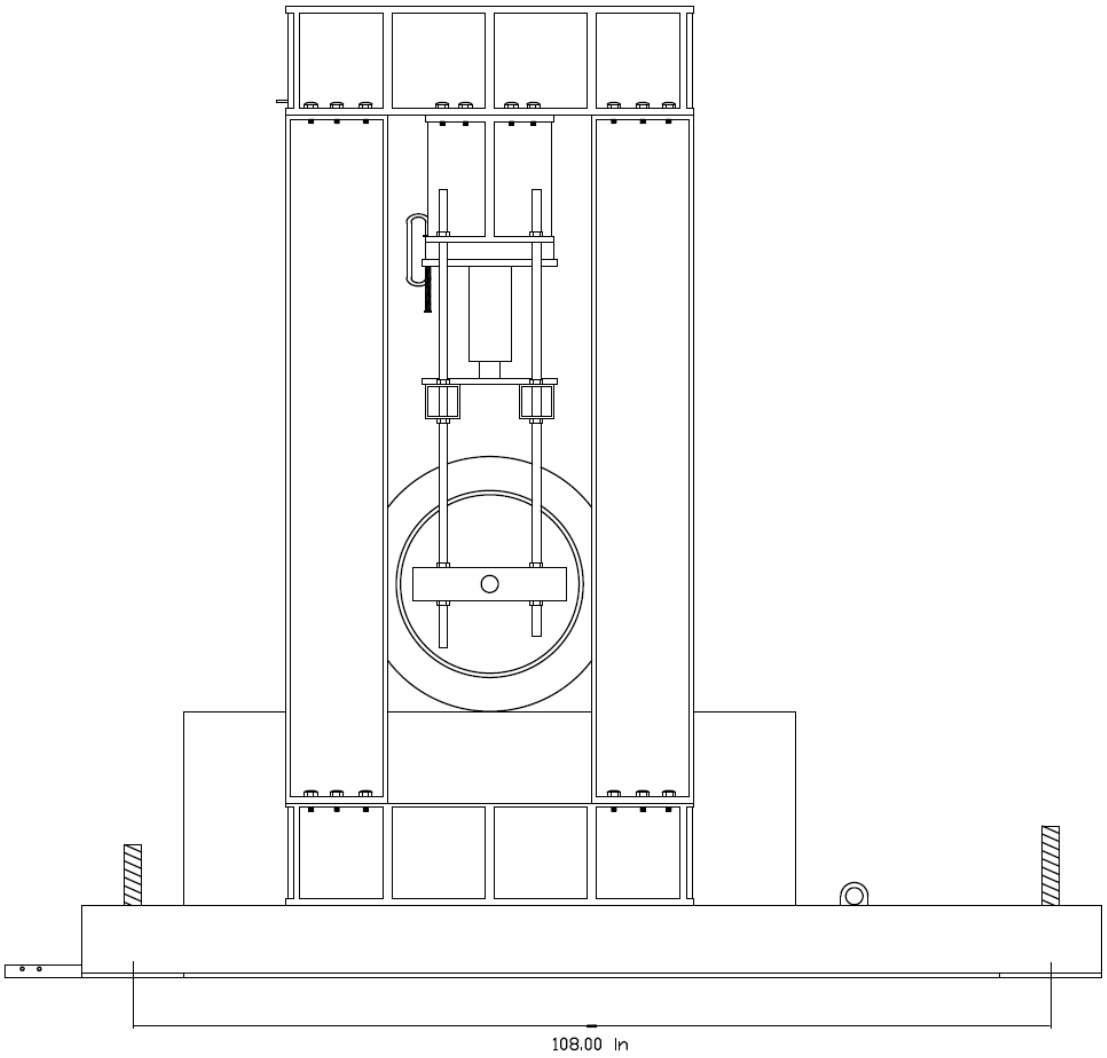
108.00 In

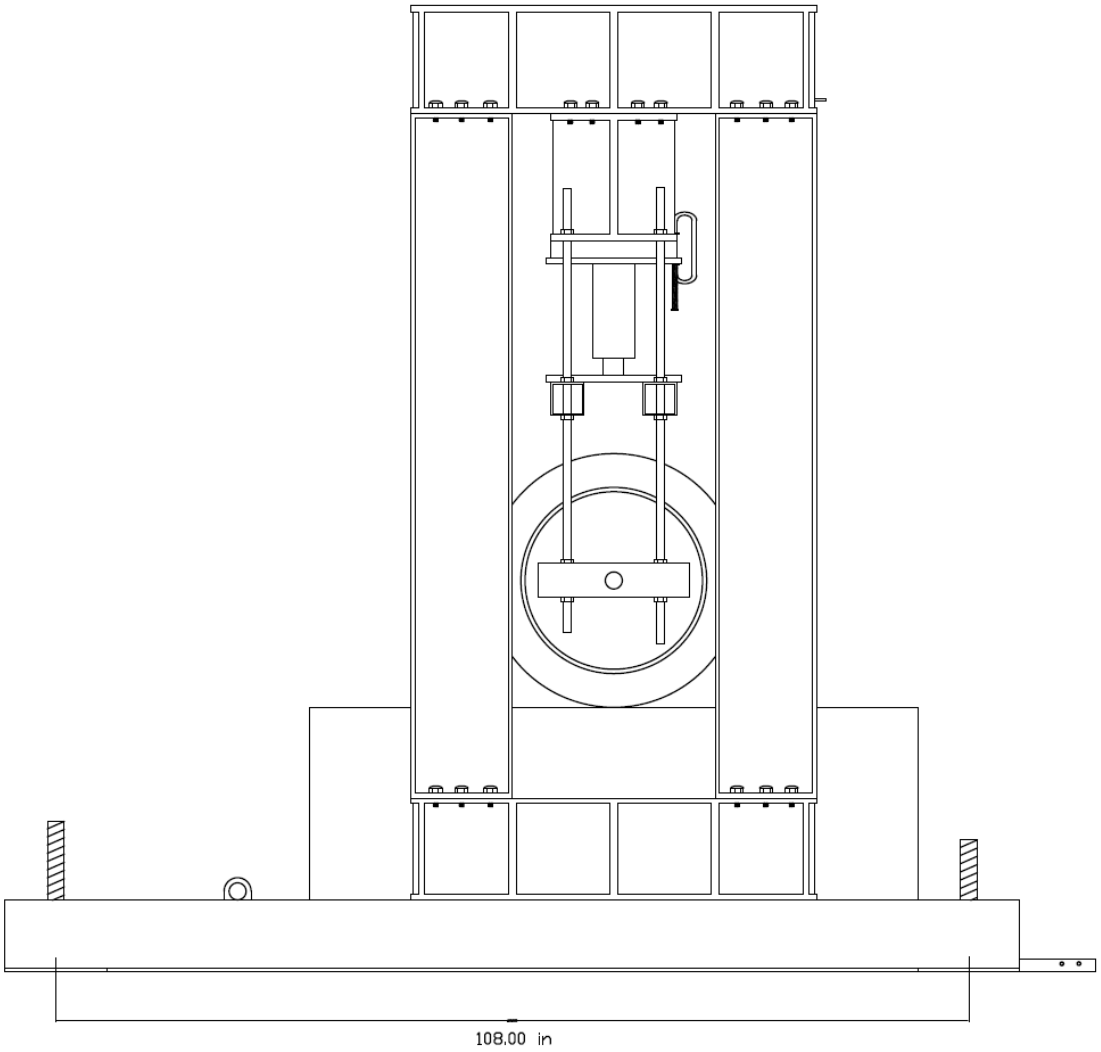
108.00 in

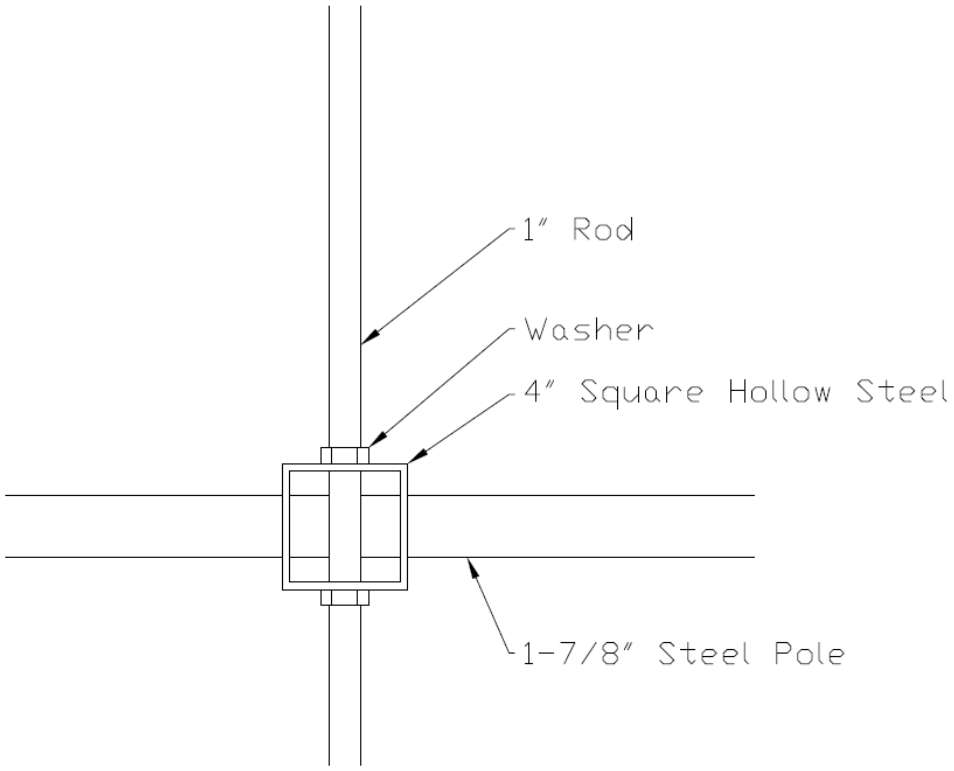

Callout A

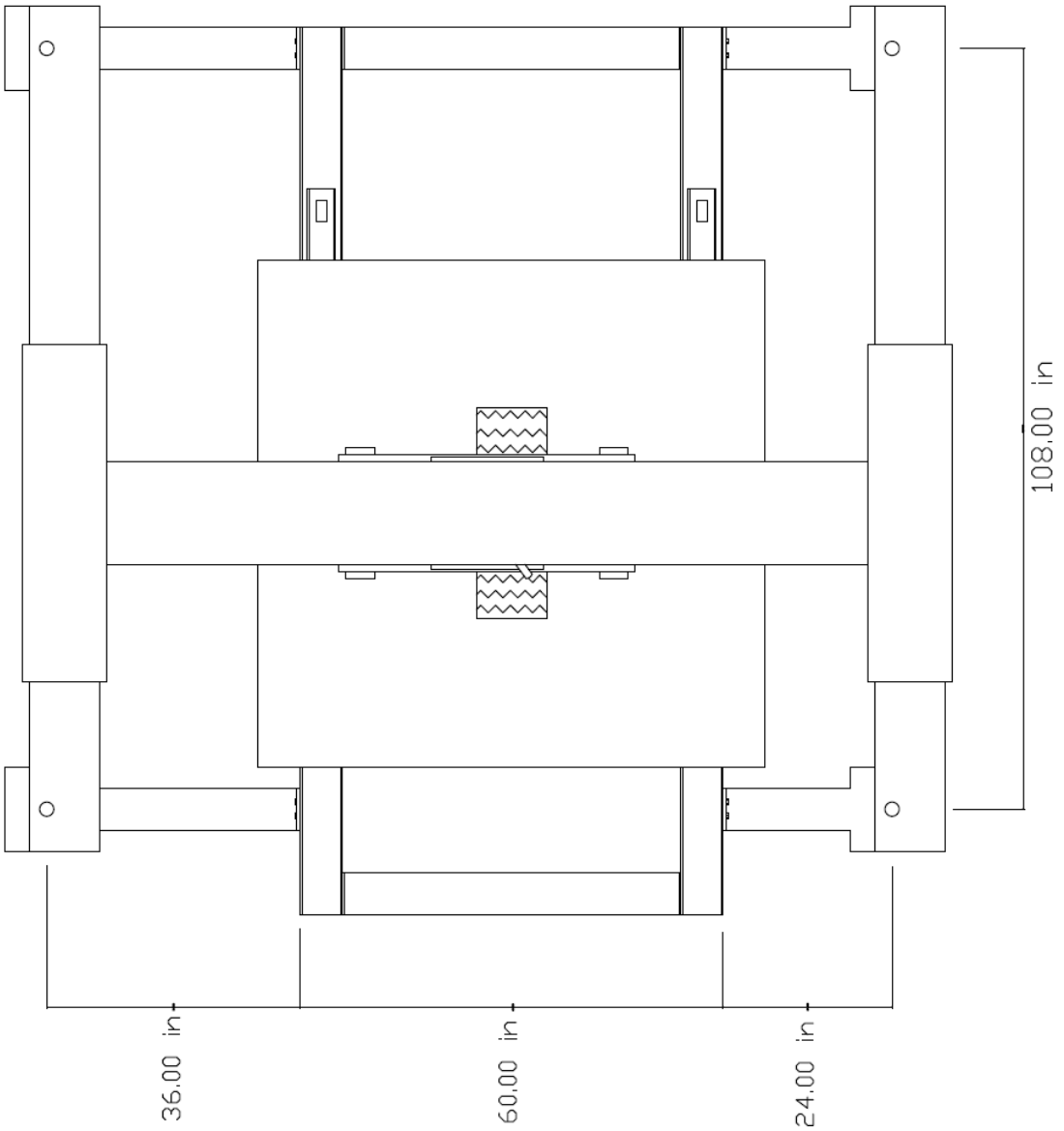
108.00 in
36.00 in
60.00 in
24.00 in

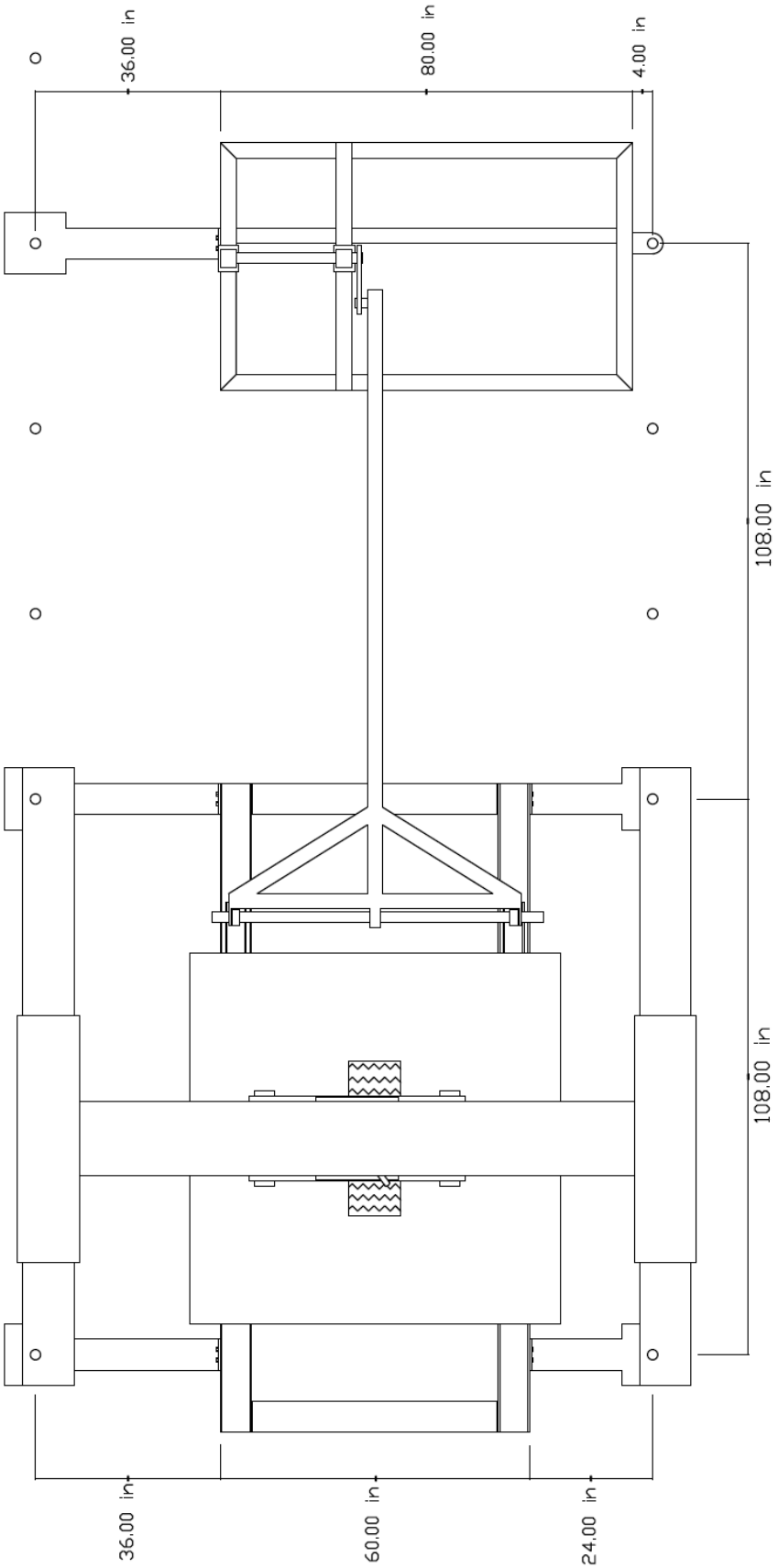
36.00 in
80.00 in
4.00 in
108.00 in
108.00 in
36.00 in
60.00 in
24.00 in

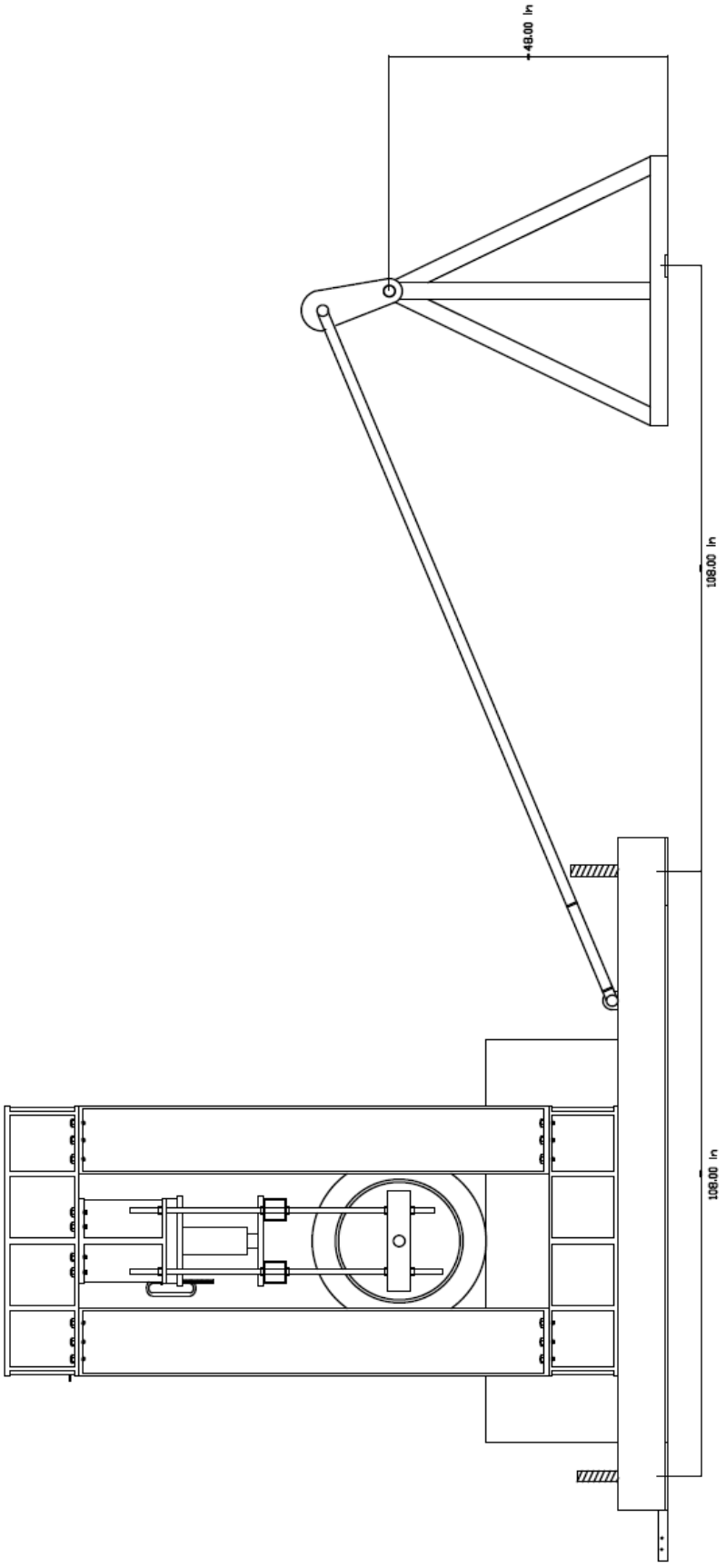
48.00 in
108.00 in
108.00 in